POLITECNICO DI TORINO

Corso di Laurea Magistrale in Ingegneria per l'Ambiente e il Territorio

Tesi di Laurea Magistrale

Automated Landing Site Optimisation Model for Human Mission to Mars

Relatore

Prof. Marilena Cardu

Candidata

Costanza Caruzzo

Marzo 2018

To my grandfather Gian Carlo

ABSTRACT

Successfully sending humans to Mars will represent one of the greatest achievements of the mankind. To ensure the crews' safety and ongoing mission success the selection of an optimised landing site for the construction of a human base is highly critical. Site selection will require a multidisciplinary effort with significant planning to implement a successful strategy that is both flexible and adaptable.

In this research, the development of a tool constructed in ArcGIS ModelBuilder which seeks to automate and optimise the landing site selection process for the first human mission to Mars will be discussed. The core focus of this work is to improve the selection process replacing time consuming and subjective manual analysis of datasets with an automated flexible model based on defined engineering constraints. To test and validate the effectiveness of the model, the constraints used for the landing of the Mars Science Laboratory (MSL) rover Curiosity at Gale Crater were incorporated into the tool. After workflow validation, the model was run on other proposed human exploration zones.

The model works by integrating images analysis tools and provides an output map that reflects the desired engineering constraint requirements. The workflow is structured into three main phases, which consists of: (1) Data processing, (2) Engineering parameter map layer development, (3) Raster reclassification. The reclassified output maps are then combined into a single map, which summarises all the properties analysed. This map represents a quantitative, fast and effective way to evaluate where it is and is not possible to land safely within an exploration zone, to identify the optimal landing areas from an engineering point of view, and to compare different exploration zones proposed for this pioneering mission.

A distinctive aspect of the model is its flexibility. The classification principles, the associated indexes, the weight of the implemented parameters may be varied, and further parameters can be entered to the workflow as required. The choice to grant flexibility to this work is consistent with the dynamic mission's objectives and constraints evolution.

The tool may be further optimised by the incorporation of a local resources analysis, which represent a fundamental requirement for a feasible and sustainable Off-Earth human mission.

AKNOWLEDGEMENTS

The development of this thesis would not have been possible without encouragement and support received from many people.

I would like to express my sincere gratitude to my supervisor Professor Marilena Cardu for her precious guidance and continuous motivation, passion and enthusiasm that guided me during the thesis development.

I sincerely would like to thank Professor Serkan Saydam for introducing me to this challenging Off-Earth mining topic, for giving me the possibility to develop this thesis at the UNSW Australia, and for providing me continuous support during my permanence at the School of Mining Engineering. I would also like to thank Sophia Casanova for her guidance and constructive feedback about the ideas I developed throughout this project. I would also like to acknowledge Kimie, Yesenia and Carlos for their valuable comments on this work and for the great time spent together at the School.

I would like to express my very profound gratitude to my parents Simona and Giacomo for providing me with unfailing support and continuous encouragement throughout my years of study at Politecnico di Torino and everything I could possibly hope for to achieve my goals.

I would really like to thank Matteo for pushing me to follow my dreams and for inspiring me with his great passion and dedication to the engineering field.

Last but certainly not least, I would really like to thank my peers and great friends Gaia, Elisa, Mariangela and Stefania for our cooperation and friendship that made this way lighter and pleasant, and Caterina for her patience and constant support that have been fundamental to accomplish this thesis.

TABLE OF CONTENTS

LIST OF FIGURES

LIST OF TABLES

LIST OF TERMS

BFR	Big Falcon Rocket
CCF	Concentric Crater Fill
CheMin	Chemistry and Mineralogy
CNSA	China National Space Administration
CTX	Context Camera
DAN	Dynamic Albedo of Neutrons
DEM	Digital Elevation Model
DM	Deuteronilus Mensae
DTM	Digital Terrain Model
EMC	Evolvable Mars Campaign
ESA	European Space Agency
EZ	Exploration Zone
GC	Gale Crater
GCM	General Circulation Model
GER	Global Exploration Roadmap
GIS	Geographical Information System
GLF	Glacial-like Features

HEOMD	Human Exploration and Operations Mission Directorate
HiRISE	High Resolution Imaging Science Experiment
HLS^2	Human Landing Site Selection
HRSC	High Resolution Stereo Camera
HSO-SAG	Human Science Objectives Science Analysis Group
ICE WG	ISRU and Civil Engineering Working Group
ISS	International Space Station
ISRO	Indian Space Research Organization
ISRU	In-Situ Resource Utilization
JMARS	Java Mission-Planning and Analysis for Remote Sensing
JPL	Jet Propulsion Laboratory
JAXA	Japan Aerospace Exploration Agency
LDA	Lobate Debris Aprons
LS	Landing Site
LVF	Lineated Valley Fill
MAV	Mars Ascent Vehicle
MAVEN	Mars Atmosphere and Volatile Evolution
MBC	Mars Base Camp
MEGDR	Mars MGS MOLA Elevation Model

MER	Mars Exploration Rover
MGS	Mars Global Surveyor
MOLA	Mars Orbiter Laser Altimeter
MOM	Mars Orbiter Mission
MOXIE	Mars Oxygen In-Situ Utilization Experiment
MRO	Mars Reconnaissance Orbiter
MSL	Mars Science Laboratory
M-WIP	Mars Water In-Situ Resource Utilization Planning
NASA	National Aeronautics and Space Administration
ODY	Mars Odyssey
PM	Protonilus Mensae
ROI	Region of Interest
SHARAD	Shallow Radar
SLS	Space Launch System
SMD	Science Mission Directorate
THEMIS	Thermal Emission Imaging System
TGO	ExoMars Trace Gas Orbiter
UAE	United Arab Emirates
URSS	Union of Soviet Socialist Republics

1 INTRODUCTION

Since 1965, when Mariner 4 spacecraft found a place in history collecting the first close-up photographs of Mars, an increasing interest in pioneering space led humanity to realise several successful missions over the time. The subsequent exploration decades provided a huge amount of data that allowed scientists investigating the Red Planet and making important discoveries, such as finding evidence of widespread presence of both liquid water that flowed on the surface during the past times and glacial ice that is actually present below the surface.

New horizon goals have been established to find signs of past life on the planet and Mars represents the next tangible frontier to expand the human presence beyond Earth.

The National Aeronautics and Space Administration (NASA) is working to land the first humans on its surface on 2033 and both space industries and politicians are demonstrating a growing interest to achieve this goal.

The global interest to emplace the first crew on Mars generates a synergy between industries and space agencies that are developing a complex architecture, which represents a logistic and supply chain challenge rather than a technological challenge (NASA, 2016b). The strategy to colonize the planet must be flexible and resilient to changes, requiring a technological advance in different areas, such as In-Situ Resource Utilization (ISRU), Off-Earth mining techniques and extraction technologies.

To ensure crews' safety and ongoing mission success, the selection of an optimised landing site for the construction of a human base is highly critical. Site selection will require a multidisciplinary effort with significant planning phases to implement a successful strategy that is both flexible and adaptable.

Demonstrating the ability to produce commodities from local resources represents a fundamental requirement to both reduce and ideally eliminate the reliance on Earth and to plan a feasible and sustainable mission to Mars. Water represents the highest priority both for propellant production and life support. In 2016, NASA funded a "first-order" analysis of questions related to potential water resource deposits on the Red Planet, named ISRU Planning (M-WIP).

With the aim of selecting a candidate location where crews will land, live and work, initially for a short and then for an extended period of time, both scientific and resource objectives have been fixed to maximise the astrobiological return and the human operation sustainability. In addition to these requirements, a set of engineering parameters, driven by operational considerations, are defined to select the landing site within the exploration zone where human activities will take place.

1.1 Research objectives

This thesis aims to assist in the selection of the landing site for the human mission to Mars.

The key research objectives are to:

i. Develop a flexible model based on defined engineering constraints, allowing the automated selection of an optimised landing site location within a proposed exploration zone for the human mission to Mars;

ii. Validate model effectiveness;

iii. Run the model on different exploration zones located on Mars;

iv. Propose possible configurations of the landing and habitation sites within an exploration zone;

v. Incorporate the output results with a local glacial resources analysis.

To provide an adequate context, a solid foundation of knowledge, and justifications to the project undertaken, a review of the available literature has been firstly conducted in Sections 2, 3 and 4. This analysis was not intended to be an exhaustive review of all the information sources, but rather an overview to highlight that the evolution of Mars' exploration requires a multidisciplinary approach to achieve its goals and that the dualism

between engineering and geology plays a fundamental role to select the optimum landing site for a sustainable human mission.

Concluding this review, a project overview was conducted in Section 5 to highlight the major objectives and tasks of this work.

Section 6 describes in detail the methodology followed to develop the model, with both its strengthens and limitations.

The results obtained are presented in Section 7 and discussed in Section 8.

Finally, conclusions and recommendations are provided in Sections 9 and 10.

2 MARS EXPLORATION

2.1 Evolutionary stream in Mars exploration

Retracing the steps of Mars exploration in past and present times, outlining future goals for the next missions already planned, and also providing an overview of both industrial and political statements, allow contextualising the project that has been developed in this thesis. Indeed, the evolutionary stream in Mars exploration gives a general idea of both the actual state of knowledge and the future objectives that have been fixed, looking towards landing the first humans on Mars.

2.1.1 Previous and present missions to Mars

Since the pioneering launch of Mariner 4 spacecraft that has been done by the United States in 1964, four entities have successfully completed their missions on Mars: NASA (National Aeronautics and Space Administration), ESA (European Space Agency), ISRO (Indian Space Research Organization) and the Soviet Union (see Table 2-1).

Between 1964 and 1971, NASA built and sent to Mars four spacecrafts named Mariner, relatively small robotic explorers carrying a host of scientific instruments, as cameras and remote sensors, which weighted less than half a ton (NASA, n.d.c).
Mariner 4, which has been launched in 1964, collected the first close-up photographs of Mars after an eight-month voyage: these 21 pictures recorded and showed lunar type impact craters on the surface of the planet (NASA, n.d.c).
In 1969 the first dual mission to Mars has been completed by Mariner 6 and 7: they returned respectively 75 and 126 images of the heavily cratered surface of the planet and analysed both the surface and the atmosphere with remote sensors (NASA, n.d.c).
Mariner 9 was the first artificial satellite of Mars that achieved its orbit in November 1971, returning more than 7000 high-quality images of the surface of Mars in about one year of mapping and measurements (NASA, n.d.c). It allowed recognizing both great volcanoes and valleys, revealing a global dust storm that obscured the whole globe of the

planet, providing the first close-up photographs of Phobos and Deimos, which are the two small and irregular Mars' moons (NASA, n.d.c).
Between 1960 and 1973 the URSS' Mars Program took place with the aim of exploring Mars with flyby probes, orbiters and landers. Subsequently of some failed missions, Mars 3 spacecraft was launched in 1971. It consisted in a lander and an orbiter: the lander-orbiter system entered into Mars' orbit and then the lander separated and descended to the surface of the Red Planet. Mars 3 lander has been the first spacecraft that landed safely on Mars although the transmission of data stopped after 20 s for unknown reasons (NASA, n.d.d); on the contrary, Mars 3 orbiter recorded data for approximately 8 months (NASA, n.d.b).
Mars 5 lifted off in 1973 and transmitted 60 images showing Valles Marineris (Mitchell, 2004), the largest and deepest canyon feature of the Solar System (NASA, n.d.b).

In 1975 NASA's Viking Project found a place in the history of Mars' missions: two identical spacecraft, Viking 1 and Viking 2, each consisting of a lander and an orbiter, were launched (NASA, n.d.k). For the first time, two American spacecrafts landed safely on Mars after eleven months of transit time. Both landers and obiters operated far beyond their designed lifetimes, transmitting photographs that surpassed expectations in quality and quantity (NASA, n.d.k). The landers provided the first close-up images of the surface, determined the means size of the atmospheric aerosol and monitored variations in atmospheric opacity over several Martian years (NASA, n.d.k). The orbiters' cameras mapped 97% of the surface of Mars observing new and puzzling features on it, and the orbiters' infrared thermal mappers and atmospheric water detectors acquired a massive quantity of data that have been used to understand the global meteorology of the planet (NASA, n.d.k). The Viking missions also determined that the residual north polar ice cap is made of water ice rather than frozen carbon dioxide (NASA, n.d.k). Unfortunately, despite an unexpected chemical activity in the Martian soil has been discovered, no clear evidence of microbial life has been found (NASA, n.d.k).

Mars Global Surveyor (MGS), a NASA's global mapping mission, began in 1996 with the aim of studying the entire Martian surface, atmosphere and interior. MGS examined the entire planet and revealed ancient signs of water such as gullies and debris flow

features, and an accumulation of hematite, a well-crystalized ferric oxide that originate from thermal activity (NASA, n.d.f).

Mars Pathfinder returned extensive data on Martian weather factors such as whirlwinds called dust devils which mix dust into the atmosphere, pressure and temperature variations, and early morning water ice clouds in the lower atmosphere that evaporate when the temperature becomes warmer (NASA, n.d.g). Mars Pathfinder also conducted chemical analyses on rock and soil that appeared high in silica (NASA, n.d.g).

In 2001, Mars Odyssey (ODY) orbiter has been launched. This mission represents NASA's longest-lasting spacecraft that is still operating, and it enabled scientists both to make the first global map of chemical elements and minerals distribution and to identify regions with subsurface water ice.
Images and measurements derived from this mission aided to identify potential landing sites for rovers and landers on Mars including the Mars Exploration Rovers (MER) Spirit and Opportunity, the Mars Phoenix lander and the Mars Science Laboratory's (MSL) Curiosity rover (NASA, n.d.a).

The two MER Spirit and Opportunity landed on Mars on 2004 and surpassed the expected lifetime of more than 15 times: their spectrometers provided evidence that salty water saturated the rock, which is rich of sulphate-salt minerals.

In 2005, NASA launched a multipurpose spacecraft named Mars Reconnaissance Orbiter (MRO) to provide detailed images of the Red Planet to enable evaluating potential safe landing sites for rovers and landers, combining both radar observation and satellite imagery (NASA, n.d.h). The MRO also carries a sounder to find subsurface water, a second camera for medium-resolution images that provides a broader geological and meteorological context and other instruments to analyse how dust and water are transported in the atmosphere.

Mars Phoenix lander, scheduled for launch in 2007, arrived on Mars' surface in 2008. It has been designed to study the history of water and to search complex organic molecules

in the ice-rich soil of Mars (NASA, n.d.j). It has been the first lander that identified water ice beneath the surface: indeed, the Phoenix lander dug through the sublimation protective layer to the water ice below with a robotic arm and brought both ice and soil to the lander platform for detailed chemical and geological analysis (NASA, n.d.j).

In 2012, NASA's Mars Science Laboratory (MSL) mission set down Curiosity rover, a large mobile laboratory, at Gale Crater. After few weeks from landing, Curiosity identified an area with evidence for stream flow where water coursed vigorously in the past time (NASA, n.d.i). Then some drilled samples have been analysed and evidence for life in Mars' early history has been proved: water not too acid or salty that flowed on the planet's surface, a chemical energy source, and other key elements for life provided confirmation about a habitable environment during past times (NASA, n.d.i). Curiosity also identified a methane amount in Mars' atmosphere (NASA, n.d.i).

Between 2013 and 2016, NASA's Mars Atmosphere and Volatile Evolution (MAVEN), ISRO's Mars Orbiter Mission (MOM), and ESA's ExoMars Trace Gas Orbiter (TGO) have been successfully sent into orbit with the main aim of studying the Martian atmosphere (NASA, n.d.b).

Table 2-1 provides a summary of all the successful missions over the time.
APPENDIX A reports both failed and successful missions over the decades of exploration.

Table 2-1. Historical summary of successful missions (modified from NASA, n.d.b)

Launch Date	Name	Country	Reason/Results
1964	Mariner 4	US	Returned 21 images
1969	Mariner 6	US	Returned 75 images
1969	Mariner 7	US	Returned 126 images
1971	Mars 3 Orbiter/Lander	USSR	Orbiter obtained approximately 8 months of data and lander landed safely, but only 20 seconds of data
1971	Mariner 9	US	Returned 7329 images
1973	Mars 5	USSR	Returned 60 images; only lasted 9 days

1973	Mars 6 Orbiter	USSR	Occultation experiment produced data
1975	Viking 1 Orbiter/Lander	US	Located landing site for lander and first successful landing on Mars
1975	Viking 2 Orbiter/Lander	US	Returned 16000 images and extensive atmospheric data and soil experiments
1996	Mars Global Surveyor	US	More images than all Mars Missions
1996	Mars Pathfinder	US	Technology experiment lasting 5 times longer than warranty
2001	Mars Odyssey	US	High resolution images of Mars
2003	Mars Express Orbiter	ESA	Orbiter imaging Mars in detail and lander lost on arrival
2003	Mars Exploration Rover - Spirit	US	Operating lifetime of more than 15 times original warranty
2003	Mars Exploration Rover - Opportunity	US	Operating lifetime of more than 15 times original warranty
2005	Mars Reconnaissance Orbiter	US	Returned more than 26 terabits of data (more than all other Mars missions combined)
2007	Phoenix Mars Lander	US	Returned more than 25 gigabits of data
2011	Mars Science Laboratory	US	Exploring Mars' habitability
2013	Mars Atmosphere and Volatile Evolution	US	Studying the Martian atmosphere
2013	Mars Orbiter Mission (MOM)	ISRO	Develop interplanetary technologies and explore Mars' surface features, mineralogy and atmosphere
2016	ExoMars Orbiter	ESA	Orbiter studying Martian atmosphere and EDL demo lander lost on arrival

2.1.2 Future missions to Mars

Successively to these exploration decades, which allowed acquiring a vast amount of data that have been used to investigate different aspects related to Mars, twelve space agencies defined the Global Exploration Roadmap (GER) with the aim to expand human presence in space (NASA, 2016b). Achieving this aim requires to accomplish a sequence of subsequent goals, that are to (1) emplace facilities and infrastructures on Mars' surface, (2) landing crews for short periods of time, and (3) enable humans to live on Mars and to be Earth-independent for an extended period of time (see Figure 2-1).

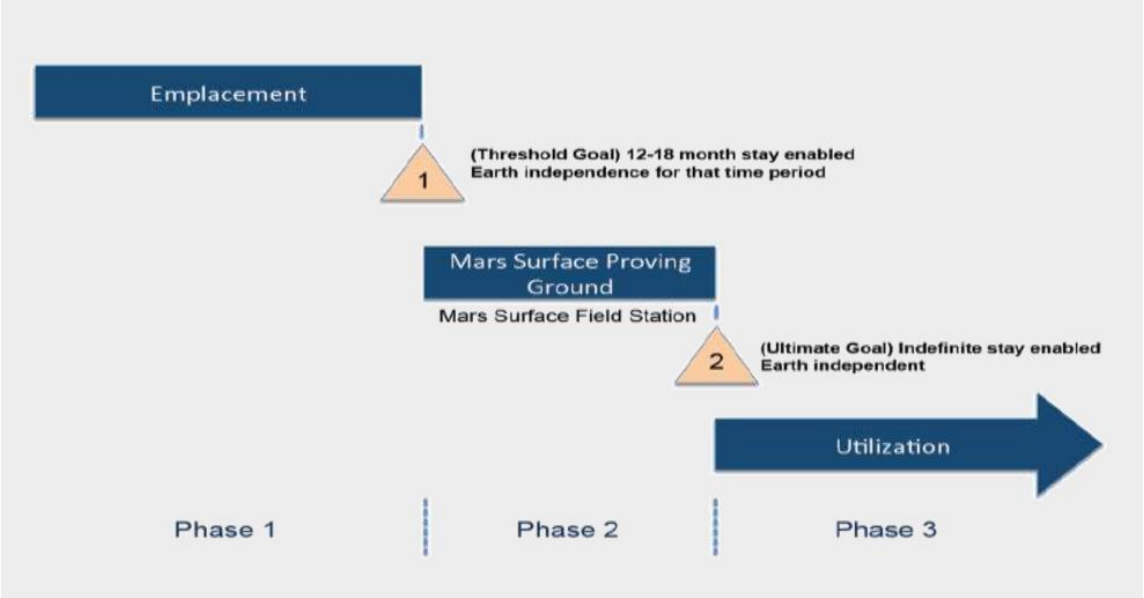

Figure 2-1. Mars Surface Field Station evolution (Bussey and Hoffman, 2016)

Nowadays, future missions have already been planned with the aim of collecting further data and information that will be useful to safely emplace the first humans on Mars.

In 2018, NASA's InSight mission will be launched with the aim of understanding both past and present planetary interior and its role in generating the ancient Mars' magnetic field, in the volcanic activity and in producing a wet and warm habitable environment during the past times (Explore Mars Inc., 2017).

In 2020, several upcoming missions will be accomplished (Explore Mars Inc., 2017): NASA's Mars 2020 rover will be launched with the aim of collecting samples from Mars and of producing oxygen from local atmosphere as part of the Mars Oxygen In-Situ Utilization Experiment (MOXIE); ESA's ExoMars 2020 rover will land on Mars' surface to find signs of past life with the aid of a drilling robotic arm that will excavate 2 m below the surface; the United Arab Emirates (UAE) are developing Hope orbiter with the objective of creating a global weathering map; SpaceX agency is projecting to launch its first Red Dragon for testing this technology; the China National Space Administration (CNSA) scheduled the launch for both a lander and an orbiter to explore the Martian atmosphere and terrain searching for signs of past life.

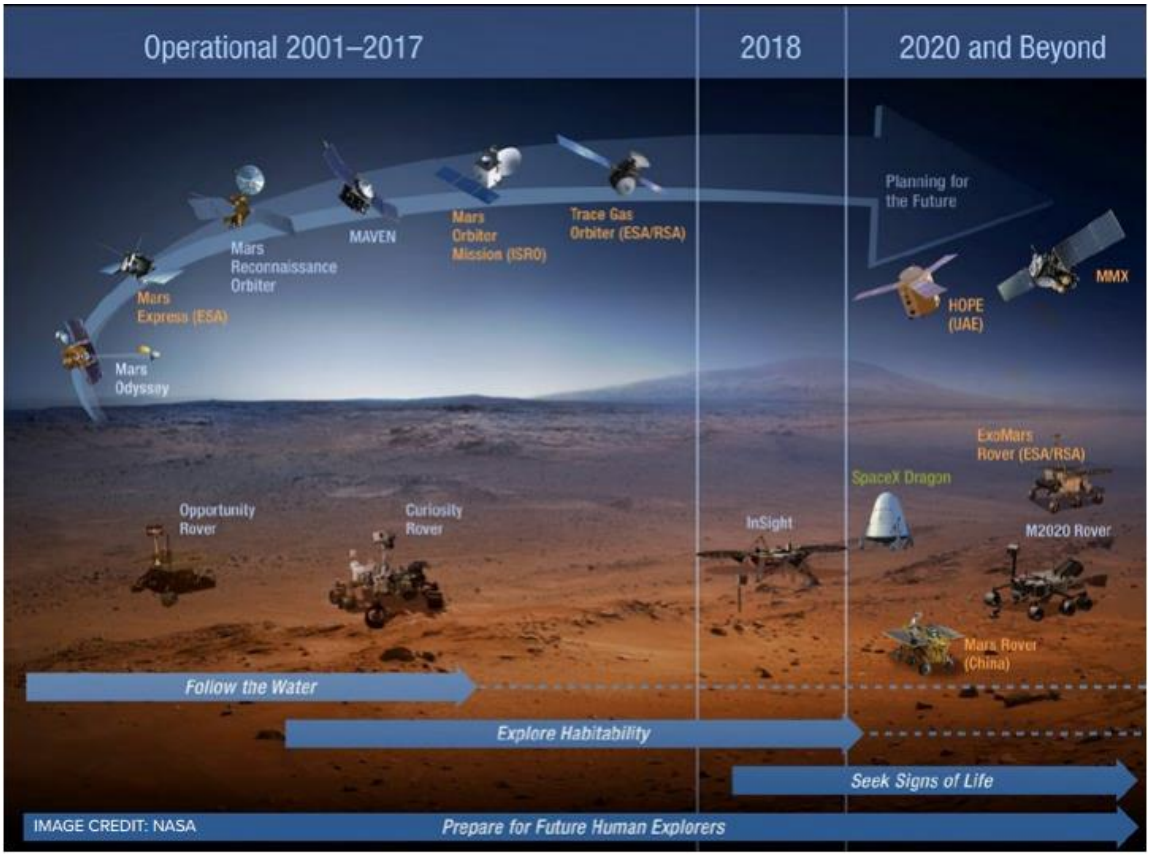

Figure 2-2. Present and future missions for Mars exploration (Explore Mars Inc., 2017)

Beyond that, in 2024 the Japan Aerospace Exploration Agency (JAXA) will be launching the Martian Moons Exploration mission (MMX) to return samples from Phobos and to understand both mechanical and gravitational aspects of Mars' moons (Explore Mars Inc., 2017).

Further missions have not been yet approved by NASA beyond 2020. Nevertheless, the Next Generation Mars Reconnaissance Orbiter mission and the Mars Sample Return mission are actually under study; these missions will be useful to solve some uncertainties in order to reduce risks associated with human landing on Mars (Explore Mars Inc., 2017).

All these projects, which are summarised in Table 2-2 and Table 2-3, highlight how research is quickly moving towards a time rich in scientific discoveries.

Table 2-2. Future missions actually under development (modified from Explore Mars Inc., 2017)

Launch Date	Name	Country	Reason/Aim
2018	InSight	US	Quantitative understanding of the internal structure of the planet, evaluation of any local areas of seismic risk and analysis of Mars' weather
2020	Mars 2020	US	MOXIE ISRU demo, caching for sample return
2020	Hope 2020	UAE	Global weather mapping
2020	ExoMars 2020 rover	ESA	Investigate signs of life
2020	Red Dragon SpaceX	US	Technology demonstration mission: first use of supersonic retro-propulsion in a Mars lander

Table 2-3. Future missions actually under study (modified from Explore Mars Inc., 2017)

Launch Date	Name	Country	Reason/Aim
2022/2024	Next Generation Mars Reconnaissance Orbiter	US	Martian system resource reconnaissance for ISRU of Mars and its moons
2024	Martian Moon Exploration	JAXA	Phobos sample return; critical insight into the potential for Martian moons to support ISRU

Not defined yet	Mars Sample Return	US	More detailed biological analysis, due diligence to address toxicity and potential biological risks

2.1.3 Architectures and systems: agency and industry statements

The human exploration of Mars is getting closer every day because of a multinational combined effort of space agencies and industries that continue to design a structured architecture for the pioneering journey to the Red Planet. The goal for the first landing of humans to Mars' surface has been set on 2033: this date can be considered reasonable from both technological and economical sides, and also to maintain political and public support (Explore Mars Inc., 2017).

Expanding human presence to Mars requires a combined interaction between different technical activities that must be balanced by non-technical constraints such as affordability, feasibility, engagement and interest (Explore Mars Inc., 2017).

As consequence, the pioneering approach to enable human expansion beyond Earth must be flexible and resilient to changes, because of the large number of variables and unknowns that characterise the project itself.

2.1.3.1 NASA's Journey to Mars

Aligning its activities with GER, NASA is looking towards landing the first humans on the surface of the Red Planet in the early 2030's, with a long term human sustainable missions on Mars as its final goal. To accomplish this goal, NASA is defining a long-term, flexible and sustainable architecture for space exploration called Evolvable Mars Campaign (EMC) (Bussey and Hoffman, 2016).

The challenge of allowing humans to live, operate and work safely on Mars for extended periods of time requires the preparation of a three-phase project named "Journey to Mars" (see Figure 2-3). This strategy, developed by a multidisciplinary collaboration on a global scale, passes through three thresholds, each with increasing challenges: (1) from "Earth Reliant" human spaceflight program, (2) through the "Proving Ground" of cislunar space, (3) to an "Earth Independent" capability. Earth Reliant exploration constitutes the initial

phase of the “Journey to Mars” and both scientific and technological researches occur aboard the International Space Station (ISS) from 2000. ISS is testing life support and crew health systems, habitat modules and other technologies needed to reduce reliance on Earth looking towards long-duration missions; the Proving Ground phase will analyse how to conduct operations in an Off-Earth environment by operating in a cislunar space; using knowledge acquired in ISS and in cislunar space, Earth Independent activities will allow to advance science and technology to go to Mars not only to visit the planet but to stay (NASA, 2016b).

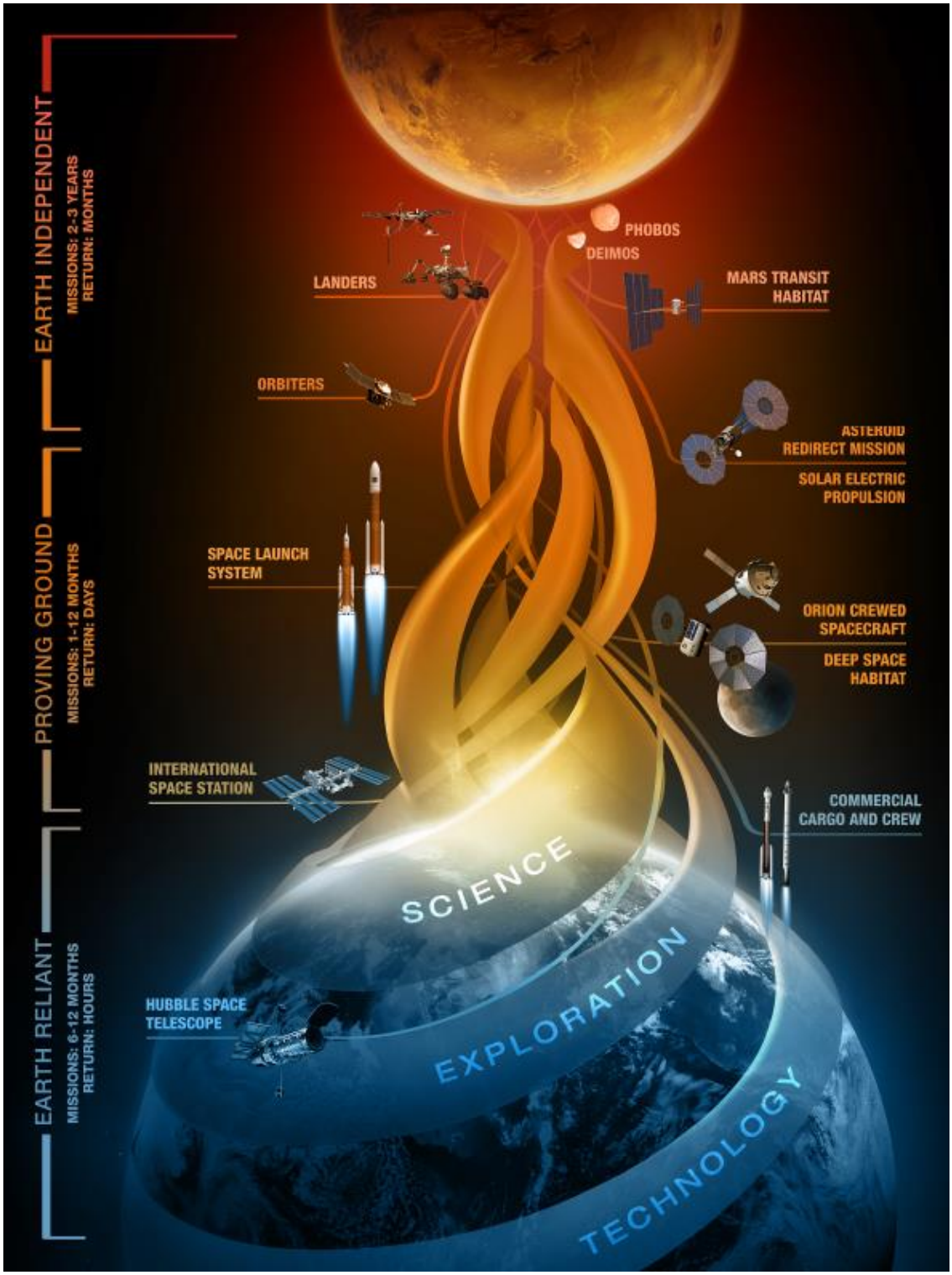

Figure 2-3. Multiple phases and evolutionary streams in NASA's EMC (NASA, 2016b)

2.1.3.2 JPL's Minimal Mars

The Jet Propulsion Laboratory (JPL) conducted an independent research to evaluate the affordability of a possible plan to realize two separate campaigns: the first one to place astronauts in Mars orbit in 2033 and the second one to land humans on the surface of the Red Planet in 2037. The challenge of a crewed travel to Mars has been broke up in two parts with the aims of minimizing both development and mission risks, avoiding unnecessary complexity and spreading the costs (Explore Mars Inc., 2017; Jet Propulsion Laboratory, n.d.). This architecture allows integrating the expensive and complex development of technologies, such as in-situ propellant production and cryogenic propellant, after doing a preliminary evaluation of the human risk of travelling to Mars (Explore Mars Inc., 2017). Crew's safety is placed in emphasis in all the phases of the travel: indeed, injury or loss of life could cripple the mission.

JPL's program establishes to connect all the future challenges with the previous missions, using them as backup knowledge (Explore Mars Inc., 2017). For this reason, the Mars vehicle will be tested on the Moon before launching it to Mars: the low gravity environment can provide a simulation for the landing phase, for the surface operations and for the ascending phase (Explore Mars Inc., 2017). Consequently, the lunar mission constitutes a rehearsal for the following ones on Mars.

2.1.3.3 Lockheed Martin's Mars Base Camp

The American global aerospace, defence, security and advanced technologies company Lockheed Martin is developing a crewed Mars laboratory orbiter concept named Mars Base Camp (MBC) that proposes to launch astronauts into Mars orbit around 2028, providing a blueprint to NASA's Journey to Mars (Lockheed Martin, n.d.). The MBC concept may answer to fundamental science questions to prepare for a safe human landing on Mars (Explore Mars Inc., 2017); indeed, two Orion crew modules will be launched to explore Mars's moons Deimos and Phobos and will tele-robotically operate on Mars' surface, also bringing samples back to the orbiting base camp; then a crewed, single-stage, descent and ascent re-usable surface lander will be used to perform sortie missions on Mars (Explore Mars Inc., 2017): each mission, involving up to four scientist-astronauts, could last in two weeks and return to the orbiting MBC without surface

refuelling (Lockheed Martin, n.d.). This lander system is powered by engines that use liquid hydrogen and liquid oxygen propellants generated from water (Lockheed Martin, n.d.).

2.1.3.4 Boeing Cislunar and Mars

Boeing's architecture is based on an initial phase of cislunar proving ground before trying to visit Mars. Nowadays, Boeing is collaborating with NASA to develop the Space Launch System (SLS) heavy lifter, a powerful launch vehicle for deep-space missions (Explore Mars Inc., 2017). The first step of Boeing's design will be positioning a space station in cislunar space named Deep Space Gateway (Explore Mars Inc., 2017; Boeing, n.d.). After testing Mars vehicle prototype named Deep Space Transport vehicle, a series of missions will be launched from the cislunar Gateway to Mars' moons and also to Mars' surface with remote operations. The architecture culminates with the first crewed mission on the surface of Mars (Explore Mars Inc., 2017).

Figure 2-4. Boeing Mars architecture: from cislunar to Mars exploration (Boeing, n.d.)

2.1.3.5 SpaceX's Mars Architecture

SpaceX aspirational goal is to deliver a large quantity of cargo and people to Mars, with the aim of enabling humanity to become a multi-planetary species. To reach this colonization goal, the first cargo mission to Mars has been planned in 2022, with the objectives of confirming water resources and placing the first infrastructures that will supply all the human activities to the Red Planet (SpaceX, 2017); then, a crewed mission for preparing the environment for next crew flights and for building a propellant deposit has been targeted for 2024 (SpaceX, 2017).

To achieve these ambitious results, SpaceX's architecture is focused on spacecrafts' full reusability as fundamental step to enable people living Off-Earth.

In 2012, the company launched Falcon 9, the first rocket able to fly again, carrying satellites and Dragon spacecraft (SpaceX, 2016). Dragon has been the first commercial spacecraft that delivered cargo to the ISS and came back to Earth safely (SpaceX, 2017). It was designed with the aim of carrying both human and cargo to space (SpaceX, 2017). In February 2018, Falcon Heavy, the most powerful operational rocket with the ability to lift over 54 tons, has been successfully tested.

In September 2017, SpaceX CEO and Lead Designer Elon Musk introduced the next generation vehicle named Big Falcon Rocket (BFR) (SpaceX, 2017). BFR will provide transportation to both cargo and humans to Mars, replacing Falcon 9 and Falcon Heavy (SpaceX, 2017). After delivering the payload on Mars, BFR will refill by making use of propellant produced in-situ (see Figure 2-5). For this reason, Mars' In-Situ Resource Utilization (ISRU) plan is required: water resources located on Mars will be fundamental to produce propellant to come back to Earth.

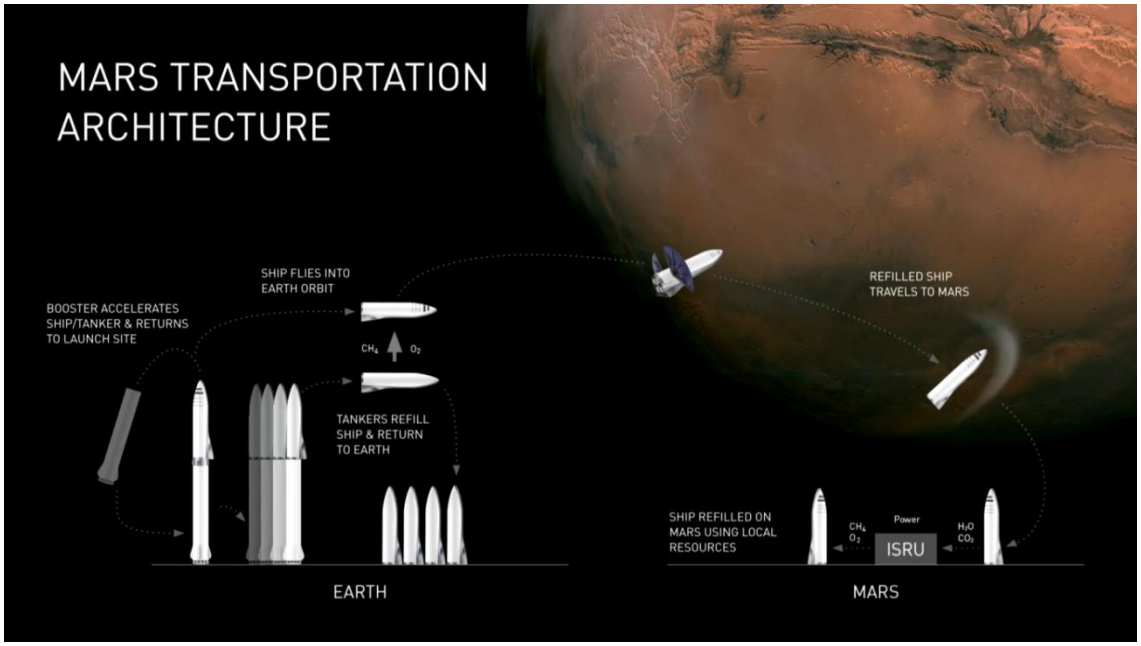

Figure 2-5. BFR: SpaceX's BFR technology (Human Mars, 2017)

2.1.4 Presidential Statements

As delineated in Sections 2.1.1 and 0, NASA, ESA, ISRO and URSS currently have operational missions on Mars and, in 2020, JAXA, UAE and CNSA will also launch missions to Mars.

Even though the effort to land the first human crew to Mars is multinational, the United States of America acts as primary sponsor to pursue this objective (Explore Mars Inc., 2017).

In October 2016, less than one month before the election, President Barack Obama indicated the next steps of the American's space history: send humans on Mars' surface and return the crew safely to Earth by the 2030's, with the future ambition to stay for an extended period of time on this planet (Explore mars Inc., 2017).

During his inaugural address, President Donald Trump stated that the World stand at the birth millennium for human expansion across Solar System, without mentioning Mars. Indeed, in December 2017, he changed the national space policy, signing a new space directive that refocuses the US' space program on human exploration and discovery of the Moon, laying the foundation for a following human Mars exploration (NASA, 2017).

NASA will align presidential directives, looking towards returning humans to the Moon (NASA, 2017); however, the space agency will maintain the established objectives to send humans to Mars in the 2030's (Explore Mars Inc., 2017).
Despite Trump's directive changes human deep space exploration priorities, the lunar mission will provide valuable knowledge for the following Mars missions. Indeed, this concept is consistent with most of the described Mars' exploration architectures that define a cislunar technology testing phase as necessary to test technologies before landing humans on Mars.

2.2 Water on Mars

Achieving the goal of landing humans on Mars, initially for a short and then for an extended period of time, requires demonstrating the ability of producing commodities from local resources. A sustainable crewed mission considers water as a fundamental resource both for life support and propellant production, to reduce and ideally eliminate reliance on Earth. As delineated in Section 2.1, Mars exploration program returned a huge amount of data over the years and proved water resources existence in different chemical and physical states (Saydam et al., 2015). Moreover, several upcoming missions to investigate and define usable reserves have already been planned.
Hence, "follow the water" is the concept that must be followed to project a sustainable Mars habitability.

In 2016, NASA funded a "first-order" analysis of questions related to potential water resource deposits on Mars. This scoping analysis, named Mars Water In-Situ Utilization (ISRU) Planning (M-WIP), was undertaken by Abbud-Madrid et al.; this study provides guidance regarding issues involving the potential use of Mars' water deposits and it is based on the following objectives:

1. Describing hypothetical water "reserves" on Mars;
2. Evaluating technologies for water extraction;
3. Providing a first draft analysis of the production system considering both known and potential geological variations;

4. Preparing a description concerning with preliminary implications for future exploration campaigns (Abbud-Madrid et al., 2016).

Abbud-Madrid et al. (2016) have conducted this analysis by defining four different potential water resource types, which are:

1. Sub-surface glacial ice;
2. Natural concentration of poly-hydrated sulphate minerals;
3. Natural concentration of phyllosilicate minerals;
4. Regolith.

Actually, the extraction of water from other sources, such as the Martian atmosphere, recurring slope lineae, permafrost and high latitude ice, is considered far outside of what is practical on the surface of Mars for both technical and logistical reasons (Abbud-Madrid et al., 2016).

The concept of "reserves" in this context has been modified from the legal meaning used in terrestrial mining practice (see Figure 2-6). Indeed, an Off-Earth reserve is the in-situ raw material proven to be feasible to be extracted and processed but that has not been either extracted or processed yet (Abbud-Madrid et al., 2016).
As defined by Beaty et al. (2016), a reserve represents "the essential interface between exploration and production" (see Figure 2-7) and it is possible to classify a reserve as "proven" if the risk that the raw material is not extractable, or is not processable or is not present as modelled is sufficiently low (Abbud-Madrid et al., 2016).
The threshold confidence value for a proven reserve is 99% and NASA will define an acceptable level of risk of failing to make acceptable discoveries: in Mars ISRU Application, astronauts' lives depend on the possibility of exploit and use local resources (Abbud-Madrid et al., 2016).

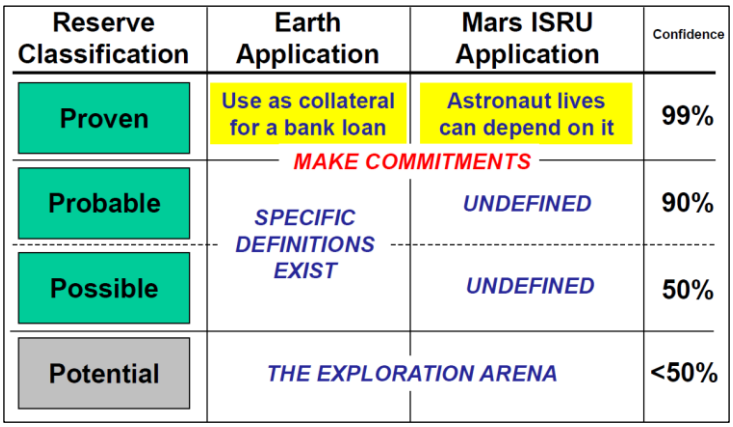

Figure 2-6. Concept of Reserve: comparison between Earth and Mars (Abbud-Madrid et al., 2016)

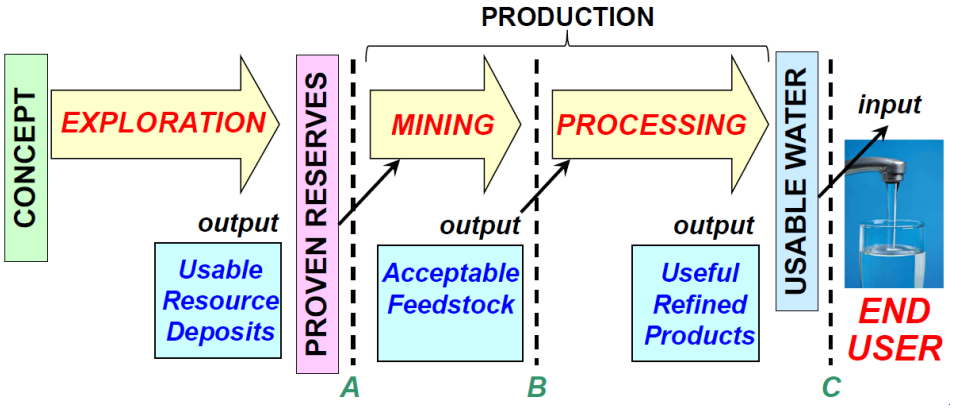

Figure 2-7. The Exploration-Production Flow (Beaty and al., 2016)

2.2.1 In Situ Resource Utilization (ISRU)

Stating that pioneering space is firstly a logistics and supply chain challenge than a technological challenge, it is necessary to develop a new strategy to achieve a sustainable human presence on Mars by breaking the chain that connect the Red Planet to Earth: this self-reliant architecture is called In-Situ Resource Utilization (ISRU).

ISRU technology will enable both to operate in space in a new way and to achieve Earth independence by converting local resources as water, which is present on Mars in different forms and zones, in rocket propellant, radiation shielding and consumables for life support systems (NASA, 2016b). This feedstock production will provide economic benefits for Mars missions, because ISRU system will reduce the launch payload of the Mars Ascent Vehicle (MAV) used to transport humans from Mars' surface back to Earth (NASA, 2016b).

2.2.2 ISRU Resources

Water extraction on Mars constitutes a challenge for several reasons: while various resources have been hypothesised, further data acquisitions and analysis are required to confirm the deposits' extent; furthermore, the delineation of usable reserves requires knowledge of the production system but also the design of the production system requires knowledge of reserves: this relationship, defined by Beauty et al. (2016), is a chicken-egg issue that highlight how exploration and engineering need to advance together; in addition to that, mining water on Mars is a priority for a feasible and sustainable mission to the Red Planet.

As identified in the M-WIP analysis, four water resource types are actually considered extractable and processable:

1. Sub-surface glacial ice;
2. Natural concentration of poly-hydrated sulphate minerals;
3. Natural concentration of phyllosilicate minerals;
4. Regolith (Abbud-Madrid et al., 2016).

The following Sections will provide a further necessary description of these resources and summarises the essential attributes of these four reference cases.

Table 2-4. Essential attributes of the four proposed reference cases for mining water on Mars (Abbud-Madrid et al., 2016)

Essential Attribute	A. Ice	B. Poly-hydrated Sulfates	C. Clay	D. Typical Regolith (Gale)
Depth to top of deposit (stripping ratio)	Variable (1-10 m)	0 m	0 m	0 m
Deposit geometry, size	Bulk	Bulk	Bulk	Bulk
Mechanical character of overburden	Sand	NA	NA	NA
Concentration and state of water-bearing phase within the minable volume				
- Phase 1	90% ice	40% gypsum[1]	40% smectite[2]	23.5% basaltic glass[3]
- Phase 2	--	3.0% allophane[4]	3.0% allophane[4]	3.0% allophane[4]
- Phase 3	--	3.0% akaganeite[5]	3.0% akaganeite[5]	3.0% akaganeite[5]
- Phase 4	--	3.0% smectite[2]	3.0% bassanite[6]	3.0% bassanite[6]
- Phase 5	--	--	--	3.0% smectite[2]
Geotechnical properties				
- large-scale properties ("minability"), e.g. competence, hardness	Competent – hard	Sand – easy	Sand – easy	Sand – easy
- fine-scale properties ("processability"), e.g.competence, mineralogy	No crushing needed	No crushing needed	No crushing needed	No crushing needed
The nature and scale of heterogeneity	variation in impurities	±30% in Concentration	±30% in concentration	±30% in concentration
Distance to power source	1 km	1 km	1 km	100 m
Distance to processing plant	1 km	1 km	1 km	100 m
Amenability of the terrain for transportation	flat terrain	flat terrain	flat terrain	flat terrain
Presence/absence of deleterious impurities	dissolved salts	None	None	Perchlorate (?)
First order power requirements	TBD	TBD	TBD	TBD
Not considered:				
Planetary protection implications	TBD	TBD	TBD	TBD

2.2.2.1 Sub-surface glacial ice

The presence of glacial ice has been detected on Mars at different latitudes: indeed, at latitudes higher than 60°, it is present at depths of tens of centimetres below a sublimation layer, while at latitudes lower than 60°, the ice quantity is inferior, but it is possible to assess its presence from patterned ground and sublimation pitting also at latitudes as low as 30° (Carr and Head, 2009). A significant amount of near-surface ice should also be present at latitudes inferior to 30°, but orbiter spectrometers' resolution is not high enough to detect these resources (Carr and Head, 2009). However, despite for some of these glacial features we have no information about whether residual ice remains and at what depth (Dickson et al., 2012), it has been demonstrated that subsurface ice is present not only at the poles, but also in the mid-latitudes of Mars.
The process of water transportation from the poles to the other regions, which brings to a redistribution of ice around the planet, has been driven by obliquity changes. A detailed explanation of this phenomenon and of the characteristics of Glacier-like Features (GLF), that are named Lineated Valley Fill (LVF), Lobate Debris Aprons (LDA) and Concentric Crater Fill (CCF), is furnished in Section 3.1.4.

Because of the engineering and mission constraints associated with polar exploration, mid-latitudes ice provides a valid alternative to extract water on Mars.
Dickson et al. (2012) conducted a survey related to the GLF located in mid-latitude regions on Mars to understand the global extent of glacial ice accumulation and the distribution of ice-related flow features. These features have been identified with the Context Camera (CTX) on-board the Mars Reconnaissance Orbiter (MRO) (Dickson et al., 2012). As shown in Figure 2-8, evidence of ice existence is given by LVF, LDA and CCF.
The abundance of these glacial bodies is evident, and it has great importance for the Landing Site (LS) selection to plan a sustainable human mission to Mars.

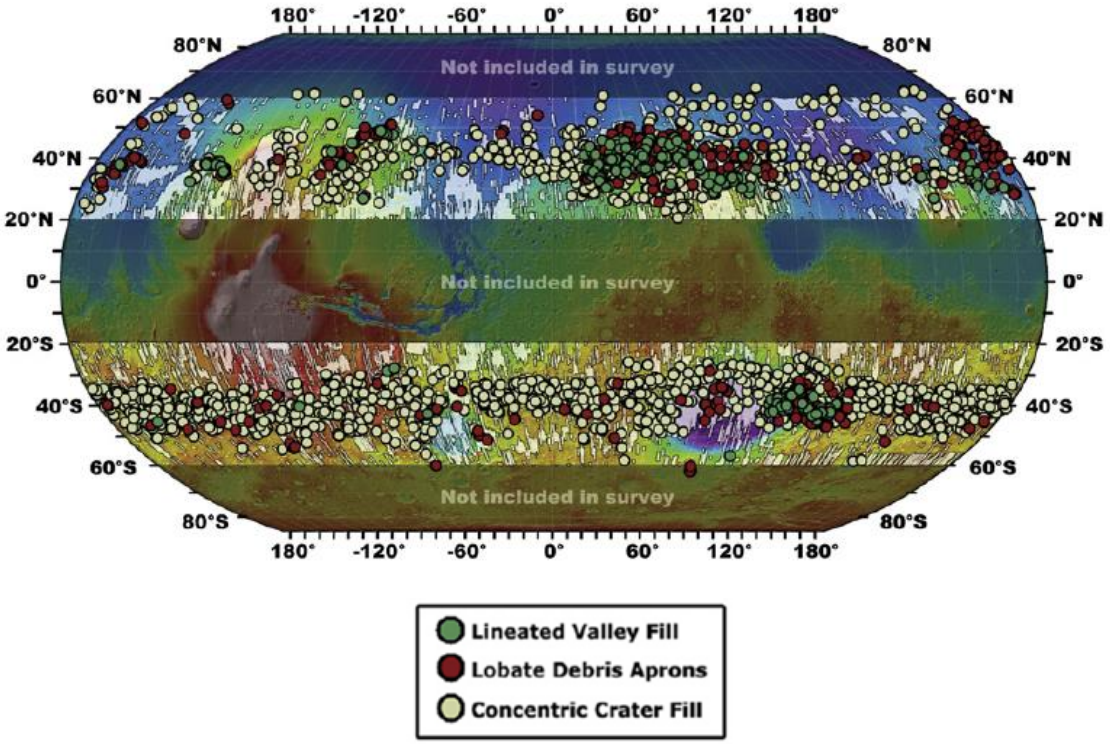

Figure 2-8. Glacier-like Features (GLF) map (Dickson et al., 2012)

Dickson et al. (2012) also note the presence of exposed ice in recent impact craters named "mold-craters" along with evidence given by MOR's Shallow Radar (SHARAD) instrument that also proved the existence of ice in the mid-latitude of Mars.

SHARAD data showed that Glacier-like Features are protected by sublimation till layer that is composed by an unsorted collection of rocks, cobbles, sand and fine sedimentary material with a thickness that is in the order of 1-10 m (Abbud-Madrid et al., 2016; Hoffman et al., 2016). Below this overlying residue, a solid layer of water ice could be 100's to 1000's of meters thick (Hoffman et al., 2016).

M-WIP study proposed to mine ice deposits or by open pit methods or by down-hole heating methods. The first option requires removing the overburden, the second one drilling it before the ice extraction (Hoffman et al., 2016). As reported by Abbud-Madrid et al., the break-even depth of cover is around 2 or 3 meters thick. The removal of ice's overburden involves mechanical and energetic difficulties; however, buried glacial ice deposits may represent the most concentrated source of water on Mars and, if compared with any mineral cases, the ice case would involve less mass and energy for transportation and processing (Hoffman et al., 2016). As consequence, if engineering challenges with

mining buried ice could be resolved, glacial ice is considered a promising resource for the future human missions on Mars.

2.2.2.2 Aqueous Minerals

Over the last 15 years, space exploration provided a huge amount of data with an increasing level of detail that have been used to investigate different aspects related to the Red Planet and to understand what Mars is like and how it arrived at its present state.

This improvement made significant progress also in understanding Mars' mineralogy and composition. ODY orbiter enabled scientists to make both the first global map of chemical elements and minerals distribution using infrared spectroscopy (NASA, n.d.a). Spirit, Opportunity and Curiosity rovers conducted chemical analysis of samples on Mars' surface (Ehlmann and Edwards, 2014) to improve the level of information. Physical erosional processes mixed and redistributed minerals, which subsequently undergo anhydrous oxidation and chemical alteration due to liquid water interaction (Ehlmann and Edwards, 2014).

Representing the most promising granular resource deposits, poly-hydrated sulphate minerals have been found on different locations on Mars and they can contain a significant water concentration (Ehlmann and Edwards, 2014). In Table 2-5 it is possible to compare water concentration by weight of different poly-hydrated sulphate minerals that have been detected on Mars.
Figure 2-9 presents a master compilation of all aqueous mineral detections on Mars that has been realised by Ehlmann and Edwards (2014): it includes phyllosilicates, silicates, chlorides, carbonates and sulphates.

Table 2-5. Poly-hydrated sulphate minerals detected on Mars with water concentration by weight (Ehlmann and Edwards, 2014)

Name	Formula	%H_2O
Epsomite	($MgSO_4 \cdot 7H_2O$)	51
Melanterite	$FeSO4 \cdot 7H_2O$	45
Gypsum	$CaSO_4 \cdot 2H_2O$	21

Kiserite	(MgSO4.H_2O)	13
Bassanite	$CaSO_4 \cdot 0.5H_2O$	6
Szomolnokite	$FeSO_4 \cdot H_2O$	11

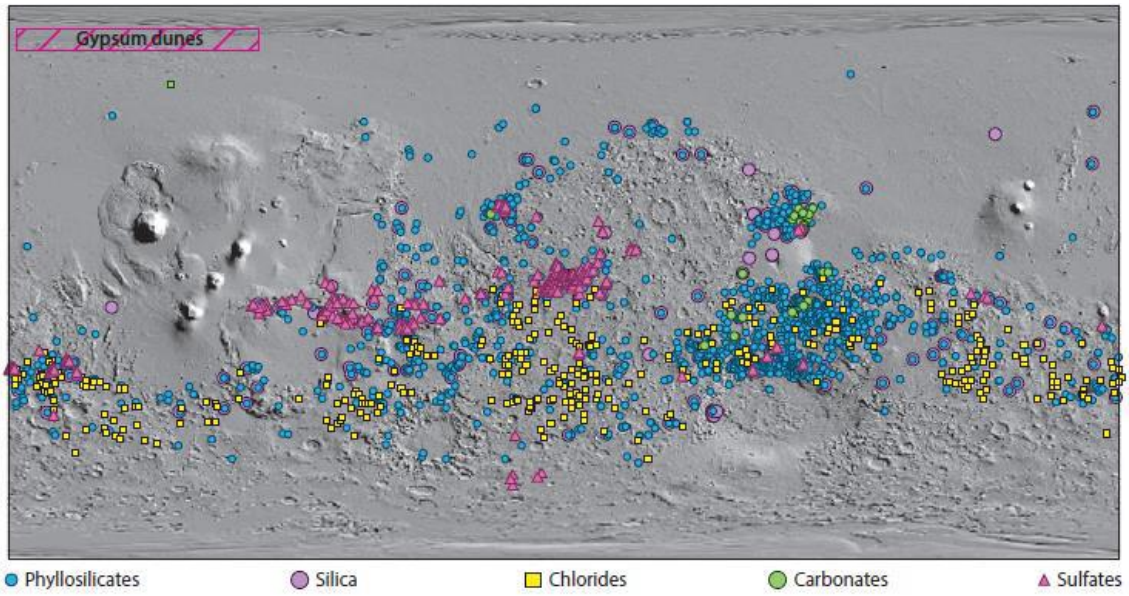

Figure 2-9. Global distribution of aqueous minerals (Ehlmann and Edwards, 2014)

Despite granular cases are sensitive to the nature and scale of the mechanical heterogeneity of the ore deposit, and also to the distance between the mine and the processing plant, aqueous minerals provide an excellent opportunity to extract water on Mars (Abbud-Madrid et al., 2016).

2.2.2.3 Martian regolith

In M-WIP study, Abbud-Madrid et al (2016) defined regolith as "the entire layer or mantle of fragmental and loose, incoherent, or unconsolidated rock material, of whatever origin that nearly everywhere forms the surface and that overlies more coherent bedrock". This implies that Martian regolith encompasses "soil, dunes, talus, rubble, airfall dust and ejecta" (Abbud-Madrid et al, 2016).

Although regolith is widespread present on Mars' surface, differences in its mechanical properties can be noticed and, for this reason, it is not equally amenable to ISRU operations (Abbud-Madrid et al., 2016).

Rover and lander missions to Mars' surface allowed analysing samples of regolith. Curiosity rover, which landed in Gale Crater, identified a contact of three different geologic units and then sampled a mudstone in this location. A detailed scientific analysis of the test results and mineralogy of the sample taken in Yellowknife bay location of Gale Crater has been provided by Vaniman et al. (2014). The Chemistry and Mineralogy (CheMin) instrument onboard Curiosity rover identified detrital basaltic minerals, calcium sulphates, iron oxide and hydroxides, iron sulphides and smectite clays present in the Martian regolith (Vaniman et al., 2014).

The Dynamic Albedo of Neutron (DAN) instrument carried by Curiosity rover supported the existence of bound hydrogen in Martian regolith. The results have been analysed by Litvak et al. (2014): they concluded that, in a 15-meters traverse in Gale Crater, there was a significant variation in the hydrogen levels. Indeed, the upper layer water content was around 1.4-1.7% and the lower level content was 2.4-2.9%, with a vertical average of 2.1-2.7% (Litvak et al., 2014).

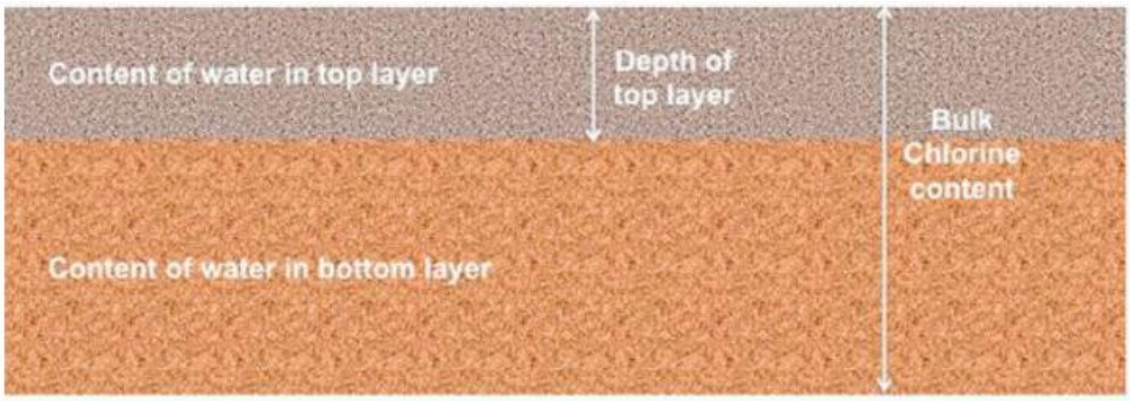

Figure 2-10. Two-layer subsurface model proposed by Litvak et al. (2014) used for DAN data analysis

Mitranofov et al. (2014) conducted a separate study of DAN data and stated that, for the diurnal sublimation effect in the first 10-20 cm layer, a model with a single layer distribution of water is not adequate to analyse water variation. They also concluded that water is present in three different forms in Martian regolith: (1) structurally bound water inside minerals, (2) adsorbed water over the surface of grains, and (3) free water ice in the porous volume (Mitranofov et al., 2014). The third form is not stable at temperature and pressure of Gale Crater. Therefore, the research focus should be on the first two forms of water (Mitranofov et al., 2014).

As for the aqueous minerals, Martian regolith case is sensitive to nature and scale of mechanical heterogeneity of the ore deposit, and to distance between mine and processing plant (Abbud-Madrid et al., 2016). However, M-WIP study assumed that Martian regolith can be found in all the candidate landing sites without exploration. As consequence, transportation demands would be minimized (Abbud-Madrid et al., 2016).

2.2.3 First human mission ground rules

A nominal quantity of 16 metric tons of water per crew has been assumed to meet the requirements established for a fully fuelled MAV and for production of oxygen for life support (Abbud-Madrid et al., 2016). The ISRU production window for Liquid Oxygen-only (LOX) or LOX/Liquid Methane (LCH_4) resources is 480 days: as consequence, it will be necessary to launch the ISRU system to produce propellant and oxygen prior to the crew arrival on Mars' surface (Abbud-Madrid et al., 2016). This timeline organization will allow (1) reducing mission's risk because astronauts' lives depend on these resources and also (2) producing goods for the subsequent crews (Abbud-Madrid et al., 2016). Indeed, multiple missions will take place in the same Exploration Zone (EZ) on Mars.

Successively to a provisional landing site selection based on analysis of available datasets, at least one robotic lander mission on the surface of Mars is considered fundamental to prove the existence of identified water reserves and to reduce the geological risk. The effective presence of these strategic resources will allow a feasible and sustainable human presence on Mars (see Figure 2-11).

Despite some disadvantages described before, the natural scale of Glacial-like Features (GLF) present on Mars is far larger than the minimum required to produce 16 metric tons needed per crew (Abbud-Madrid et al., 2016). Moreover, the chance to discover a glacial ice deposit that would yield less than 16 metric tons is considered non-existent (Abbud-Madrid et al., 2016). For these reasons, glacial ice Regions of Interest (ROIs) represent fundamental features that must characterise the EZ on the Red Planet to achieve the goal of a sustainable human mission.

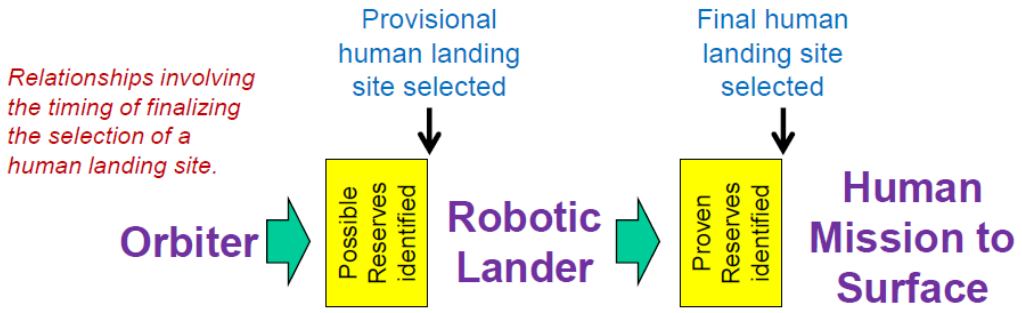

Figure 2-11. Proven reserve identification as prerequisite for the site selection for the human mission to Mars (Abbud-Madrid et al., 2016)

2.3 Exploration Zone (EZ) and Landing Site (LS) selection

As discussed in Section 2.1.3.1, NASA is developing a long-term, flexible and sustainable architecture for space exploration called Evolvable Mars Campaign (EMC) to accomplish the goal of landing the first humans to Mars (Bussey and Hoffman, 2016). This research is delineating all the aspects of the mission such as the launch from Earth, the transit to and from Mars, and all the operations on the surface of Mars (Bussey and Hoffman, 2016).

The starting point of the project development consists of defining a process for the evaluation of candidate locations where the human crew could land, live and work on the Martian surface (LPI, 2015). For this reason, a specific nomenclature that describes all the required elements for the Martian site has been defined.

The location where human activities will take place is named Exploration Zone (EZ); the EZ is a collection of Regions of Interest (ROIs) that are located within approximately 100 kilometres from a centralized Landing Site (LS) (LPI, 2015). ROIs are relevant areas for scientific investigation and/or development or maturation of capabilities and resources that are fundamental for a sustainable human presence on Mars (LPI, 2015). Hence, it is possible to classify the ROIs between Scientific Regions of Interest (SROIs) and Resources Regions of Interest (RROIs).

The goal is to find an EZ that can maximise both the scientific return and the human operation sustainability (LPI, 2015).

The EZ also contains a Habitation Site (HS) that will be used by multiple human crews during time, as noted in the Landing Site/Exploration Zone Workshop for Human Missions to the Surface of Mars announcement. Indeed, multiple human missions are going to be planned in the same EZ: across multiple missions, all the necessary infrastructure will be emplaced and Mars' surface "field station" will evolve, such that multiple crews across multiple missions will develop the life system at this HS and will regularly depart from this location on traverses to explore the ROIs (LPI, 2015).

Figure 2-12 shows a possible EZ layout configuration for a human mission to Mars: both RROIs and SROIs are present around the HS that is close to the LS.

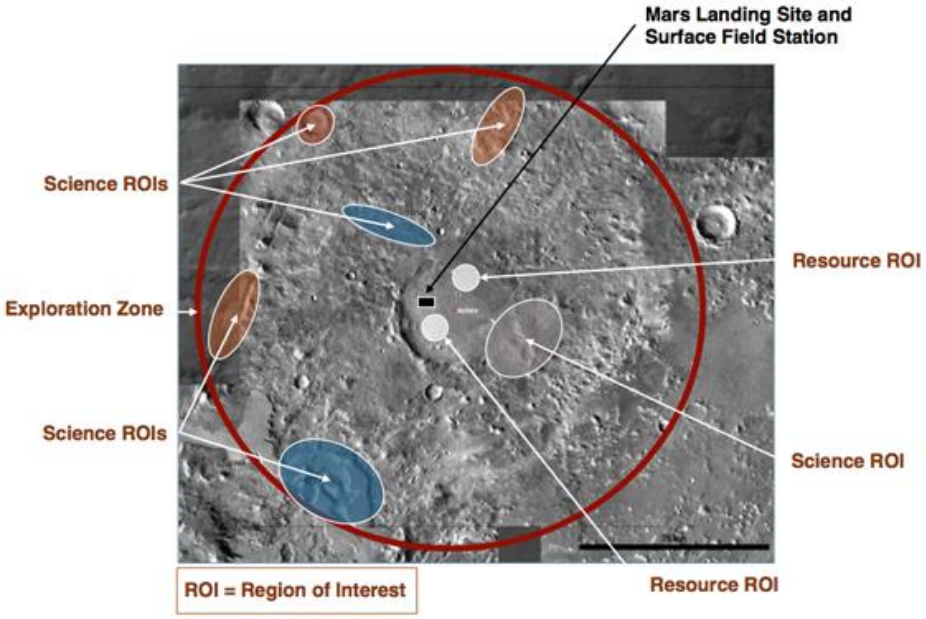

Figure 2-12. Exploration Zone Layout Consideration (NASA, 2015)

Site selection criteria for un-crewed missions have been extensively developed (Clarke et al., 2017). Some recent examples of this process include the MSL/Curiosity, Mars Exploration Rover (MER) and Phoenix missions.

To what may concern site selection's methodology of the EZ for the crewed mission to Mars, a criterion emerged at the first HLS^2 workshop that has been held at the Lunar and Planetary Science Institute of Huston on October 2015.
As shown in Figure 2-13 and summed up in

APPENDIX B, forty-seven possible EZs for the first crewed mission to Mars have been proposed during this workshop. This selection has been carried out by the cooperative effort of the NASA's Human Exploration and Operations Mission Directorate (HEOMD) and the Science Mission Directorate (SMD). HEOMD is responsible for the future human mission preparation and SMD is responsible for the on-going Mars Exploration Program of robotic vehicles in orbit and on the surface of Mars (Bussey and Hoffman, 2016).

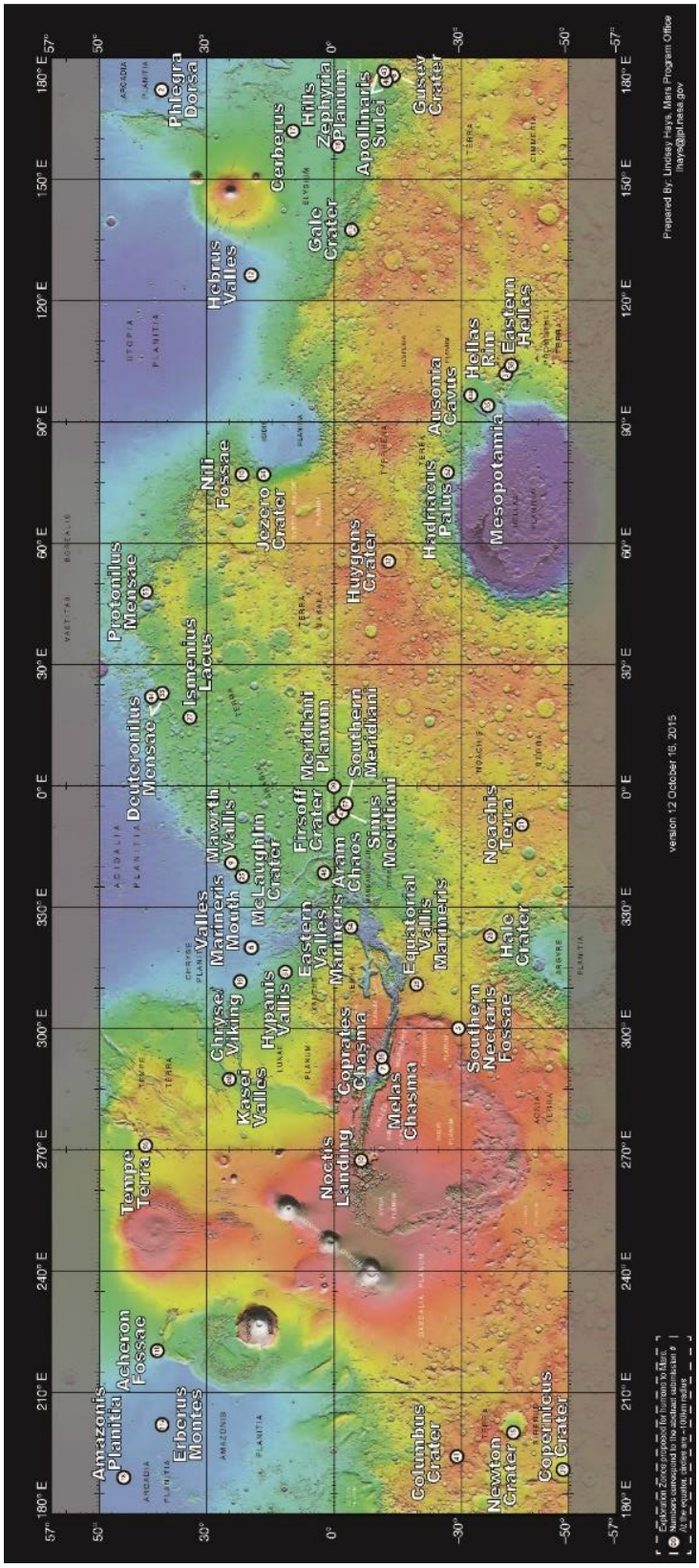

Figure 2-13. Potential EZ for the Human Mission to the Surface of Mars (Bussey and Hoffman, 2016)

With the aim to select these EZs, some guidelines have been written: the proposed EZs should contain a set of ROIs that collectively meet the threshold/required criteria as well as several qualifying/enhancing criteria that are given by both Scientific and Resource Objectives (LPI, 2015). These EZs must satisfy some Engineering Constraints that are fundamental for the mission success (LPI, 2015).

Figure 2-14 summarises the flow of criteria that have been considered to determine possible EZs in which the crews will land and live.

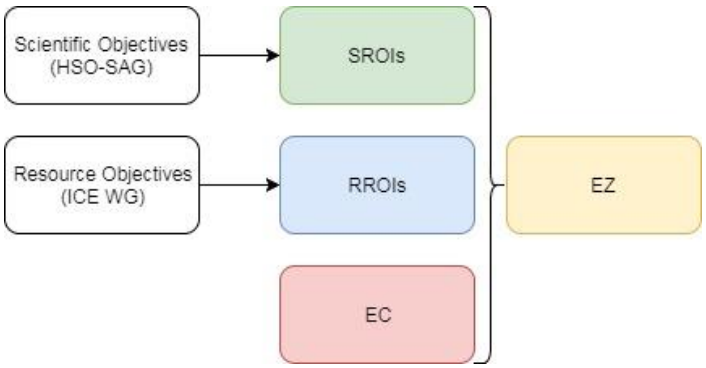

Figure 2-14. Summary of the EZ's evaluation criteria

The EMC develops during time in a dynamic way: it determines that the objectives and constraints and their priority for the human Mars mission should significantly change over the years. This is consistent with the concept of developing a flexible architecture that is resilient to changes, for multiple reasons such as the number of variables involved into the project itself and the collected datasets that grow in quantity and quality over the time: it allows to find additional information to improve the planned system in order to achieve the goal of a human "Journey to Mars".

2.3.1 Scientific Objectives: SROIs Criteria

In 2015, the Human Science Objectives Science Analysis Group (HSO-SAG) outlined the Scientific Objectives that might be considered for a human mission and used to construct a set of ROIs criteria which can be useful to identify an EZ with high potential for scientific discoveries.

The team states that the science objectives and priorities for Mars should change significantly prior to 2030 (LPI, 2015).

The scientific objectives for the crewed mission to Mars have been classed in four groups:

A. Astrobiology;

B. Atmospheres;

C. Geology;

D. Cross Cutting (LPI, 2015).

These scientific objectives were used to construct a set of SROIs criteria. Two types of criteria have been determined: "Threshold" and "Qualifying". The threshold criteria represent the highest priority and "must have" for any potential ROI and, consequently, the qualifying ones are other high priority criteria that add breadth to the scientific potential and address fundamental scientific questions (LPI, 2015).

The SROIs criteria that have been evaluated by HSO-SAG are summed up in the following table.

Table 2-6. Science Objectives for a crewed mission to Mars (LPI, 2015)

		Site Factors
Astrobiology	Threshold	Potential for past habitability and/or Potential for present habitability/refugia
	Qualifying	Potential for organic matter, w/ surface exposure
Atmospheric Science	Threshold	Noachian/Hesperian rocks w/ trapped atmospheric gasses
	Qualifying	Meteorological diversity in space and time High likelihood of surface-atmosphere exchange Amazonian subsurface or high-latitude ice or sediment High likelihood of active trace gas sources
Geoscience	Threshold	Range of Martian geologic time; datable surfaces Evidence of aqueous processes Potential for interpreting relative ages
	Qualifying	Igneous rocks tied to 1+ provinces or different times Near surface ice, glacial or permafrost Noachian or Pre-Noachian bedrock units Outcrops with remnant magnetization Primary, secondary, and basin-forming impact deposits Structural features with regional or global context Diversity of aeolian sediments and/or landforms

2.3.2 Resource Objectives: RROIs Criteria

The ISRU and Civil Engineering Working Group (ICE WG) was tasked with delineating a set of Resource Objectives that satisfies NASA's goal of a permanent and sustainable human presence on Mars' surface with the purpose of minimizing and ideally eliminating reliance on Earth (LPI, 2015). Hence, the necessity of providing air, water, food, shelter for basic human needs and power, propellant and building materials for critical operational needs, represents a basis to achieve mission's goals.
All these concepts have been grouped in two broad categories: In Situ Resource Utilization (ISRU) and Civil Engineering (CE). However, despite other fundamental concepts as food production do not ideally fit in these given categories, they have been included in the research (LPI, 2015).

Three main Resource Objectives have been identified for ISRU and CE within an EZ on Mars and these will be used for guidance during the EZ selection (LPI, 2015):

A. Demonstrate the ability to prospect for and extract useful commodities from local materials and resources as soon as possible (LPI, 2015).

The highest priority related to this objective is water: indeed, as discussed in the previous chapter, it constitutes a strategic resource for propellant production and life support (LPI, 2015).
Metals, silicon and structural building material have secondary priority: they will be important for in-situ fabrication of spare parts and repairs (LPI, 2015).

B. Demonstrate the ability to manipulate the surface for infrastructure emplacement and protection of hardware (LPI, 2015).

The highest priority related to this objective is related to foundation improvement and surface stabilization (LPI, 2015).
Of secondary importance are capabilities to build structures and enhance radiation shielding for the crew (LPI, 2015).

C. Demonstrate capabilities to reduce reliance on supplies from Earth using indigenous materials, resources, and the environment (LPI, 2015).

The highest priority of this objective is food production because it is one of the largest consumable items that must be imported from Earth in the current mission scenarios. So, the ability to produce food on Mars will improve the mission sustainability (LPI, 2015). Of secondary priority are in-situ manufacturing and construction with locally derived feedstock: the aim is to minimize long term costs, logistics, and crew risk (LPI, 2015).

These objectives have been used to establish a set of RROIs criteria to guide the selection of proposed EZs for the human Mars mission (LPI, 2015).

The desire to build a quantitative selection process sometimes must face with the actual lack of datasets that do not currently exist. As a result, the term "potential" has been introduced into some criteria to indicate indirect evidence that a candidate site meets one or more of these criteria (LPI, 2015). Sites that satisfy these "potential" criteria may become (1) targets for gathering additional data using instruments on existing and future spacecraft as well as (2) focus of specific analysis by qualified teams using existing and future datasets (LPI, 2015).

The RROIs criteria that have been determined by ICE WG are summed up in the following Table.

Table 2-7. Resources Objectives for a crewed mission to Mars (LPI, 2015)

Site Factors

Water Resources	Threshold	Potential for ice or ice/regolith mix and/or Potential for hydrated minerals Quantity for substantial production Potential to be minable by highly automated systems Located less than 3 km from processing equipment site Located no more than 3 m below the surface Accessible by automated systems
	Qualifying	Potential for multiple sources of ice, ice/regolith mix and hydrated minerals Distance to resource location can be > 5 km Route to resource location must be (plausibly) traversable
Civil Engineering	Threshold	~ 50 km^2 region of flat and stable terrain with sparse rock distribution 1-10 km length scale: < 10° Located within 5 km of landing site location
	Qualifying	Located in the northern hemisphere Evidence of abundant cobble sized or smaller rocks and bulk, loose regolith Utilitarian terrain features
Food Production	Qualifying	Low latitude No local terrain feature(s) that could shadow light collection facilities Access to water Access to dark, minimally altered basaltic sands
Metal/Silicon Resource	Threshold	Potential for metal/silicon Potential to be minable by highly automated systems Located less than 3 km from processing equipment site Located no more than 3 m below the surface Accessible by automated systems
	Qualifying	Potential for multiple sources of metals/silicon Distance to resource location can be > 5 km Route to resource location must be (plausibly) traversable

2.3.3 Engineering Constraints

One of the most important aspects that determine the feasibility of the human Mars mission is to evaluate the engineering factors that will help to define the allowable locations within a proposed EZ.
These constraints and considerations have already been determined. However, they will be refined and improved over several years (LPI, 2015).
The evaluation of EC is driven by a set of operational considerations, such as:

- The need to organise multiple safe campaigns in the same EZ;
- The need to protect the emplaced infrastructures by debris projections associated with landing;
- The need to provide the HS with all the facilities required to support both human life and activities such as habitation areas, local work areas, ISRU infrastructures, supporting utilities for power production and mobility zones (LPI, 2015).

All these operations imply EC that are summed up in Table 2-8.
These ECs have been associated in classes, which are:

- CC: Contour Conditions;
- LS: Landing Site requirements;
- HS: Habitation Site requirements;
- CPR: Crew Pressurized Rover requirements;
- G: Geometry.

Some of the EC listed in the following Table have been acquired from the Mars Science Laboratory (MSL) process of selection of Curiosity rover LS.

Table 2-8. Current EZ requirements for the human Mars mission (modified from LPI, 2015)

#	Class	EC	Target value	MSL
1	CC	Latitude	50°N to 50°S	
2	CC	Elevation	Altitude ≤+2 km (MOLA)	
3	LS	Terrain relief	100-130 m over 1000 m baseline	x
4	LS/HS	Slope	< 15° over 20 m length scale	x
5	LS	Rock height	0.5% probability of at least one ≤ 0.55 m high rock in 4 m^2 area (rock abundance <8%)	x
6	LS/HS	Surface wind	<15 m/s (steady); <30 m/s (gusts); steady winds never exceed 40 m/s	x
7	LS	Load Bearing surface	High thermal inertia, low albedo, not dominated by dust	
8	CPR	Slope	< 30º, paths ~5x wider than rover width	
9	CPR	Rock height	< 20% coverage by obstacles > radius of rover wheel (0,55 m)	
10	G	LZ radius	100 m	
11	G	LS blast zone	~1 km	
12	G	LS area	25 km^2	
13	G	EZ radius	~100 km	
14	G	Exclusion zones	1 - 5 km radius from excluded element (e.g., nuclear power system)	

All the LS's EC will be analysed in Section 6.1.3 because they represent the basic parameters used to build the automatic model developed in this project.

2.4 Conclusion statement

Concluding this review on the evolutionary stream in Mars exploration, on water resources presence on the Red Planet and on the required parameters for EZ and LS selection, a solid foundation of knowledge has been developed for this project.

EC analysis will assist in developing the model to satisfy the objectives of this thesis, and the strategic importance of mining water on Mars underlines the need of finding a synergy between engineering and geology.

Although finding evidence for past life represents one of the fundamental objectives of the human mission to Mars, crew's safety is placed in emphasis in all the phases of the "Journey to Mars": indeed, injury or loss of life could cripple the mission.

This technical priority clearly highlights the importance of a careful evaluation of EC for the EZ/LS selection.

However, the trend that has to be followed is trying to find an EZ that should maximise both the astrobiological return and the human operation sustainability (LPI, 2015).

3 GEOLOGIC HISTORY AND PRESENT DAY ENVIRONMENTAL CONDITIONS OF MARS

The aims of the Chapter are both defining the environmental conditions of the planet and creating an overview on the main geological periods occurred on Mars, with a specific focus on Glacier-like Features (GLF) generated during the Amazonian period. Indeed, the most distinctive characteristic of this geologic era is the formation of features related with ice presence, accumulation and movement (Carr and Head, 2009). GLF have great importance for In Situ Resources Utilization (ISRU) plan because they represent significative resources of water on the planet and because they are strongly related with the concept of water as "analysis guiding principle" for the sustainable human mission to Mars.

The past decades of exploration provided a huge amount of data with an increasing level of detail that have been used to investigate different aspects related to the Red Planet and to understand what Mars is like and how it arrived at its present state. This improvement has been driven by an effort to acquire compositional data to understand the history of the planet since the Mariner and Viking missions, by the capabilities of orbital instruments with increasing spectral and spatial resolution over the time, by in-situ exploration and measurements done by rovers and landers (Ehlmann and Edwards, 2014).

3.1 Geologic history of Mars

The geologic history of Mars has been subdivided in three different age groups that followed the origin and early times of the planet: Noachian, Hesperian and Amazonian periods. Each of these periods has been characterised by the formation of different geologic features that establish the division into age groups (Carr and Head, 2009).
The nomenclature of the three periods is based on type localities and not on the properties of the rock (Carr and Head, 2009): the Noachian named from the Noachis region that is

a heavily cratered area, the Hesperian named from the Hesperia Planum that is a broad lava plain and the Amazonian named from the younger Amazonia Planum.
The Noachian period extended from Hellas formation that is estimated from 4.1 to 3.8 Gya ago (Carr and Head, 2009) to 3.7 Gya ago. The Hesperian period is likely ended around 2.9 and 3.3 Gya ago, when the Amazonian period began (Carr and Head, 2009; Hartmann and Neukum, 2001). However, these boundaries between periods should incorporate significant errors (Carr and Head, 2009).

The following Table provides a summary of the main geologic events and features that characterised the different age groups with variable intensity a frequency. Despite the technologic development provided datasets with an increasing level of detail, some uncertainties have not been solved yet and the puzzling role of these unknowns makes the challenge of studying Mars extremely interesting.

Table 3-1. Summary of the main characteristics of each martian geological period

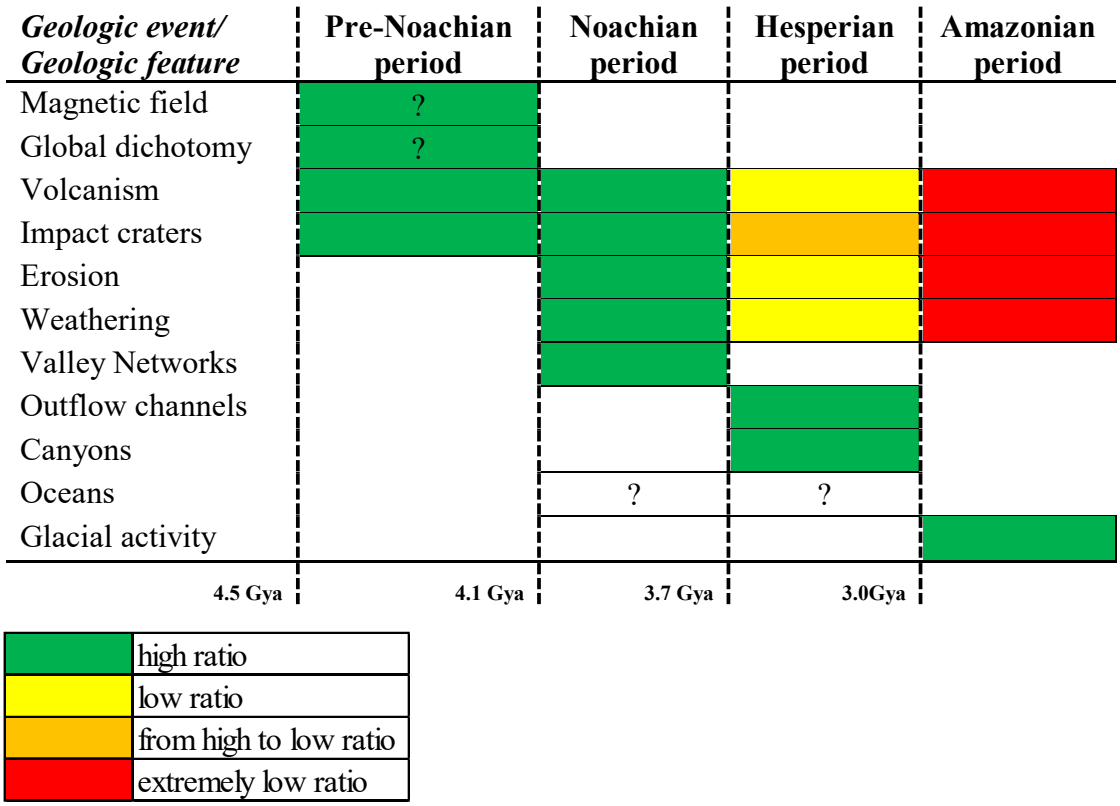

3.1.1 Origin and early times

The Solar System formation and evolution began 4.6 Gya ago with the gravitational collapse of a small part of a giant molecular cloud (Bouvier and Wadhwa, 2010). The Nebular Hypothesis Model, developed by Swedenborg, Kant and Laplace in the 18th century and then improved and refined after the dawn of the space age in the 1950's, suggests that most of the collapsing mass had been collected in the centre forming the Sun, while the rest had formed a protoplanetary disk or solar nebula that originated planets, moons, asteroids, and other small Solar System bodies (Boss and Durisen, 2005). At present time, the accepted method by which the planets formed is accretion: at the first phase of their formation process, planets began as dust grains that were in orbit around the central protostar. These grains have been aggregated by direct contact into clumps up to 200 m in diameter. Consequently, these clumps collided to form planetesimals that are larger bodies with an average diameter of 10 km (Goldreich and Ward, 1973). Over the course of the next few million years, planetesimals gradually increased through further collisions (Goldreich and Ward, 1973). The high temperature of the inner Solar System did not allow the condensation of volatile molecules like water and methane, so the planetesimals were made from compounds with high melting points, such as metals like iron, nickel and aluminium and rocky silicates. Mercury, Venus, Earth and Mars, also known as inner planets, have been generated from these rocky bodies (Zabludoff, 2003). Mars accumulated and differentiated into crust, mantle and core within a few tens of millions of years of Solar System formation: by 4 Gya ago, over 70% of the crust would have accumulated (Carr and Head, 2009).

The mineralogy of Mars has been analysed with the aid of spectrometers carried by spacecraft, rovers and landers, in-situ tests on the surface and remote sensing from orbit. As shown in Table 3-2, the most abundant chemical elements are silicon, oxygen, iron magnesium, aluminium, calcium and potassium (Ehlmann and Edwards, 2014); these elements are the main components of igneous rocks and are of primary importance on crust composition. Other elements, as titanium, chromium, manganese and sulphur are less abundant, but they have a great importance in composition of many accessory minerals as weathering products, dust and soils (Ehlmann and Edwards, 2014). Hydrogen is present both as water ice and hydrated minerals (Ehlmann and Edwards, 2014). Carbon

is present as carbon dioxide in the atmosphere and as dry ice at the poles (Ehlmann and Edwards, 2014).

Table 3-2. Minerals detected on Mars from landed and orbital datasets analysis (Ehlmann and Edwards, 2014)

	Class	Group/Mineral/Phase	Formula
Primary	Framework silicates	Olivines	$(Mg, Fe)_2SiO_4$
		Orthopyroxenes	$((Mg, Fe)_{0.95+x}, Ca_{0.05-x})Si_2O_6$
		Clinopyroxenes	$(Ca, Mg, Fe)Si_2O_6$
		Plagioclase feldspars	$(Ca, Na)(Al, Si)AlSi_2O_8$
		Alkali feldspars	$(K, Na)AlSi_3O_8$
	Sulfides	Pyrrhotite	$Fe_{1-x}S$
		Pyrite/marcasite	FeS_2
	Oxides	Magnetite	$Fe_{3-x}Ti_xO_4$
		Ilmenite	$FeTiO_3$
Secondary	Oxides	Hematite	Fe_2O_3
		Goethite	$FeO(OH)$
		Akaganeite	$Fe(O, OH, Cl)$
	Phyllosilicates (clay minerals)	Fe/Mg smectites (e.g., nontronite, saponite)	$(Ca,Na)_{0.3-0.5}(Fe,Mg,Al)_{2-3}(Al, Si)_4O_{10}(OH)_2 \cdot nH_2O$
		Al smectites (e.g., montmorillonite, beidellite)	$(Na, Ca)_{0.3-0.5}(Al, Mg)_2(Al, Si)_4O_{10}(OH)_2 \cdot nH_2O$
		Kaolin group minerals (e.g., kaolinite, halloysite)	$Al_2Si_2O_5(OH)_4$
		Chlorite	
		Serpentinee	$(Mg, Fe^{2+})_5Al(Si_3Al)O_{10}(OH)_8$
		High-charge Al/K phyllosilicates (e.g., muscovite, illite)	$(Mg, Fe)_3Si_2O_5(OH)_4$ $(K, H_3O)(Al, Mg, Fe)_2Al_xSi_{4-x}O_{10}(OH)_2$
	Other hydrated silicates	Prehnite	$Ca_2Al(AlSi_3O_{10})(OH)_2$
		Analcime	$NaAlSi_2O_6 \cdot H_2O$
		Opaline silica (n > 0), quartz (n = 0)	$SiO_2 \cdot nH_2O$
	Carbonates	Mg/Ca/Fe carbonates	$(Mg, Fe, Ca)CO_3$
	Sulfates	Kieserite (MgSO4·H2O); szomolnokite (FeSO4·H2O); Fe(II)-, Fe(III)-, and Mg-	$(Fe, Mg)SO_4 \cdot nH_2O$

	polyhydrated sulfates	
	Gypsum (n = 2), bassanite (n = 0.5), anhydrite (n = 0)	$CaSO_4 \cdot nH_2O$
	Alunite	$KAl_3(SO_4)_2(OH)_6$
	Jarosite	$KFe_3(OH)_6(SO4)_2$
	Not a named mineral	$Fe_3^+SO_4(OH)$
Chlorides	Chlorides	e.g., NaCl, $MgCl_2$
Perchlorates	Perchlorates	e.g., $(Mg, Ca)(ClO_4)_2$

Little is known about the pre-Noachian period that extended from the planet formation around 4.5 Gya ago to Hellas formation that is estimated from 4.1 to 3.8 Gya ago (Carr and Head, 2009). This loss of information is related to the fact that most of geologic records have been almost completely erased over the time.
However, it can be stated that the main characteristics that typified the pre-Noachian period are:

- Magnetic field presence;
- Global dichotomy boundary formation;
- Volcanism;
- Cratering events.

The MGS mission gained the surprising result of discovering large magnetic anomalies mostly in the southern highlands (Acuña et al., 1999; Connerney et al., 1999). However, the action of impacts destroyed these anomalies that are mostly absent around the large impact basins such as Hellas, Utopia, Argyre and Isidis (Solomon et al., 2005) and the effect of tectonic activities striped some anomalies in the southern uplands (Connerney et al., 1999). As consequence, this lack of information does not allow studying and interpreting the ancient Mars magnetic field in a proper way.

One of the main open questions related to Mars is the origin of its crustal dichotomy, a global boundary that divides the planet into the northern lowland third and the southern upland two-thirds (McGill and Squyres, 1991): indeed, both time and mode of formation are big uncertainties.

As discussed by Carr and Head (2009), the crustal dichotomy can be described in three different ways that do not everywhere coincide:

- As difference in elevation, which results in a bimodal distribution with 5.5 km of difference between the two hemispheres;
- As difference in crustal thickness, that varies on average from 60 km south of the dichotomy boundary to 30 km north of the dichotomy boundary;
- As differences in crater densities across the boundary, despite the lower density of impacts north of the boundary may be a superficial difference; indeed, a densely cratered surface may have been covered by younger deposits from the Hesperian and Amazonian periods.

The dichotomy boundary formation possibly represents the oldest geologic event that is recorded in the surface configuration (McGill and Squyres, 1991; Nimmo and Tanaka, 2005). Despite this evidence, the time of formation constitutes a big uncertainty: the crustal dichotomy could have formed between the crust formation time 4.5 Gya ago and the generation of the oldest superimposed impact basins such as Utopia and Chryse around 4.1 Gya ago according to Frey (2003) chronology and 3.8 Gya ago according to the cataclysm model (Carr and Head, 2009).

The second uncertainty related to the crustal dichotomy is its mode of formation.
Literature from McGill and Sqyres (1991) provides a detailed insight into the origin process of the crustal dichotomy. Three different hypotheses have been proposed and each of those is consistent with some of the geological and geophysical evidences available but is not completely coherent with some other aspects. The three contending hypotheses for the origin of the dichotomy are:

- Origin by endogenic processes;
- Origin by a single mega-impact;
- Origin by multiple overlapping impacts.

As argued by McGill and Sqyres (1991), each hypothesis should survive three tests:

- It must account for the observed plan shape and the apparent depth of the Martian northern lowland;
- It must be physically consistent;
- It must be coherent with geological and geophysical data.

None of the three hypotheses can survive the three tests without considering some additional processes.

Figure 3-1 represents Mars' topography based on data acquired by the Mars Orbiter Laser Altimeter (MOLA; Smith and others, 2001), an instrument installed on NASA's Mars Global Surveyor (MGS) spacecraft. This Digital Elevation Model (DEM) furnishes a clear view of how the global dichotomy boundary sharply divides the planet.

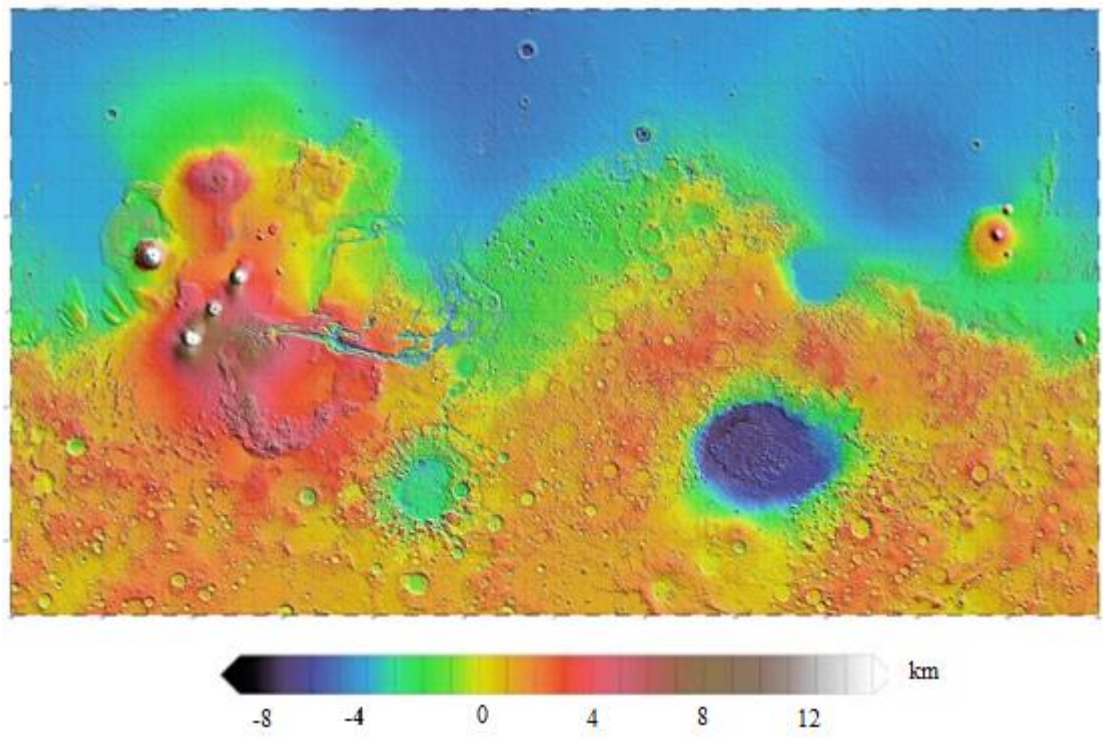

Figure 3-1. Mars Orbiter Laser Altimeter (MOLA) Digital Elevation Model (DEM)

Although geomorphic evidence of the early times volcanism has been mostly destroyed by following events, the rate of the phenomenon was likely coupled to the heat flow, so it may have started high and then declined rapidly during the first few hundred million years. Tharsis, a volcanic plateau, may have started to build during this period, also if there are no records of the start of its accumulation that ended at the end of the Noachian period 3.7 Gya ago (Carr and Head, 2009).

Any volcanic phenomenon would have been accompanied by outgassing of volatiles such as water and sulphur (Carr and Head, 2009). However, the amount of water and other volatiles that should have been generated in this period is very uncertain due to different factors. These factors, which have been summarised by Carr and Head (2009), are the mix of materials that formed the planet, the efficacy of outgassing of water and retention in the accretion phase, timing and amount of any late volatile rich additions to the planet after global fractionation and losses due to hydrodynamic escape, effectiveness of the impact erosion and upper atmosphere processes in removing water and, finally, the amount of volcanic outgassing subsequent to the accretionary period. The great number of variables makes difficult to place strong constraints on a model that should describe the amount of water that has been generated during the early history of Mars.

If surface conditions during the early times are actually very uncertain, one certainty is that Mars' surface has been episodically disrupted by impact events that formed large basins (Carr and Head, 2009). These craters ejected large amounts of rock vapour and rock melt, evaporated any oceans that might have been present, raised up the temperature of the planet surface by several hundred K (Carr and Head, 2009). Hence, surface temperature remained above freezing for years after each large impact event. As consequence, the amount of water that has been injected into the atmosphere during both the impact phenomena and the warming of the surface and subsurface could rain out over years. The magnitude of each precipitation phenomenon has been time dependant on the impact size (Carr and Head, 2009).

3.1.2 Noachian period

The Noachian period extended from Hellas formation, which is estimated from 4.1 to 3.8 Gya ago (Carr and Head, 2009), to 3.7 Gya ago.
The main phenomena that characterised the Noachian are:

- An extremely high rate of cratering;
- A high rate of erosion;
- A high rate of weathering;
- A high rate of volcanism;
- Valley networks formation;
- Possible ocean presence.

The Noachian period started with the formation of Hellas, the largest impact structure on Mars with a diameter of about 2300 km (Schultz and Frey, 1990).
As discussed by Carr and Head (2009), after this event many impacts larger than 100 km in diameter modified the surface of Mars: indeed, the planet-wide number of impacts with a diameter with this order of magnitude is approximately 300, with a density in the Noachian terrain that is about 2×10^{-6} km^{-2}. A crater model that has been developed by Ivanov (2001) suggests that 4 Gya ago the frequency of formation of a crater with a diameter of 100 km was one per every million years. This result is consistent with the chronological model that establishes Hellas formation 4.1 Gya ago and with the global number of craters with this size.
These impact events have distributed ejecta around the planet activating, as consequence, a great hydrothermal activity close to the impact sites. As discussed in Section 3.1.1, the main effects of these phenomena are temperature rising up and water injection in the atmosphere. These conditions are at the base of precipitation phenomena that, during the Noachian, have been at least episodic (Carr and Head, 2009) as suggested by the widespread dissection of the Noachian terrains.

To create a focus on the magnitude of Hellas crater, if the developed models of the Noachian crater size distribution suggest that craters with a diameter between 500 and 1000 km would have deposited around 300 m of ejecta all around the planet, Hellas would have deposited 500 m alone (Carr and Head, 2009).
As discussed by Carr and Head (2009), the rate of resurfacing by impacts was high if compared with resurfacing by volcanism, despite during this period the volcanic activity has been high: for this reason, at the 100-m scale, the Noachian terrain is dominated by craters.

Most of the volcanic activity has been likely concentrated in Tharsis, where a volcanic pile approximately 9 km high and 5000 km across have been accumulated (Phillips et al., 2009). This event deformed the lithosphere of Mars on a global scale and, comparing the amount of water contained in Tharsis' magmas to the Hawaiian basalts range, a global equivalent of a layer of water 120 m deep would have been outgassed (Phillips et al., 2009).
The rate of volcanism started high and declined rapidly during the first few hundred million years during the Noachian (Carr and Head, 2009).
As anticipated, the Noachian terrain is scarce of geomorphic evidence for volcanism. Despite this scarcity, most of the materials exposed in the southern cratered uplands are likely volcanic rocks sometimes reworked by impacts: these materials are mainly basalts rich in low calcium pyroxene with olivine (Carr and Head, 2009).
Where olivine is present, the upper layer of the Noachian terrain has not been extremely altered by weathering. However, the lower levels of Noachian terrain section are characterised by the widespread presence of hydrated silicates, which indicates aqueous alteration prior to deposition of the olivine rich units (Carr and Head, 2009).

The aqueous alteration of basalts, a phenomenon that distinguished the Noachian period, produced a range of phyllosilicates such as nontronite, saponite, montmorillonite and Fe-rich chlorites (Murchie et al., 2008): so, weathering action excavated the surface and exposed these older materials.

Close to the end of this geological period, the hydrous weathering has been stopped by climate changes: indeed, surface temperature became lower and the atmosphere was drier than during the previous times.
However, as detailed in Carr and Head (2009) literature review, the geomorphic evidence for valley networks and the presence of phyllosilicates in Noachian terrains, the groundwater movement and surface water at Meridiani and chlorine rich deposits in local lows, all suggest at least episodic warm conditions during the Noachian. Despite these conditions, greenhouse models during these early times indicate that the global temperature did not raised up sufficiently to allow widespread precipitation because of Mars' distance from the Sun (Kasting, 1991).

The Noachian erosion rates have been between 2 and 5 orders of magnitude higher than during the following times. For this erosion decline, the Hesperian craters preserve all the primary impact features and textures, while the Noachian ones have highly eroded rims. However, the Noachian erosion average, that has been around 5 μm per year, has been lower than terrestrial rates.

Part of the Noachian terrain is dissected by valley networks that represent the river drainage basins of Mars. The origin of these features is likely related to groundwater sapping although precipitation and hydrothermal circulation have recharged the groundwater system to enable episodic flows.
Although widespread dissection of Noachian terrain, large floods have likely been rare.

One of the most controversial issues is the eventual presence of oceans on Mars during past times. However, the Noachian time is the one that suggests big evidence for warm conditions under which oceans might be present. As stated by Carr and Head (2009), two possible shorelines have been identified by Moore and Wilhelms (2001) and the absence of valleys in the Noachian terrain of north west Arabia Terra may be related to burial by sediments (Howard et al. 2015a, b). However, there is not a clear geomorphic evidence for Noachian oceans, also because it may have been vulnerable to erosional activity (Head et al., 2002).

3.1.3 Hesperian period

The Hesperian period was initially considered as delineation between old post-Noachian plains such as Hesperia Planum and Lunae Planum and younger plains such as Amazonis Planum and Tarsis Planum. Subsequently, it has been quantitatively associated to the number of superimposed craters (Scott and Tanaka, 1986; Strom et al., 1992): the crater density suggests that the period extended from the heavy bombardment 3.7 Gya ago to 3 Gya ago (Hartmann and Neukum, 2001).
The main characteristics of the Hesperian period are:

- A steep decrease of weathering and erosion phenomena;
- A steep decrease of valley networks formation;
- A lower rate of volcanism that formed extensive lava plains;
- Cratering activity;
- Formation of the largest outflow channels;
- Canyon systems formation.

The steep decline of erosional rate, weathering and valley formation phenomena firstly suggest that the likely common climate conditions favourable to aqueous alteration of the Martian surface were rare in the Hesperian period.
Despite the decrease in valley networks formation, there are some examples of Hesperian and even Amazonian features especially on volcanoes (Carr and Head, 2009). However, their formation conditions have been completely different from the ones generated during the Noachian period: Fassett and Head (2008) recognise that the later valley networks have been originated from geothermal melting of snowpack on the volcanoes and not by a global climate change.

On the contrary, most of the larger outflow channels have been formed in this geological period, particularly in the late Hesperian. The main question concerning these channels is whether they have been carved by liquid water or by lava flows.
As suggested by Carr and Head (2009), a fluvial origin for most of the large outflow channels seems secure and their abrupt starts indicate that they have been originated from a rapid release of a big amount of stored water and not from the precipitation water immediately drained by the surface. This storage should have been generated by an aquifer, a lake or an ice deposit.

The Martian canyon system that formed during the Hesperian, known as Valles Marineris, is the deepest and largest of the Solar System and represents one of the most puzzling issues of the Martian geology: the unknowns are related to how and when they formed, to the composition of interior layered deposits, to the possibility for canyons to contain lakes and how the lakes formed and dissipated (Carr and Head, 2009).

A huge polar ice deposit has been generated during the Hesperian and, nowadays, the remnants are known as Dorsa Argentea Formation, that is a south circumpolar unit (Carr and Head, 2009).

3.1.4 Amazonian period

The Amazonian period began 3 Gya ago and extends to present time.
Although the length of this period comprises two thirds of the history of Mars, the surface modification related to volcanism, impact cratering and tectonism is modest and, as during the Hesperian period, the rate of weathering and erosion has been extremely low.

The most distinguishing feature of the Amazonian period is the evidence of the abundant ice action, especially at mid and high latitudes (Carr and Head, 2009). As consequence, the Glacial-Like Features (GLF) in the mid-latitude of the planet named Lineated Valley Fill (LVF), Lobate Debris Aprons (LDA) and Concentric Crater Fill (CCF), and most of the ice accumulated at the poles, are the main typifying glacial bodies of this era.

As discussed by Carr and Head (2009), ice presence has been detected with neutron and gamma-ray spectrometer measurements: at latitudes higher than 60°, it is present at depths of tens of centimetres below a sublimation layer, while at latitudes lower than 60°, the ice quantity is inferior, but it is possible to assess its presence from patterned ground and sublimation pitting also at latitudes as low as 30°. A significant amount of near-surface ice should also be present at latitudes inferior than 30° but, unfortunately, the resolution of the orbiter spectrometers, that is of few hundreds of km, is not high enough to detect these resources.

Surface ice stability is sensitive to Mars' obliquity changes and the transport and redistribution of water between ground ice, surface ice and atmospheric reservoirs is consistent with the variation of orbital parameters (Laskar et al., 2004). For these reasons, during periods of high obliquity (> 40°) the polar ice should be sublimed and driven from the poles to be transported to the tropical regions where it saturates the atmosphere and condense onto the surface (Jakosky and Carr, 1985; Carr and Head, 2009). The reverse phenomenon occurs at low obliquities, when equatorward the ice is mobilized, and it should be stable only in the high latitude areas.
Mercury, Venus, Earth and Mars did not have a primordial obliquity at the origin (Laskar and Robutel, 1993): each of the inner planets has had a nearly zero obliquity at the

beginning and a chaotic behaviour has driven them to their actual values. Both Mercury and Venus have undergone large changes of obliquity that varied between 0° and 90° and, after these periods, their current obliquities have been reached thanks to dissipative effects (Laskar and Robutel, 1993). After passing through a chaotic phase, Earth has reached the actual state of obliquity after Moon capture (Laskar and Robutel, 1993). On the contrary, at present time the obliquity of Mars is still in a chaotic zone: indeed, the planet is far from the Sun and has no a satellite big enough to create tidal interactions able to slow and stop the process (Laskar and Robutel, 1993). Laskar and Robutel (1993) found a Mars' large chaotic zone that ranges from 0° to 60°. Laskar et al. (2004) conducted a statistical analysis of the obliquity history of Mars and developed a dynamic model of its orbital evolution over the last 250 Mya. This model allows estimating Mars obliquity variations during the Amazonian period that has been evaluated of 40° on average during this time, with a 63% probability that it reached 60° in the last Gya. At obliquities higher than 54°, the pole insolation is higher than the equator one (Carr and Head, 2009), and the Sun effect causes ice migration at lower latitudes. During the time when Mars exceeded the average value of 40° for a sustained period, a significant migration of ice occurred from the poles' ice rich zones to mid-latitudes, causing prolonged snow and ice accumulation and forming an extensive system of valley glaciers (Head and Marchant, 2006 a,b).

This large amount of ice generated features, LVF and LDA, that modified the geomorphic surface of a portion of the dichotomy boundary called fretted terrain. Fretted terrain and fretted channels are well developed in the northern part of Arabia Terra (Sharp, 1973) and are the most topographically distinctive landforms that typify the dichotomy boundary in the northernmost margins of Protonilus and Deuteronilus Mensae between 30° and 50° N (Morgan et al., 2009).

Fretted terrains formed prior to middle Hesperian and the associated LVF and LDA represent the modification of fretted topography during the late Amazonian (McGill, 2000). At the origin, the dichotomy boundary dominated by fretted terrain was defined by linear valleys that extended from the southern highlands to the northern plains, by isolated plateaus and mesas that become progressively smaller to the north (Sharp, 1973) (see Figure 3-1). This formation has been modified by two degradation features: LDA,

that originate from isolated mesas and the escarpment flanks, and LVF, that line the fretted valley floors (Squyres, 1978).

Figure 3-2 and Figure 3-3 furnish some examples of pattern that are generated on Mars surface by LVF and LDA features.

In Figure 3-2 a LVF/LDA system is showed. LVFs' lineations are aligned in downslope direction and converge together at the mouth of the alcove; a large scale LDA is fed by individual lobes of LDA that emerge from indentations (Morgan et al., 2009).

Figure 3-3 shows a divergence of flow around a 5 km mesa. The flow originates from small lobes within alcoves to the west of the image (small arrows) and flows out the north and east around isolated mesas (Morgan et al., 2009).

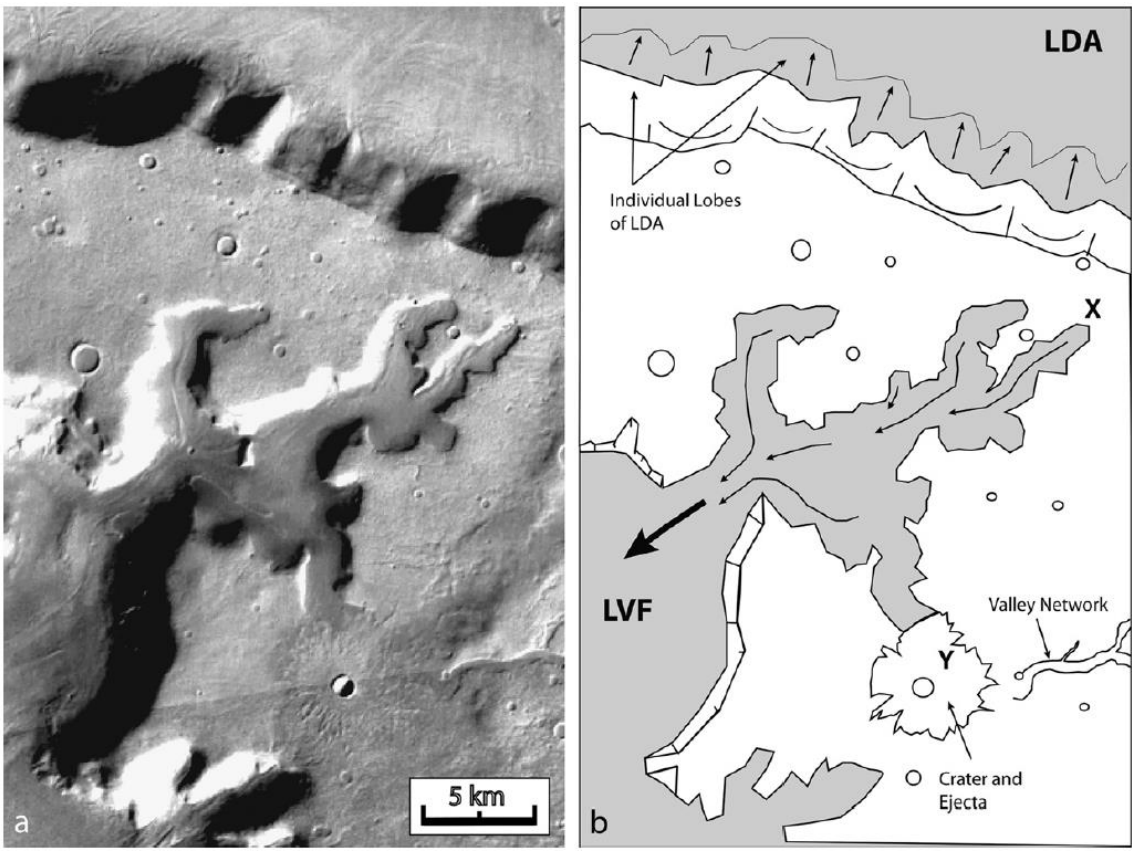

Figure 3-2. (a) portion of 1589 HRSC image; LVF and LDA system (Morgan et al., 2009)

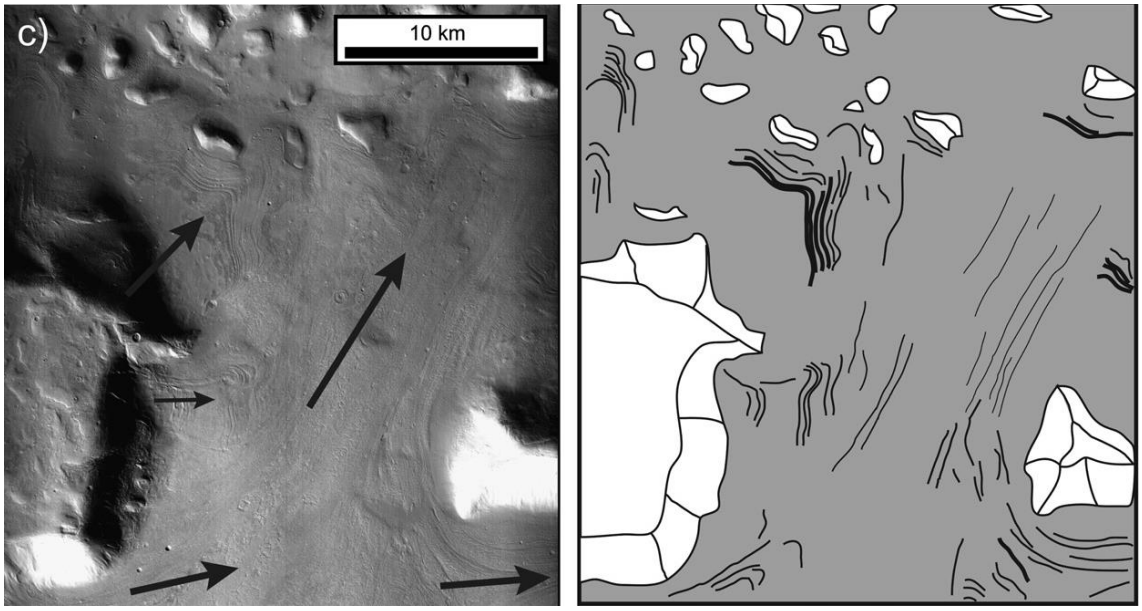

Figure 3-3. (c) CTX image P13_006239_2240; evidence of flows originated by mesa (Morgan et al., 2009)

Literature from Morgan et al. (2009) provides an insight into the three different hypotheses proposed for the origin of LVF and LDA:

1. Mobilization of ancient regolith rich in water that contributed to both fretted terrain and LVF/LDA formations;

2. Water vapour atmospheric diffusion into talus formations that generated viscous flows along flanks of walls of the valley and along the margins of massifs;

3. A glacial origin.

The third hypothesis, that considers LVF and LDA as debris-covered glaciers, supposes that significant precipitation of ice and snow have been verified during periods of higher obliquity and that they have been followed by glacial flows and by the development of sublimation till of rock and soil as protection of the ice resource (Head et al., 2006a, b). Carr and Head (2009) argue that (1) the presence of ring-mold craters, which are superimposed impacts on these glacial features that detect the presence of relatively pure subsurface ice located at shallow depths by bringing it back to the surface, (2) the flow

patterns that carve the valley floors, and (3) the prominent sublimation features all support the debris-covered glacier hypothesis.
In summary, according to the glacial origin model, LVF and LDA represent debris-covered glaciers that formed in the Amazonian when climate change caused snow and ice precipitation that accumulated preferentially in the northern mid-latitude of Mars. In this scenario, regional snow and ice deposit caused glacial flows in valleys (LVF) and at the margin of massifs (LDA). Then debris from adjacent valley walls and massisfs created a sublimation layer that buried and protected the ice from sublimation when climate conditions changed.

The other ice landform that characterises the Amazonian period is named Concentric Crater Fill (CCF). CCF has been classically described as a crater-interior unit with multiple rings or lines concentric with the crater rim (Sqyres, 1979).
Figure 3-4 shows a CCF that is clearly separated from the interior crater wall talus slopes. White lines indicate track of the underlying topographic profile.
The typical surface texture that has been analysed from High Resolution Imaging Science Experiment (HiRISE) images is called “brain terrain” (Levy et al., 2009) and Figure 3-5 reports this typical pattern.

These features are commonly present along the dichotomy boundary in the northern mid-latitude in regions containing abundant LVF and LDA.

As for the LDA and LVF, different hypotheses on CCF formation have been done. The three proposed mechanisms of formation for CCF are (Levy et al., 2010):

1. An ice-free process as an aeolian crater-filling process;
2. An ice-assisted talus creep;
3. A glacial origin.

Despite the widespread presence of dunes on the interior of a crater at both high and low latitudes, dune morphology is readily discernible from “brain terrain” texture that

characterises the surface of these craters. This dissimilarity between dunes and "brain terrain" textures significantly suggests that the origin of CCF is not primarily aeolian (Levy et al., 2010). The analysis of high-resolution images reveals that the surface layered pattern is a visual effect due to the closely spaced lineation that characterises the "brain terrain" texture (Levy et al., 2010).

The second proposed mechanism of formation suggests that CCF may have been originated from a talus ice-mobilization from crater rims. Talus are rock deposits that originated from an avalanche of material along a slope and that accumulated downslope (Jet Propulsion Laboratory, 2015). However, in some locations, CCF and talus slopes are topographically distant by tens to hundreds of meters of relief (Levy et al., 2010) and it suggests that talus slopes and CCF are made by different materials. In addition to this factor, CCFs are identified in craters that are characterised by a range of different rim morphologies, which vary from well-defined to eroded, suggesting that CCFs did not simply formed by a talus shed mobilization from crater rims (Levy et al., 2010).

The third hypothesis is the most significant one: Levy et al. (2010) analysed Context Camera (CTX) and HiRISE datasets and stated that CCF is a significant component of Amazonian aged glacial landsystem on Mars. Indeed, CCF, LVF and LDA have many common characteristics. They are commonly present in the same regions of Mars; as delineated for LDA and LVF, the widespread presence of ring-mold craters has been detected also on CCFs' surfaces: Levy et al. (2010) argue that these craters indicate the presence of near-surface ice and they examined the depth-diameter ratios of filled craters and concluded that, in many locations, hundreds of meters of ice may be present below the sublimation till; CCF formed in the late Amazonian, around 60 and 300 Mya ago, consistently with the formation ages of LVF and LDA: the morphological analysis of CCF in the proximity of the other features suggests that CCF, LDF and LVF are all part of an integrated glacial landsystem (Levy et al., 2010).
For all these reasons, CCF, LDF and LVF are Glacial-Like Features (GLF) that typifies the mid-latitude of Mars.

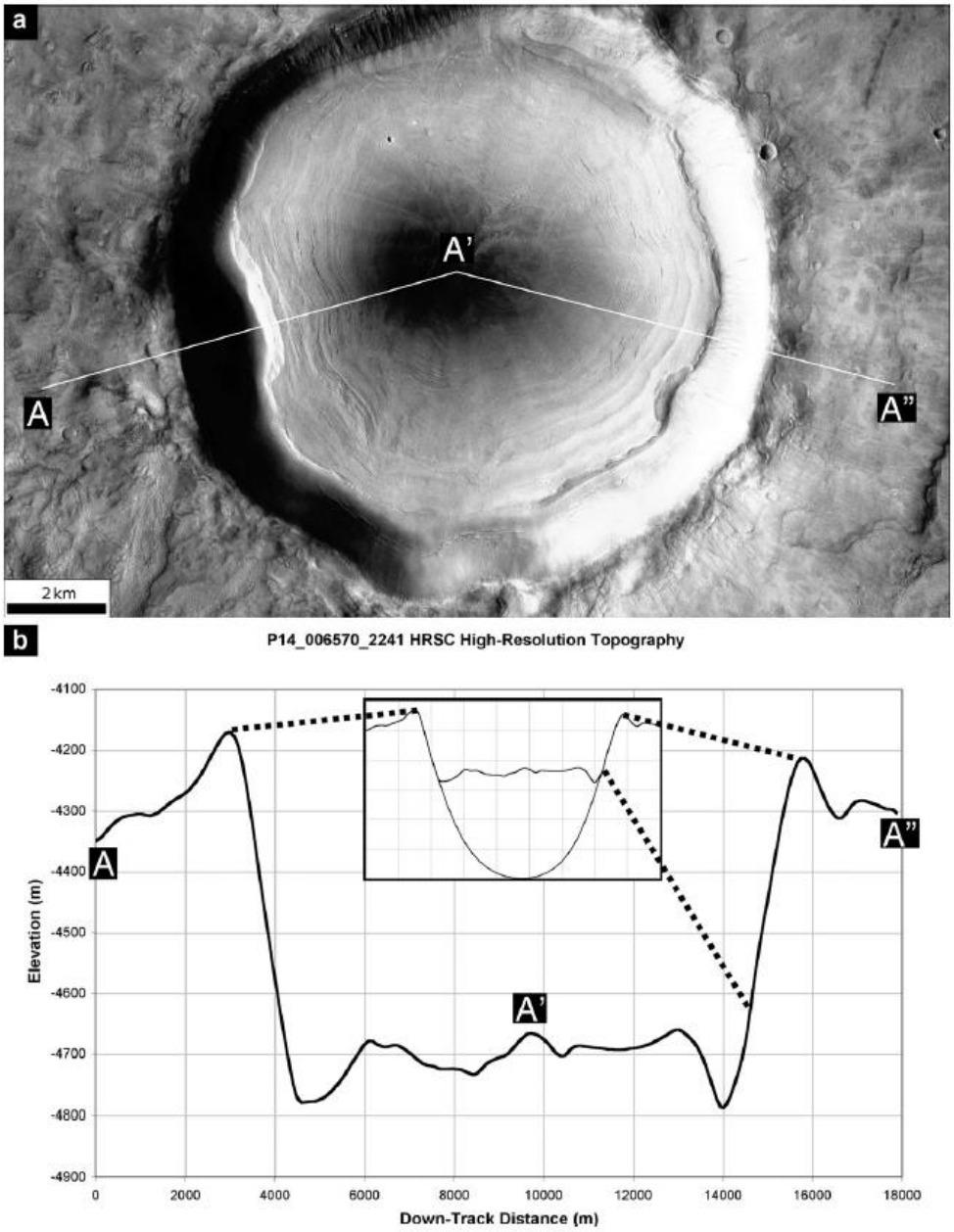

Figure 3-4. (a) Portion of P14_006570_2241 HRSC image; Classic CCF clearly separated from the interior crater wall talus slopes; white lines indicate track of topographic profile; illumination from left; (b) HRSC high-resolution DTM topographic profile across CCF-containing crater (Levy et al., 2010)

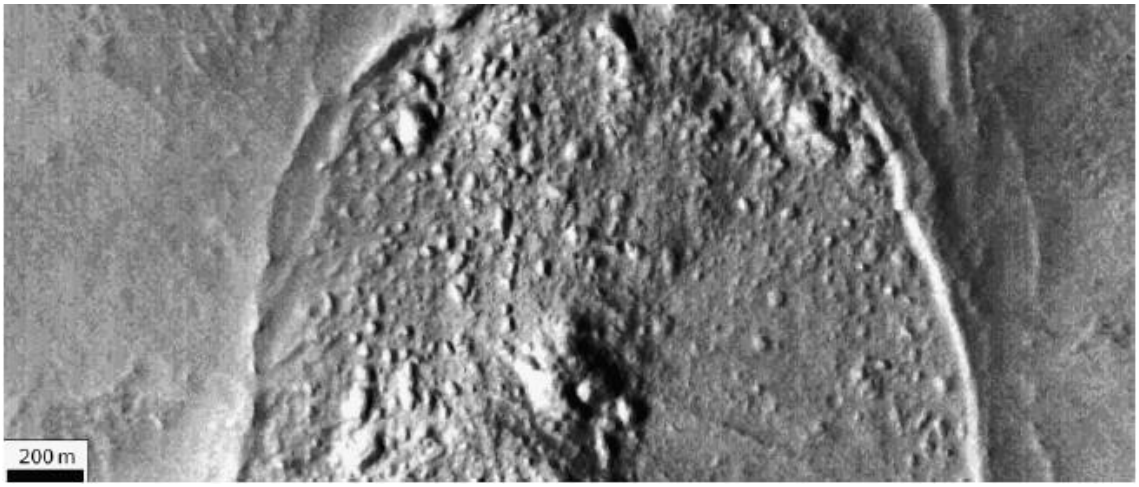

Figure 3-5. Typical "brain terrain" texture within CCF's surface (Levy et al., 2010)

3.2 Present day environmental conditions

The peculiar harsh environment that characterises Mars constitutes a great challenge for a feasible crewed mission. Indeed, it is fundamental to identify all the environmental conditions of the future human Exploration Zone (EZ) to provide an adequate robust system of facilities for life support and mining operations.
The variables that describe Mars' conditions vary significantly between locations. For this reason, it is recommended that they will be carefully evaluated in future studies for the EZ and Landing Site (LS) selection. However, a global overview on several factors that are consistent across locations and a comparison between Mars and Earth's parameters will be provided in this section.

Mars' gravity is 3.711 m/s^2, the 37.9% of Earth's one (NASA, 2016a).

The atmosphere of Mars is composed of approximately 96% carbon dioxide, 1.9% argon, 1.9% nitrogen, and traces of free oxygen, carbon monoxide, water and methane, among other gases (Mahaffy et al., 2013). The high percentage of carbon dioxide significantly influences atmospheric pressure. The average value of atmospheric pressure on the Martian surface is 600 Pa, about 0.6% of Earth's mean sea level pressure of 101.3 kPa, and it ranges from the minimum peak of 30 Pa on Olympus Mons to a maximum value of 1155 Pa in Hellas Planitia (NASA, 2016a). This pressure is well below the Armstrong limit for unprotected human bodies (NASA, 2016a) and this highlights the importance of considering this factor as fundamental for crews that will land on Mars because humans cannot survive in an unpressurized environment.
Pressure fluctuations, which are due to a season carbon dioxide condensation at the poles of the planet, vary as much as 20% (Leovy, 2001).

Mars temperature is characterised by both daily and seasonal extreme fluctuations. Indeed, Mars has an eccentric orbit and it is about $206.2 \cdot 10^6$ km from the Sun at perihelion and $249.2 \cdot 10^6$ km at aphelion, with an actual tilt of axis of 25º (NASA, 2016a). The average length of a Martian sidereal day named sol is 24 h 37 m 22.663 s and the orbital period is 687 Earth days long (NASA, 2016a). During summer solstice, daylight duration

can approach 15 hours, which are reduced to 9 during the winter solstice. Temperature on Mars can vary between 30 ºC to -140 ºC (NASA, 2016a).

Both horizontal variations of temperature and associated pressure variations drive the planetary wind system (Leovy, 2001). This general circulation model is based on observation and numerical simulation models. Obviously, this parameter varies a lot around the planet, but the reduced atmospheric pressure gives the benefit that wind does not pose a significant operational threat (NASA, 2016b). Engineering Constraints (EC) for LS and Habitation Site (HS) selection define that local wind velocity does not have to exceed 15 m/s on average and 30 m/s during gusts of wind.

The following table summarises all the parameters described in this section and compared them to Earth's values.

Table 3-3. Comparison between Mars and Earth environmental parameters

Parameter	Mars	Earth
Length of day	24 h 37 m 22.663 s	23 h 56 m
Orbital period	687 Earth d	365.25 d
Perihelion	$206.6 \cdot 10^6$ km	$147.1 \cdot 10^6$ km
Aphelion	$249.2 \cdot 10^6$ km	$152.1 \cdot 10^6$ km
Tilt of axis	25º	23.5º
Gravity	3.71 m/s^2	9.81 m/s^2
Atmospheric composition	96% carbon dioxide <2% argon <2% nitrogen <1% other	78% nitrogen 21% oxygen 1% other
Atmospheric pressure	maximum 1155 Pa minimum 30 Pa average 600 Pa	maximum 108.56 kPa minimum 87 kPa sea level 101.3 kPa
Temperature	maximum 30 ºC minimum -140 ºC average -63 ºC	maximum 58 ºC minimum -88 ºC average 14 ºC

3.3 Conclusion statement

This chapter provided an overview on the geologic history and present day environmental conditions of Mars. The analysis of these topics highlights the complexity of the Red Planet and the huge number of variables that must be considered to plan a feasible and sustainable human mission to Mars.

Nevertheless, Mars is the next tangible frontier to expand the human presence beyond Earth and a background of the Glacier-like Feature (GLF) that will be fundamental for In Situ Resources Utilization (ISRU) plan has been provided.

4 CONCLUSION STATEMENT ON BACKGROUND RESEARCH

In concluding this literature review, it can be noticed that considerable time was spent researching for this topic to properly understand this research area and to provide a solid foundation of knowledge and a global context for the work developed through this thesis. Furthermore, the literature reviewed in the previous chapters has been successful in providing a sufficient base for the development of automated landing site optimisation model for human mission to Mars: indeed, the review identified the priority of defining a method for the selection of a Landing Site (LS) location within an Exploration Zone (EZ) with a solid Engineering Constraints (EC) base. However, planning a feasible and sustainable crewed mission to the Red Planet requires strategic presence of resources within the EZ. Both the needs of land safely and mining resources represent fundamental concepts to achieve the goal of a successful mission to Mars, requiring close cooperation and synergy between engineering and geology complementary fields.

This literature review also provided some ideas for possible future developments of the model proposed in this thesis, because of the critic view acquired during the conducted analysis on this topic.

5 PROJECT OVERVIEW

To ensure the successful development and completion of the project by respecting the pre-fixed deadlines, a detailed schedule was set at the beginning of the work. By following this plan, all the steps to achieve the objectives were respected, looking towards reaching the aim of the thesis.

The main benefit of following the project schedule was the possibility to adapt to changeable circumstances: indeed, the objectives and outcomes evolved during the time for different reasons such as the flexibility of the topic itself, the growing knowledge of the theme under study, and the necessity to optimise the model after the analyses of datasets and results.

Despite the flexibility of the project, the following aim and objectives constituted the milestones that were followed and developed to upon completion of the work.

5.1 Project Objectives

5.1.1 Aim

The aim of the work is to propose an automated landing site optimisation model for human mission to Mars.

5.1.2 Objectives

The key research objectives are to:

i. Develop a flexible model based on defined engineering constraints, allowing the automated selection of an optimised landing site location within a proposed exploration zone for the human mission to Mars;

ii. Validate model effectiveness;

iii. Run the model on different exploration zones located on Mars;

iv. Propose possible configurations of the landing and habitation sites within an exploration zone;

v. Incorporate the output results with a local glacial resources analysis.

5.2 Project Outline

5.2.1 Major tasks

To properly develop the research project, this was subdivided in its major tasks that are explicated in this section.

5.2.1.1 Research phase

The literature review represents a fundamental component of the study conducted during the whole development of the project. Starting from an initial general global study of the research area, the review was focused on specific topics to provide a solid foundation of knowledge. This background allowed developing the core idea of the work, supporting and strengthening the thesis itself, providing a proper context for the work and generating ideas for future developments.
The review of the available literature provided in Sections 2 and 3 of this thesis assisted in completing *i, ii, iii, iv, v* objectives.

5.2.1.2 Modelling phase

The use of ArcGIS *ModelBuilder* allowed creating a flexible automated model to satisfy *i* objective. The modelling task was subdivided into two different phases: (1) the initial one to understand how the Software and its tools work, with the scope of both acquiring a critical use of GIS instrument and maximizing its functionalities, and (2) a second phase to develop the model based on defined engineering parameters.

5.2.1.3 Critical evaluation of results and optimisation phases

Factors identified during the literature review enabled to evaluate the results in a critical way, to clearly proof that the model works properly and to optimise the model itself. In this optimisation process the core idea was to shape the model as much resilient to condition changes as possible. The finalised result is a flexible and adaptive model useful to satisfy *iii*, *iv* and *v* objectives.

5.2.1.4 Discussion and recommendation phases

The results obtained by running the finalised model were interpreted and justified. This analysis provided the base for proposing future possible developments of the work.

5.2.2 Required Resources

Different resources were identified to accomplish the project:

- JMARS 3.7.7 Software;
- Google Earth Pro 7.1 Software;
- ArcMap 10.3.1 GIS Software.

6 AUTOMATED LANDING SITE OPTIMISATION MODEL FOR HUMAN MISSION TO MARS

After several decades of space exploration, successfully sending humans beyond Earth will represent one of the greatest achievements of the mankind. As strongly justified in Sections 2 and 3, Mars represents the closest boundary for a feasible space human mission.

Despite the great importance of the scientific interest related to find evidence of past life during the human "Journey to Mars", a technical approach plays a fundamental role to successfully drive a crew to the Red Planet for the first time. To ensure crews' safety and ongoing mission success, the selection of an optimised landing site for the construction of a human base is highly critical. Site selection will require a multidisciplinary effort with significant planning phases to implement a successful strategy that is both flexible and adaptable.

The development of a tool constructed in ArcGIS *ModelBuilder*, which seeks to automate and optimise the landing site selection process for the first human mission to Mars, will be discussed in this Section.
The core focus of this work is to improve this selection process replacing time consuming and subjective manual analysis of datasets with an automated flexible model based on defined engineering constraints.
To test and validate the effectiveness of the model, the constraints used for the landing of the Mars Science Laboratory (MSL) rover Curiosity at Gale Crater were incorporated into the tool. After workflow validation, the model was run on other proposed human exploration zones.

The model works by integrating images analysis tools and provides an output map that reflects the desired engineering constraint requirements. The workflow is structured into

three main phases, which consists of: (1) Data processing, (2) Engineering parameter map layer development, (3) Raster reclassification. The reclassified output maps are then combined into a single map, which summarises all the properties analysed. This map represents a quantitative, fast and effective way to evaluate where it is and is not possible to land safely within an exploration zone, to identify the optimal landing areas from an engineering point of view, and to compare different exploration zones proposed for this pioneering mission.

The tool may be further optimised by the incorporation of a local resources analysis, which represent a fundamental requirement for a feasible and sustainable Off-Earth human mission. As justified in Section 2, the highest priority is related to mining water on Mars both for life support and propellant production; metals, silicon and structural building material have secondary priority (LPI, 2015).

A distinctive aspect of the model is its flexibility. The classification principles, the associated indexes, the weight of the implemented parameters may be varied, and further parameters can be entered to the workflow as required. The choice to grant flexibility to this work is consistent with the dynamic mission's objectives and constraints evolution.

Section 6 shows the methodology that has been followed to build the model. Starting from data selection process, data analysis and model parameters will be described in detail.

6.1 Methodology

This Section outlines the methodology followed to automate and optimise the landing site selection process for the first human mission to Mars.
Data selection process, data analysis mechanism and parameters implemented in the workflow will be analysed in detail. The assumptions made in this project and the model flexibility will be properly justified.

6.1.1 Data Selection

The model built with ArcGIS *ModelBuilder* works by integrating images analysis tools and provides an output map that reflects the desired engineering constraint requirements shown in Table 6-1. Indeed, the analysis of three-dimensional planetary images allows investigating different surface structures and topography aspects that constitutes the base for a safe landing on Mars and a source of important information for both a geological and geomorphological interpretation of the planet surface.

Different publicly available sources described below have been used (1) to collect the input datasets required by the developed workflow, (2) to conduct a visual comparison between the generated maps and high-resolution images of Mars' surface both to validate and to optimise the model by the incorporation of a local resources analysis.

Section 6.1.1.1 will analyse sources and properties of datasets implemented in the model and used for this study. Section 6.1.1.2 will define which proposed exploration zones will be processed with the developed workflow.

6.1.1.1 Data Source

This Section is subdivided on the base of four different data sources that were used to develop this project.
Table 6-1 shows how sources are coupled with datasets types and resolution.
All the dataset names analysed in this work are listed in APPENDIX C.

Table 6-1. Summary of sources and properties of analysed data

Source	Data Acronym / Layer name	Resolution [m/pixel]
Astropedia Lunar and planetary cartographic catalogue	MOLA DEM	436
High Resolution Stereo Camera view online interface	HRSC DTM	75
	HRSC image	12.5
Google Earth Pro	CTX	5.6
Java Mission-planning and Analysis for Remote Sensing	*Oct 2015 Proposed EZs* layer	
	Mars 2035 Thermal Inertia Mask layer	
	TES Thermal Inertia layer	
	Annual average wind speed layer	
	Annual maximum wind speed layer	

- **Astropedia Lunar and planetary cartographic catalogue**

The Mars MGS MOLA Elevation Model 463 m (MEGDR) is a Digital Elevation Model (DEM) available in Astropedia Lunar and planetary cartographic catalogue (Astropedia, n.d.). It is based on data acquired by Mars Orbiter Laser Altimeter (MOLA) installed on NASA's Mars Global Surveyor (MGS) spacecraft (Astropedia, n.d.). MOLA instrument collected more than 600 million individual elevation measurements between 1999 and 2001 that were used to create a global DEM with an absolute vertical accuracy of approximately 10 metres (DLR, 2017). As consequence of MGS polar orbit, MEGDR's horizontal resolution is poorer than the vertical one, varying from 300 metres close to the poles to several kilometres near to the equator (DLR, 2017).

The image is a raster map that represents the whole surface of the Red Planet with a resolution of 463 m/pixel (Astropedia, 2017). A raster file is an image that defines space as an array of equally sized cells arranged in rows and columns and composed of single or multiple bands (Esri, n.d.); each cell has attribute values and location coordinates

associated. For this reason, MEGDR constitutes a useful instrument to analyse the global planet configuration and to find direct evidence of the dichotomy boundary that divides the planet into the northern lowland third and the southern upland two-thirds.

- **High Resolution Stereo Camera (HRSC) view online interface**

The cooperation between the Planetary Sciences and Remote Sensing Group at the Institute of Geosciences at Freie Universität Berlin and the DLR Institute for Planetary Research at German Aerospace Center produced the HRSC view online interface, an HRSC image archive where data can be viewed and accessed since 2007 (Freie Universität Berlin, n.d.).

HRSC was developed by the DLR Institute for Planetary Research and this constitutes the Germany fundamental contribution to ESA's Mars Express mission: for the first time a special stereo camera continuously acquiring images of Mars' surface in three dimensions and in colour (DLR, 2017).

The laser radiation pulses transmitted by the spacecraft to the planet are reflected by Mars' surface and received back to the spacecraft, which determines the distance between the pulse origin and the Red Planet considering the round-trip times (DLR, 2017). This acquired information allows representing surface elevation.

HRSC Digital Terrain Model (DTM) represents the ground surface with a 75 m/pixel resolution. The HRSC image resolution is of 12.5 m/pixel (Freie Universität Berlin, n.d.). The typical HRSC's swath is 52 km and its minimum strip length is 300 km (DLR, 2017). HRSC DTM were used as input data to process Elevation, Slope, Terrain Relief and Rock Height engineering parameters described in Section 6.1.3.

- **Google Earth Pro**

Google Earth Pro's Mars Planet extension allows having access to a wide range of spacecraft imagery, such as CTX, HRSC, HiRISE, CRISM an MOC.

Context Camera (CTX) images were accessed through this data source. CTX is an instrument installed on Mars Reconnaissance Orbiter (MRO) that returned more than 26 terabits of grayscale images (NASA, n.d.b).

The typical dimensions of a CTX image can be 30 km wide and 160 km long, and the resolution is 5.6 m/pixel (DLR, 2017).

MRO was launched by NASA in 2015 to enable evaluating the potential safe Landing Sites (LS) for rovers and landers, combining both radar observation and satellite imagery (NASA, n.d.h). For this reason, CTX resolution is high enough to perform a detailed visual analysis of collected data to integrate the model with a local resources investigation.

- **Java Mission-planning and Analysis for Remote Sensing (JMARS)**

The JMARS Software is a publicly available Geospatial Information System (GIS) developed by ASU's Mars Space Flight Facility to archive data and to provide tools for data-analysis and mission planning (JMARS, n.d.). JMARS provides access to images, raster files, mosaics, compositional maps (Christensen et al., 2009), and various maps and imagery already processed.
JMARS will be adopted in this project as instrument to consult the proposed landing areas for the first human mission to Mars, to collect information related to surface thermal inertia, and to obtain data related to atmospheric conditions such as the annual maximum and average wind speed.

As described in Section 2, forty-seven EZ have been proposed at the First Landing Site/Exploration Zone Workshop for Human Missions to the Surface of Mars in October 2015 (see Figure 2-13 and APPENDIX B). These sites contain a set of Regions of Interest (ROIs) that collectively meet the threshold/required criteria as well as several qualifying/enhancing criteria that are given by both Scientific and Resource Objectives (LPI, 2015). These EZs have also to satisfy Engineering Constraints (EC) that are fundamental for the mission success (LPI, 2015).
All these EZ are mapped on JMARS' *Oct 2015 Proposed EZs* layer, and this material will be used for the creation of EZ shapefiles on ArcMap, the datasets that provide geometrical information related to the EZ (see Section 6.1.3).

Successfully landing humans to Mars requires to select a safe rocky site with a relatively low rock abundance and a low level of dust on the surface. These physical properties are closely coupled with surface temperature and, as consequence, with surface's thermal inertia and albedo measures.

Mars Global Surveyor Thermal Emission Spectrometer (MGS-TES) acquired temperature measures at the top of the atmosphere directly related to the surface temperature (Planetary Science Institute, 2012). A numerical thermal inertia map with a 3 km/pixel resolution was developed by Christensen with TES data collected between 1997 and 2003. As input dataset for the model, a shapefile for each analysed EZ was created using *Mars 2035 Thermal Inertia Mask* layer. This mask generated for the human EZ selection process used Christensen TES map to exclude areas with low thermal inertia *I*, considering I = 100 $Jm^{-2}K^{-1}s^{-1/2}$ as threshold value.

An example of *Mars 2035 Thermal Inertia Mask* within Protonilus Mensae EZ is shown in Figure 6-1. The white zones represent sites within thermal inertia is lower than the required threshold value. Indeed, Figure 6-2 shows how the associated value of thermal inertia of a purple area, which in Figure 6-1 is represented in white colour, is lower than 100 $Jm^{-2}K^{-1}s^{-1/2}$.

The following table highlights the correlation between thermal inertia and geological properties of the surface. Colours associated to different values of thermal inertia refers to MGS-TES Christensen map.

This correlation reflects the fundamental importance of thermal inertia evaluation for the landing site selection: a safe rocky formation has high heat capacity and displays high thermal inertia.

Table 6-2. TES Thermal inertia map: correlations between colours and geologic formations (modified from Planetary Science Institute, 2012)

Thermal Inertia	Map Colours	Formation
Lowest	Purple to dark blue	Loose fine surface dust and very few rocks
Medium	Green to yellow	Coarser loose particles, crusted fines, a fair number of scattered rocks, and/or perhaps a few scattered bedrock outcrops

Higher	Red to white	Combination of coarse sand, dune sand, strongly-crusted fines, abundant rocks, and/or scattered bedrock exposures

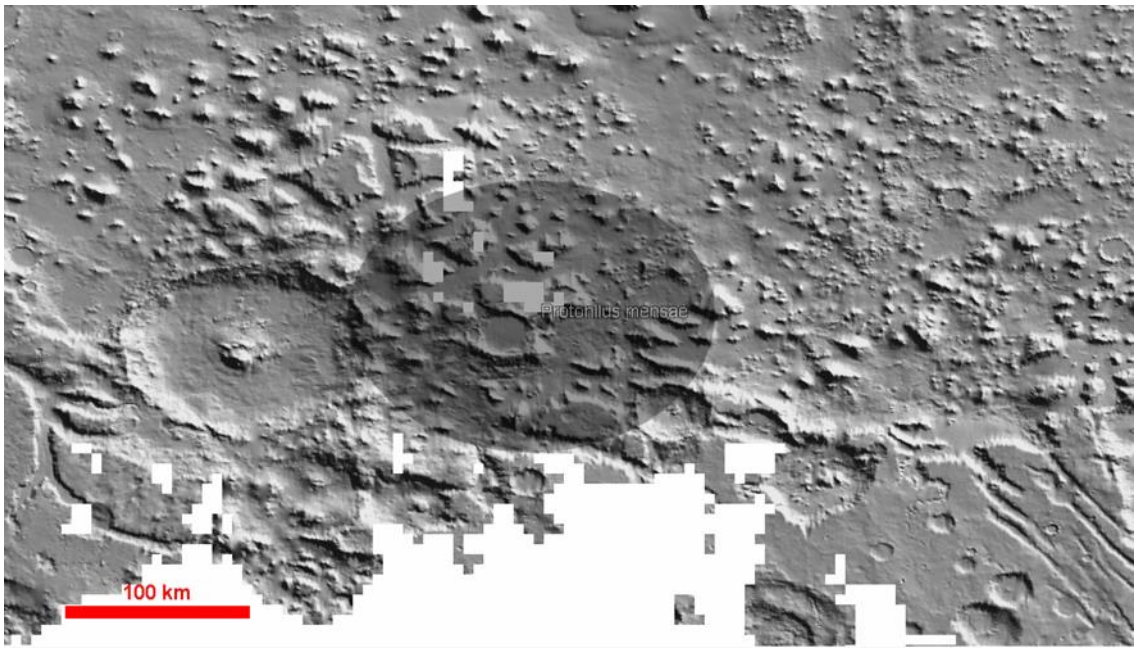

Figure 6-1. JMARS *Mars 2035 Thermal Inertia Mask* layer in Protonilus Mensae EZ; white areas have an associated thermal inertia I < 100 $Jm^{-2}K^{-1}s^{-1/2}$

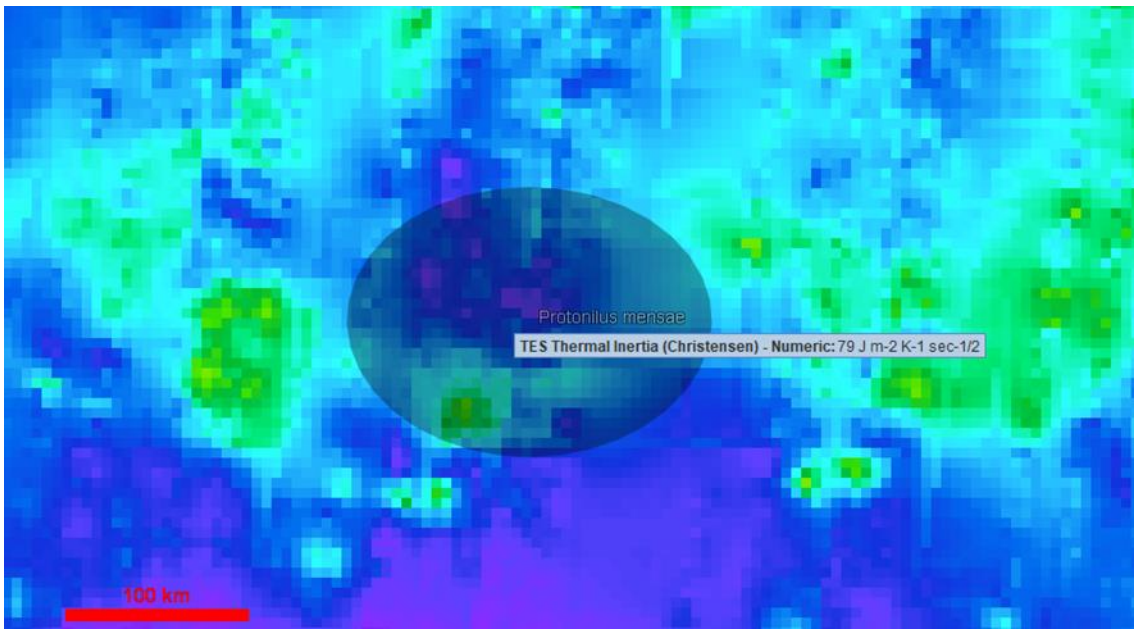

Figure 6-2. *JMARS TES Thermal Inertia (Christensen) + 1 plot* layer in Protonilus Mensae EZ

Wind speed represents another fundamental atmospheric condition for the success of this pioneering mission. As shown in Figure 6-3 and Figure 6-4, JMARS provides *Annual average wind speed* and *Annual maximum wind speed* layers, two masks that indicate wind speed in meters per second on the base of the Ames General Circulation Model (GCM) in the 26th Martian year. The planetary wind system is driven by both horizontal variations of temperature and associated pressure variations (Leovy, 2001) and the GCM is based on observation and numerical simulation models.

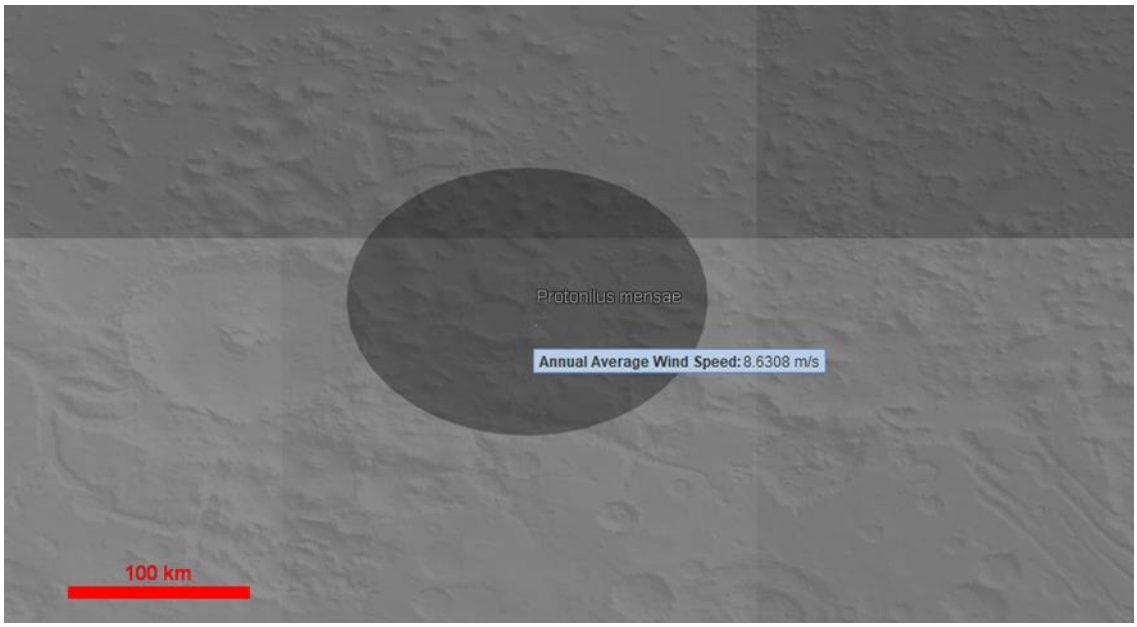

Figure 6-3. JMARS *Mars 2035 Annual Average Wind Speed* layer in Protonilus Mensae EZ

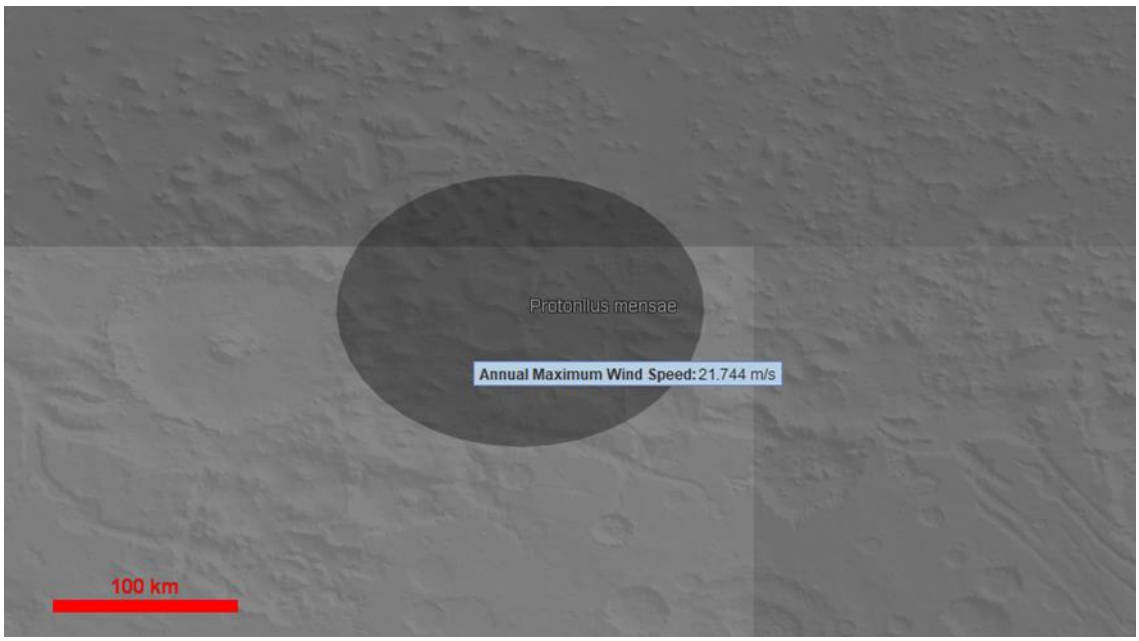

Figure 6-4. JMARS *Mars 2035 Annual Maximum Wind Speed* layer in Protonilus Mensae EZ

6.1.1.2 Sites Selection

The model was run on different proposed human Exploration Zones (EZs), that are:

- Gale Crater;
- Protonilus Mensae;
- Deuteronilus Mensae I;
- Deuteronilus Mensae II.

Gale Crater EZ was chosen to test and validate the effectiveness of the model. Indeed, the constraints used for the landing of the Mars Science Laboratory (MSL) rover Curiosity on Gale Crater were incorporated into the tool developed in this project.
After workflow validation, the model was run on the other proposed human EZ and the obtained results are reported in Section 7 and discussed in Section 8.

6.1.2 Data Analysis

Successfully sending humans to Mars will represent one of the greatest achievements of the mankind. A significant multidisciplinary effort is needed to achieve the goal of safely land crews on Mars' surface and to ensure ongoing mission success the selection of an optimised landing site requires to implement a flexible and adaptable strategy.
In this Section, the tool built in ArcGIS ModelBuilder which seeks to automate and optimise the landing site selection process for the first human mission to Mars will be discussed.

6.1.2.1 Model Workflow

The core focus of this work is to improve the selection process replacing time consuming and subjective manual analysis of datasets with an automated flexible model based on defined engineering constraints.

The global model is developed with ArcGIS *ModelBuilder* (see Section 6.1.2.2), that is a visual programming application for working with maps and geographic information.

To test and validate the effectiveness of the model, the constraints used for the landing of Mars Science Laboratory (MSL) rover Curiosity at Gale Crater were incorporated into the tool.
After workflow validation, the model was run on other proposed human exploration zones.
The model works by integrating images analysis tools and provides an output map that reflects the desired engineering constraint requirements.
The workflow is structured into three main phases, which consists of:

1) Data processing: a sequence of operation tools is performed to convert raw data into usable form;

2) Engineering parameter map layer development: the input dataset is processed with an appropriate tool to obtain a map for each engineering parameter associated to an EC. This phase furnishes a set of raster files that are "spatial data models that

defines space as an array of equally sized cells arranged in rows and columns" (Esri, n.d.). Each map represents a different property of the analysed EZ with a specific associated unit of measure;

3) Raster reclassification: each raster is reclassified by associating a specific index to each range of values. If the attribute value of a cell does not satisfy the engineering requirement, the associated index is 0; otherwise, the index is as higher as better is the parameter. This phase allows shifting from dimension to dimensionless maps.

The reclassified output maps are then combined into a single map, which summarises all the properties analysed. This map represents a quantitative, fast and effective way to evaluate where it is and is not possible to land safely within an exploration zone, to identify the optimal landing areas from an engineering point of view, and to compare different exploration zones proposed for this pioneering mission.

A distinctive aspect of the model is its flexibility. The classification principles, the associated indexes, the weight of the implemented parameters may be varied, and further parameters can be entered to the workflow as required. The choice to grant flexibility to this work is consistent with the dynamic mission's objectives and constraints evolution.

The tool may be further optimised by the incorporation of a local resources analysis, which represent a fundamental strategic requirement for a feasible and sustainable Off-Earth human mission.

6.1.2.2 Software

To achieve the aim of this thesis, the Geographic Information System (GIS) *ModelBuilder* application was used to build the workflow described in the previous Section.
GIS is a system that allows storing, manipulating, analysing, managing and presenting spatial and geographic data. It is provided of applications that are tools that may be used to analyse spatial information, edit data in maps and present obtained results.

ArcGIS is the extension of this system for working with maps and geographic information and *ArcMap* is the main component of its suite of geospatial processing programs.
ModelBuilder is an *ArcMap* application that may be used to create models. These models are workflows that connect geoprocessing tools into sequences by feeding each tool with the output data of the previous one. This visual programming language was used to string a sequence of tools together to analyse input datasets described in Section 6.1.1.
The programmed model allows executing a series of tools to analyse input images and obtain a final raster map that identifies the optimum Landing Site (LS) for the pioneering human mission to Mars.

6.1.2.3 Preliminary phase

The input HRSC DTM datasets were georectified before data processing phase. Indeed, DTMs are strips partially superimposed and georectification produces a digital alignment of these satellite images by intersecting a specified number of control points. This preliminary phase grants a better superposition and merging of input HRSC datasets in the data processing phase.
The reference system adopted for all the input datasets and output results is SINUSOIDAL_MARS.

6.1.2.4 Integrated approach

The model developed in this thesis is a flexible workflow that may be integrated with different data as an analysis of resources.
As justified in Section 2, meeting the Resource Objectives in the location where human activity will take place is strategically important to be able to produce commodities from local resources.

In 2015, forty-seven possible Exploration Zones (EZs) summed up in

APPENDIX B were proposed during the first HLS^2 workshop. This selection has been carried out by the cooperative effort of NASA's Human Exploration and Operations Mission Directorate (HEOMD) and Science Mission Directorate (SMD).

The EZ is a collection of Regions of Interest (ROIs) that are located within approximately 100 kilometres from a centralized Landing Site (LS) (LPI, 2015).

The presence of raw materials constitutes a milestone for the feasibility and sustainability of the project. The highest priority is related to mining water on Mars both for life support and propellant production (LPI, 2015). Metals, silicon and structural building material have secondary importance (LPI, 2015).

Although the proposed EZs completely or partially meet the fixed requirements, the LS and Habitation Site (HS) must be close to accessible resources. For this reason, proposing the optimum LS requires considering the presence of resources.

The output final raster map generated by the programmed workflow will be compared with CTX images to identify the presence of accessible glacial features in proximity of the proposed LS and HZ.

6.1.3 Model Parameters

The first fundamental requirement for human mission feasibility is to satisfy the engineering requirements called Engineering Constraints (EC) to safely land crews on the surface of Mars. Indeed, crew's safety is placed in emphasis in all the phases of the "Journey to Mars" because injury or loss of life could cripple the mission. This technical priority clearly highlights the importance of a careful evaluation of these constraints for the Landing Site (LS) selection.

Table 6-3 summarises the EC implemented in the workflow developed with ArcGIS *ModelBuilder*. These EC and relative assumptions will be delineated in this Section.

This Section will also clarify how the workflow is set up, how the tools for image analysis work and the adopted problem-solving approach.

Table 6-3. Engineering Constraints for Landing Site selection (modified from LPI, 2015)

#	EC	Target value
1	Latitude	50°N to 50°S
2	Elevation	Altitude ≤+2 km (MOLA)
3	Terrain relief	100 - 130 m over 1000 m baseline
4	Slope	< 15° over 20 m length scale
5	Rock height	0.5% probability of at least one ≤ 0.55 m high rock in 4 m^2 area (Rock abundance < 8%)
6	Surface wind	<15 m/s (steady); <30 m/s (gusts); steady winds never exceed 40 m/s
7	Load Bearing surface	High thermal inertia $I > 100\ Jm^{-2}K^{-1}s^{-1/2}$ Low albedo, not dominated by dust

This Section shows Gale Crater case study settings on ArcGIS *ModelBuilder* as example. Except for HRSC images, TES Thermal Inertia map and Wind Speed maps, that are input datasets peculiar for each proposed EZ, all the input parameters were set up in the same way for all the areas. This configuration grants a fast use of the model: indeed, it is only necessary to change input datasets and names of output files to run the workflow and analyse different EZs.

6.1.3.1 General Model

The general model developed in this thesis with ArcGIS *ModelBuilder* is subdivided in its three main phases that are (1) Data processing, (2) Engineering parameter map layer development, and (3) Raster reclassification described in detail in Section 6.1.2.1. The reclassified output maps are combined into a single map, which summarises all the analysed properties.

Figure 6-5 shows the general model run on Gale Crater Exploration Zone (EZ).

The structure of the model connects the output of each phase as input of the next one: this mechanism generates an automated flow that analyses the input raster datasets and produces the final result.

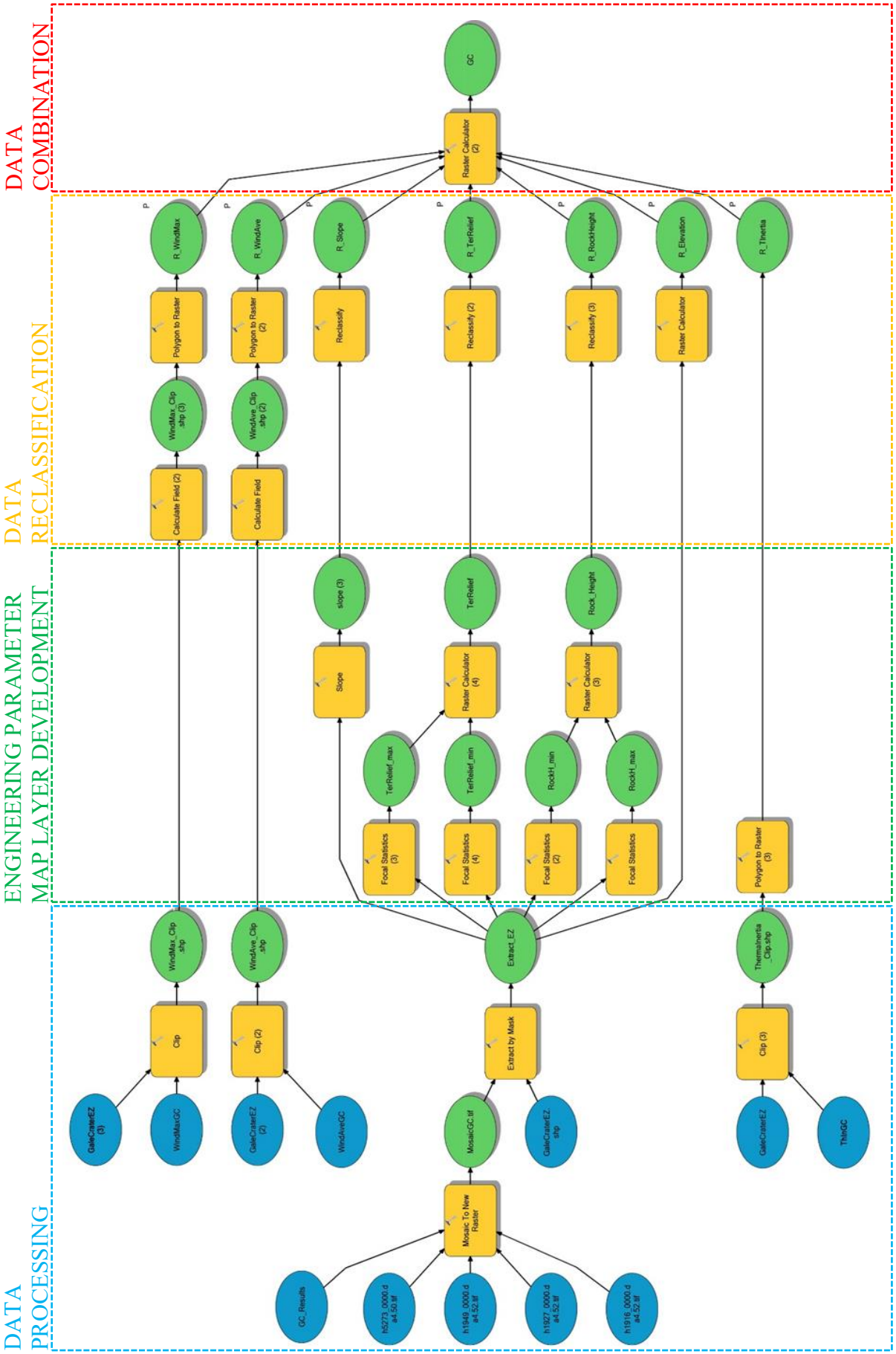

Figure 6-5. General Model

6.1.3.2 Exploration Zone Selection

The Exploration Zone (EZ) Selection phase is a preliminary phase of the model that allows merging all the input HRSC files together and extracting the proposed EZ from the merged image (see Figure 6-6).

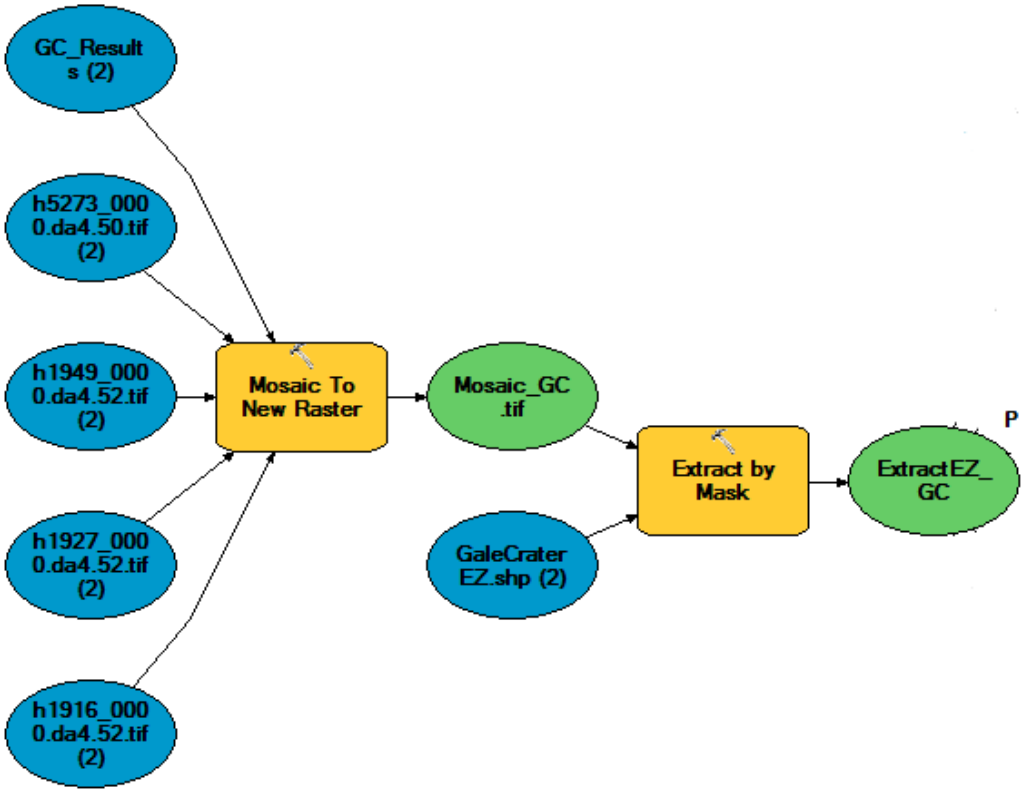

Figure 6-6. Exploration Zone Selection phase

Mosaic to New Raster tool (see Figure 6-7) merges multiple raster datasets into a new raster file. In Gale Crater case study, four different HRSC raster files with the same number of bands and bit depth were uploaded as input datasets. The merged output file has a SINUSOIDAL_MARS reference system associated and TIFF extension. The bit depth or radiometric resolution of the mosaic dataset is 32_BIT_FLOAT: the output data type is 32-bit supporting decimals. MAXIMUM Mosaic Operator is used to merge overlapping areas of the input HRSC files. Cell values in these areas will be the maximum ones of the overlapping cells. To better align these satellite images, HRSC files were preliminary georectified (see Section 6.1.2.3).

Extract by Mask tool (see Figure 6-8) extracts the cells of EZ shapefile that is the mask created on the analysed proposed area of exploration.

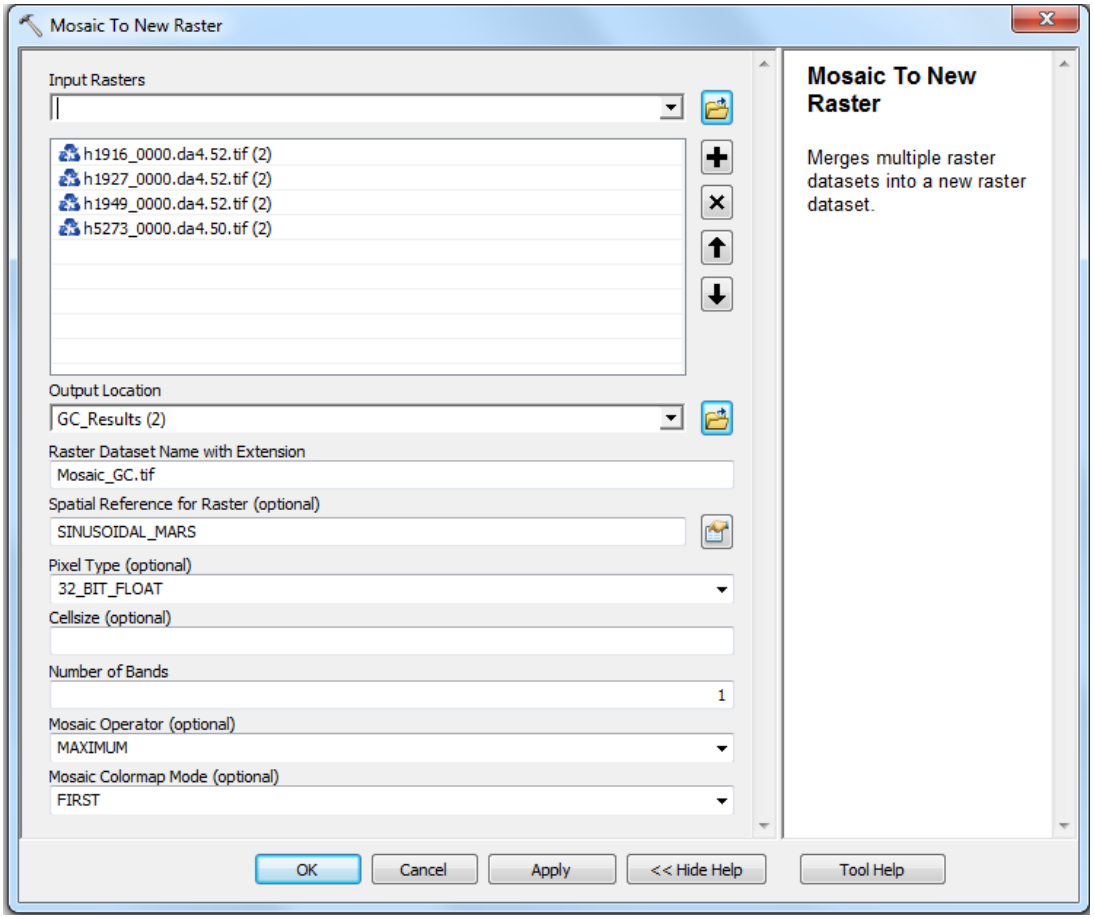

Figure 6-7. *Mosaic to New Raster* tool

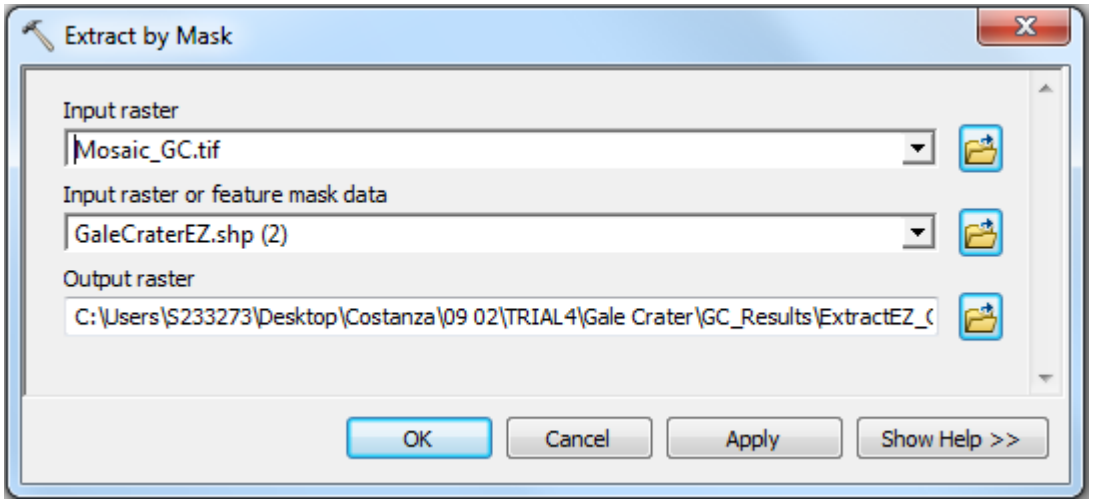

Figure 6-8. *Extract by Mask* tool

Figure 6-9 shows (a) the initial implemented HRSC datasets, (b) the mosaic output HRSC and (c) the extracted EZ.

It is possible to compare the elevation intervals. Indeed, the highest and lowest values of elevation of mosaic raster are 1830 m and -4676 m (MOLA reference system) consistently with the highest and lowest values of the four input HRSC files in Gale Crater. The extracted HRSC elevation ranges between 838 m and - 4676 m.

The extracted EZ will be the input file for Slope, Terrain Relief and Rock Height engineering parameters.

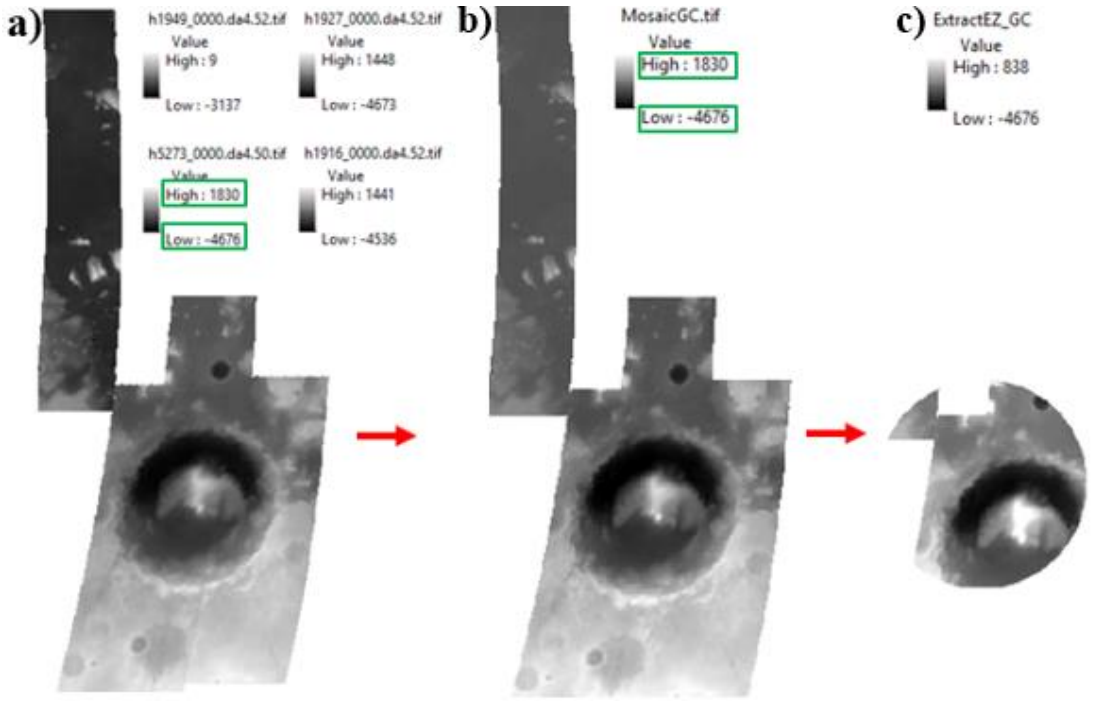

Figure 6-9. *Exploration Zone Selection* phase: a) HRSC input datasets in Gale Crater (GC); b) Merged HRSC in GC; c) GC Exploration Zone extracted from mosaic dataset

6.1.3.3 Latitude

The EZ's latitude must range between 50°N and 50°S. The developed model was run on four of the EZs proposed at the First Landing Site/Exploration Zone Workshop for Human Missions to the Surface of Mars in October 2015. These EZs satisfy this geographic requirement and, for this reason, this engineering parameter was not implemented in the automated model. As reported in APPENDIX B, Gale Crater EZ centre is located at 4.5°S, Protonilus Mensae's one at 42°N, Deuteronilus Mensae I and

II ones respectively at 39°N and 41°N. Therefore, the latitude requirement is assumed as always satisfied.

6.1.3.4 Elevation

According to Engineering Constraints (EC) for Landing Site (LS) selection, the EZ's elevation *E* must be:

$$E \leq +2km$$

in MOLA reference system.

HRSC images represent surface elevation on the base of MOLA reference system and, as consequence, the HRSC EZ output of the *Exploration Zone Selection* phase is reputed an adapt input to evaluate elevation parameter.

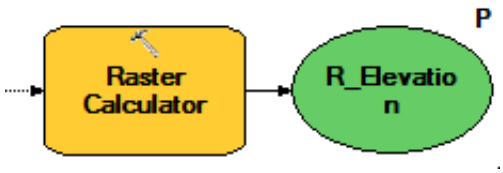

Figure 6-10. Elevation workflow

Raster Calculator tool allows building and executing a Map Algebra expression using Python syntax. The built expression is:

$$Con(\%\text{Extract\_EZ}\% \geq 2000,0,1)$$

where:

Extract_EZ is the HRSC mosaic clipped in the analysed EZ.

Con is a conditional tool that performs an if/else evaluation on each cell of the input raster file. If elevation is higher than the threshold value of 2000 m, the conditional query attributes to each of these cells a 0 value. Otherwise, the associated value is 1.

Associating a value of 1, rather than a higher value or a classification, to the cells that satisfy the prefixed elevation requirement, represent a reasonable choice. Indeed, elevation requirement is associated to environmental conditions that are considered equally acceptable if elevation is lower than 2000 m.

The final *R_Elevation* raster map represent the already reclassified elevation map.

Executing the defined Map Algebra expression allows transforming the HRSC DTM input map in a dimensionless map. This is due to the cells' associated attributes that switched from elevation with meters as unit of measure to a dimensionless index correlated to the goodness of the analysed engineering parameter.

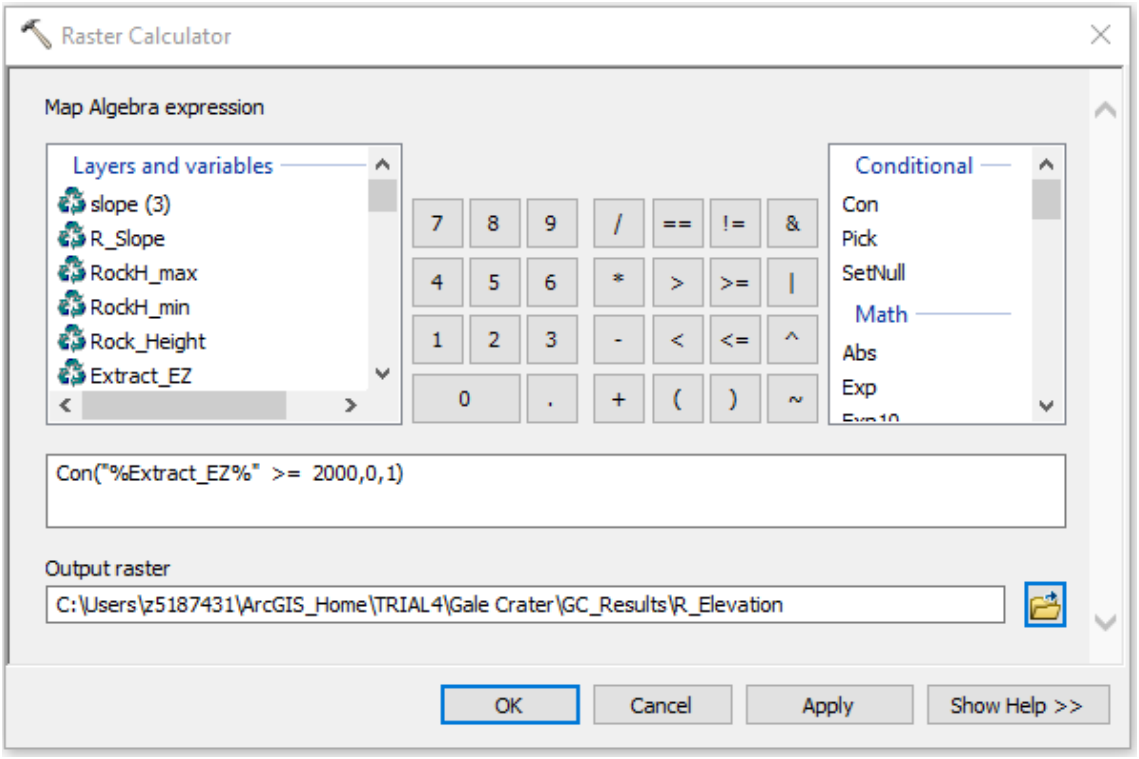

Figure 6-11. ***Raster Calculator*** **tool input set up: Elevation reclassification**

6.1.3.5 Slope

According to Engineering Constraints (EC) for Landing Site (LS) selection, the LS's slope S must be:

$$S < 15°$$

On a 20 m length scale.

HRSC DTM is used as input dataset for slope evaluation.

As shown in Figure 6-12, *Slope* tool is used for the engineering parameter map layer evaluation and *Reclassify* tool to associate an index to each reclassified range of values.

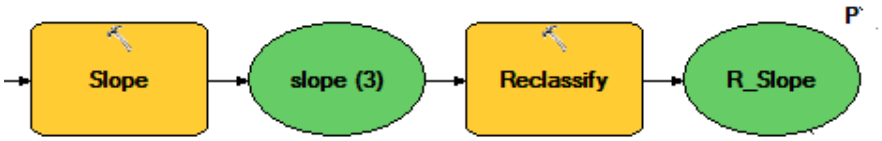

Figure 6-12. Slope workflow

Slope tool identifies the slope from each cell of a raster surface calculating the maximum elevation change in z-value over the distance between the centre of a cell and its eight neighbours' centres. The z-values of a 3x3 cell neighbourhood are ideally fitted with a plane and the slope is evaluated by the software.

The lower is the slope, the flatter is the analysed terrain; otherwise, the higher is the slope value, the steeper is the surface.

As shown in Figure 6-13, the output slope map is generated in degrees.

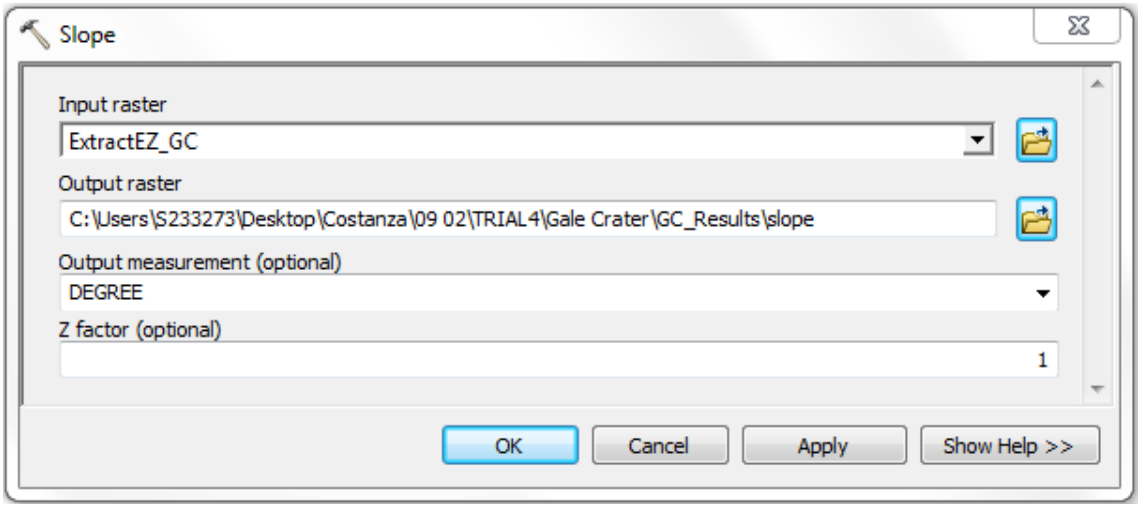

Figure 6-13. *Slope* tool

The output slope raster is reclassified with *Reclassify* tool.

This tool substitutes the attribute value of each cell with a dimensionless index as highlighted in Figure 6-14 and Figure 6-15. The cells with an associated slope between 0° and 15° are classified in 10 equal intervals (see Figure 6-16) and the other ones that does not respect the engineering requirement are excluded from this classification.

The classified acceptable slope ranges are reclassified with an index between 1 and 10; the highest index is linked to lowest slope range, while the lowest index is associated to the highest slope range.

The excluded cells with an attribute slope higher than 15° are reclassified with a 0 index. The highest slope value is assumed 90°. The choice of setting up a maximum slope that approaches vertical is consistent with the objective of creating a model adaptable to each different situation, also if 90° represents an extreme case of slope.

If necessary, slope threshold value, reclassification indexes and equal interval classification may be flexible modified and adapted to different requirements.

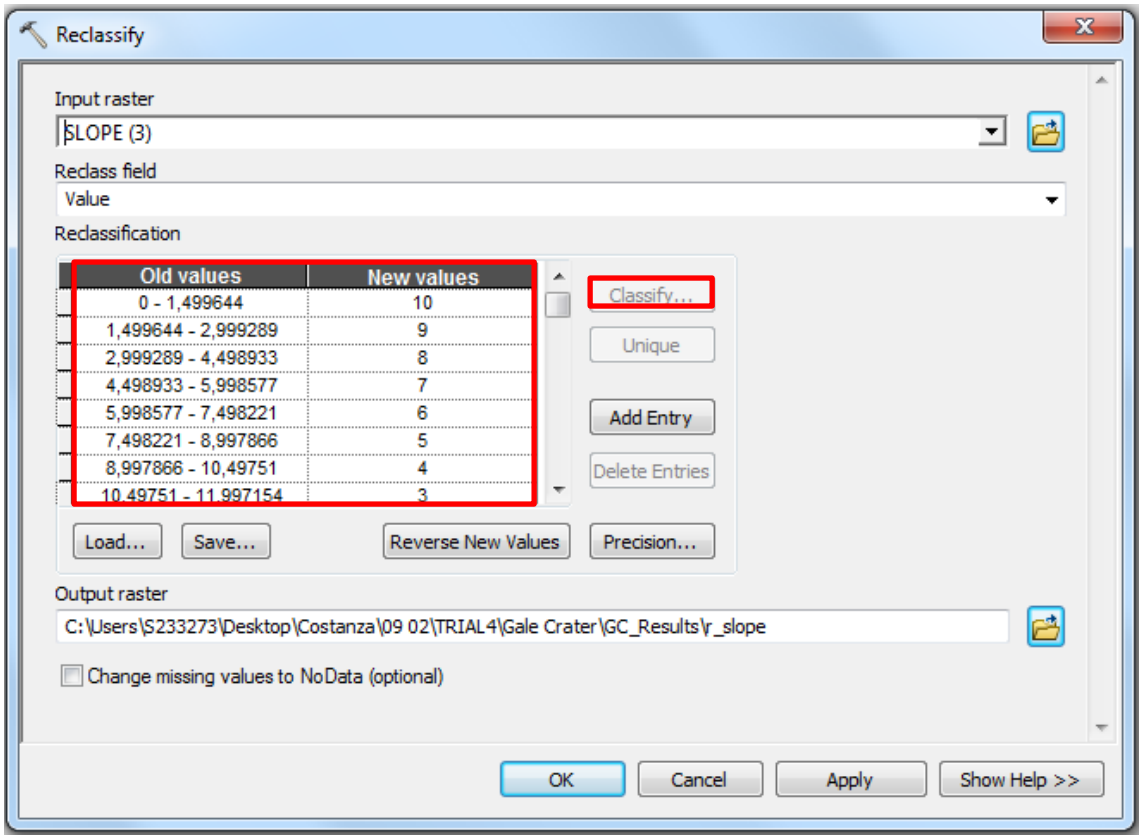

Figure 6-14. ***Reclassify*** **tool (part I): Slope reclassification**

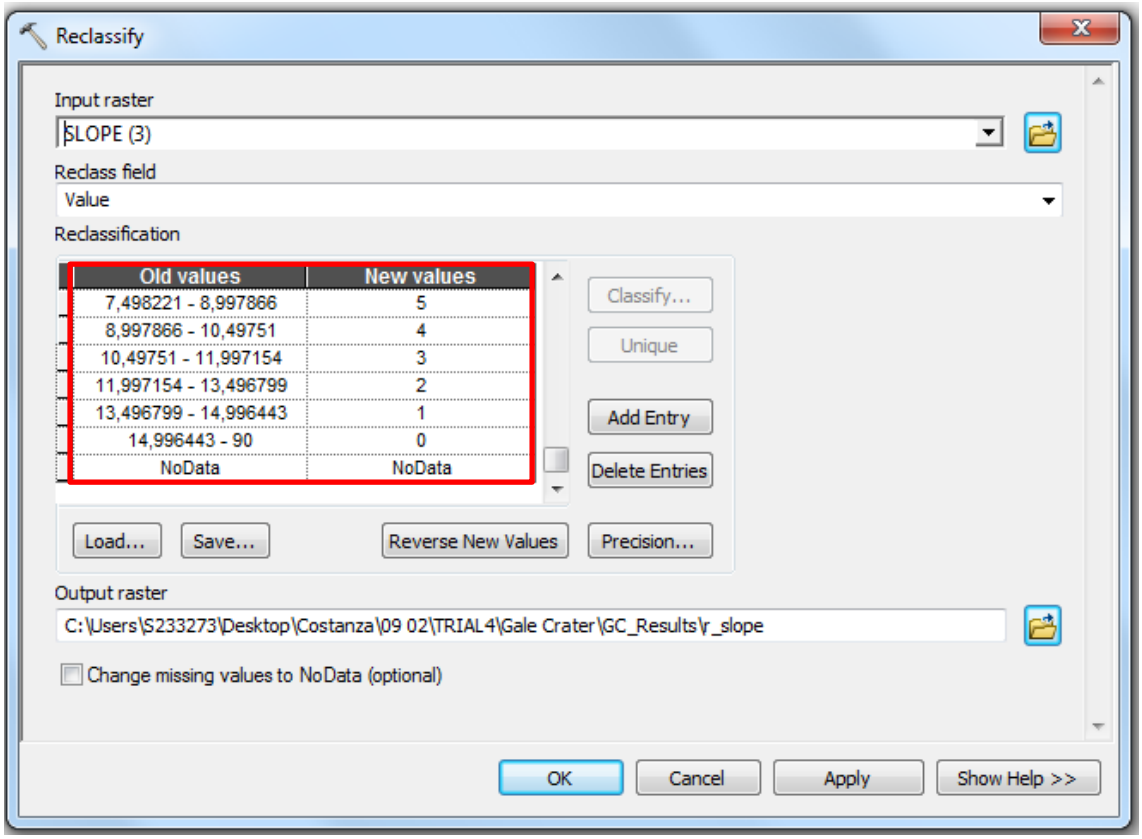

Figure 6-15. ***Reclassify*** **tool (part II): Slope reclassification**

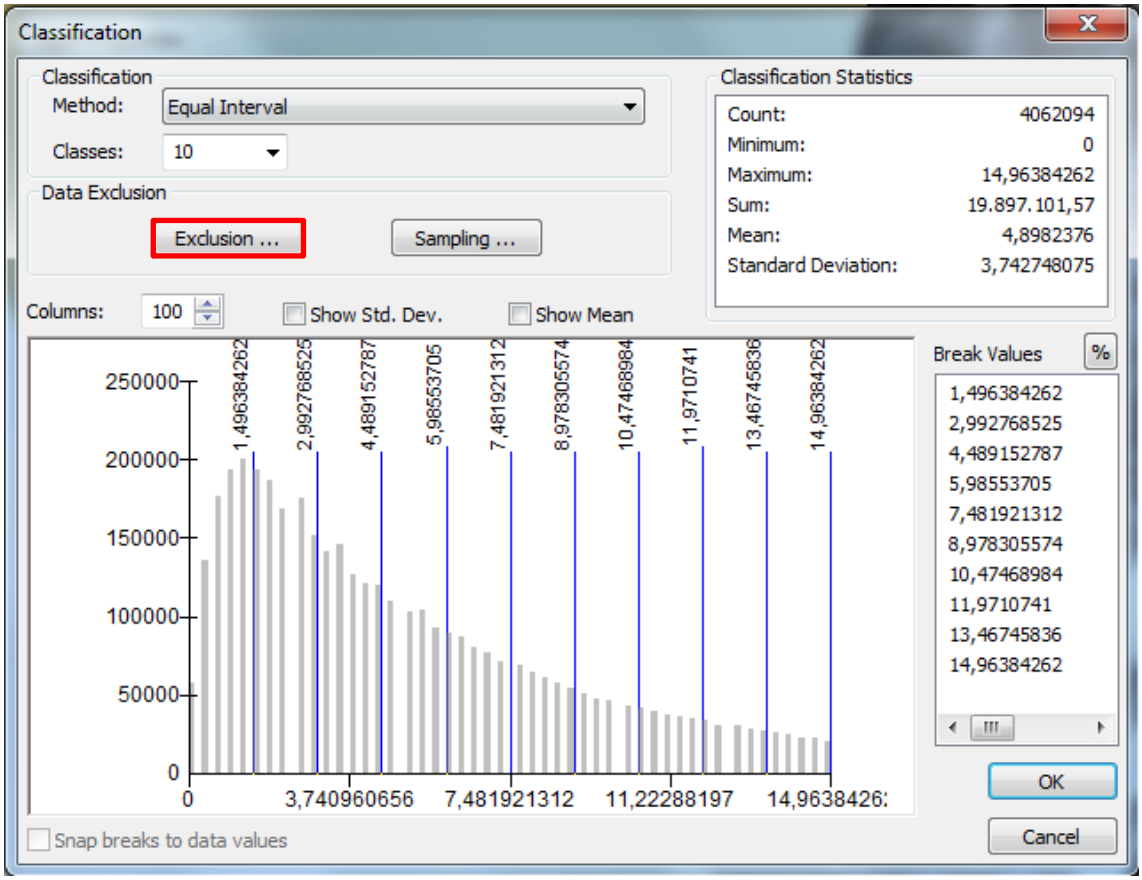

Figure 6-16. ***Classification*** **interface: Slope histogram represents the frequency of different slope angles between 0° and 15°**

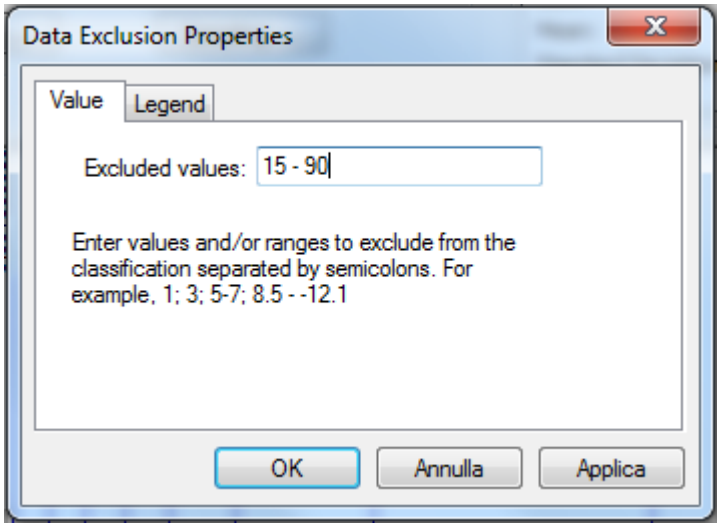

Figure 6-17. ***Data Exclusion Properties*** **interface: exclusion of slope angles between 15° and 90°**

6.1.3.6 Thermal Inertia

The list of Engineering Constraints (EC) proposed for a safe landing on Mars (LPI, 2015) includes the requirement of high thermal inertia.

To successfully emplace the crew on Mars' surface, in this model thermal inertia I is assumed:

$$I > 100\, Jm^{-2}K^{-1}s^{-1/2}$$

on the base of the constraints used for the landing of the Mars Science Laboratory (MSL) rover Curiosity at Gale Crater and of the ones set up for the future NASA's Mars 2020 mission.

Successfully landing humans to Mars requires to select a safe rocky site with a relatively low rock abundance and a low level of dust on the surface. These physical properties are closely coupled with surface temperature and, as consequence, with surface's thermal inertia and albedo measures. In the planetary science context, thermal inertia is a measure of the ability of a material to store heat during the day and reradiate it during the night time (Planetary Science Institute, 2012) and reflect both temperature oscillations and physical properties of materials. The engineering requirement of high thermal inertia is consistent with the need of landing on a rocky ground: indeed, rocks display a much higher capability to heat and remain warm during the daily cycle; on the contrary, sand and dust cool off really when temperature changes during the night.

Thermal Inertia it is defined as:

$$I = (k\rho c)^{1/2}\ \left[tiu = Jm^{-2}K^{-1}s^{-1/2}\right]$$

where:

k is thermal conductivity [W m-1 K-1];
ρ is density [kg m-3];
c is specific heat capacity [J kg-1 K-1];
tiu is thermal inertia unit (SI unit designation);

and it is related to physical properties such as grain size and degree of induration, i.e. grains cementation (Planetary Science Institute, 2012).

Figure 6-18 shows Thermal Inertia workflow.

A shapefile based on JMARS *Mars 2035 Thermal Inertia Mask* layer information is created as input for Thermal Inertia workflow. This JMARS *Mask* generated for the human EZ selection process is based on Christensen's TES Map which excludes areas with $I < 100$ $Jm^{-2}K^{-1}s^{-1/2}$ from the LS selection process. This attribute is consistent with the assumption made for this parameter in this project.

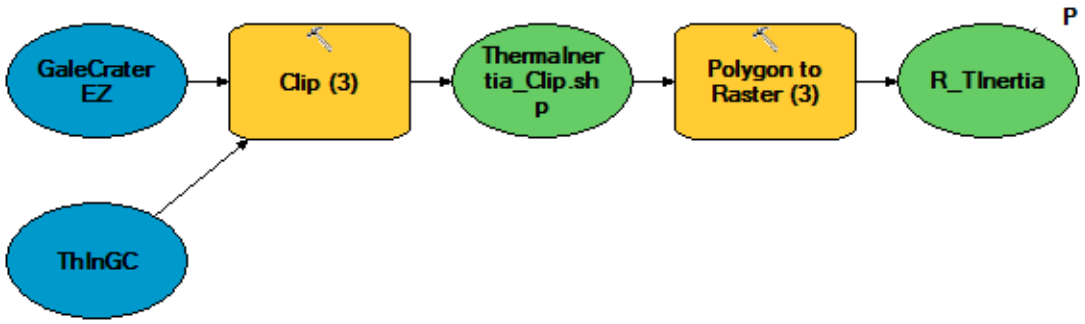

Figure 6-18. Thermal Inertia workflow

The shapefile edited on ArcGIS is a file that stores attribute information for the spatial features. This file does not have a topological geometry: for this reason, draw and edit a shapefile is fast and practical, consistently with the aim of creating a rapid first order analysis model.

Each shapefile has an associated *Attribute Table*. The thermal inertia shapefile is reclassified by creating an additional field in the attribute table: a value of 1 is associated to the zones within the engineering requirement is satisfied, otherwise a value of 0 indicates the presence of an unacceptable environmental condition.

The input thermal inertia shapefile is extracted with the overlaid EZ shapefile.

Figure 6-19 reports *Clip* tool run on Gale Crater as example: *ThInGC* shapefile generated in Gale Crater area is cut out with *GaleCraterEZ* clip feature.

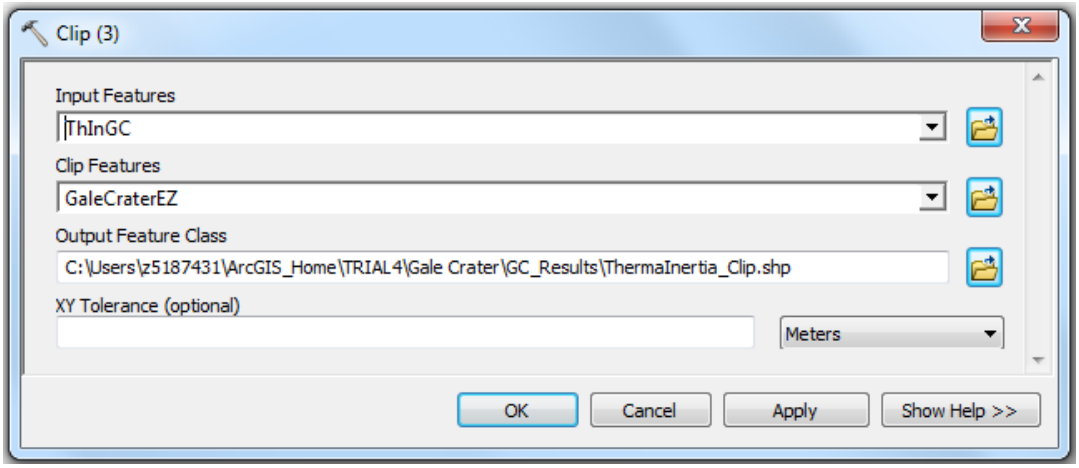

Figure 6-19. *Clip* tool: Thermal Inertia shapefile extraction

The shapefile extracted with *Clip* tool is converted to raster dataset with *Polygon to Raster* tool (see Figure 6-20). This conversion will allow associating thermal inertia information with the other raster datasets. Indeed, it is not possible to combine reclassified output maps with different file extensions into a single map. *Value field* is the field used to assigns attribute values to the output raster file. To complete this process, the index associated to the reclassification of the input feature is set up.

Cellsize parameter is the cell size for the output dataset. Consistently to HRSC DTM resolution, the input raster files used to process Elevation, Slope, Terrain Relief and Rock Height engineering parameters, a value of 75 m/pixel is chosen (see Figure 6-20).

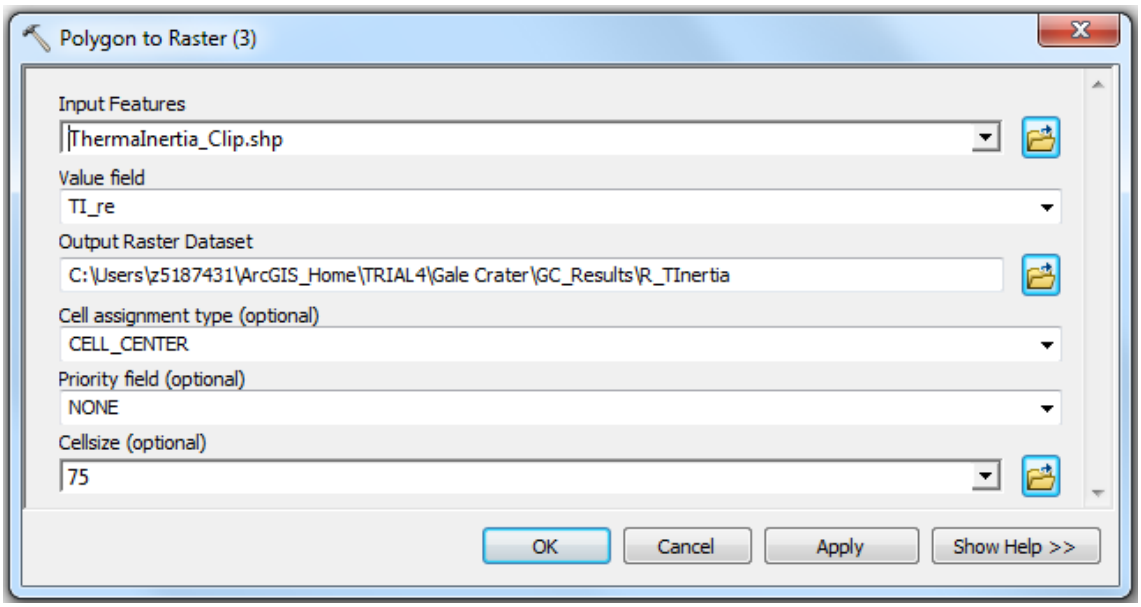

Figure 6-20. *Polygon to Raster* tool: Thermal Inertia shapefile conversion

6.1.3.7 Terrain Relief

According to Engineering Constraints (EC) for Landing Site (LS) selection, the LS's Terrain Relief *TR* must be:

$$TR < 100 \div 130\ m$$

over 1000 m baseline.

Therefore, terrain relief measures the change of vertical elevation over a baseline.

Figure 6-21 shows Terrain Relief workflow.

The core idea developed to analyse this parameter is to (1) identify the maximum elevation value on a 1000 m length scale, (2) identify the minimum elevation value on a 1000 m length scale, (3) calculate the difference between these values, and (4) reclassify the output map.

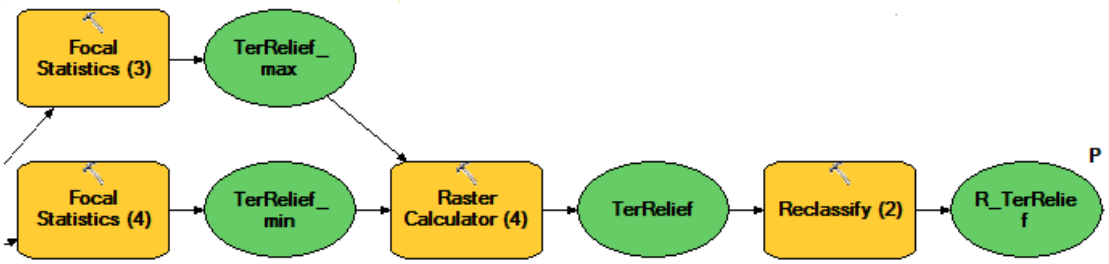

Figure 6-21. Terrain Relief workflow

Focal Statistic tool calculates a statistic of the values within a specified neighbourhood around each input cell. A square neighbourhood with both width and height of 13 cells is set up. Indeed, 13 cells of a HRSC DTM raster file with a resolution of 75 m/pixel has a length of 975 m. As consequence, analysing 13 cells constitutes a conservative choice if compared with the engineering requirement of a 1000 m baseline.

The MAXIMUM and MINIMUM Statistic types respectively calculate the highest and the lowest values of the cells in the neighbourhood.

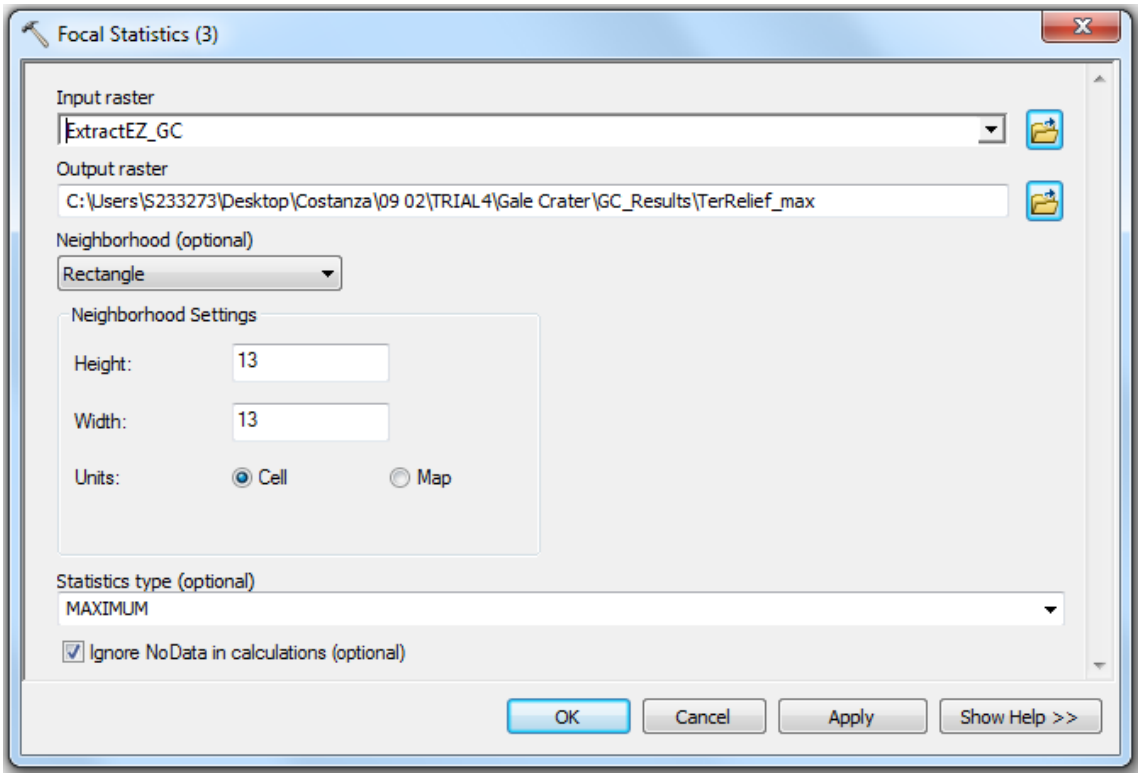

Figure 6-22. ***Focal Statistics*** **tool: evaluation of the maximum elevation value in the neighbourhood of 13 cells**

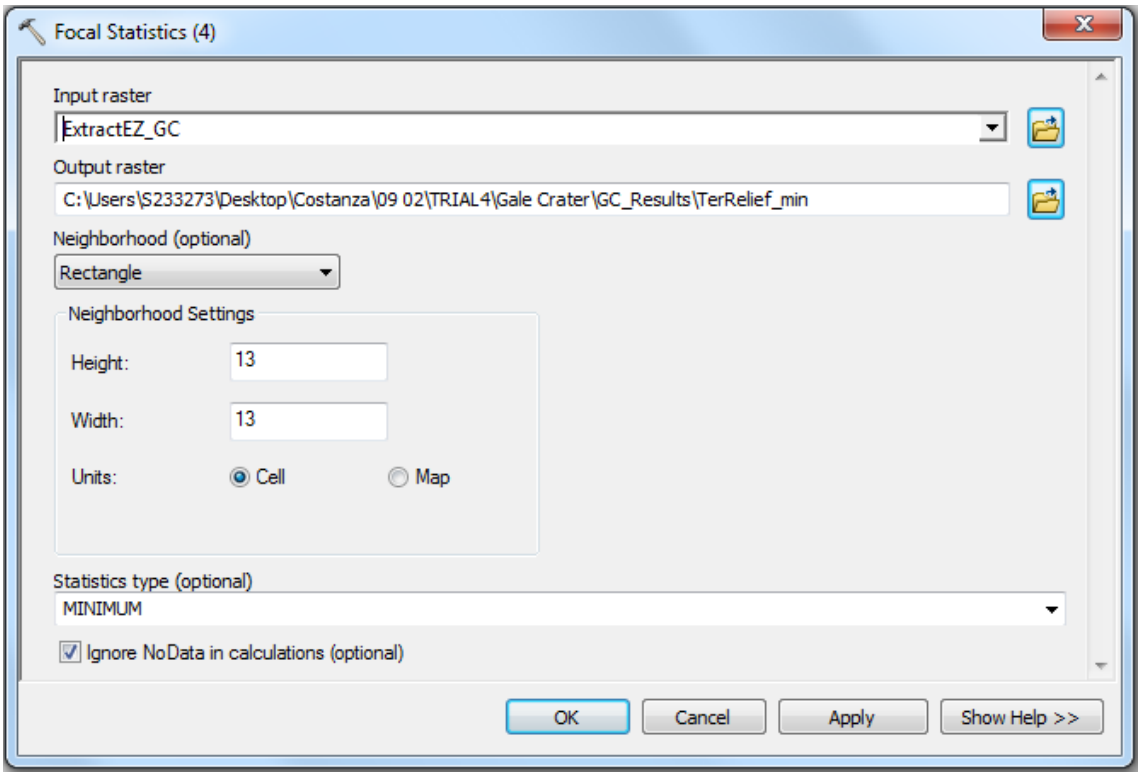

Figure 6-23. ***Focal Statistics*** **tool: evaluation of the minimum elevation value in the neighbourhood of 13 cells**

Raster Calculator tool allows building and executing a Map Algebra expression using Python syntax. This tool is used to calculate terrain relief shapefile.
The built expression is:

$$\%TerRelief\_max\% - \%TerRelief\_min\%$$

where:

TerRelief_max is the output raster map of *Focal Statistics* tool runs to evaluate the maximum elevation value in the neighbourhood of 13 cells;
TerRelief_min is the output raster map of *Focal Statistics* tool runs to evaluate the minimum elevation value in the neighbourhood of 13 cells.

Figure 6-24 reports the described process.

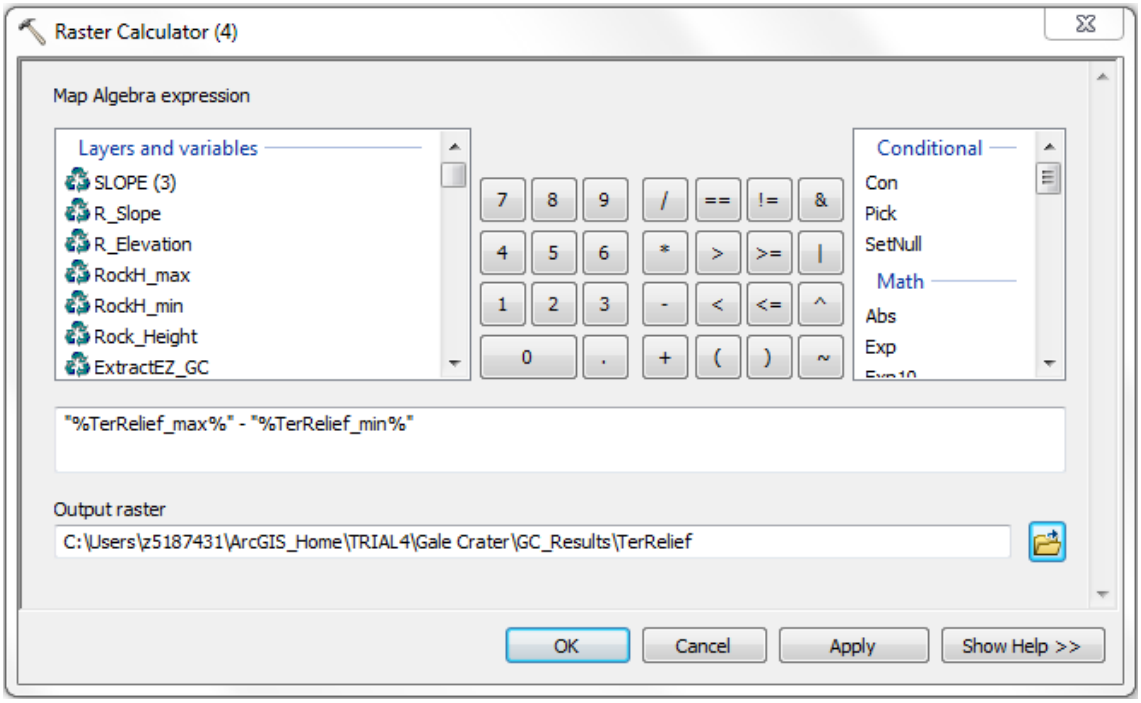

Figure 6-24. *Raster Calculator* tool: Terrain Relief shapefile generation

The output terrain relief map named *TerRelief* shows the variability of elevation over the set length scale of 975 m. This map is reclassified with *Reclassify* tool. The acceptable Terrain Relief range between 0 and 130 m is associated to a dimensionless index of 10; otherwise the cells that do not satisfy the requirement are associated to a 0 index.

Considering the conservative choice of setting a baseline of 975 m, which is shorter if compared to the admitted one, the highest terrain relief proposed value of 130 m is chosen for this reclassification.

The range of elevation, which is considered unacceptable from an engineering point of view, is set in *Reclassify* tool between 130 m and 30000 m (see Figure 6-25). This value represents the approximation of the elevation difference between the maximum and minimum values on Mars' surface. This range is calculated using *Mars MGS MOLA Elevation Model 463m*, where Olympus Mons is the highest peak with an elevation value that is around 22 km and the deepest crater is located in Hellas Planitia with an elevation value of -7.1 km. This approximation clearly represents the maximum range of elevation of the planet that won't be find within the proposed EZs and, particularly, in the Terrain Relief raster map. However, setting up this extreme range of elevation, rather than the HRSC DTM elevation interval peculiar for each EZ, efficiently responds to the need of changing the lowest number of parameters as possible to run the model on different areas. As consequence, the condition of associating a 0 value to unacceptable cells will be always be respected.

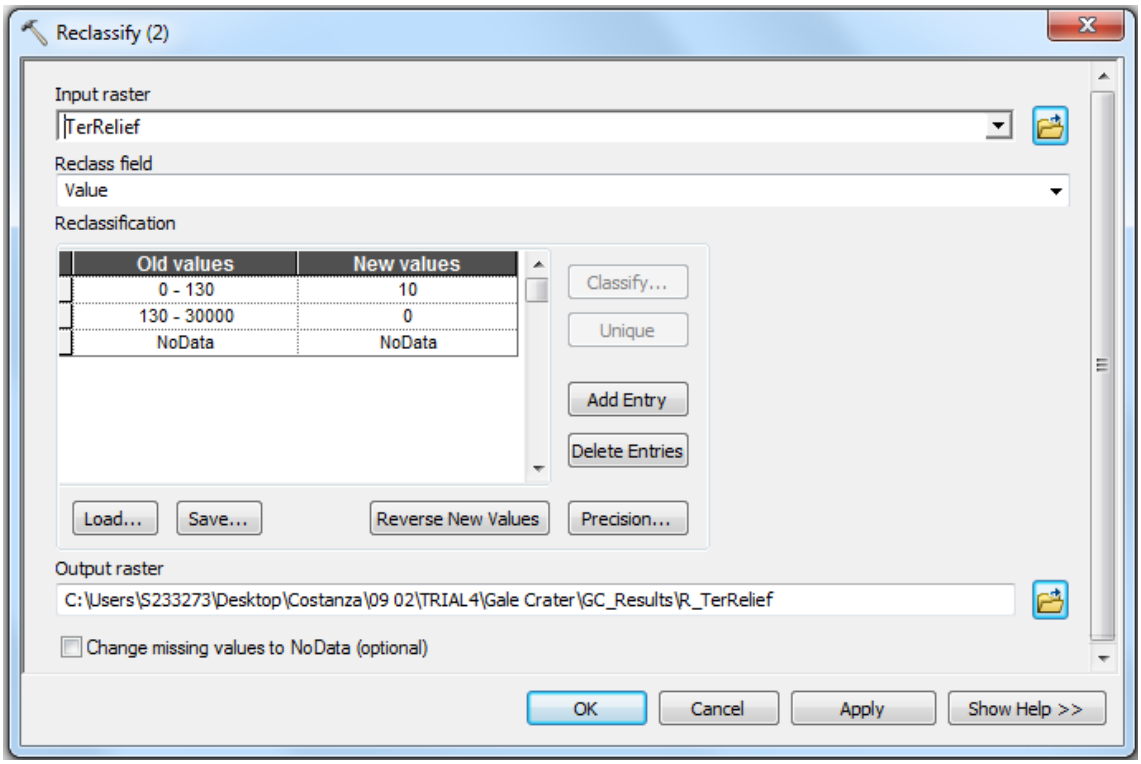

Figure 6-25. *Reclassify* tool: Terrain Relief reclassification

6.1.3.8 Rock Height

According to Engineering Constraints (EC) for Landing Site (LS) selection, the probability of finding a rock higher than 0.55 m in 4 m^2 must be lower than 0.5%. So, rock abundance must be lower than 8% to safely land on Mars' surface. This parameter is also named rock height.

Analysing this EC required making some assumptions related (1) to the processed area and (2) the rock presence probability. Indeed, the first fundamental requirement of a model that have to be run on different zones is input data availability. Unfortunately, the actual lack of high-resolution data deepened in Sections 6.1.1 and 6.1.4 does not always allow generating engineering maps with a proper level of accuracy. Rock Height evaluation constitutes a representative case because of the requirement of analysing 2 m/pixel resolution images to properly evaluate this characteristic. High Resolution Imaging Science Experiment (HiRISE) images, with its 0.3 m/pixel, may represent the proper solution. However, the few HiRISE datasets available does not satisfy the needs of the project.

The rocky bodies' presence probability is assumed 0%, rather than 0.5%. This choice of setting a more conservative and restrictive condition is reasonable considering the resolution limitations already delineated.

Rock Height workflow is shown in Figure 6-26.

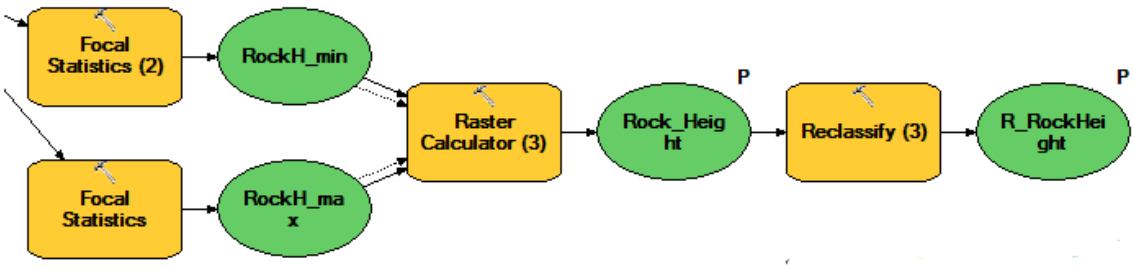

Figure 6-26. Rock Height workflow

The proposed mechanism reflects the Terrain Relief's one described in detail in the previous Section. For this reason, refer to Section 6.1.3.7 for further information. The core idea is to (1) identify the maximum elevation value over a 150 m length scale, (2)

identify the minimum elevation value over a 150 m length scale, (3) calculate the elevation difference between these values, (4) and reclassify the output map.
The length scale is a clear limitation for this parameter evaluation, but 150 m is also the minimum one that may be set up with *Focal Statistic* tool on a HRSC DTM dataset (75 m/pixel resolution). Indeed, carrying out a statistic analysis with this tool requires to set a neighbourhood of a cell: a square neighbourhood with both width and height of 2 cells, the lowest possible limit, is set up. A square composed from 2 cells of a HRSC DTM raster file with a resolution of 75 m/pixel has a side length of 150 m.

Raster Calculator tool is used to calculate Rock Height shapefile.
The built expression is:

$$\%RockH\_max\% - \%RockH\_min\%$$

where:

RockH_max is the output raster map of *Focal Statistics* tool runs to evaluate the maximum rock height in the neighbourhood of 2 cells;
RockH_min is the output raster map of *Focal Statistics* tool runs to evaluate the minimum rock height in the neighbourhood of 2 cells.

The output map shows differences between rock heights in a 150x150 m^2 area.

This map is reclassified with *Reclassify* tool. The acceptable Rock Height ranges between 0 and 0.5 m and it is associated to a dimensionless index of 10; otherwise, the cells that do not satisfy the requirement are associated to a 1 index. The association of indexes that are different from 0 implies that the cells considered unacceptable from an engineering point of view won't be excluded from the landing site selection. Indeed, the underlined lack of data highlights the need to make different assumptions. Hence, not to exclude these cells and this Engineering Constraint (EC) from this study, it is considered a reasonable choice for this study, programming a model that considers all the required parameters. Moreover, this parameter may be further optimised in the future times when HiRISE data will be available.

6.1.3.9 Annual Maximum Wind Speed

According to Engineering Constraints (EC) for Landing Site (LS) selection, the LS's maximum wind speed *v* during gusts must be:

$$v_{max,\ gust} < 30 \frac{m}{s},$$

and, steadily:

$$v_{max,\ steady} < 40 \frac{m}{s}.$$

The Maximum Wind Speed workflow is shown in Figure 6-27.

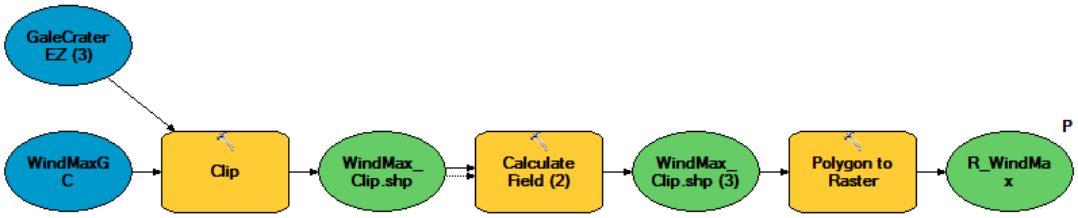

Figure 6-27. Annual Maximum Wind Speed workflow

The workflow input file is a shapefile drawn on the base of JMARS *Annual maximum wind speed* layer information (see Section 6.1.1.1). The wind velocity information associated to each area of the shapefile is joined as additional field to the attribute table of the edited non-topological map.

It is necessary to justify the choice of naming this parameter as 'annual'. Indeed, as specified in Sections 3.2 and 6.1.1.1, planetary wind system is driven by both horizontal variations of temperature and associated pressure variations (Leovy, 2001) and, on the base of this information, a General Circulation Model (GCM) is simulated. This GCM is based on different observed parameters that are related to specific time and condition. These numerical simulation models are, indeed, built for each planned mission to forecast the expected situation on Mars' surface. Wind speed parameter varies a lot around the planet, but the reduced atmospheric pressure gives the benefit that wind does not pose a significant operational threat (NASA, 2016b).
JMARS information used for drawing the input shapefiles refer to 26th Martian year.

The input maximum wind speed shapefile is extracted with the overlaid EZ shapefile. Figure 6-28 reports *Clip* tool settings on Gale Crater case study: *WindMaxGC* shapefile generated in Gale Crater area is cut out with *GaleCraterEZ* clip feature.

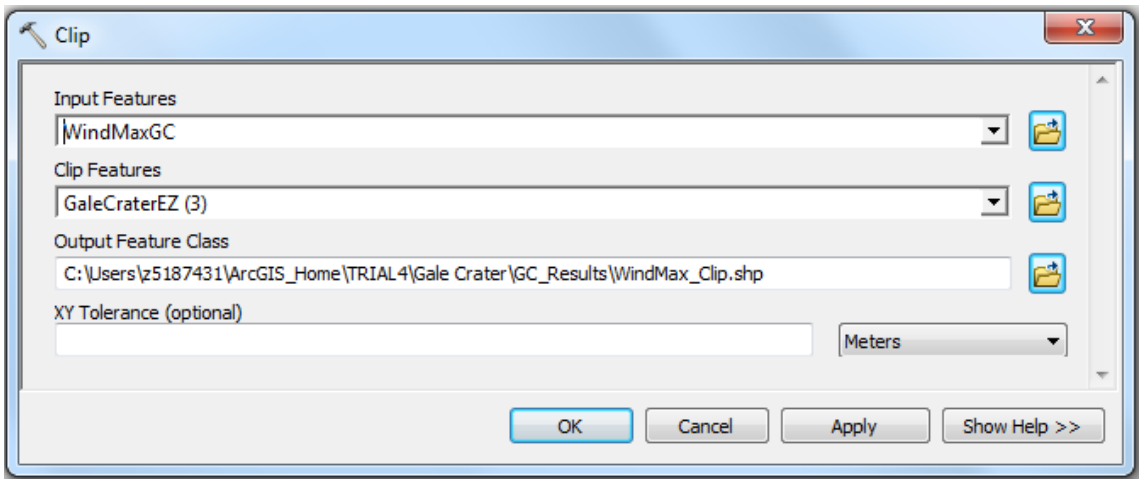

Figure 6-28. *Clip* tool: Annual Maximum Wind Speed extraction

The implemented tool used to reclassify a shapefile is *Calculate Field.* This tool allows calculating a specific field associated to a shapefile attribute that, in this case, is wind speed expressed in m/s.

Table 6-4 summarises the correlations between ranges of wind speed and indexes. To have a more conservative approach, gusts maximum velocity of 30 m/s is set up as maximum acceptable value, rather than considering the higher threshold value of 40 m/s steady wind speed. The lower ranges of wind speed are associated to higher indexes, higher ranges are linked to lower indexes.

Table 6-4. Attribute indexes associated to annual maximum wind speed ranges

v_{range} [m/s]	index [-]
0 ÷ 3.00	10
3.01 ÷ 6.00	9
6.01 ÷ 9.00	8
9.01 ÷ 12.00	7
12.01 ÷ 15.00	6
15.01 ÷ 18.00	5
18.01 ÷ 21.00	4

21.01 ÷ 24.00	3
24.01 ÷ 27.00	2
27.01 ÷ 30.00	1

To obtain the Annual Maximum Wind Speed reclassified shapefile, in which indexes associated to cells are inversely proportional to wind speed, the following expression is implemented in *Calculate Field* tool (see Figure 6-28 and Figure 6-29):

$$I_{recl} = I_{max} - int\left(\frac{v_{area}}{\left({}^{v_{max,ad}}/_{n_{classes}}\right)}\right)$$

$$= 10 - int\left(\frac{v_{area}}{\left({}^{30}/_{10}\right)}\right)$$

where:

I_{recl} is the index attributed to a specific area of the input data at the end of field calculation;
I_{max} is the maximum index of the proposed classification;
v_{area} is the value of wind speed associated to a specific area of the input shapefile;
$v_{max,ad}$ is the maximum admitted velocity;
$n_{classes}$ is the number of classes considered for reclassification process;
int( ) is a function that rounds down a real number to an integer.

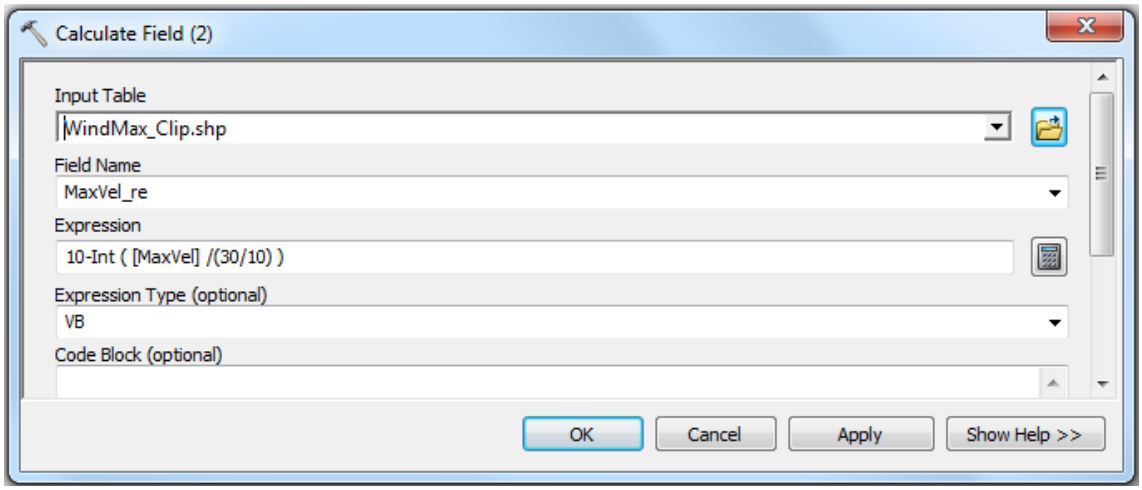

Figure 6-29. *Calculate Field* tool: Wind shapefile extraction

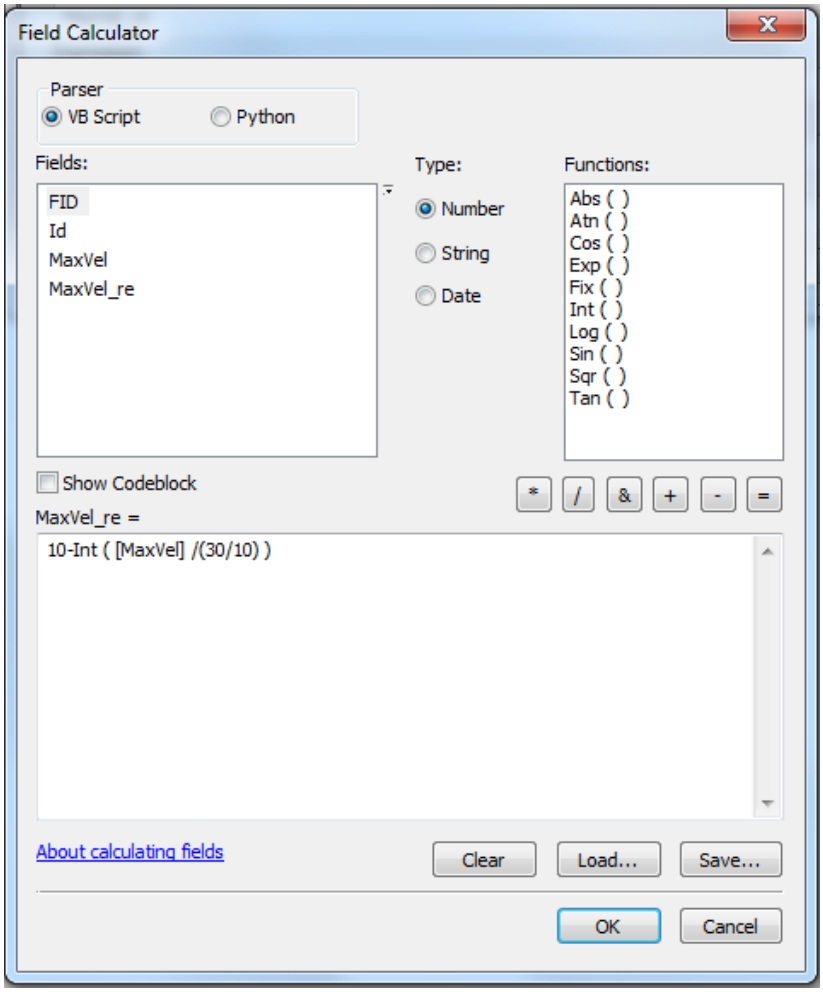

Figure 6-30. ***Field Calculator*** **tool: expression implementation**

The output shapefile is converted to raster dataset with *Polygon to Raster* tool. This conversion will allow associating wind speed information with the other raster datasets. The shapefile extracted with Clip tool is converted to raster dataset with Polygon to Raster tool (see Figure 6-20). This conversion will allow associating thermal inertia information with the other raster datasets.

Cellsize parameter is the cell size for the output dataset. Consistently to HRSC DTM resolution, the input raster files used to process Elevation, Slope, Terrain Relief and Rock Height engineering parameters, a value of 75 m/pixel is chosen (see Figure 6-31).

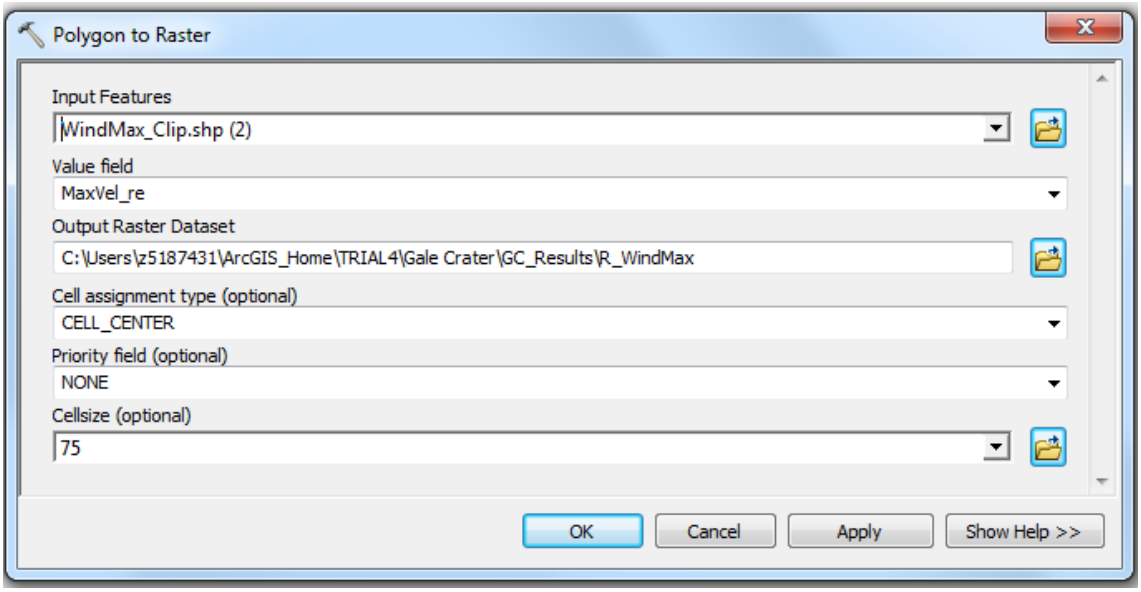

Figure 6-31. *Polygon to Raster* tool: Annual Maximum Wind Speed conversion

6.1.3.10 Annual Average Wind Speed

According to Engineering Constraints (EC) for Landing Site (LS) selection, the LS's average wind speed *v* must be:

$$v_{max,\ steady} < 15\frac{m}{s}.$$

The Maximum Wind Speed workflow is shown in Figure 6-32.

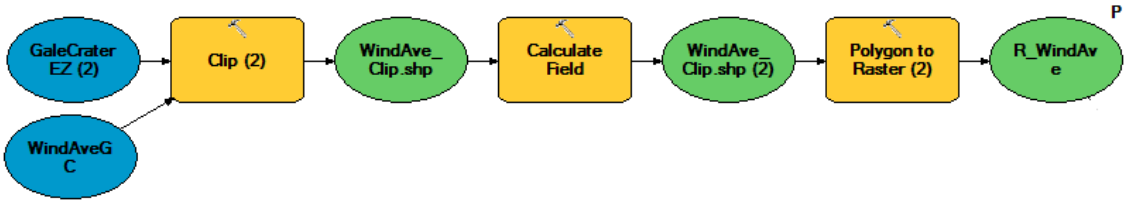

Figure 6-32. Annual Average Wind Speed workflow

The process mechanism retraces the same steps of Annual Maximum Wind Speed engineering parameter described in the previous Section.

The input workflow differences are (1) the maximum threshold velocity value that is 15 m/s rather than 30 m/s, and (2) the wind speed ranges, which are shown in Table 6-5.

To obtain further information and details related to the editing process, refer to Section 6.1.3.9.

Table 6-5. Attribute indexes associated to annual average wind speed ranges

v_{range} [m/s]	index [-]
0 ÷ 1.50	10
1.51 ÷ 3.00	9
3.01 ÷ 4.50	8
4.51 ÷ 6.00	7
6.01 ÷ 7.50	6
7.51 ÷ 9.00	5
9.01 ÷ 10.50	4
10.51 ÷ 12.00	3
12.01 ÷ 13.50	2
13.51 ÷ 15.00	1

6.1.3.11 Final Raster Map

The raster output maps obtained from the previous processes are combined into a single map, which summarises all the analysed properties.

Figure 6-33 shows the Final Raster Map calculation workflow.

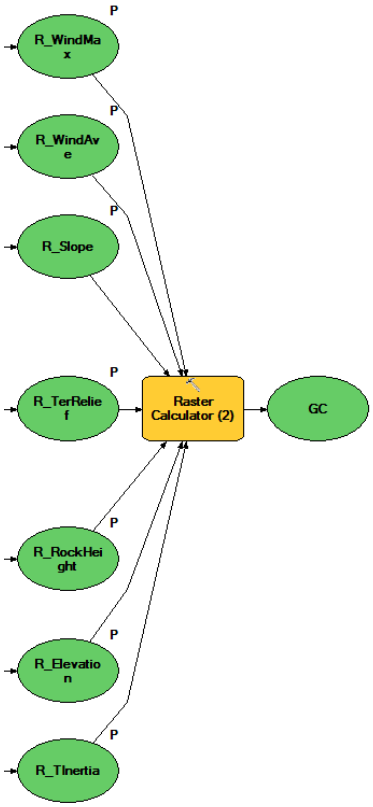

Figure 6-33. Final Raster Map workflow

Raster Calculator tool allows building and executing a Map Algebra expression using Python syntax (see Figure 6-34).
The built expression is:

$$\left[(WF \times R_{Elevation}) \times \left(WF \times R_{Slope}\right) \times (WF \times R_{ThermalInertia}) \times \left(WF \times R_{TerrainRelief}\right)\right] \times \left[\left(WF \times R_{RockHeight}\right) + \left(WF \times R_{MaxWindSpeed}\right) + \left(WF \times R_{AveWindSpeed}\right)\right]$$

where:

WF is a weight factor for the engineering parameter;
R_{xxx} is a reclassified output map obtained from previous model phases.

As shown in Figure 6-34, a WF = 1 is set up for this study. However, the choice of allowing to associate a weight to each reclassified map uploaded in the final expression constitutes one strengthen of the model built in this work. Indeed, this model can be run and used in different fields of application and this WF allows providing a higher weight to most influential parameters of the specific study. As consequence, the output map will proportionally depend on the weight that each engineering parameter assumes in each study.

The final output map is a raster file in which each cell has an attribute value determined by all the values that the same cell assumes in all the reclassified maps.

Elevation, Thermal Inertia and Terrain Relief ECs evaluation is properly conducted with the developed model and is consistent with the defined engineering requirements. Indeed, as specified in the previous Sections, these parameters have been properly evaluated by the built workflow. As consequence, it is reasonable to exclude a cell from the LS selection process if only one of these parameters result as not satisfied.
A comparison analysis between Slope evaluation on a zone where both CTX and HRSC DTM datasets are available showed that the error related to images' resolution is not relevant when the slope raster file is reclassified. For this reason, Slope reclassified map is inserted in the first part of the implemented expression.
This expression section multiplies the cells' attributes, which are the indexes associated to the maps with the reclassification process: though if only one cell has 0 as attribute value, the value of the cell in the final raster map will be 0 and it will be excluded from selection.

Rock Height, Annual Average Wind Speed and Annual Maximum Wind Speed maps are summed and, then, multiplied for the other raster maps. These parameters are affected by limitations explained in the previous Sections. Despite this aspect, it is considered reasonable to implement also these parameters in the model and to make some assumptions justified both (1) by the need of fulfil the lack of high-resolution data to properly evaluate Rock Height EC and (2) by the high variability in time and space of

Wind Speed parameter. Following this idea, the model is complete of all the EC. The choice of multiplying the sum of these parameters highlights the necessity to implement this developed model when the required data will be available.

A strengthen of the built set up is the short time required to modify the expression to update and upgrade this model.

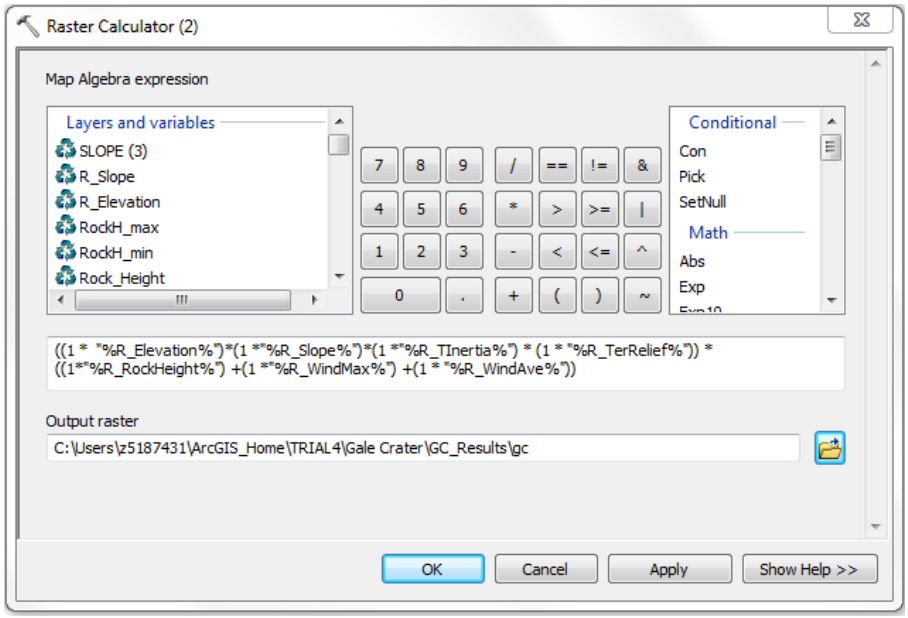

Figure 6-34. *Raster Calculator* tool: Final Raster Map expression

6.1.4 Assumptions and Justifications

The Automated Landing Site Optimization Model developed in this thesis incorporates a range of assumptions that were made where necessary to address gaps in data availability to meet project objectives. This Section both justifies the choices undertaken during the project development and underlines the necessity to improve the model with increasing data availability.

6.1.4.1 Lack of data

Despite the technological development provided data with an increasing level of detail over the years, the collected information that are growing in quantity and quality over the years are not sufficient to satisfy the actual model requirements. However, nowadays new missions have already been planned to collect further data and information that will be useful to emplace the first humans on Mars.

Rock Height engineering parameter requires to evaluate rock abundance within a 4 m^2 scale. To properly conduct this analysis, a 2 m/pixel or higher resolution is needed (see Section 6.1.3.8). High Resolution Imaging Science Experiment (HiRISE) camera provided the highest-resolution images from Martian orbit, with a 0.3 m/pixel resolution. Unfortunately, few zones have already been mapped with these high-resolution images. This lack of data does not allow to properly evaluate Rock Height parameter. Despite this gap, this variable is added in the model workflow, with the aim of upload the parameter analysis when HiRISE datasets will be available.

Slope EC must be evaluated on a 20 m length scale. Context Camera (CTX) images represent a valid alternative to HRSC DTM datasets because of the higher resolution of 5.6 m/pixel. This resolution allows to properly evaluate this engineering parameter.
CTX images have higher availability if compared with HiRISE data. However, running the model developed in this thesis on CTX present a list of disadvantages, that are related to:

1) Data availability; despite CTX's diffusion on Mars' surface is higher than HiRISE's one, different areas are not properly mapped with the Context Camera. This lack of data constitutes a great obstacle to the aim of the work that is creating an automated model for the optimisation of landing site selection: indeed, if it is not possible to run the model on the proposed EZ because input maps are not available, this first order analysis cannot be conducted;

2) Data size and geometry; CTX file size is extremely higher than HRSC one. This is due to CTX resolution of 5.6 m/pixel, around 13 times higher than HRSC DTM resolution. In addition to this, CTX typical dimensions are 30 km wide and 160 km long and HRSC typical swath is 52 km and its minimum strip length is 300 km (DLR, 2017). The direct consequence is that to cover the same surface area, it is necessary to download a higher number of CTX files. These factors imply higher time (1) to download CTX files to cover the same surface geometry and (2) to process input files with the developed model.

In addition to these observations, the error generated in analysing slope in HRSC DTM does not particularly influence the reclassified slope map (see Section 6.1.3.11).

These factors justify the choice of using HRSC DTM to conduct a fast and efficient first order analysis of Mars' surface to safely land the first crews to the Red Planet.

6.1.4.2 Albedo and Thermal Inertia

As shown in Table 6-3, a surface that presents high thermal inertia, low albedo and that is not dominated by dust is done is required to safely land the first crews on Mars. These three different aspects are directly related: indeed, a rocky ground that grants a safe landing phase has a high capacity of store heat and does not diffuse reflection of solar radiation with the same intensity of a surface dominated by dust. For both this direct correlation and the absence of a specified required value of thermal inertia and albedo, the only thermal inertia parameter is implemented in the developed model. The threshold value of thermal inertia of Mars Science Laboratory (MSL) Curiosity rover is implemented as minimum acceptable value of this model. This is consistent with the other EC acquired from the landing site selection process of MSL's spacecraft.

6.1.5 Model Flexibility

A distinctive aspect of the model developed in this work is its flexibility.

As shown in the methodology description (1) the principles adopted to reclassify input datasets, (2) the indexes associated to the different ranges of values, (3) the weight that each implemented parameter assumes for the final output map, and (4) the final expression syntax, may be easily varied. In addition to this strengthen, (4) further parameters can be entered to the workflow as required. This model may be (5) run on different exploration zones and (6) implemented when high-resolution datasets will be available.

The choice to grant flexibility to this work is consistent with the dynamic mission's objectives and constraints evolution.

This model design allows identifying the optimal landing areas from an engineering point of view and comparing different exploration zones proposed for this pioneering mission in a quantitative, fast and effective way.

7 RESULTS

This Section reports the output results obtained with the automated flexible model developed in this thesis. This tool, based on defined Engineering Constraints (EC), improves the selection process replacing time consuming and subjective manual analysis of datasets.

The model is run on four different proposed Exploration Zones (EZs): (1) Gale Crater (GC), (2) Protonilus Mensae (PM), (3) Deuteronilus Mensae I (DMI) and (4) Deuteronilus Mensae II (DMII).

Running the model on GC EZ allows testing and validating the effectiveness of the model. Indeed, the constraints used for the landing of the Mars Science Laboratory (MSL) rover Curiosity on GC were incorporated into the tool developed in this project.

The following Sections show (A) the geographical framework, (B) both the EC map layer and the reclassified raster file of (1) Elevation, (2) Slope, (3) Terrain Relief, (4) Rock Height, (5) Thermal Inertia, (6) Annual Maximum Wind Speed, and (7) Annual Average Wind Speed, and (C) the final raster map of all the analysed EZs.
Section 7.1.3 provides evidence of model effectiveness, which will be properly justified in Section 8.
Section 7.2.5 shows three different possible configurations of both the landing and habitation sites within PM EZ.
Section 7.5 reports a comparison between the obtained final maps that summarise all the analysed properties.

All this output results will be discussed and justified in Section 8.

7.1 Gale Crater Exploration Zone

7.1.1 Geographical Framework

Figure 7-1 provides the geographical framework of Gale Crater (GC) Exploration Zone (EZ). GC EZ centre is located at 4.5°S and MSL's Curiosity rover landed on this EZ in 2012 (see Figure 7-1).

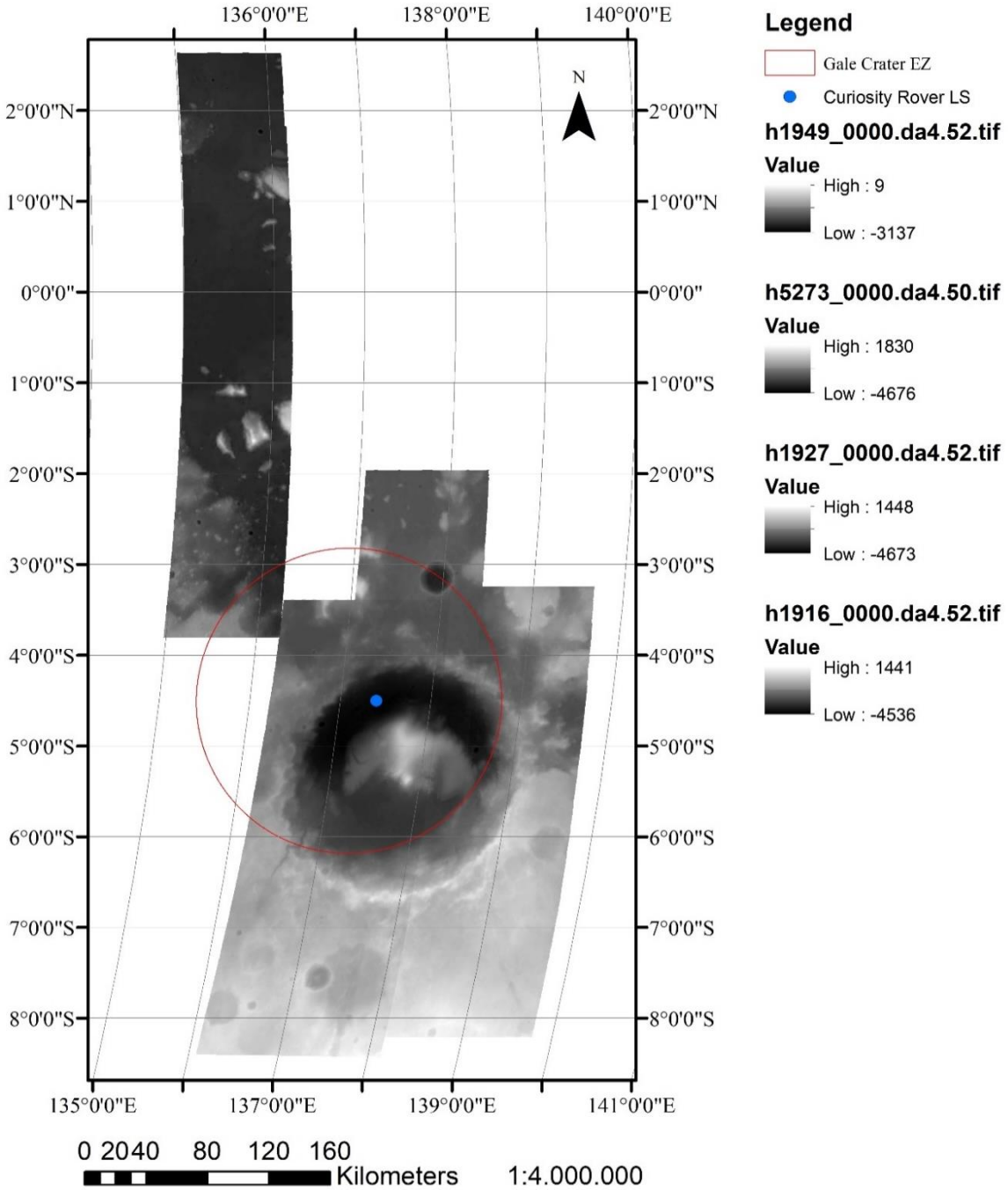

Figure 7-1. Gale Crater (GC) Exploration Zone (EZ): geographical framework; HRSC DTM images (75 m/pixel resolution)

7.1.2 Engineering Parameters Maps and Reclassified Maps

This Section reports the output maps obtained in Gale Crater (GC) Exploration Zone (EZ).

The engineering map layers of (1) Elevation, (2) Slope, (3) Terrain Relief, and (4) Rock Height are automatically generated from the workflow developed in this thesis. Otherwise, (5) Thermal Inertia, (6) Annual Maximum Wind Speed, and (7) Annual Average Wind Speed engineering map layers are drawn as shapefiles and uploaded as input files in the model (see Section *6.1.3 Model Parameters*).

All these maps show how each engineering parameter varies within GC. Each map is then reclassified by associating a specific index to a defined range of values. The associated indexes (1) are consistent with defined Engineering Constraints (see Table 6-3) and (2) are directly related to goodness of each parameter.

All the introduced maps are shown in this Section.

With the aim of better delineating all the model phases, the output raster maps obtained with *Focal Statistic* tool (see Sections 6.1.3.6 Thermal Inertia and 6.1.3.7), describing both the maximum and minimum values of Rock Height and Terrain Relief respectively in the neighbourhood of 2 and 13 cells, are exclusively reported in this Section.

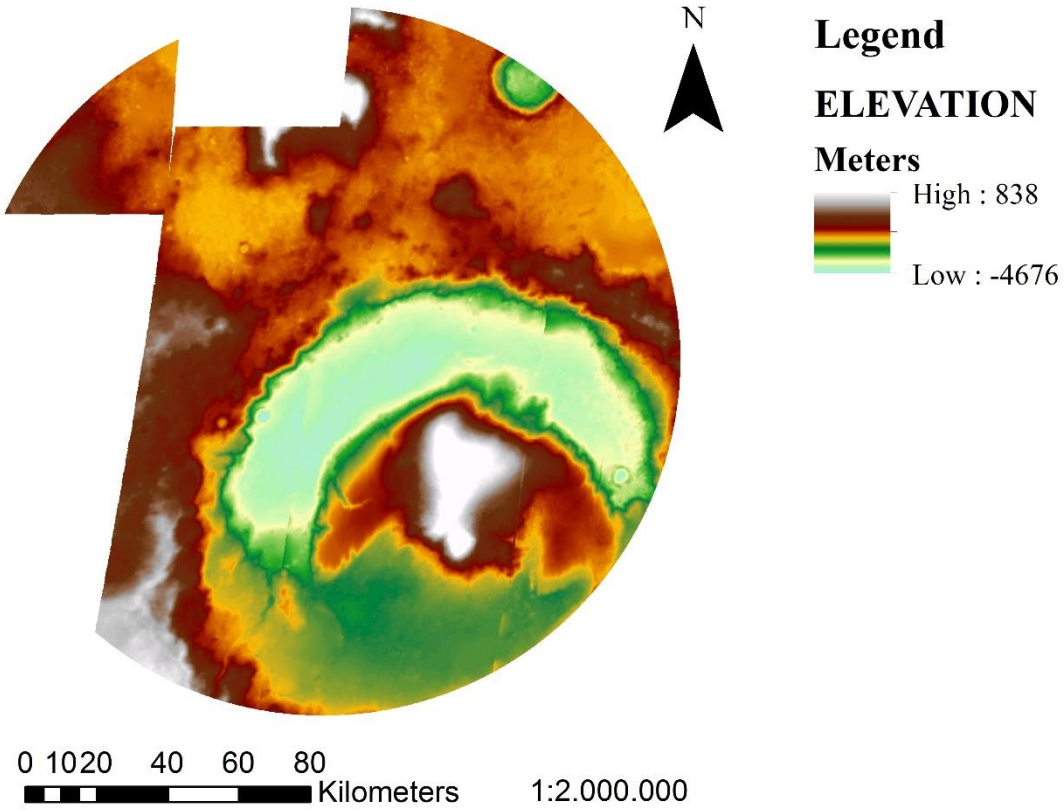

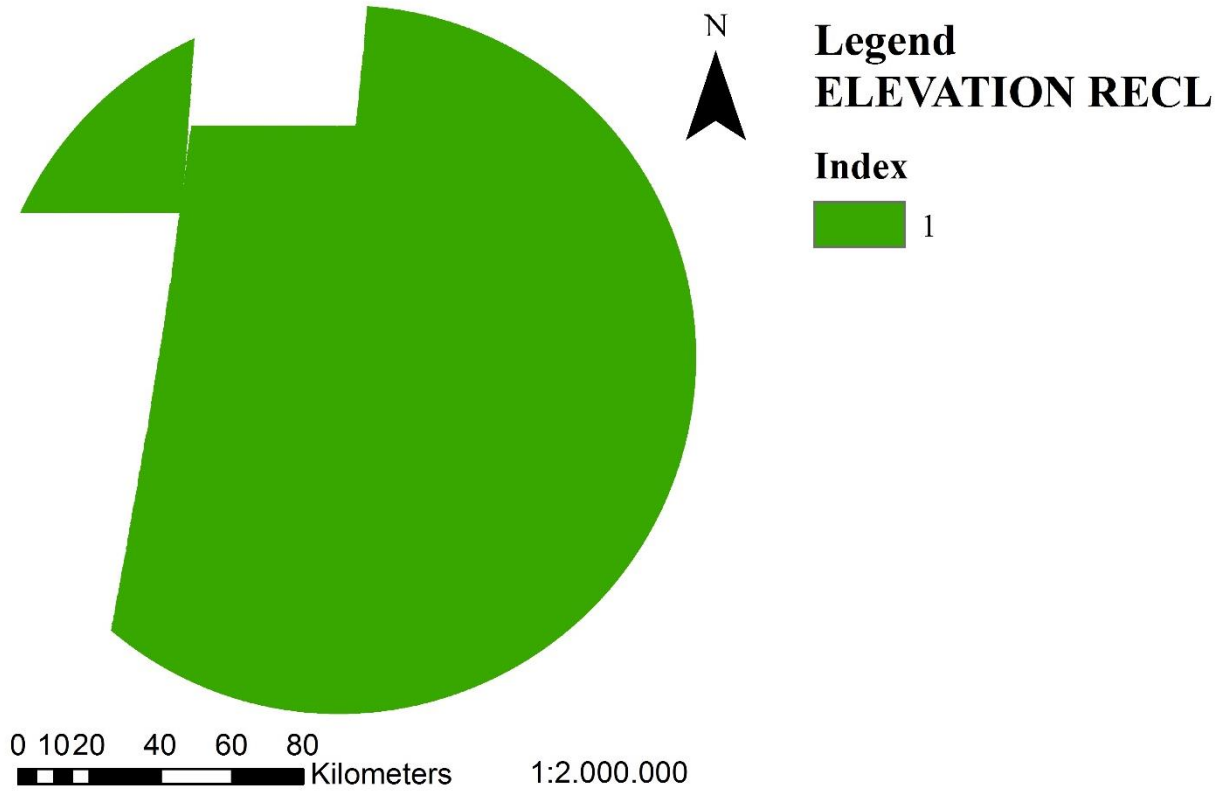

Figure 7-2. GC EZ: Elevation Map and Elevation Reclassified Map

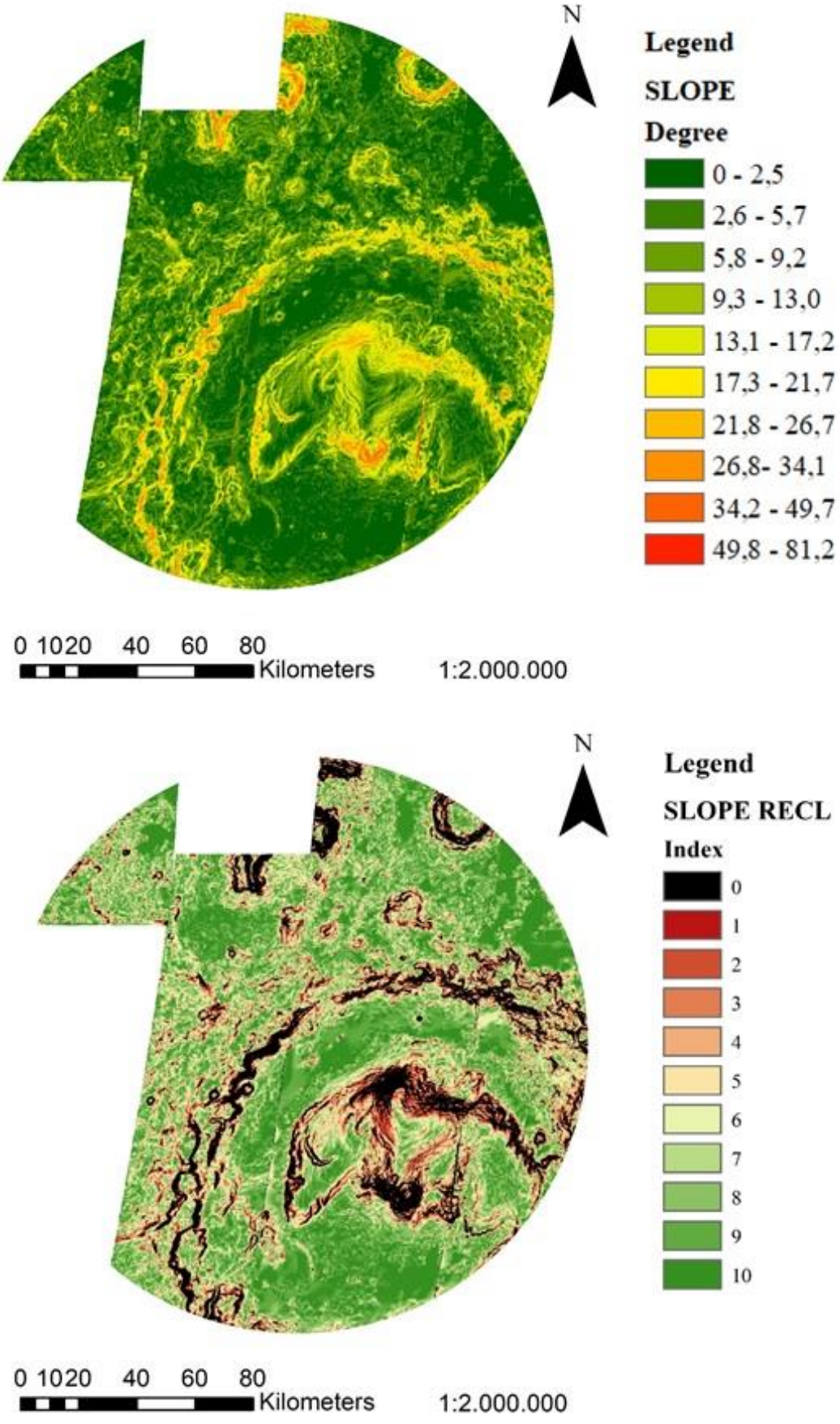

Figure 7-3. GC EZ: Slope Map and Slope Reclassified Map

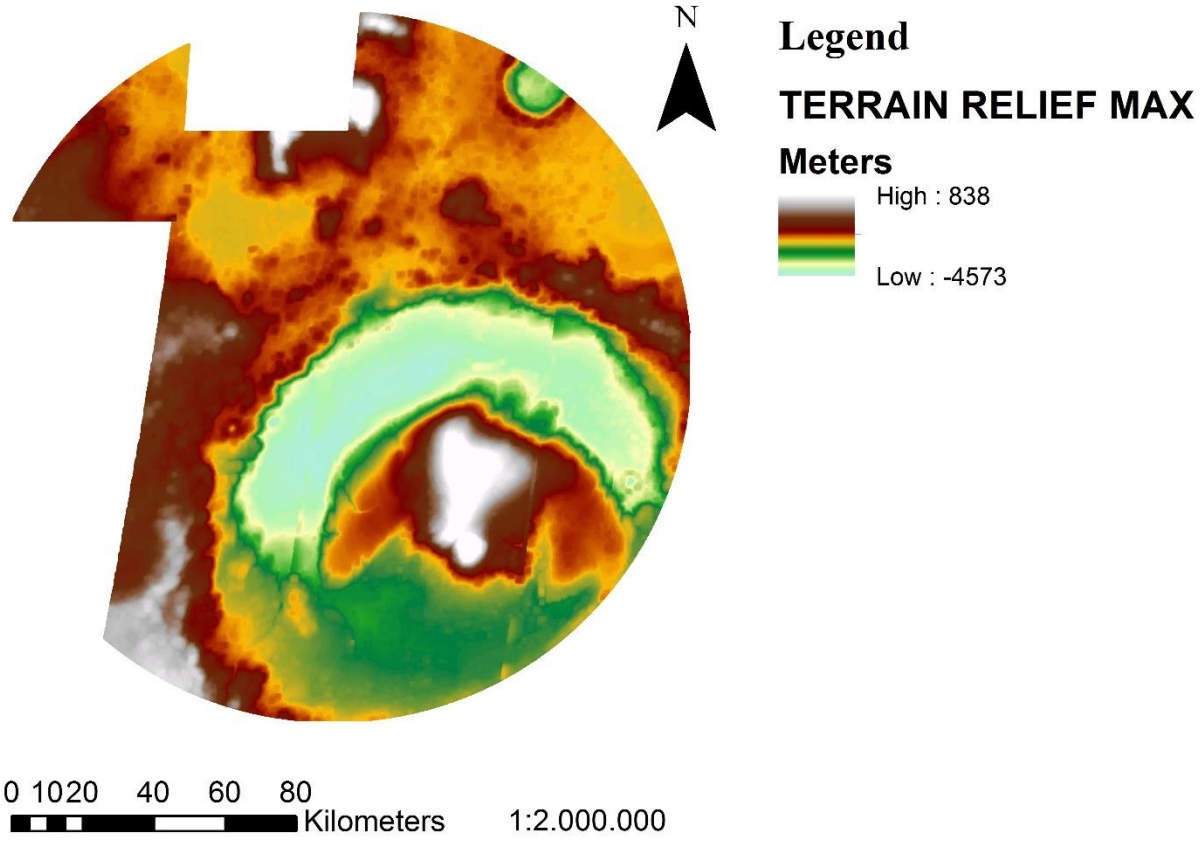

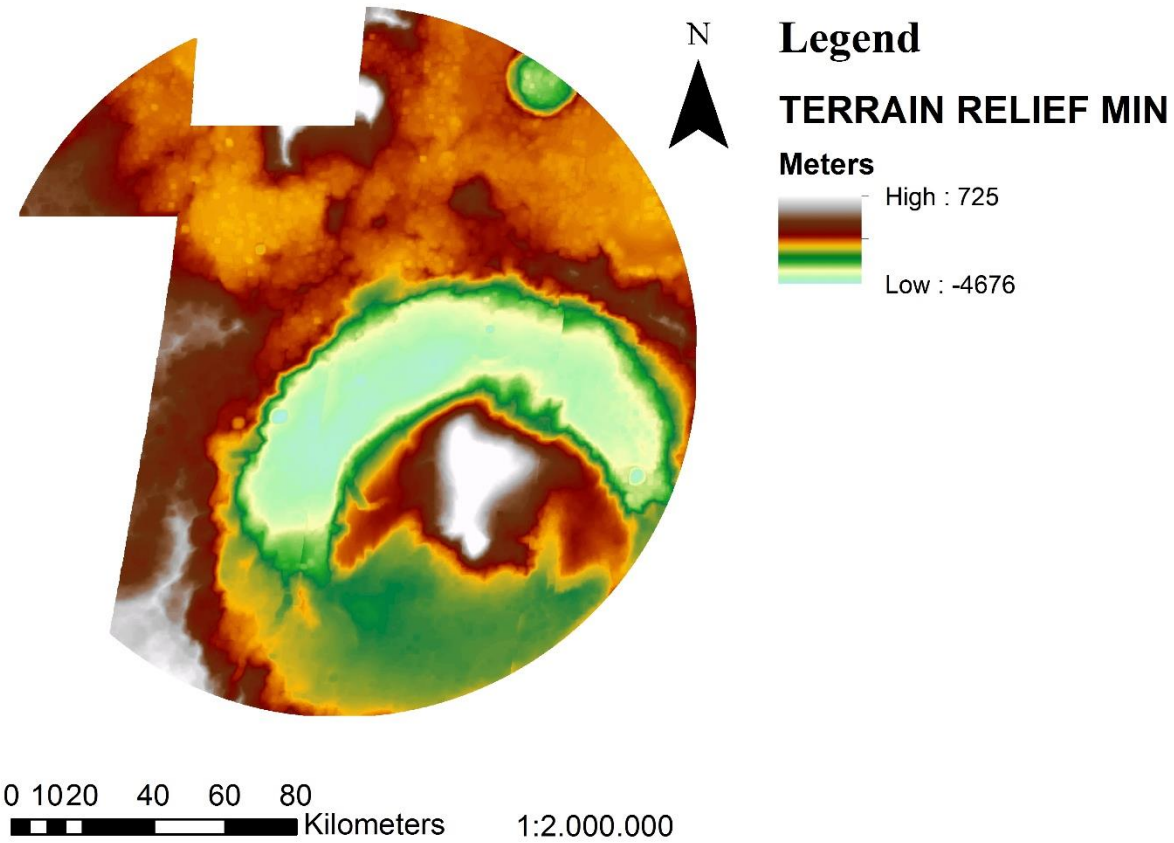

Figure 7-4. GC EZ: Maximum and Minimum Terrain Relief Maps

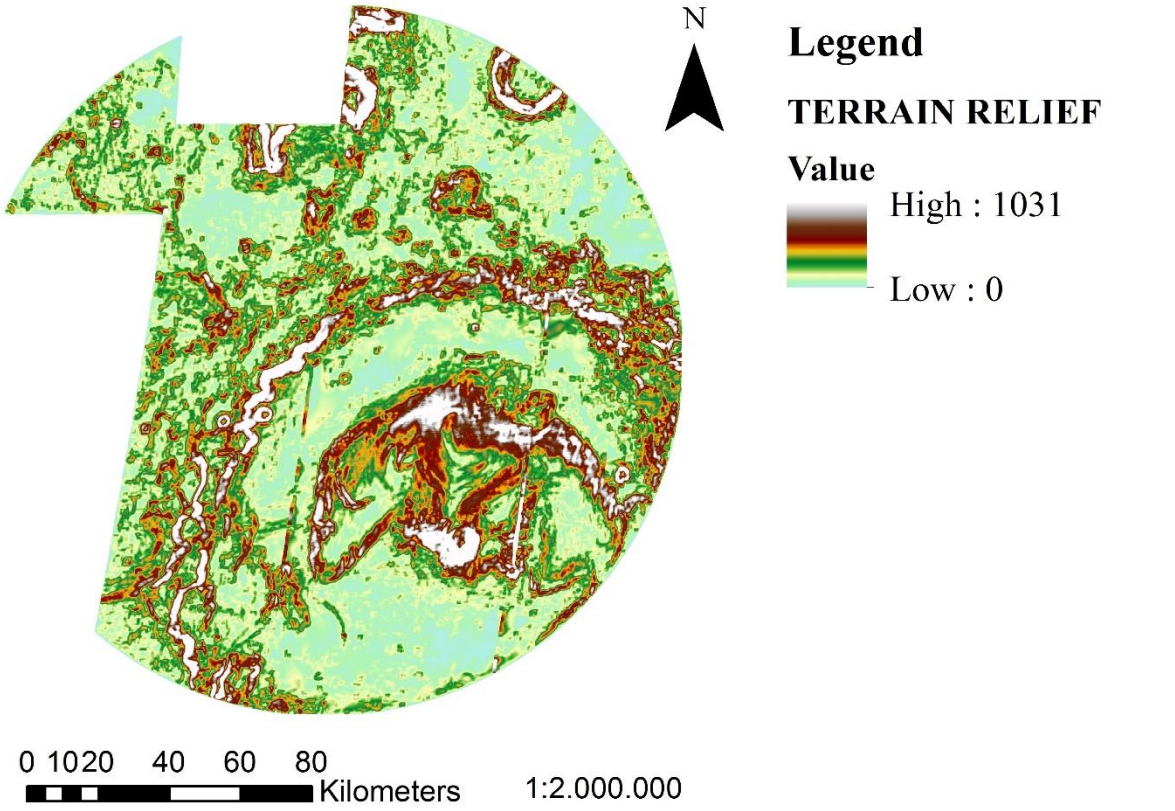

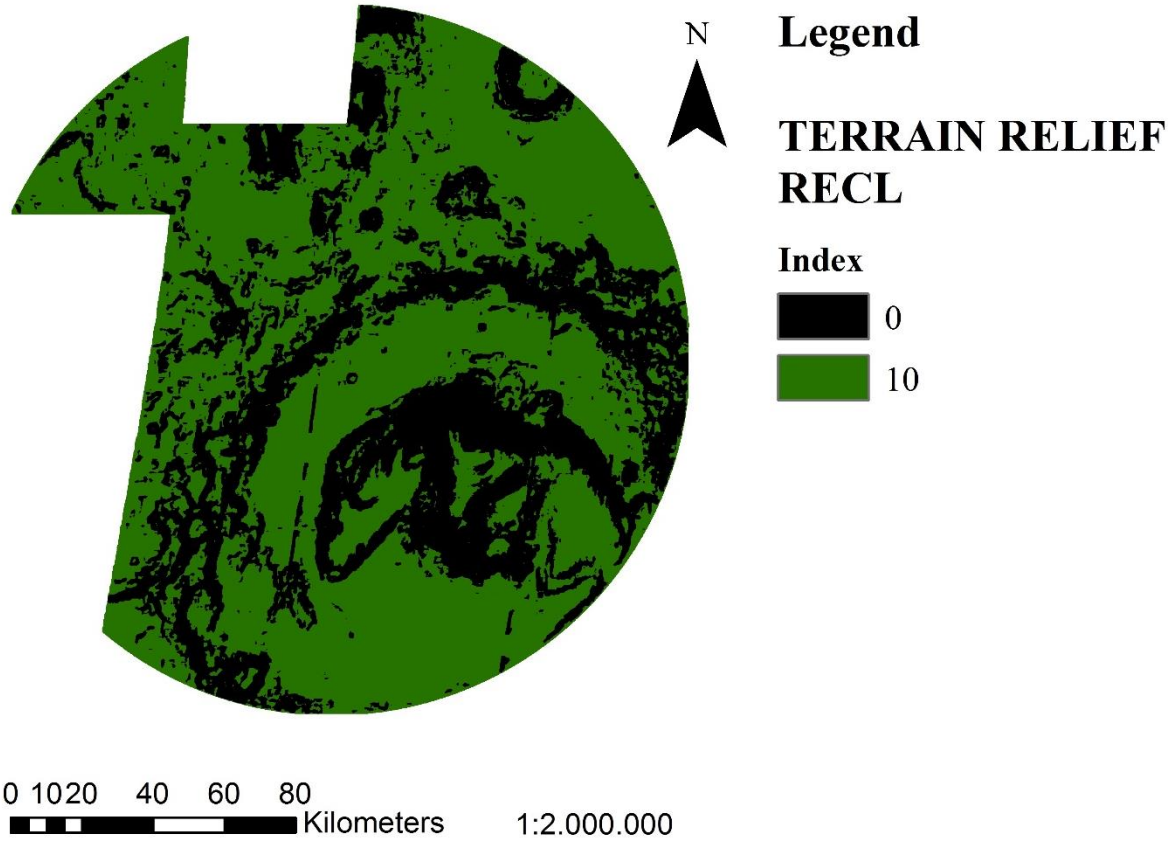

Figure 7-5. GC EZ: Terrain Relief Map and Terrain Relief Reclassified Map

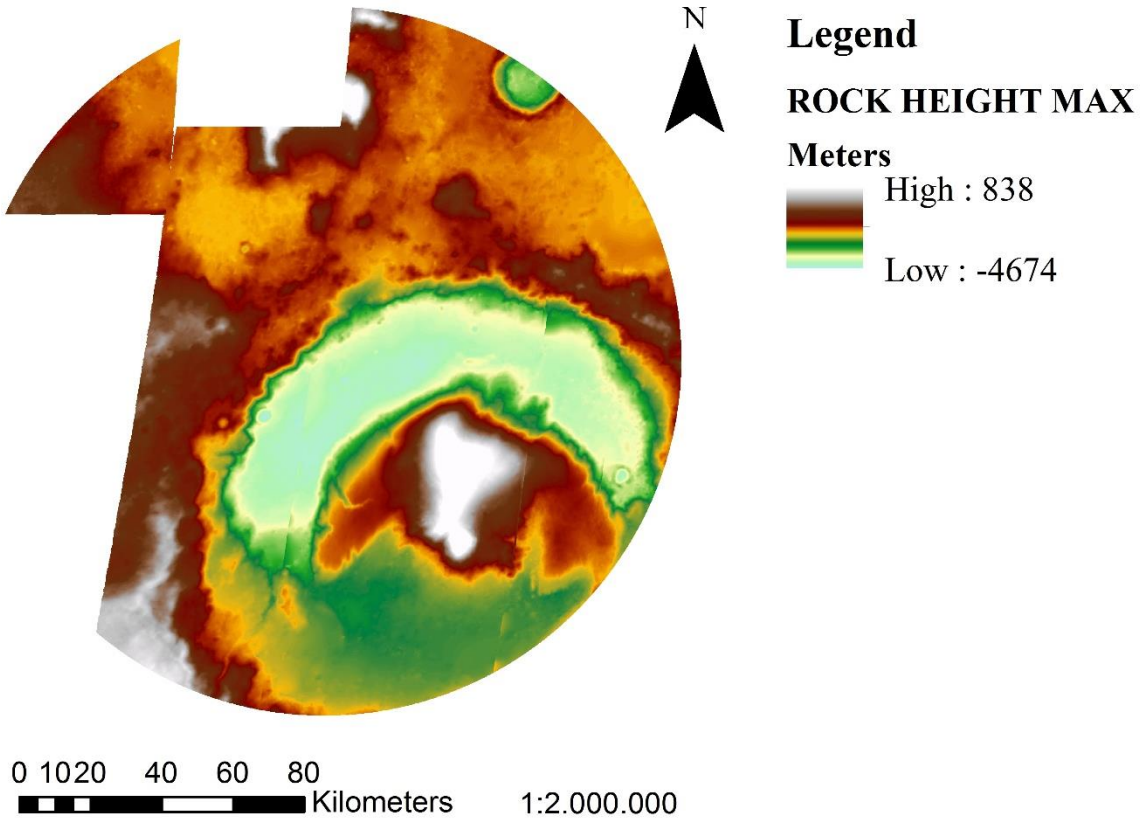

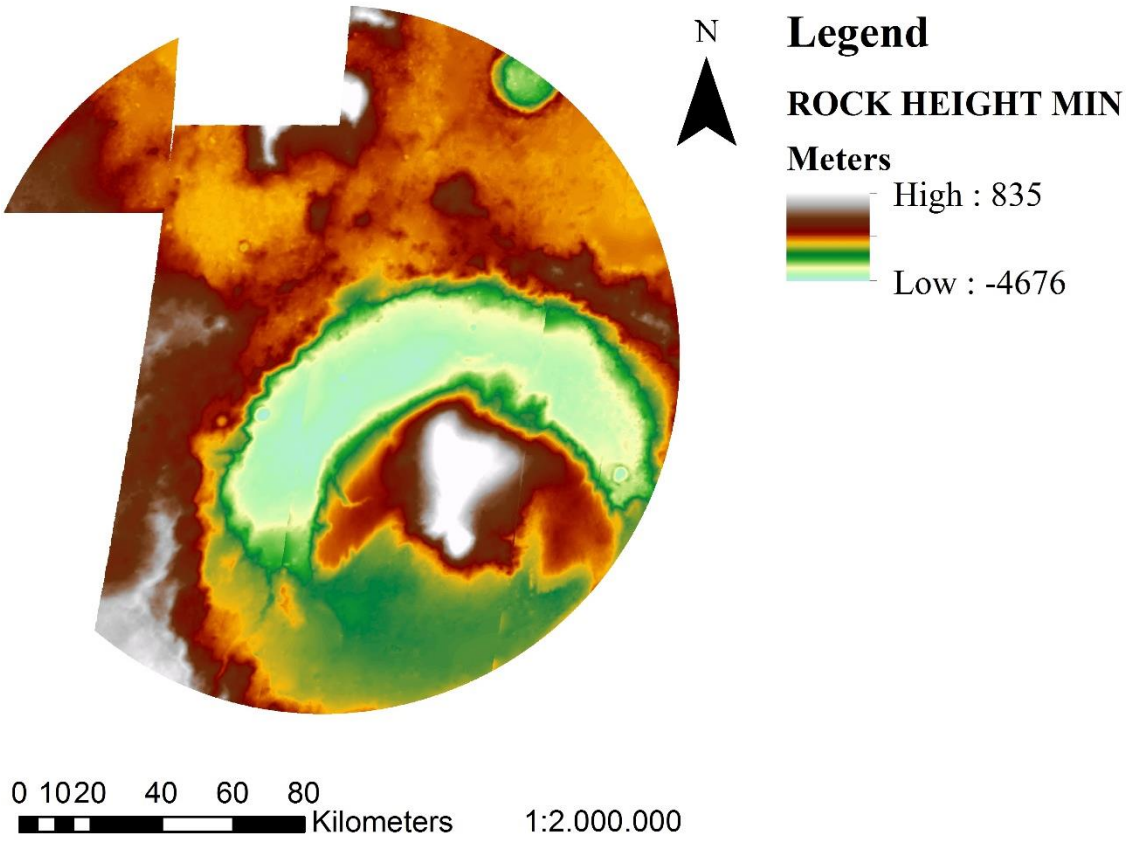

Figure 7-6. GC EZ: Maximum and Minimum Rock Height Maps

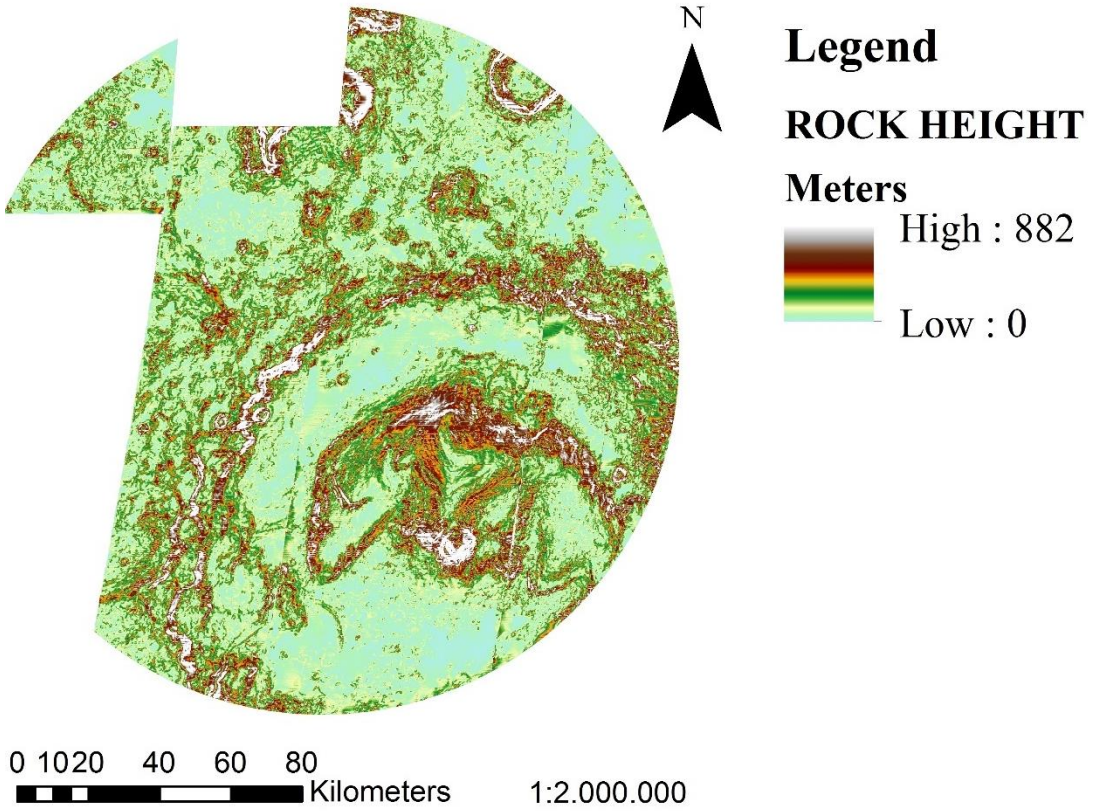

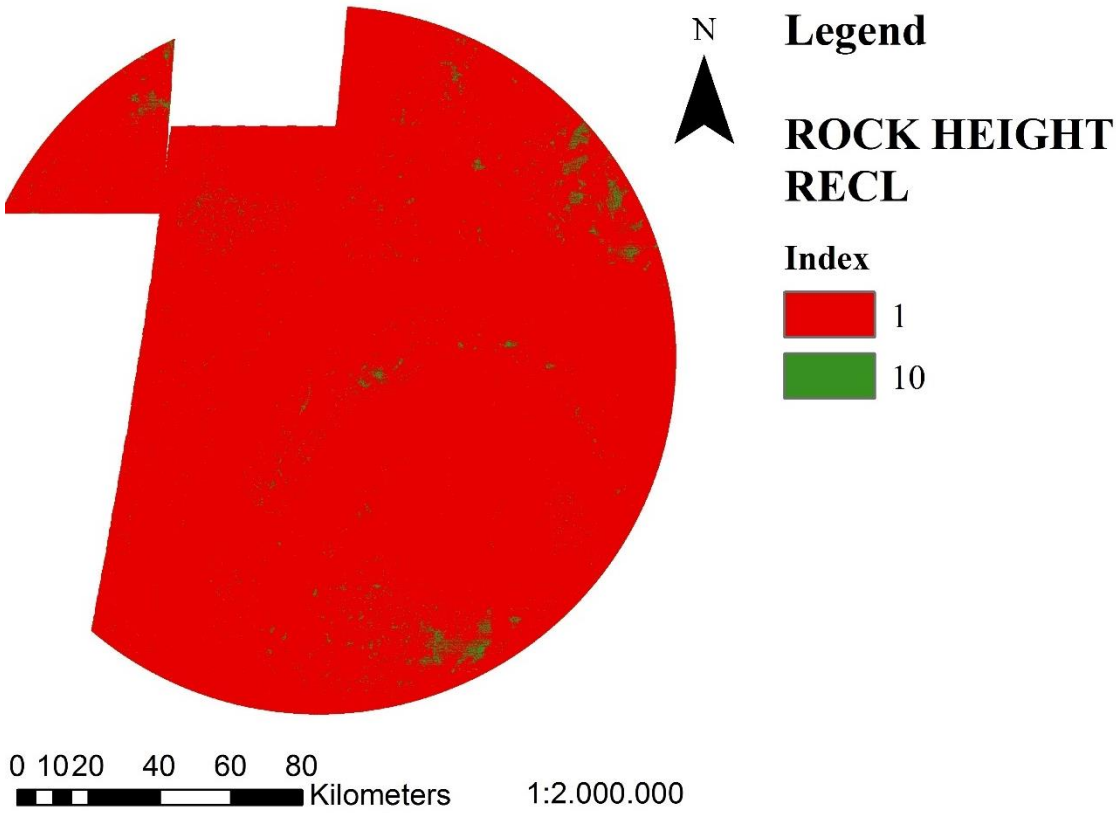

Figure 7-7. GC EZ: Rock Height Map and Rock Height Reclassified Map

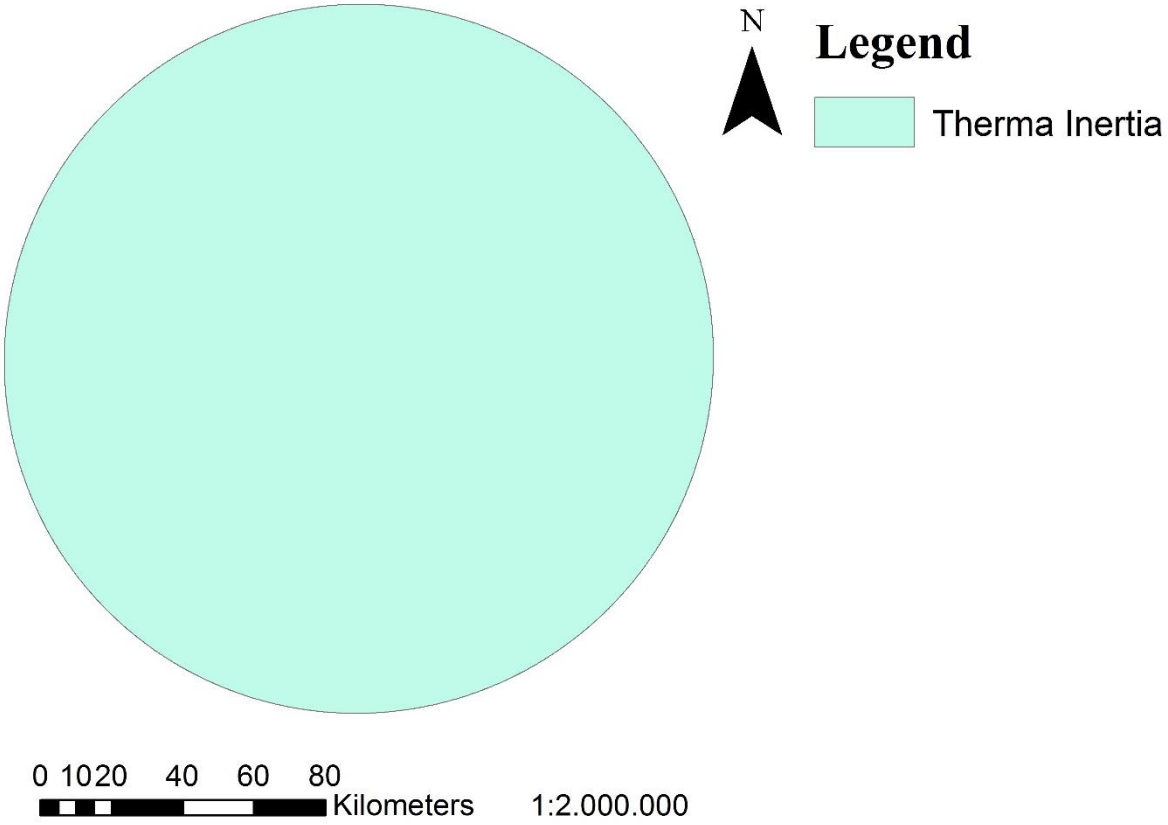

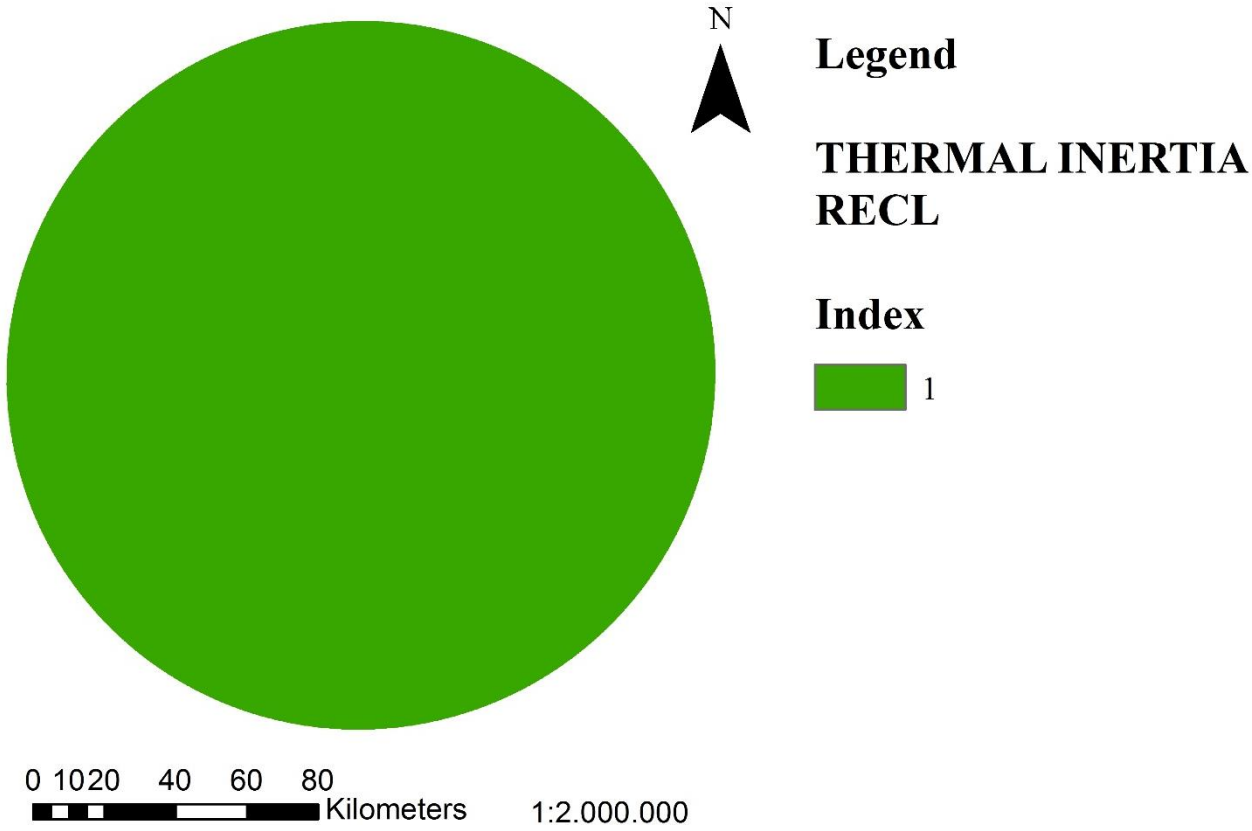

Figure 7-8. GC EZ: Thermal Inertia Map and Thermal Inertia Reclassified Map

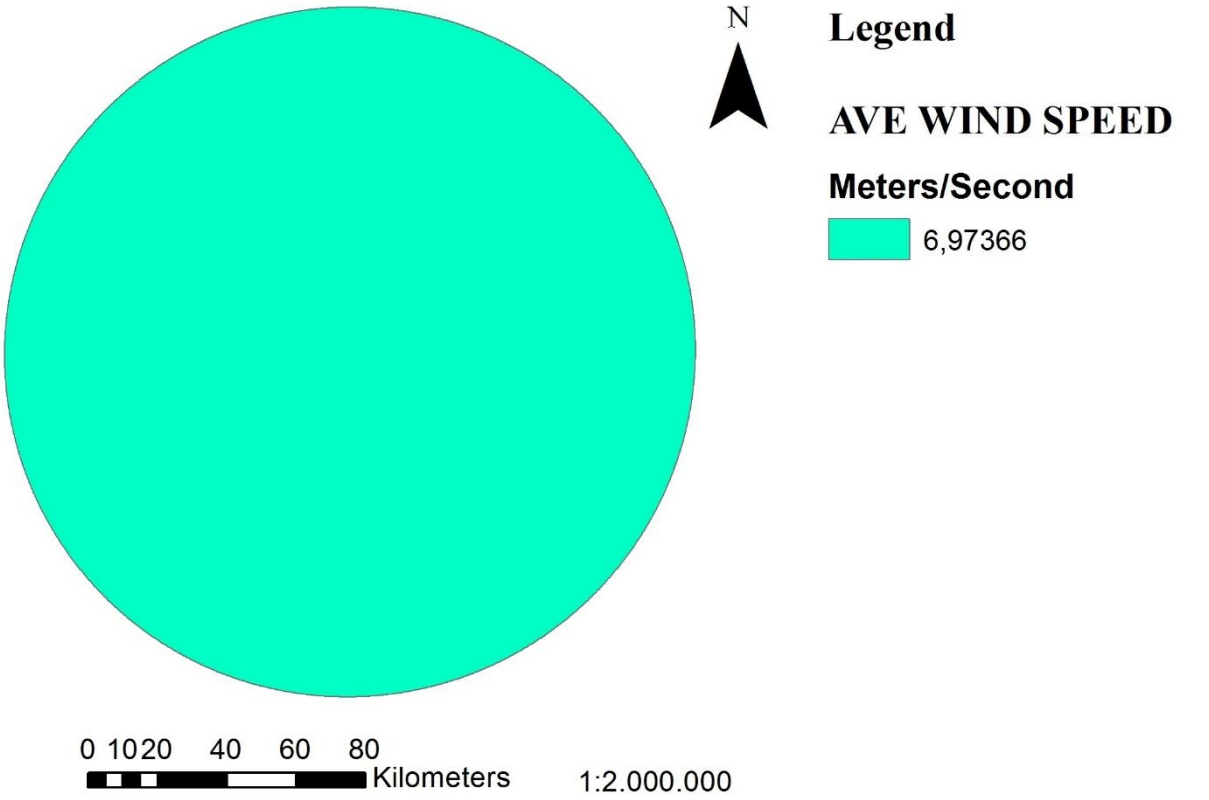

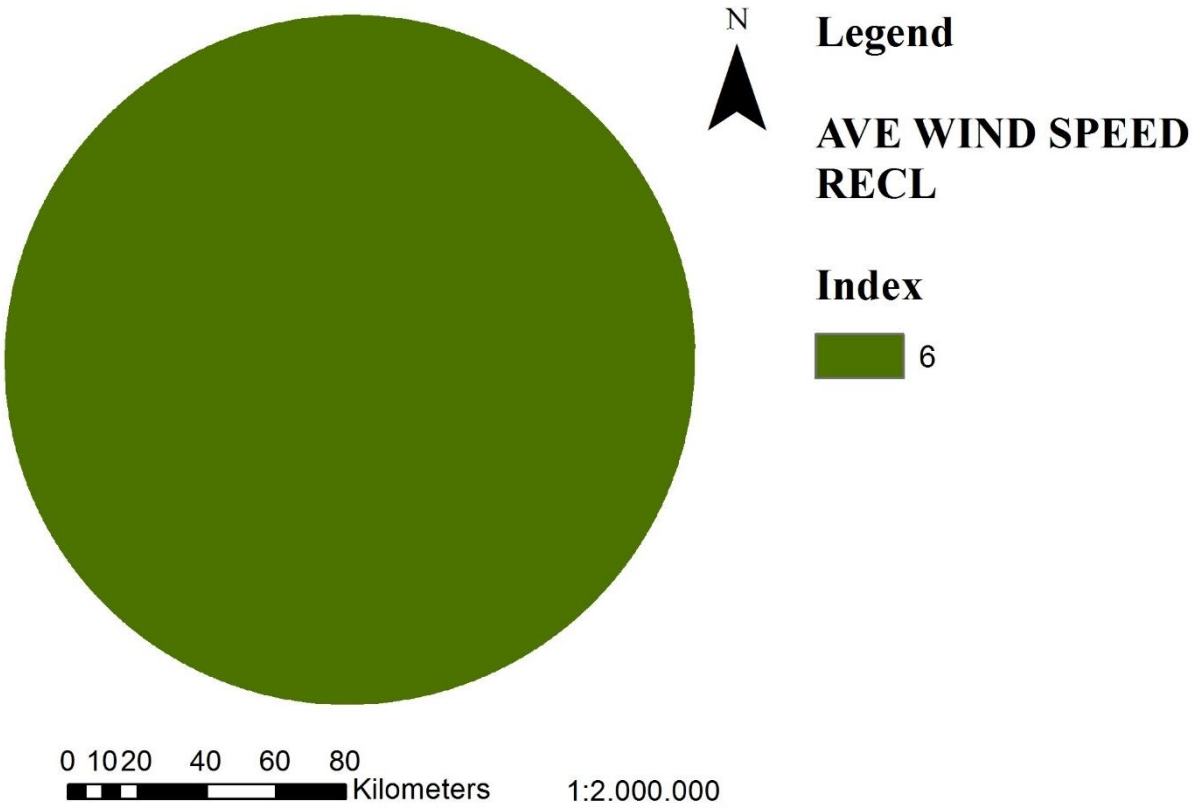

Figure 7-9. GC EZ: Annual Average Wind Speed Map and Annual Average Wind Speed Reclassified Map

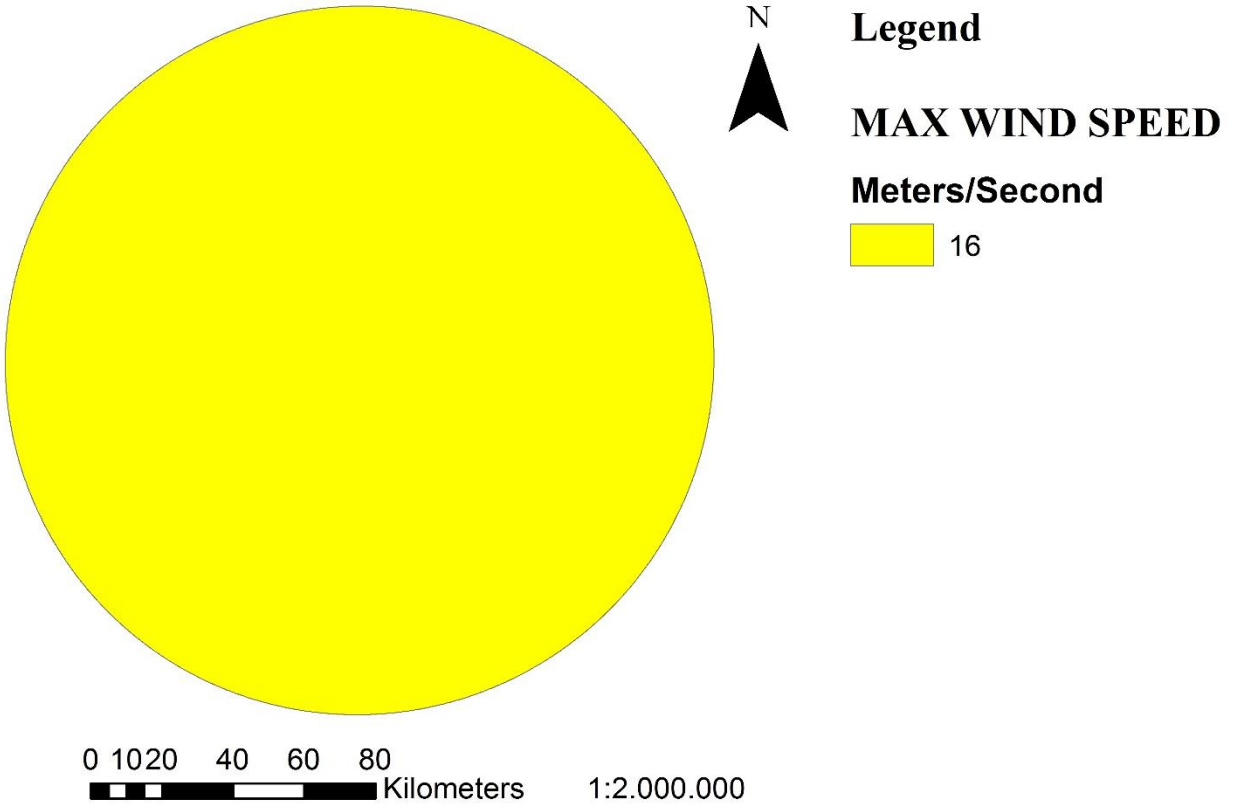

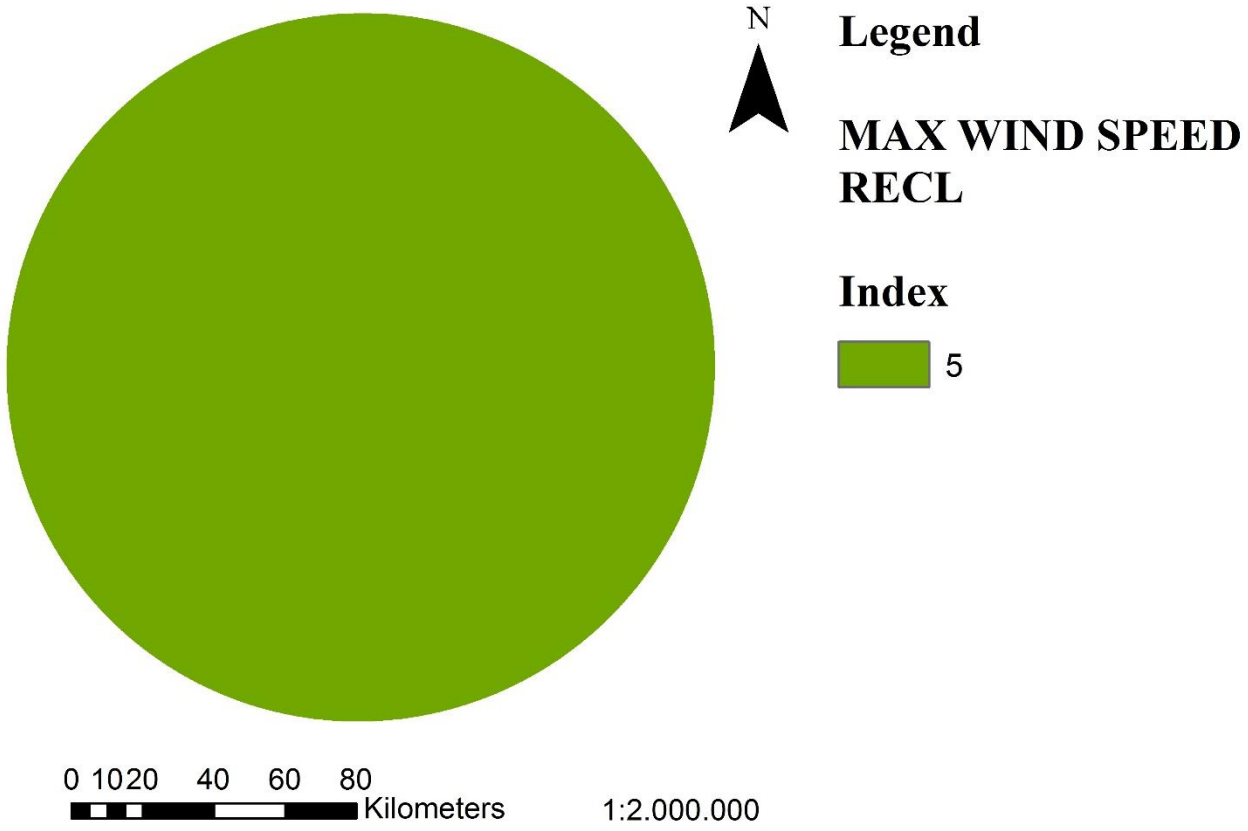

Figure 7-10. GC EZ: Annual Maximum Wind Speed Map and Annual Maximum Wind Speed Reclassified Map

7.1.3 Final map and validation of model effectiveness

This Section shows the final map obtained in Gale Crater (GC) Exploration Zone (EZ). In 2012, MSL's Curiosity rover landed on Aeolis Palus, a plain located between the northern wall of GC and Aeolis Mons, at 4.5°S latitude and 137.4°E longitude.

To test and validate the effectiveness of the model, the constraints used for the landing of Curiosity at Gale Crater were incorporated into the tool. For this reason, a comparison between the final raster map and CTX image is shown in this Section.

Furthermore, CTX datasets are placed side by side with the final raster map in different areas of the EZ: this comparison allows evaluating reliability and quality of results.

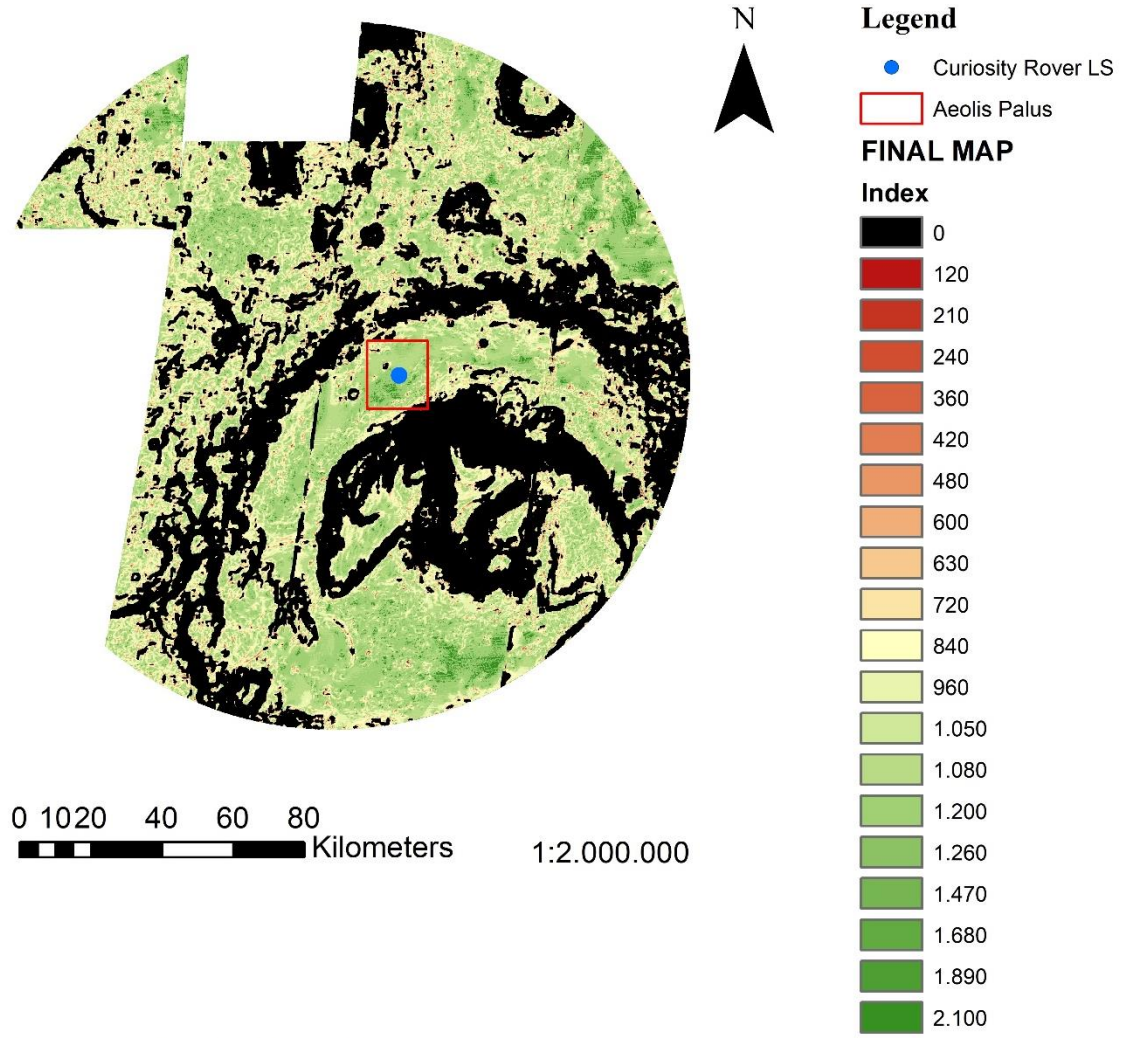

Figure 7-11. GC EZ: Final raster map and comparison between final raster map and CTX datasets in Aeolis Palus

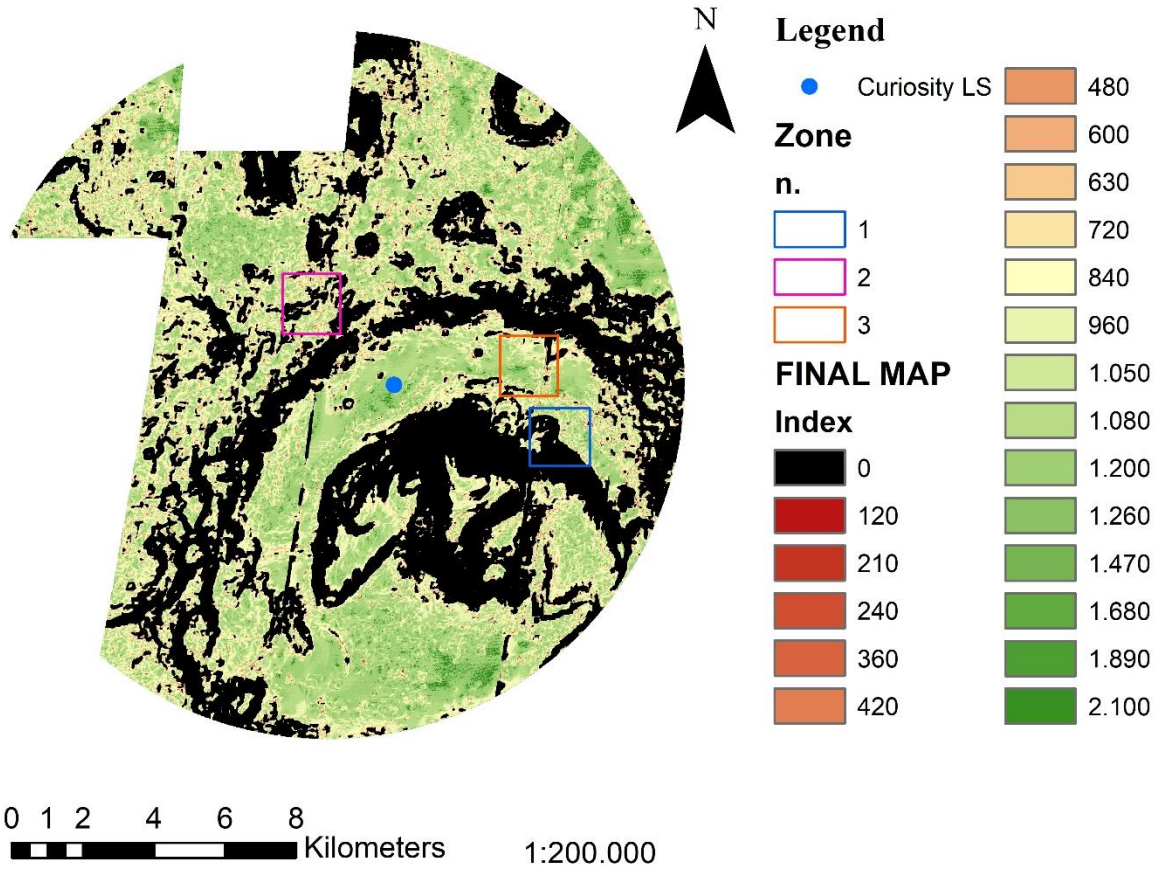

Zone 1

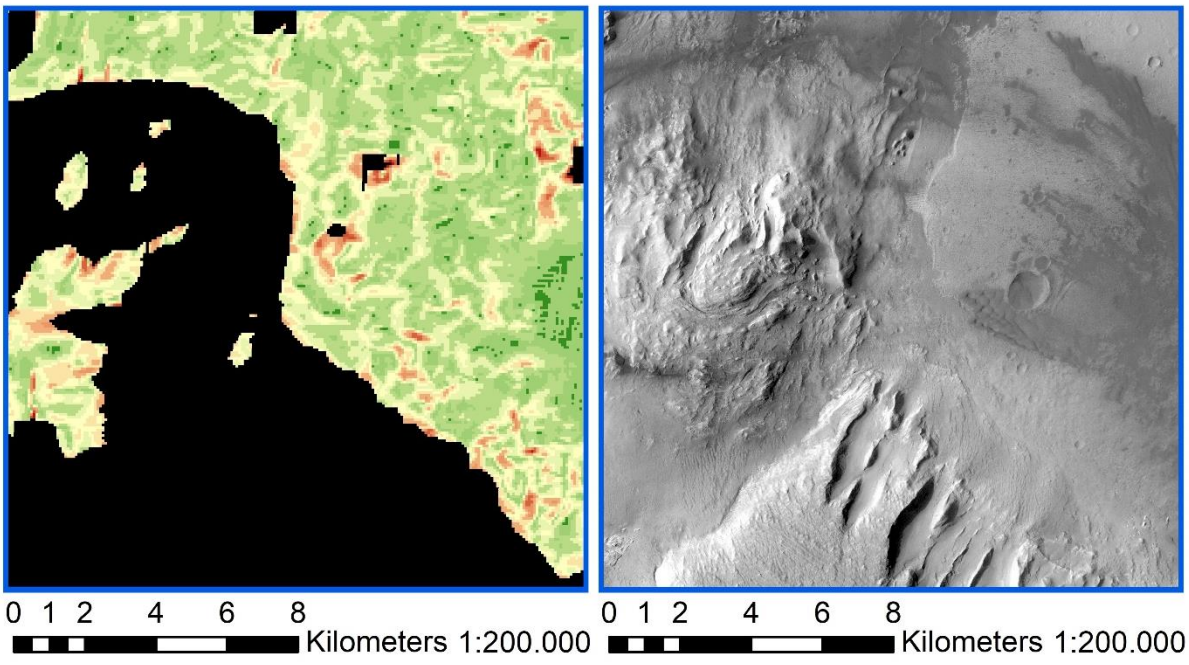

Figure 7-12. GC EZ: comparison between final raster map and CTX datasets (Zone 1)

Zone 2

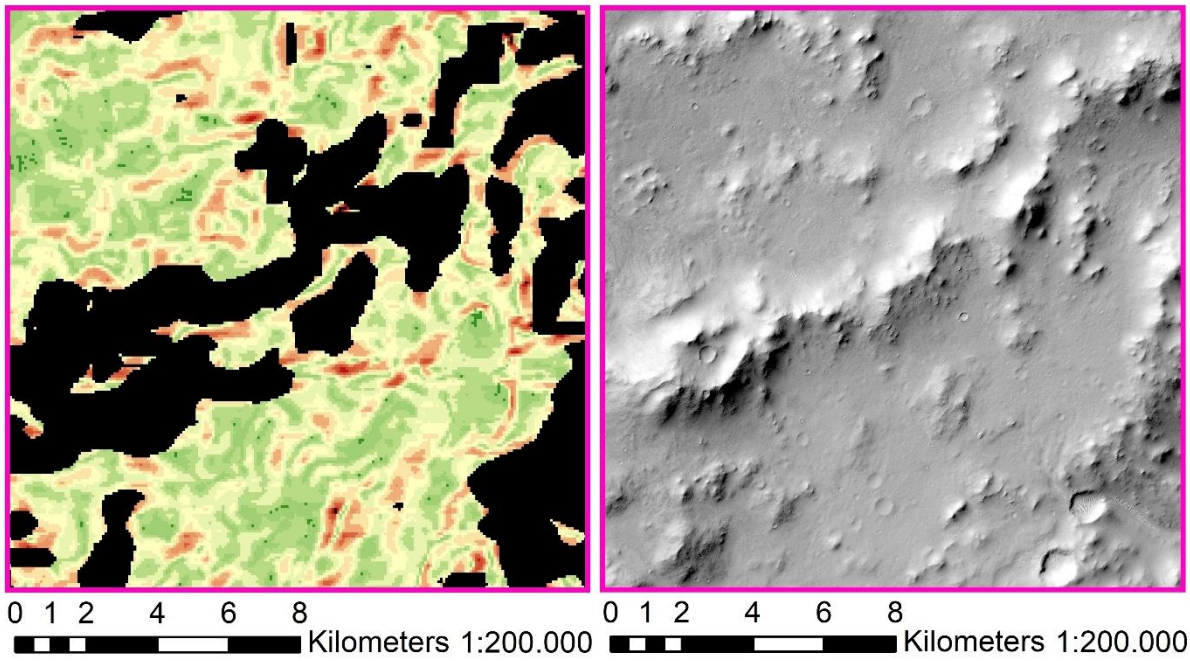

Zone 3

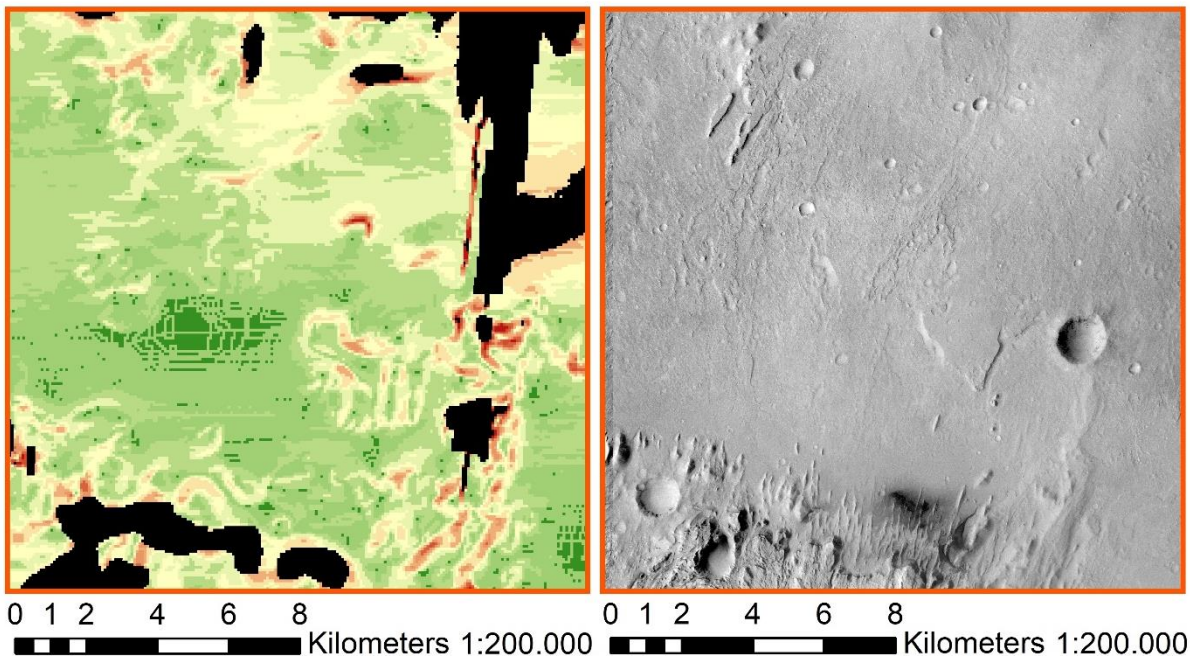

Figure 7-13. GC EZ: comparison between final raster map and CTX datasets (Zones 2 and 3)

7.2 Protonilus Mensae Exploration Zone

7.2.1 Geographical Framework

Figure 7-14 provides Protonilus Mensae (PM) Exploration Zone (EZ) geographical framework. PM EZ's centre is located at 42°N.

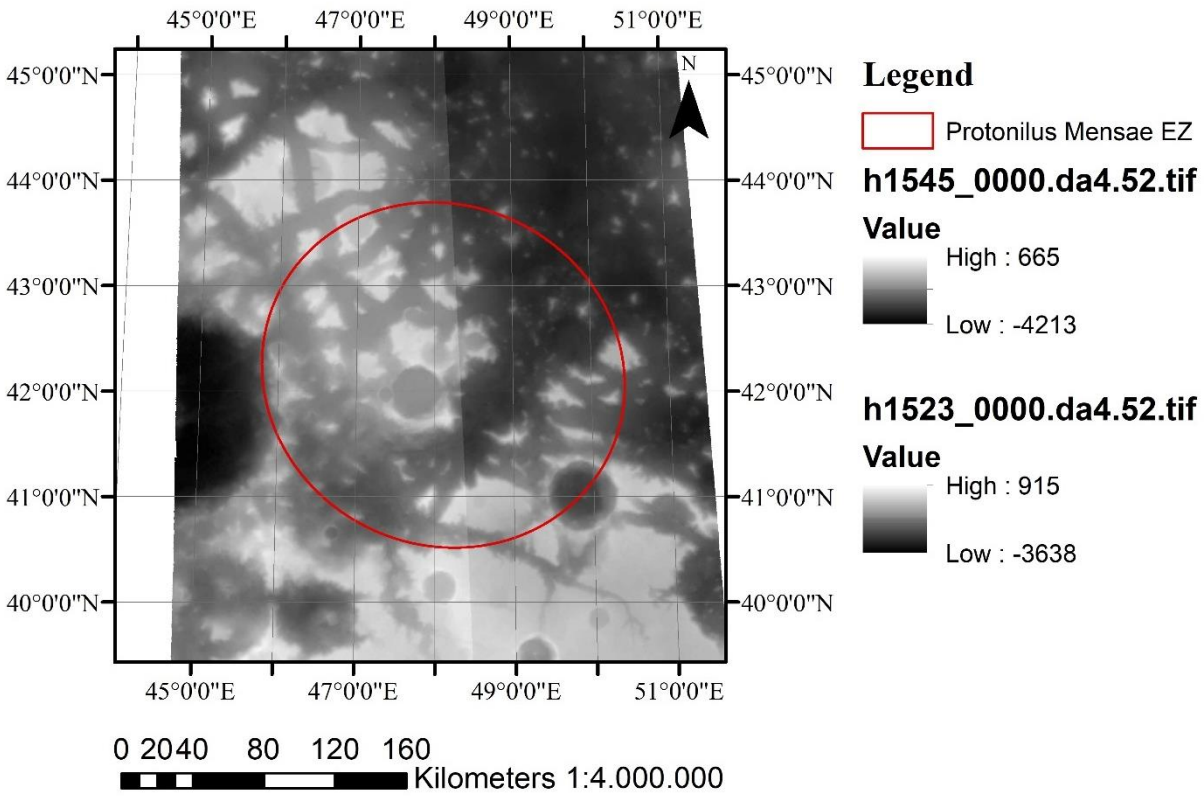

Figure 7-14. Protonilus Mensae (PM) Exploration Zone (EZ): geographical framework; HRSC DTM images 75 m/pixel resolution

7.2.2 Engineering Parameters Maps and Reclassified Maps

This Section reports the output maps obtained in Protonilus Mensae (PM) Exploration Zone (EZ).

The engineering map layers of (1) Elevation, (2) Slope, (3) Terrain Relief, and (4) Rock Height are automatically generated from the workflow developed in this thesis. Otherwise, (5) Thermal Inertia, (6) Annual Maximum Wind Speed, and (7) Annual Average Wind Speed engineering map layers are drawn as shapefiles and uploaded as input files in the model (see Section 6.1.3).

All these maps show how each engineering parameter varies within PM. Each map is then reclassified by associating a specific index to a defined range of values. The associated indexes (1) are consistent with defined Engineering Constraints (see Table 6-3) and (2) are directly related to the goodness of each parameter.

All the introduced maps are shown in this Section.

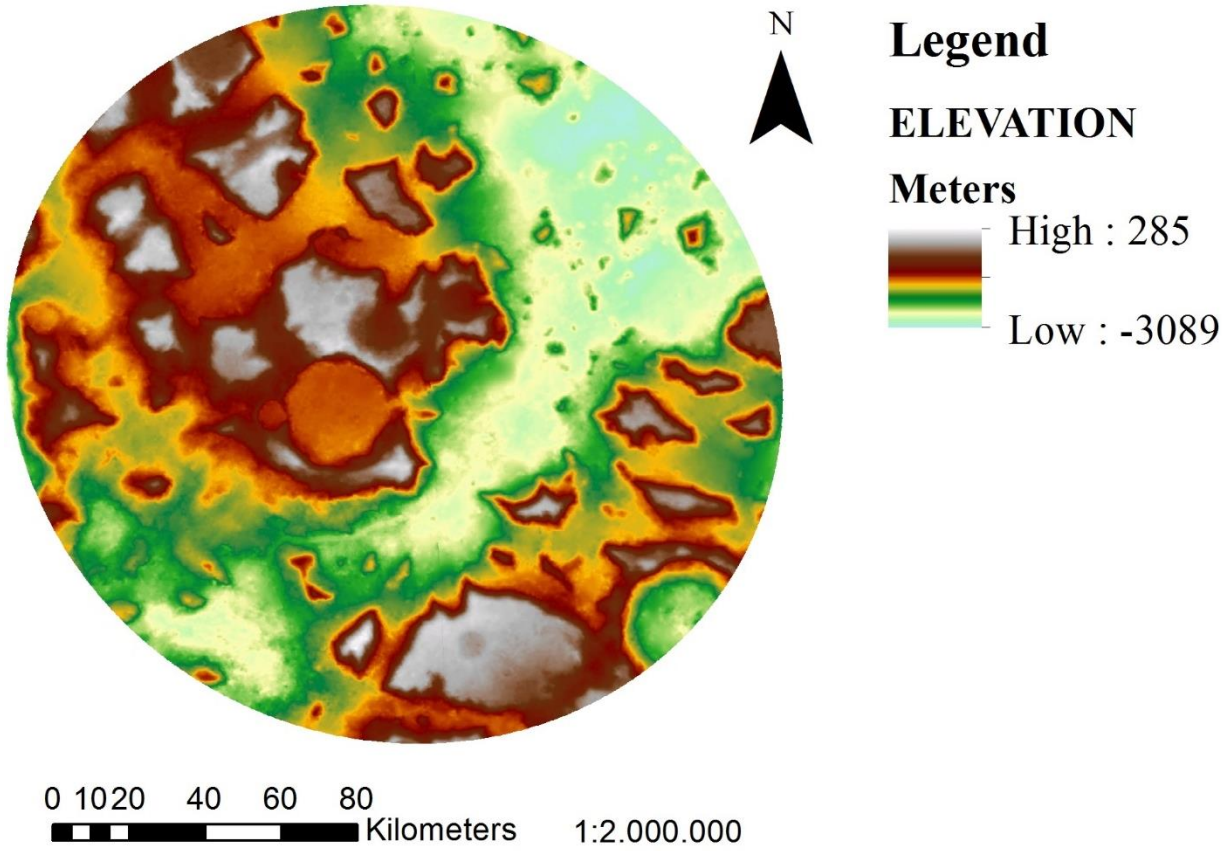

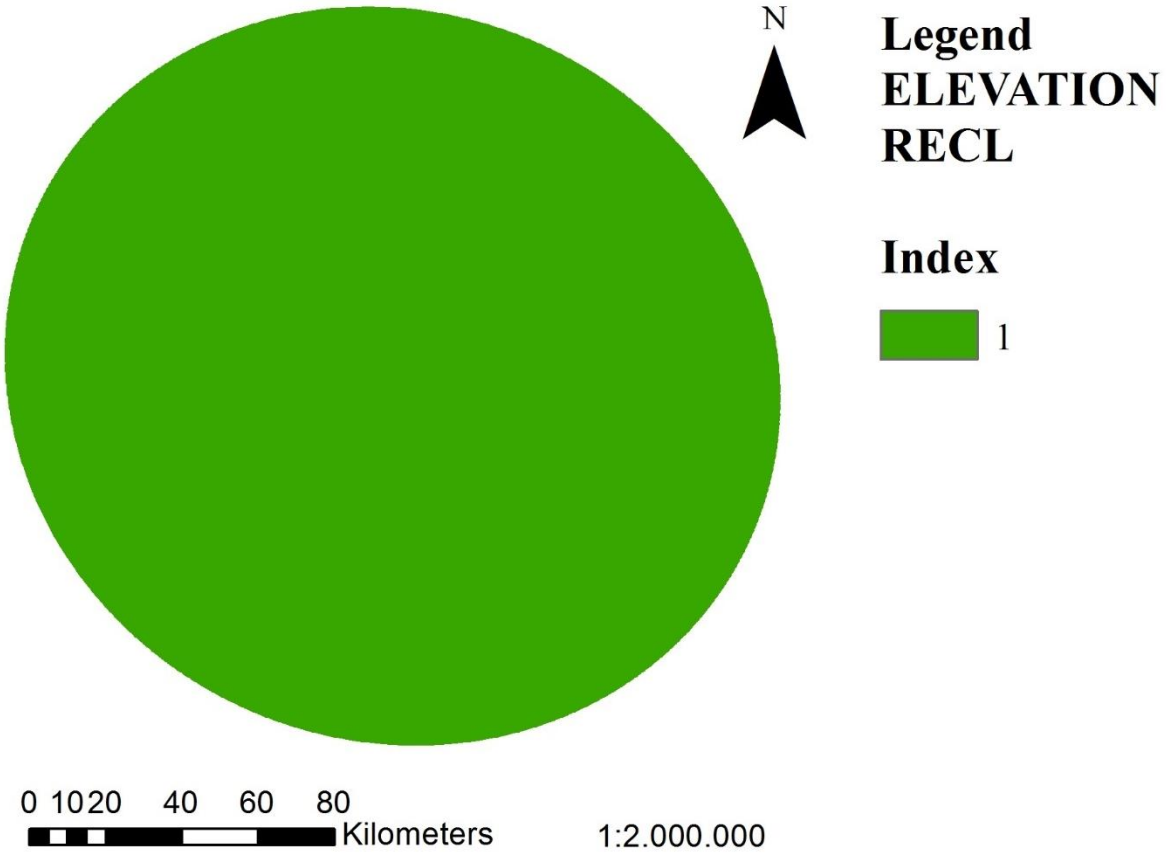

Figure 7-15. PM EZ: Elevation Map and Elevation Reclassified Map

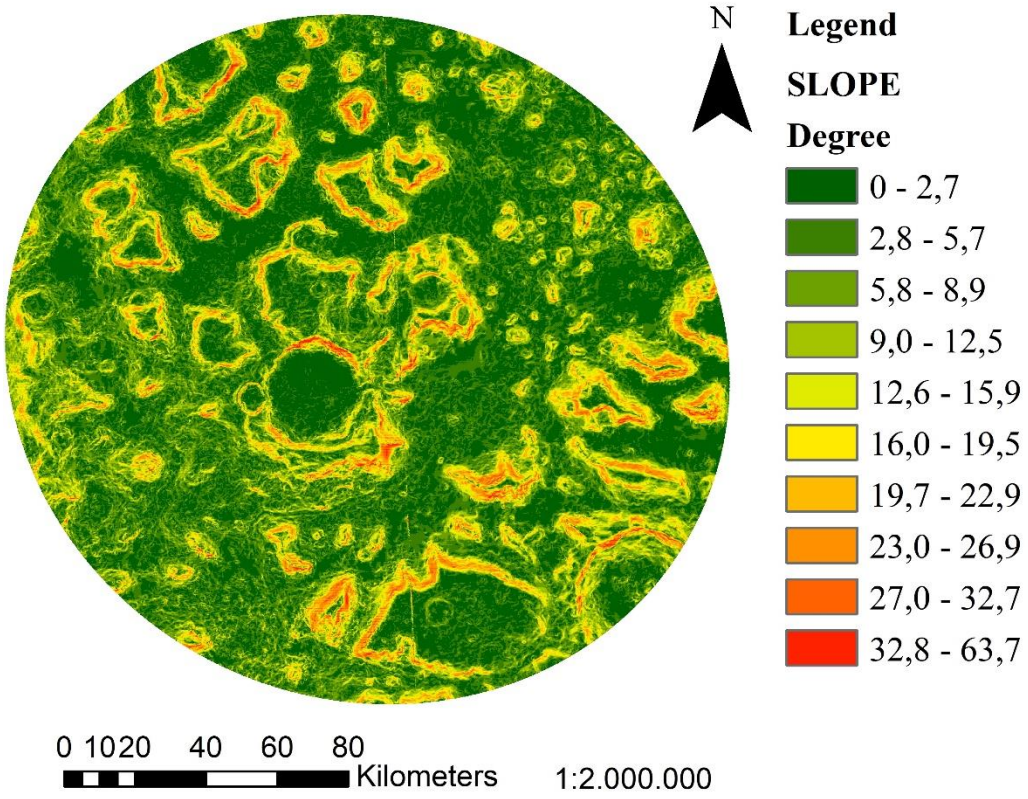

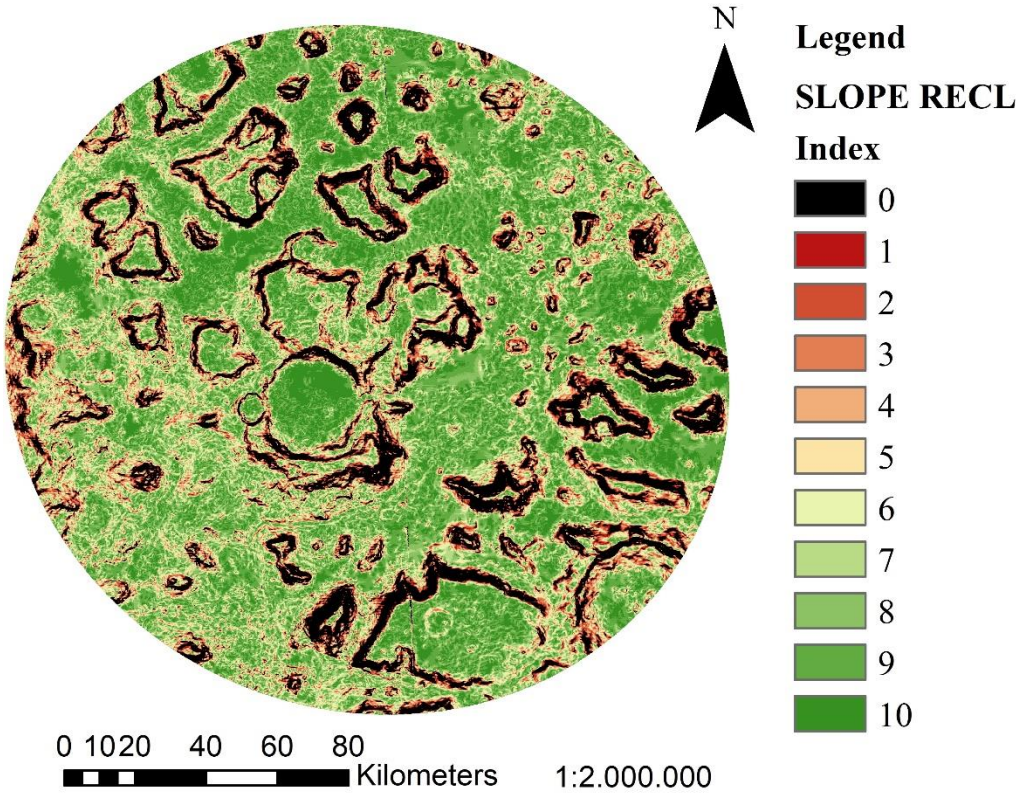

Figure 7-16. PM EZ: Slope Map and Slope Reclassified Map

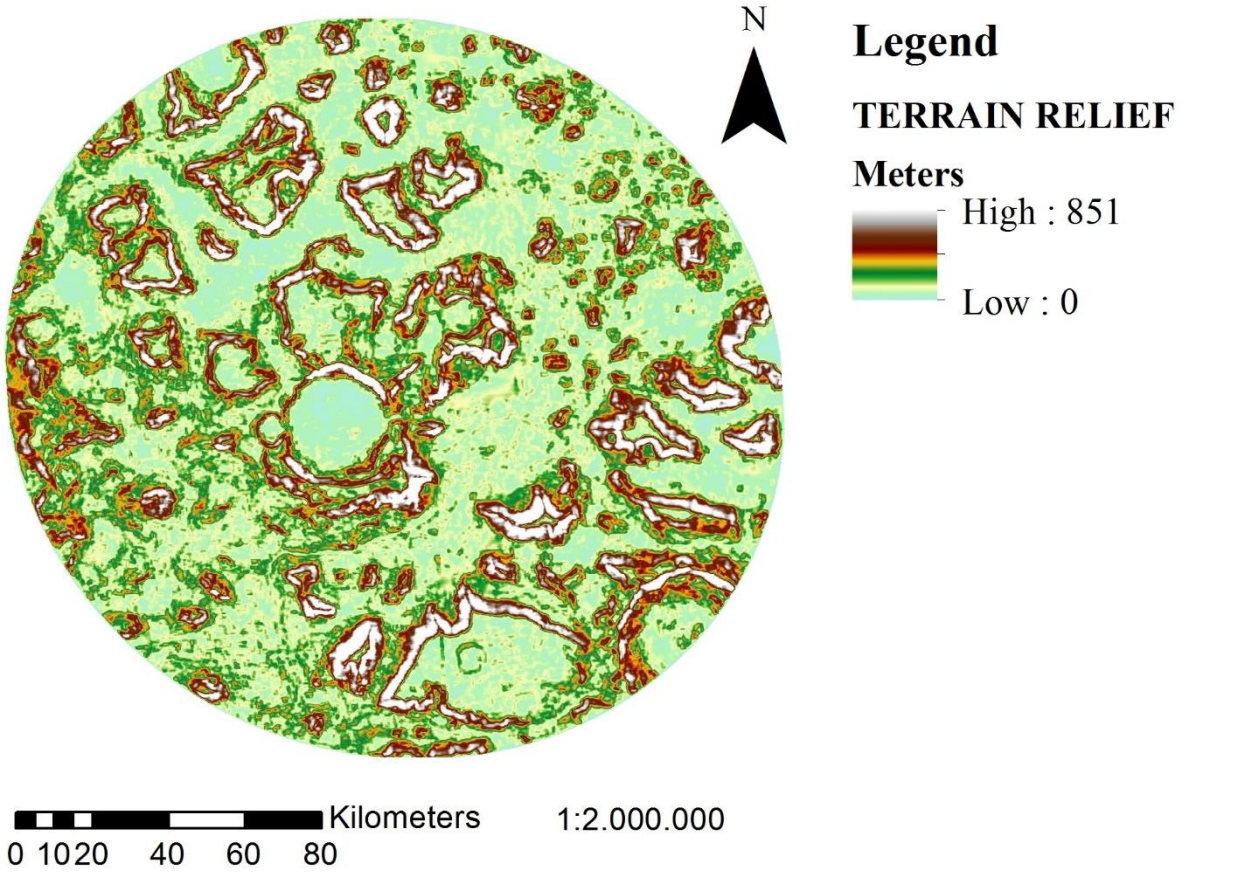

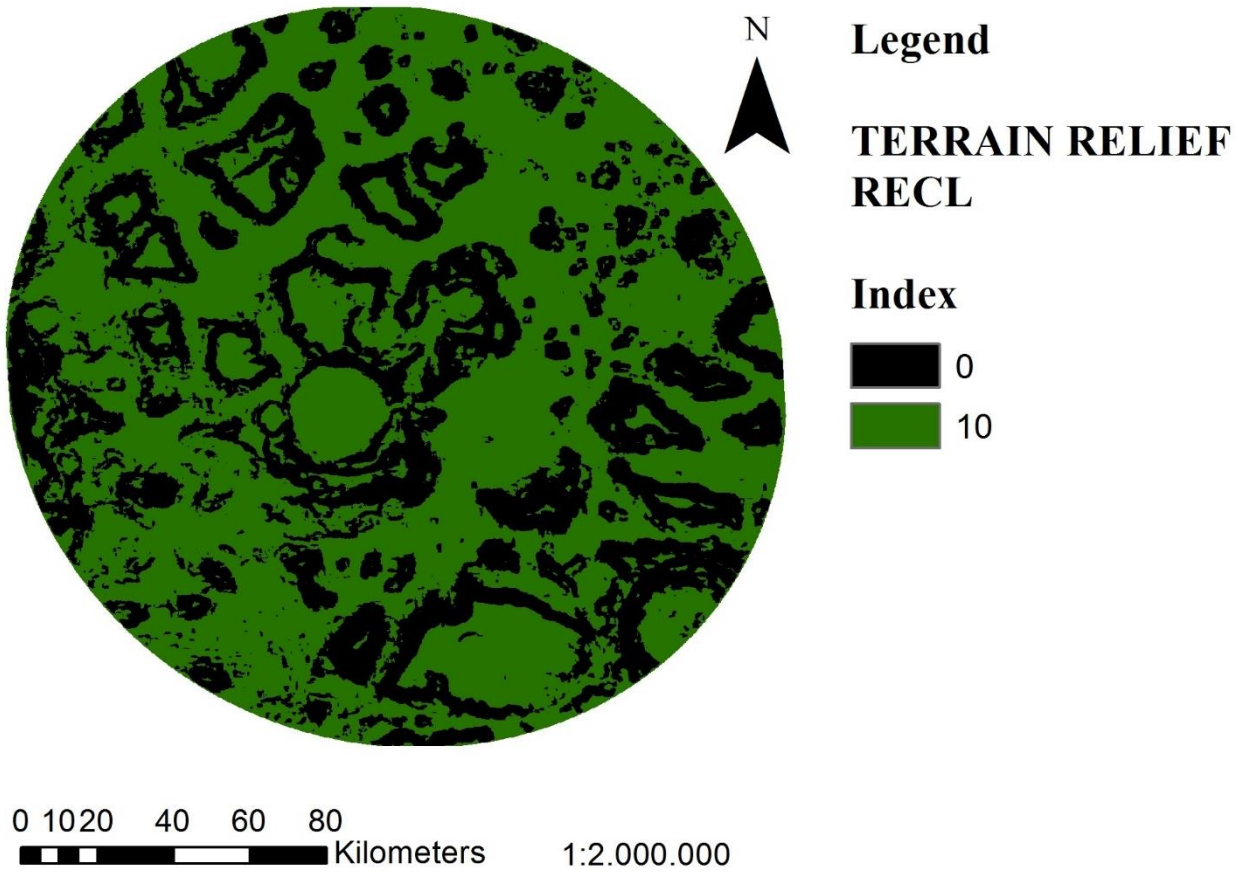

Figure 7-17. PM EZ: Terrain Relief Map and Terrain Relief Reclassified Map

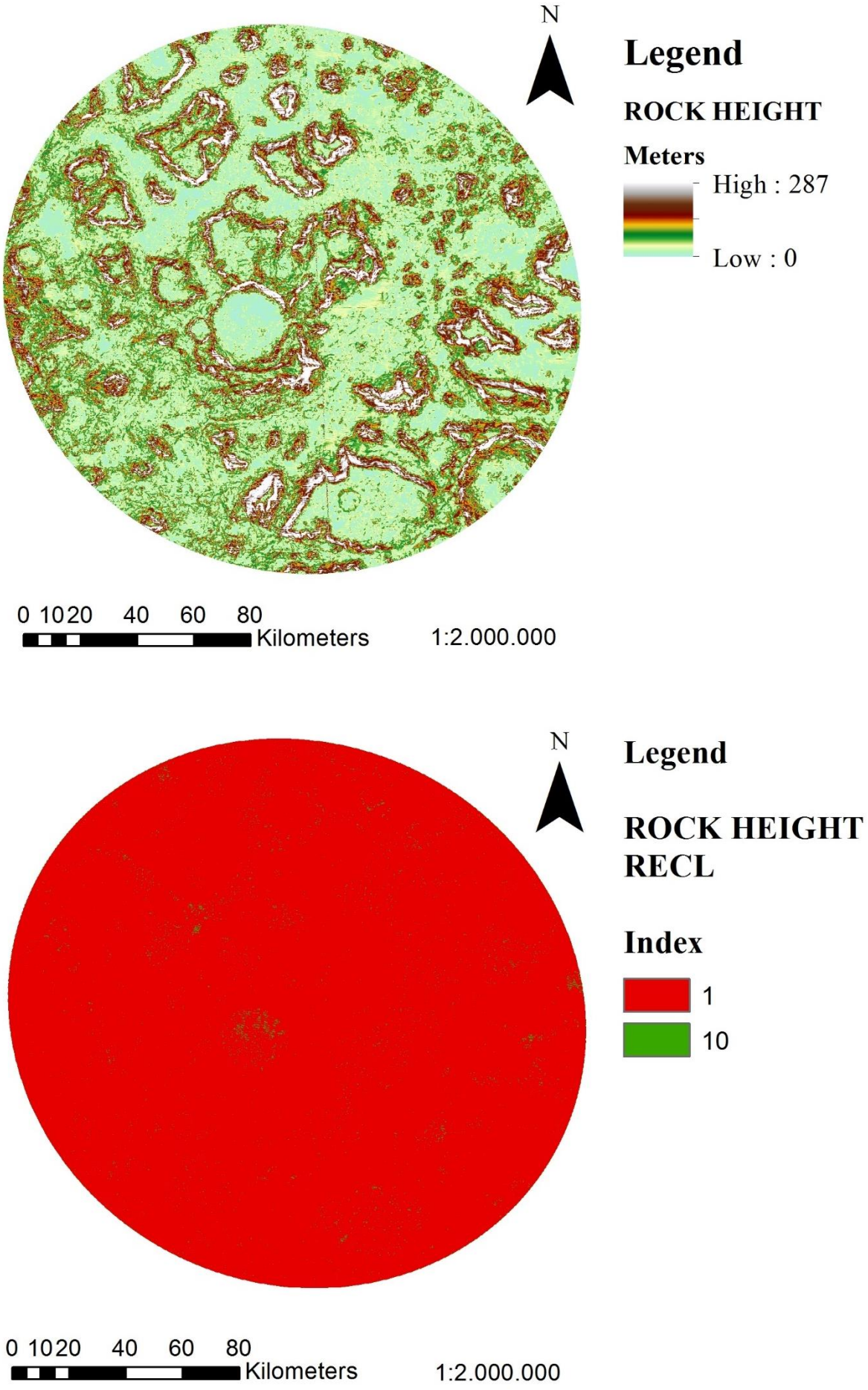

Figure 7-18. PM EZ: Rock Height Map and Rock Height Reclassified Map

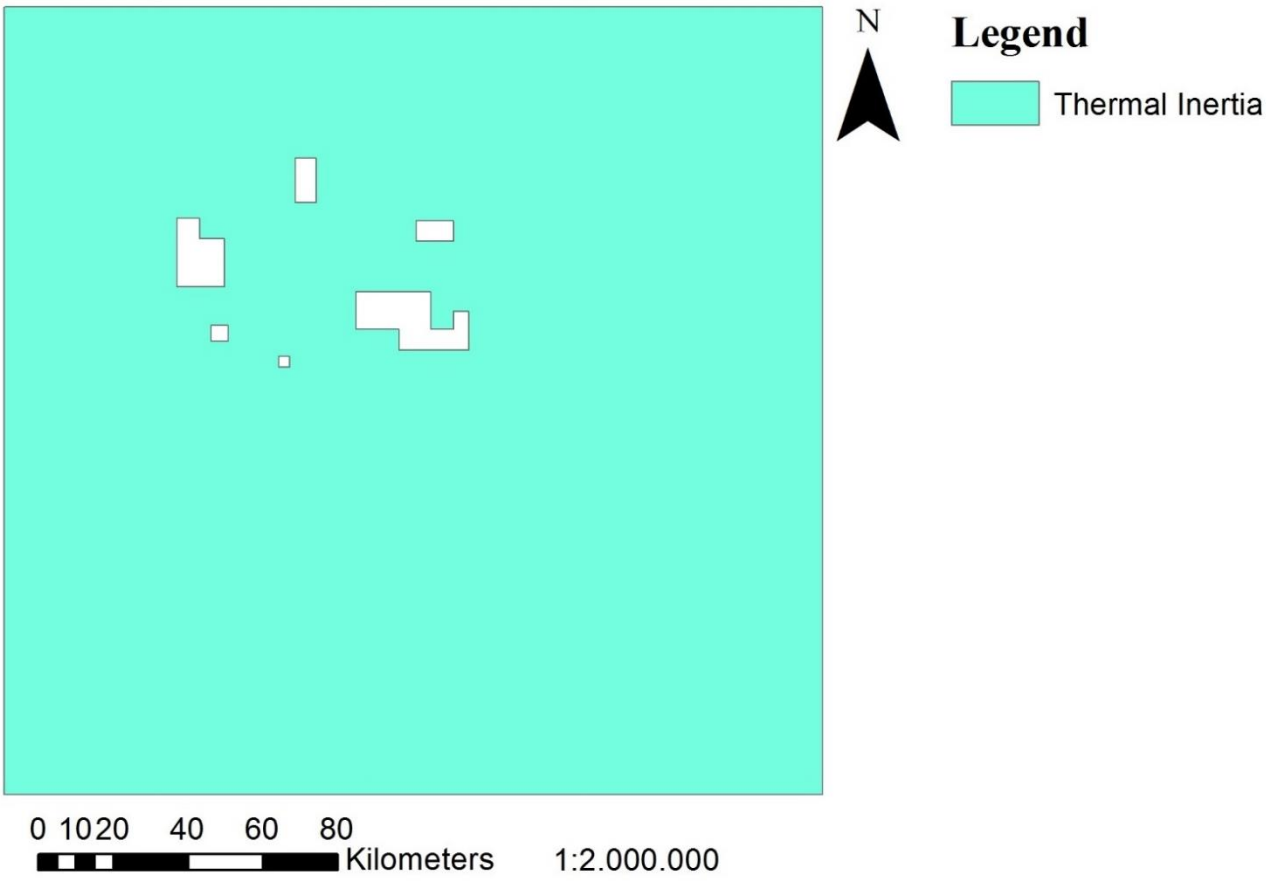

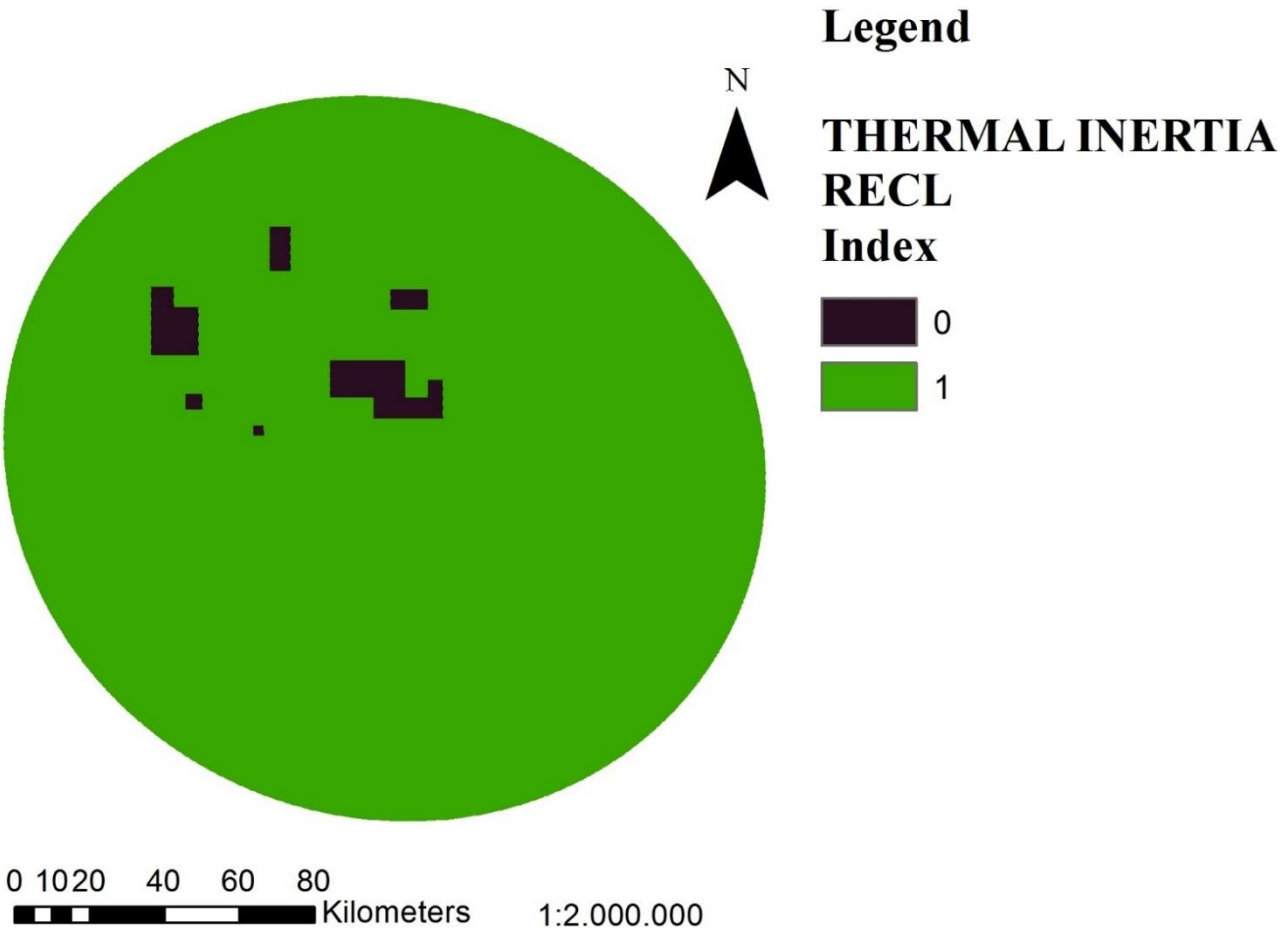

Figure 7-19. PM EZ: Thermal Inertia Map and Thermal Inertia Reclassified Map

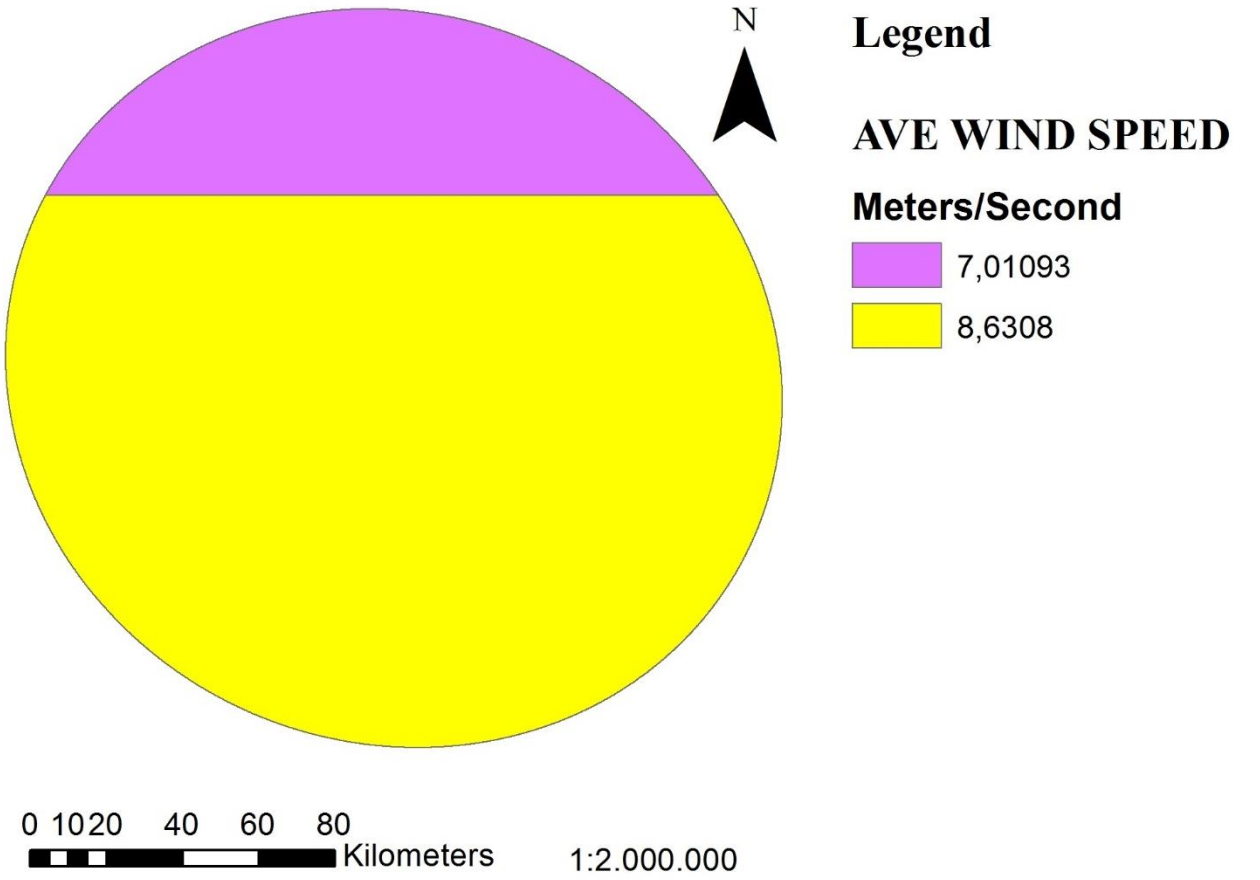

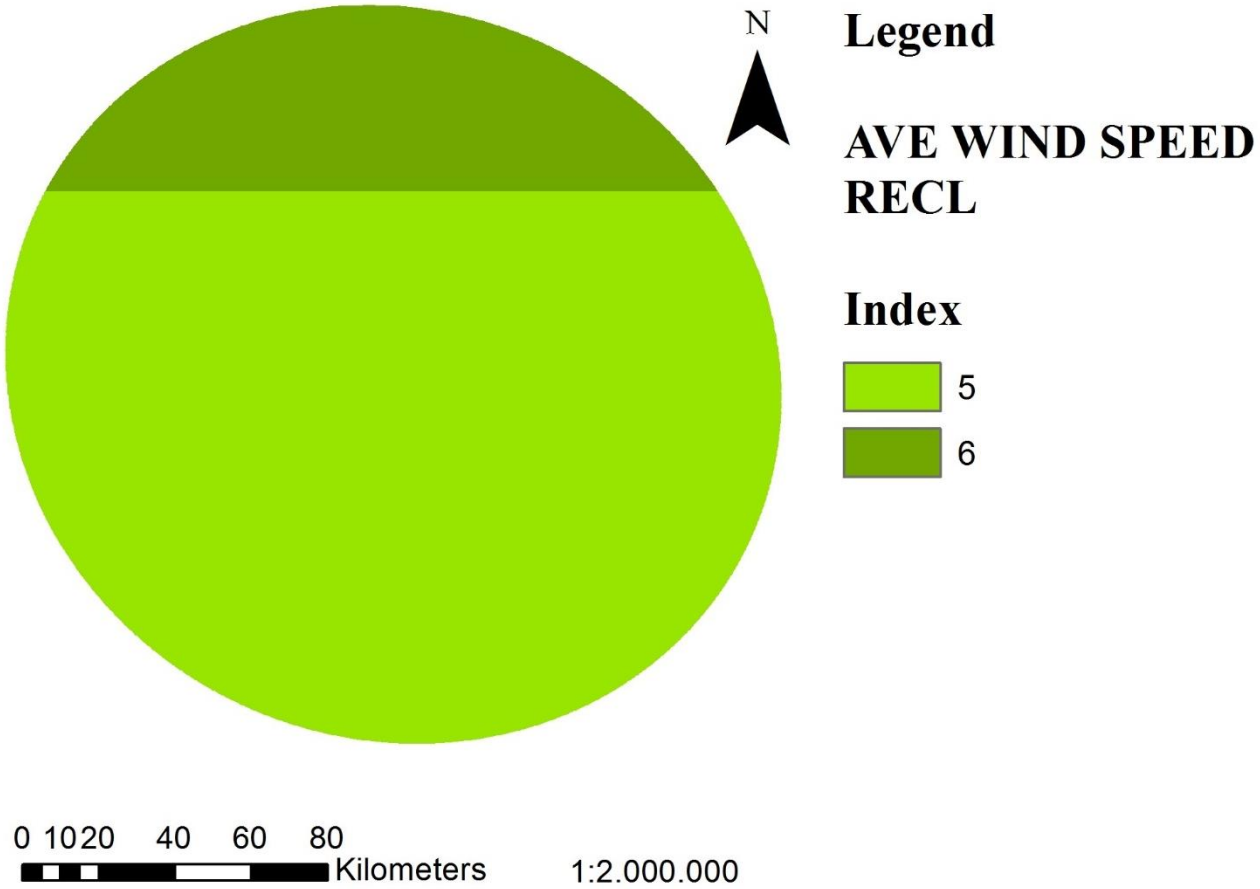

Figure 7-20. PM EZ: Annual Average Wind Speed Map and Annual Average Wind Speed Reclassified Map

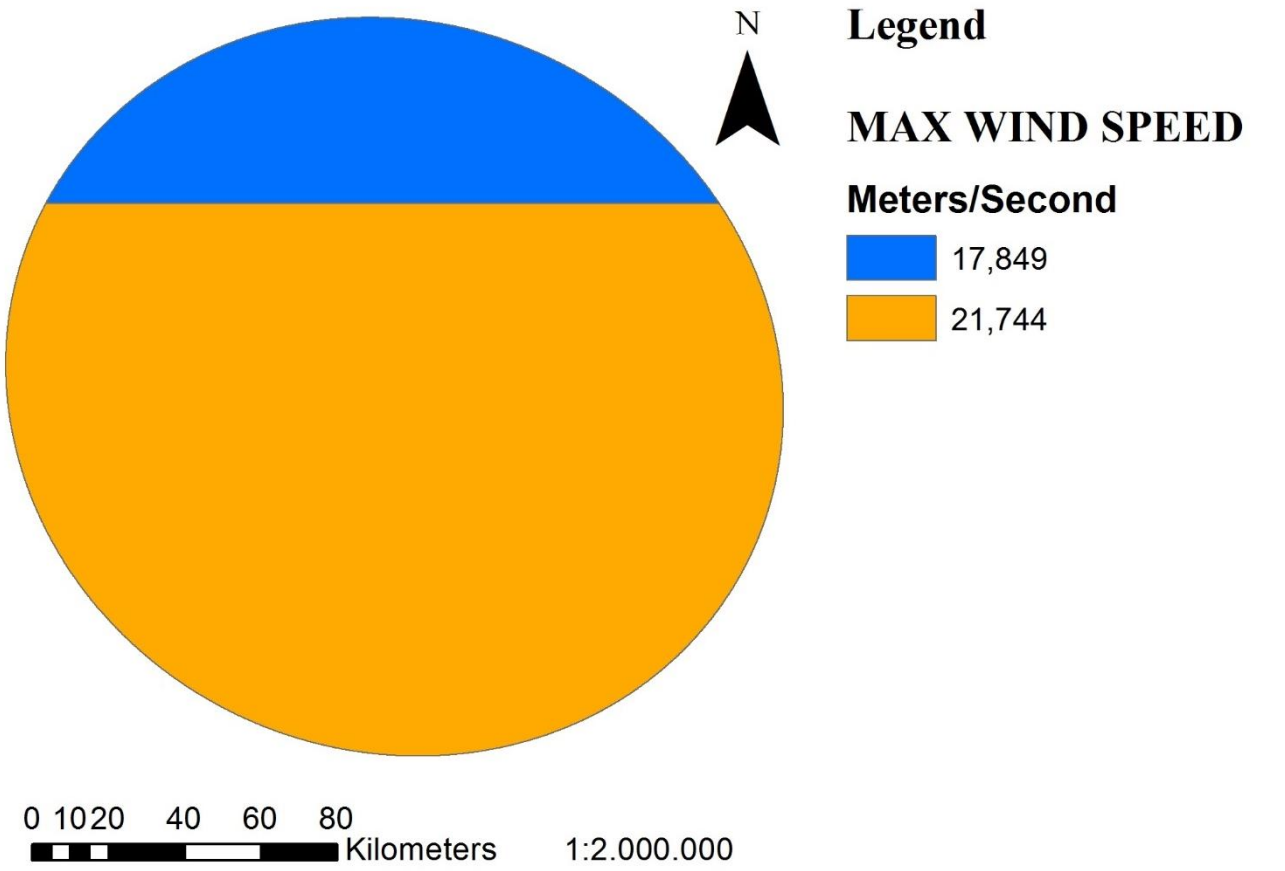

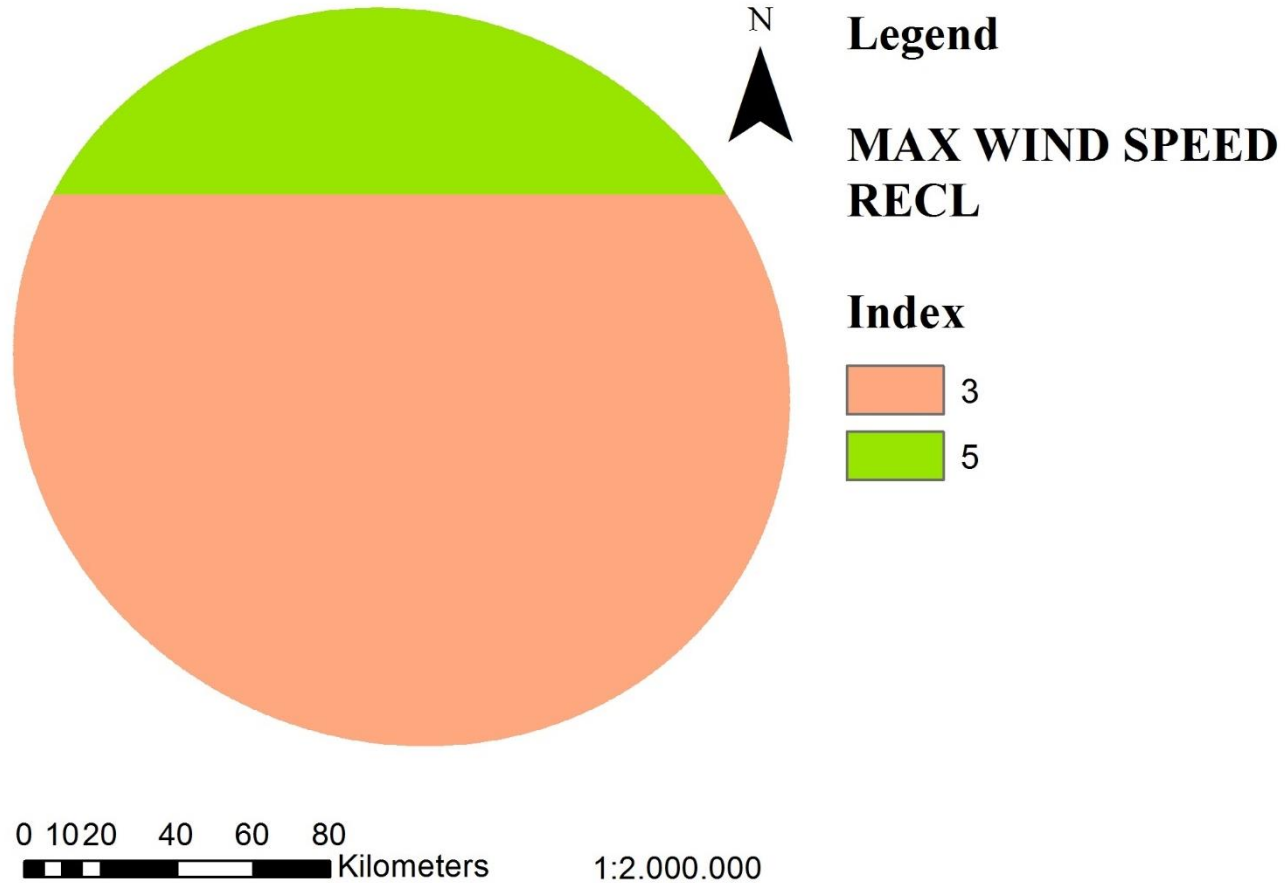

Figure 7-21. PM EZ: Annual Maximum Wind Speed Map and Annual Maximum Wind Speed Reclassified Map

7.2.3 Final Map

Figure 7-22 shows the raster map obtained as final result from the developed workflow in PM.

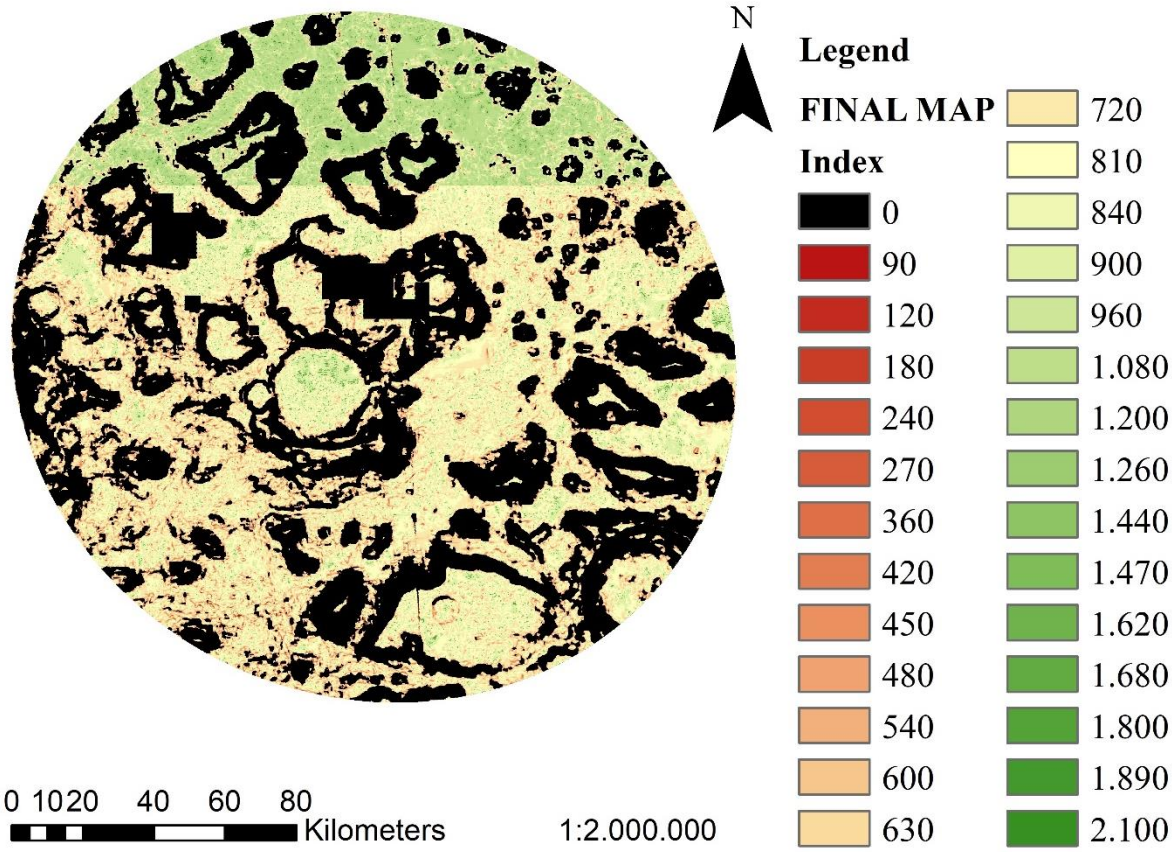

Figure 7-22. PM EZ: Final Map

7.2.4 Critical evaluation of ground geology and morphology

In this Section, CTX datasets are placed side by side with the final raster map in different areas of Protonilus Mensae (PM) Exploration Zone (EZ). This comparison allows conducting a visual analysis to properly justify the effectiveness of the model and the need of a geological analysis. Indeed, as justified in the conducted literature review, achieving the goal of a successful human mission to Mars requires the cooperation between engineering and geology complementary fields.

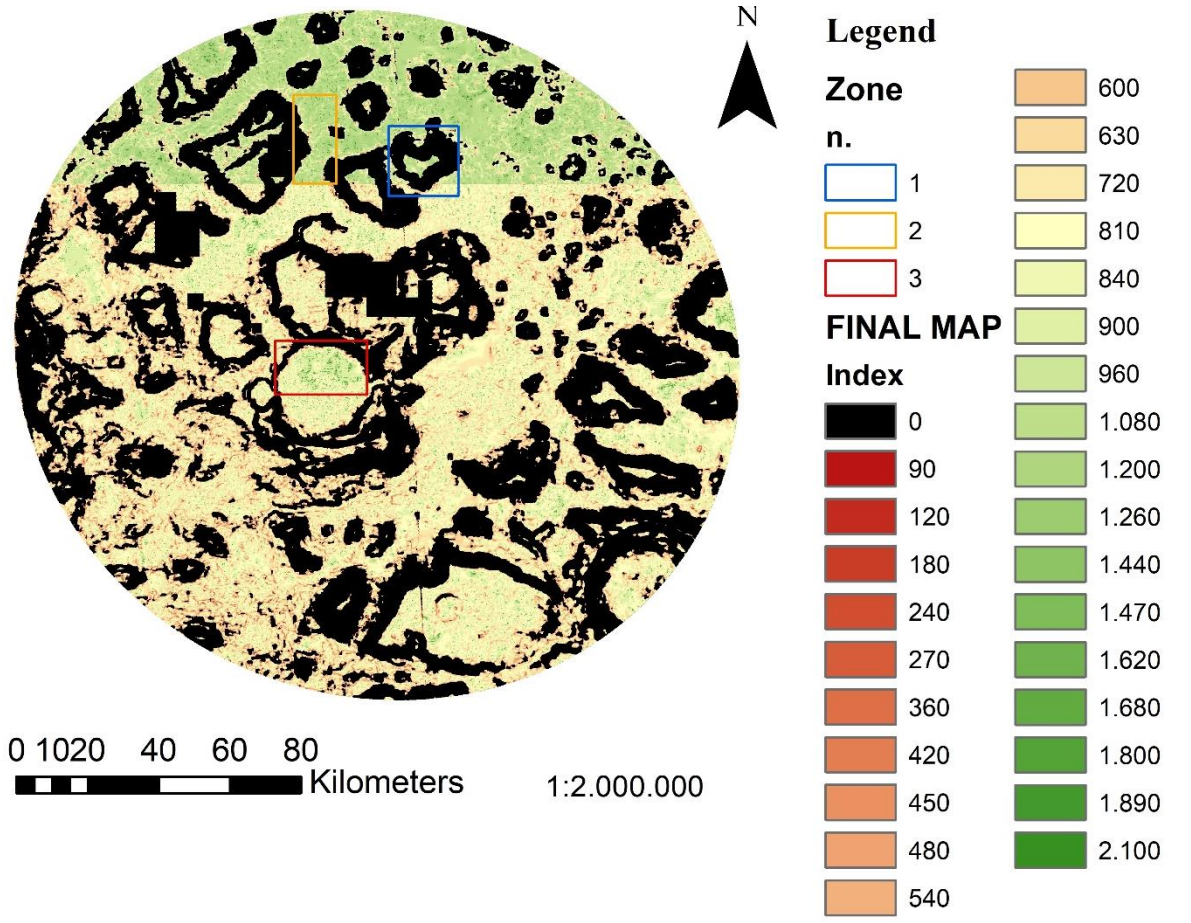

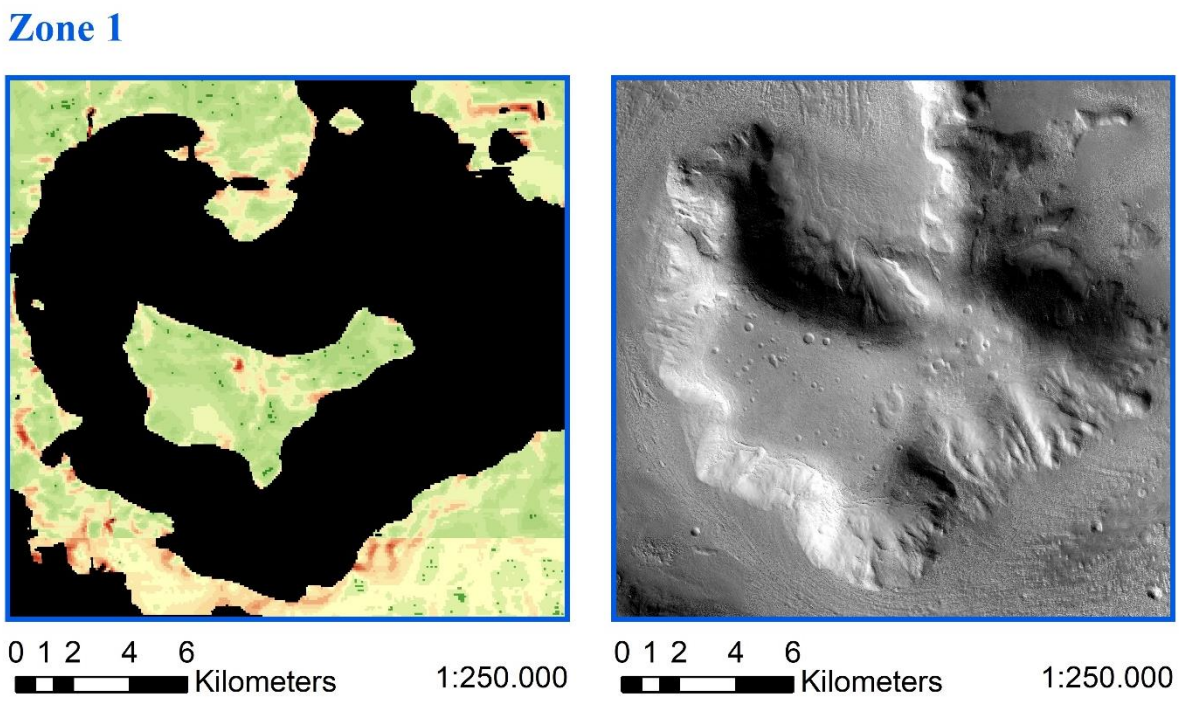

Figure 7-23. PM EZ: comparison between final raster map and CTX dataset (Zone 1)

Zone 2

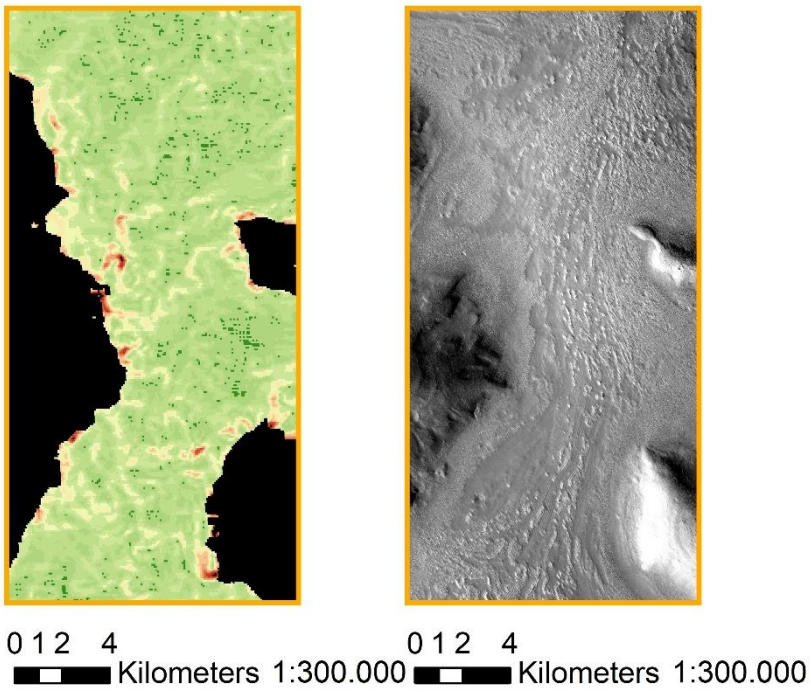

Zone 3

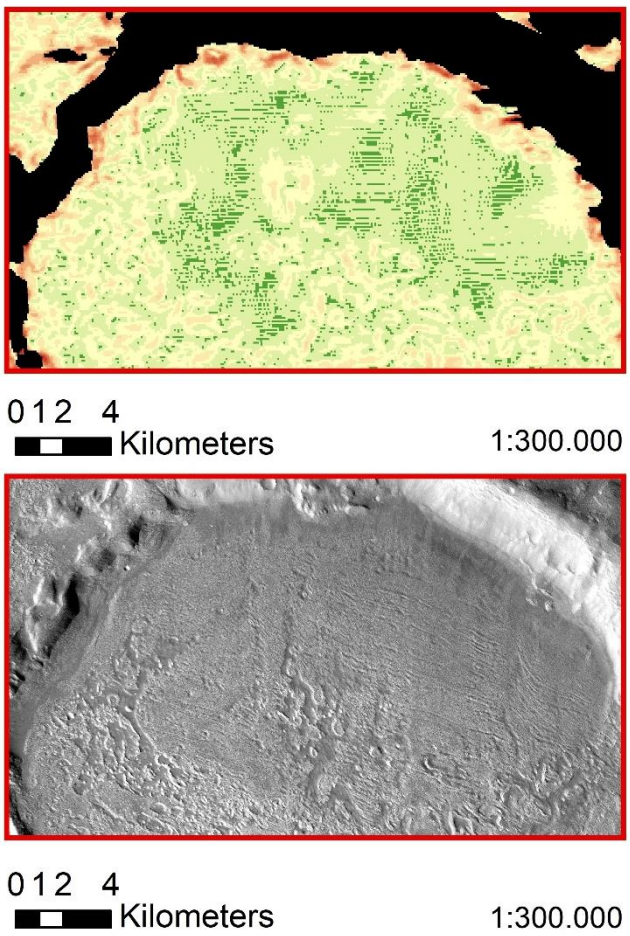

Figure 7-24. PM EZ: comparison between final raster map and CTX dataset (Zones 2 and 3)

7.2.5 Possible configurations of the Landing and Habitation Sites within Protonilus Mensae Exploration Zone

In this Section, three different possible configurations for Landing Site (LS) and Habitation Site (HS) are proposed in Protonilus Mensae (PM) Exploration Zone (EZ). The LS and HS geometrical requirements (LPI, 2015) have been respected, indeed:

$$A_{LS} \cong 25km^2,$$

where:

A_{LS} is the area of the Landing Site (LS),

$$Area_{HS} \cong 50km^2,$$

where:

A_{HS} is the area of the Habitation Site (HS),

$$d_{LS-HS} \leq 5km,$$

where:

d_{LS-HS} is the distance between LS and HS.

An additional requirement of selecting and area with a slope lower than 30° in the HS is considered in this study. This is an additional variable allows to improve the LS/HS selection facilitating movements of the crew pressurised rovers within the HS. This condition is based on LPI (2015) considerations.

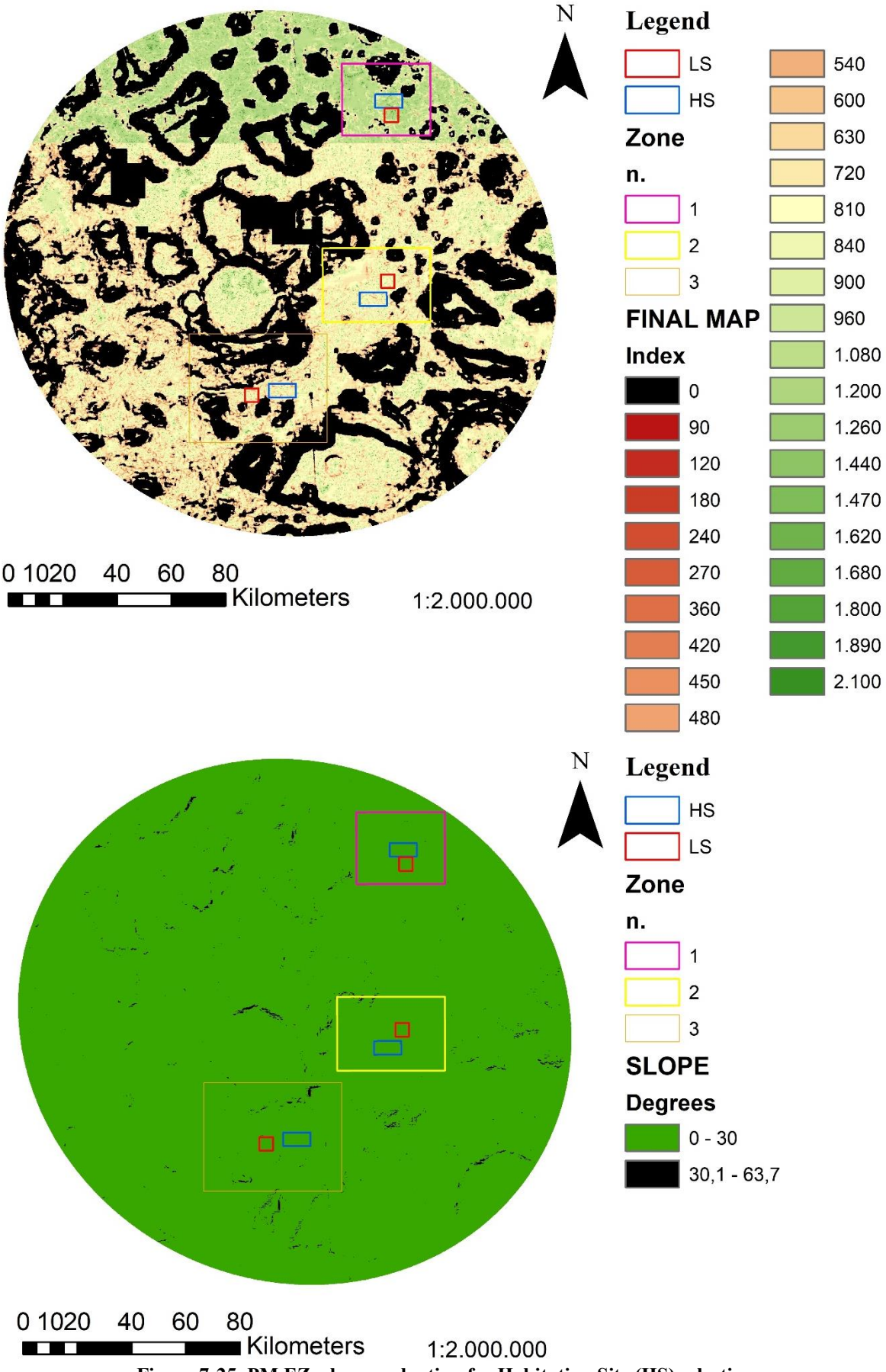

Figure 7-25. PM EZ: slope evaluation for Habitation Site (HS) selection

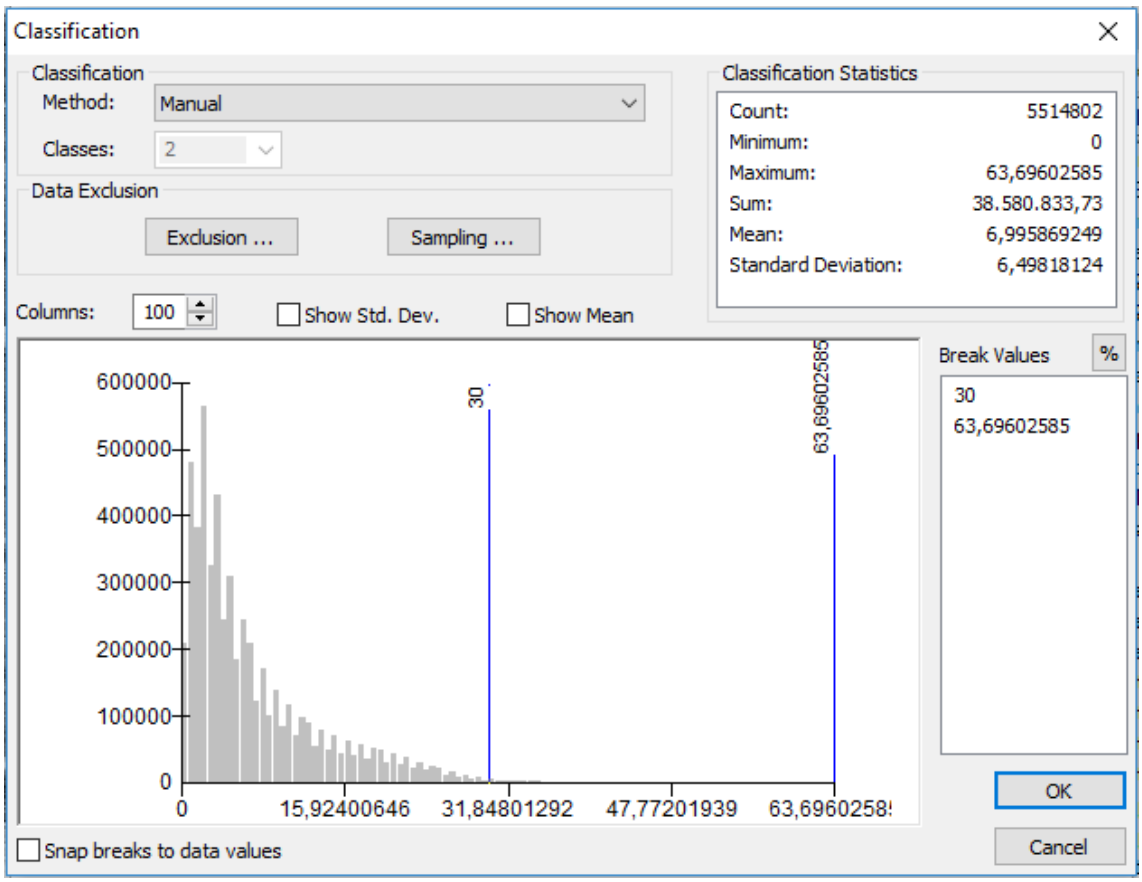

Figure 7-26. PM EZ: slope frequency histogram for Habitation Site (HS) selection

Zone 1

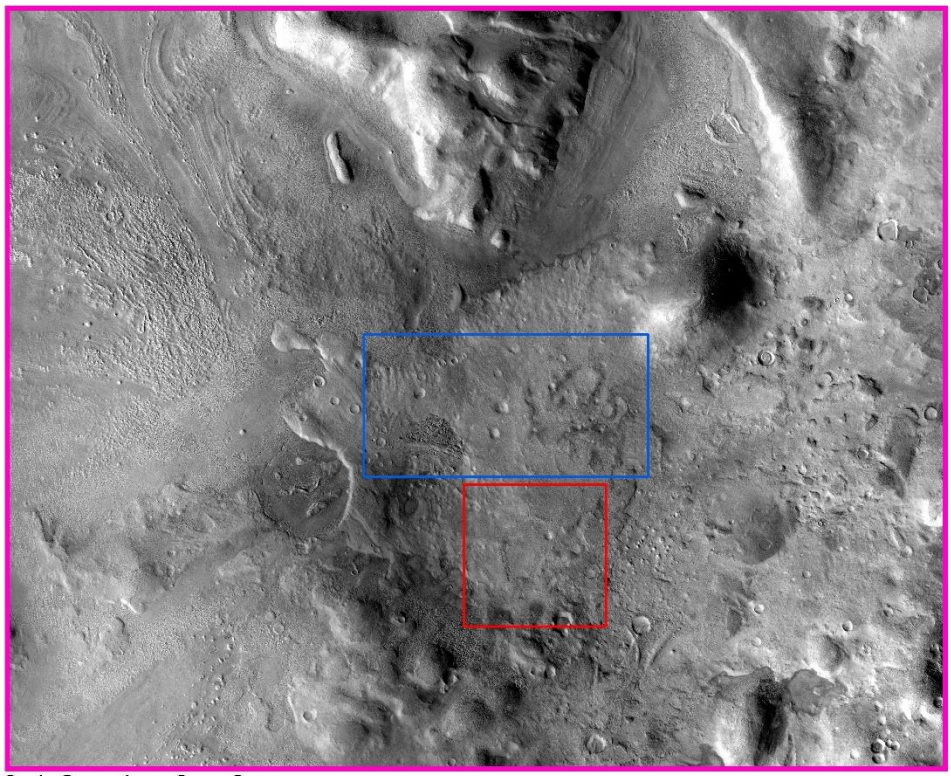

Landing Site

Area = 25 km^2

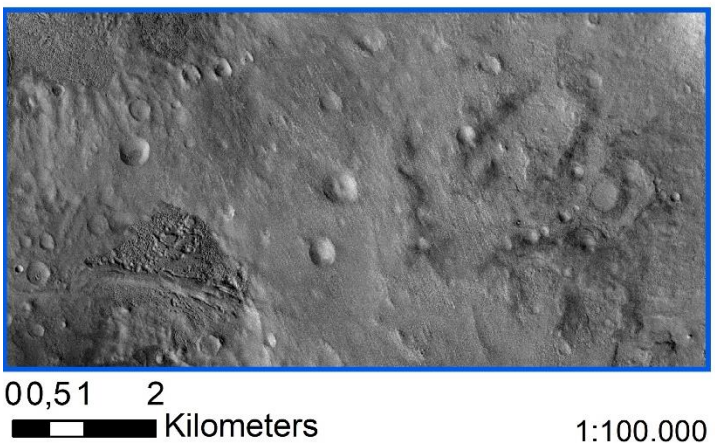

Habitation Site

Area = 50 km^2

Figure 7-27. PM EZ: Landing Site (LS) and Habitation Site (HS) possible configuration (Zone 1)

Zone 2

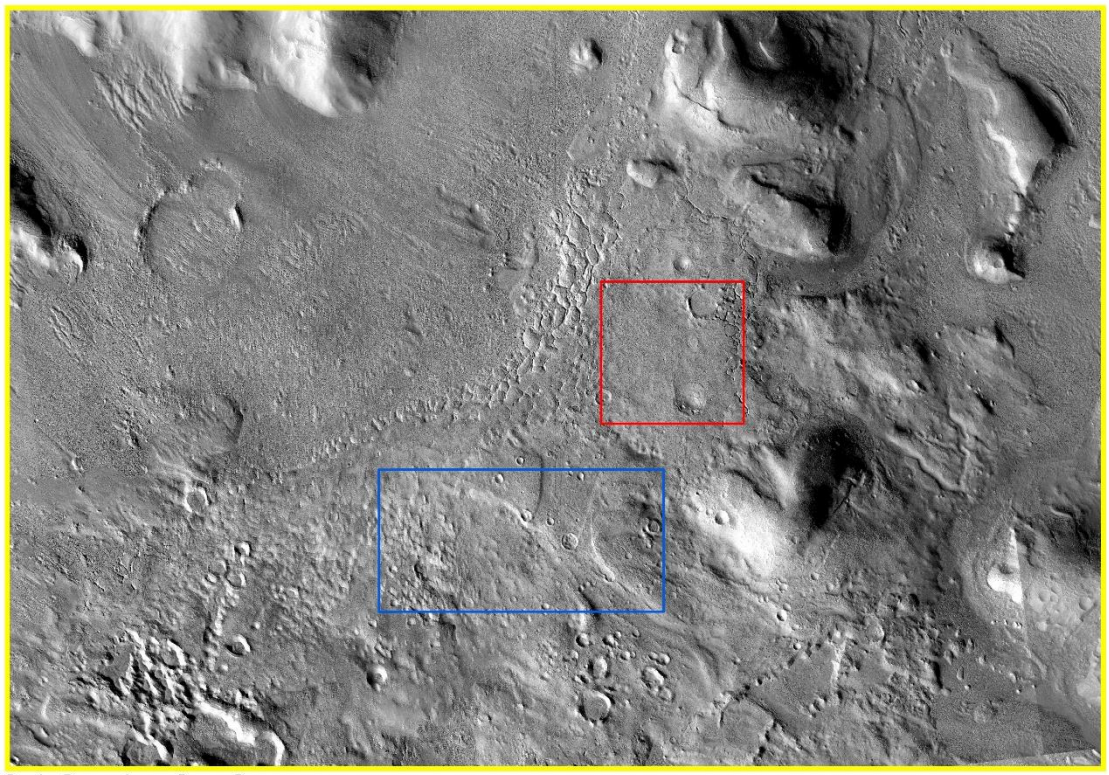

0 1 2 4 6 8
Kilometers

1:250.000

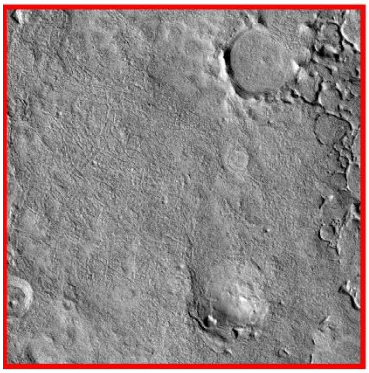

Landing Site

Area = 25 km^2

00,51 2
Kilometers 1:100.000

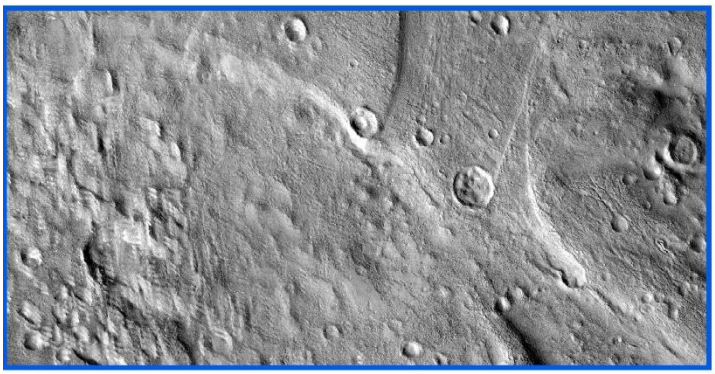

Habitation Site

Area = 50 km^2

00,51 2
Kilometers

1:100.000

Figure 7-28. PM EZ: Landing Site (LS) and Habitation Site (HS) possible configuration (Zone 2)

Zone 3

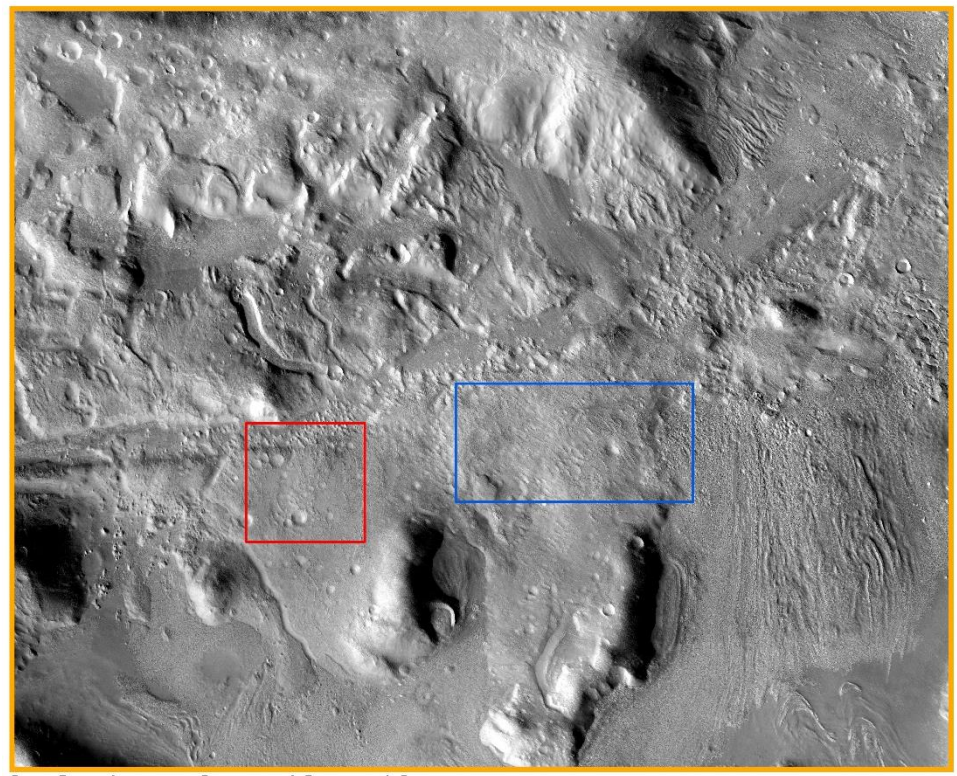

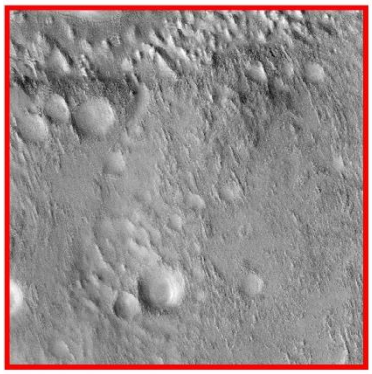

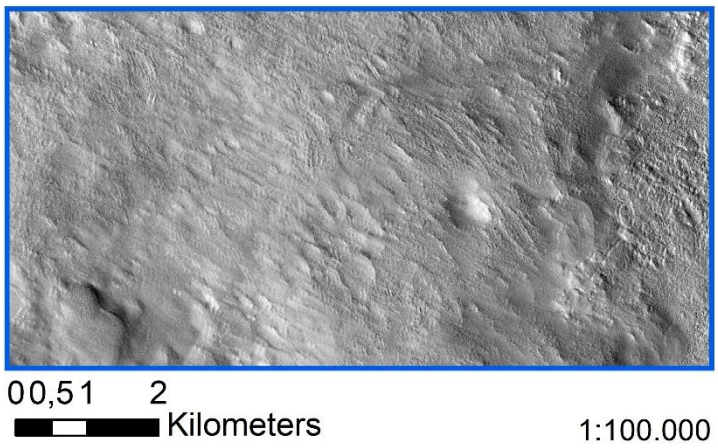

Figure 7-29. PM EZ: Landing Site (LS) and Habitation Site (HS) possible configuration (Zone 3)

7.3 Deuteronilus Mensae I Exploration Zone

7.3.1 Geographical Framework

Figure 7-30 provides Deuteronilus Mensae I (DMI) Exploration Zone (EZ) geographical framework. DMI EZ's centre is located at 39°N.

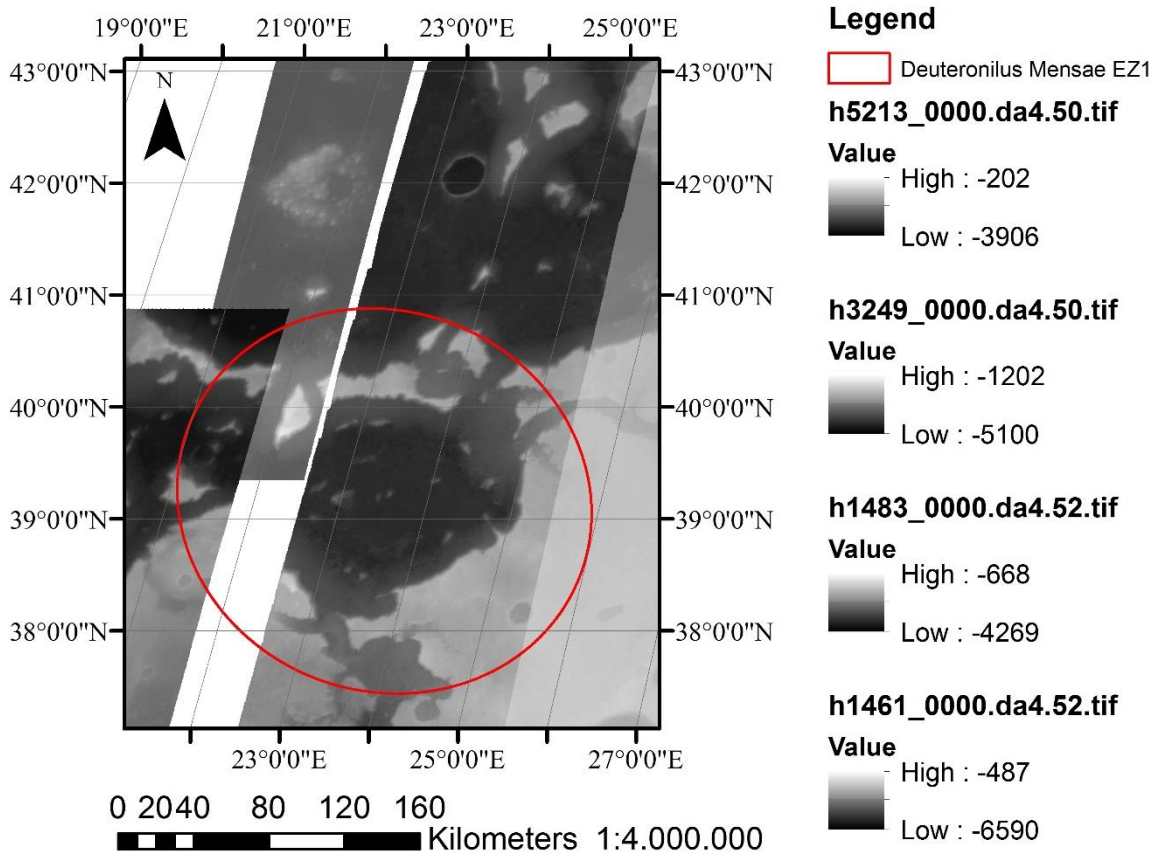

Figure 7-30. Deuteronilus Mensae I (DMI) Exploration Zone (EZ): geographical framework; HRSC DTM images 75 m/pixel resolution

7.3.2 Engineering Parameters Maps and Reclassified Maps

This Section reports the output maps obtained in Deuteronilus Mensae I (DMI) Exploration Zone (EZ).

The engineering map layers of (1) Elevation, (2) Slope, (3) Terrain Relief, and (4) Rock Height are automatically generated from the workflow developed in this thesis. Otherwise, (5) Thermal Inertia, (6) Annual Maximum Wind Speed, and (7) Annual Average Wind Speed engineering map layers are drawn as shapefiles and uploaded as input files in the model (see Section 6.1.3).

All these maps show how each engineering parameter varies within DMI. Each map is then reclassified by associating a specific index to a defined range of values. The associated indexes (1) are consistent with defined Engineering Constraints (see Table 6-3) and (2) are directly related to the goodness of each parameter.

All the introduced maps are shown in this Section.

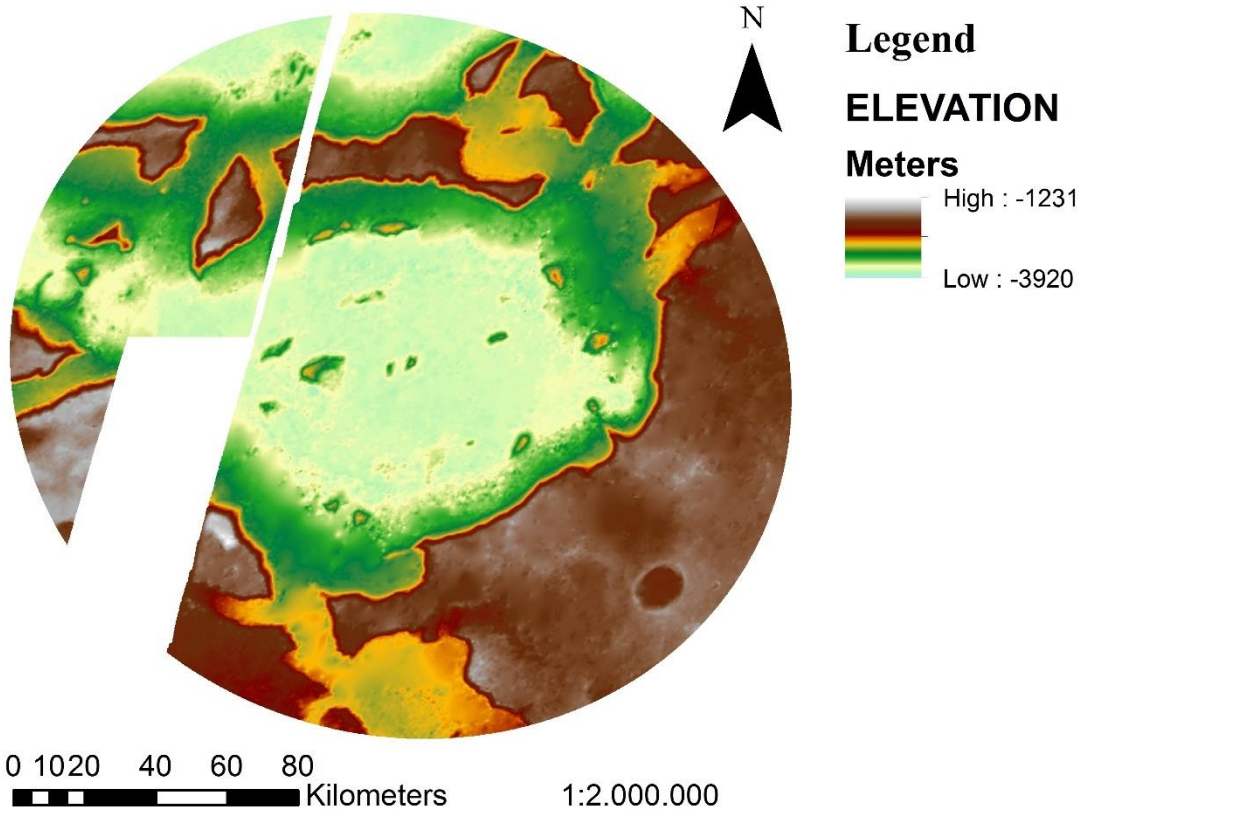

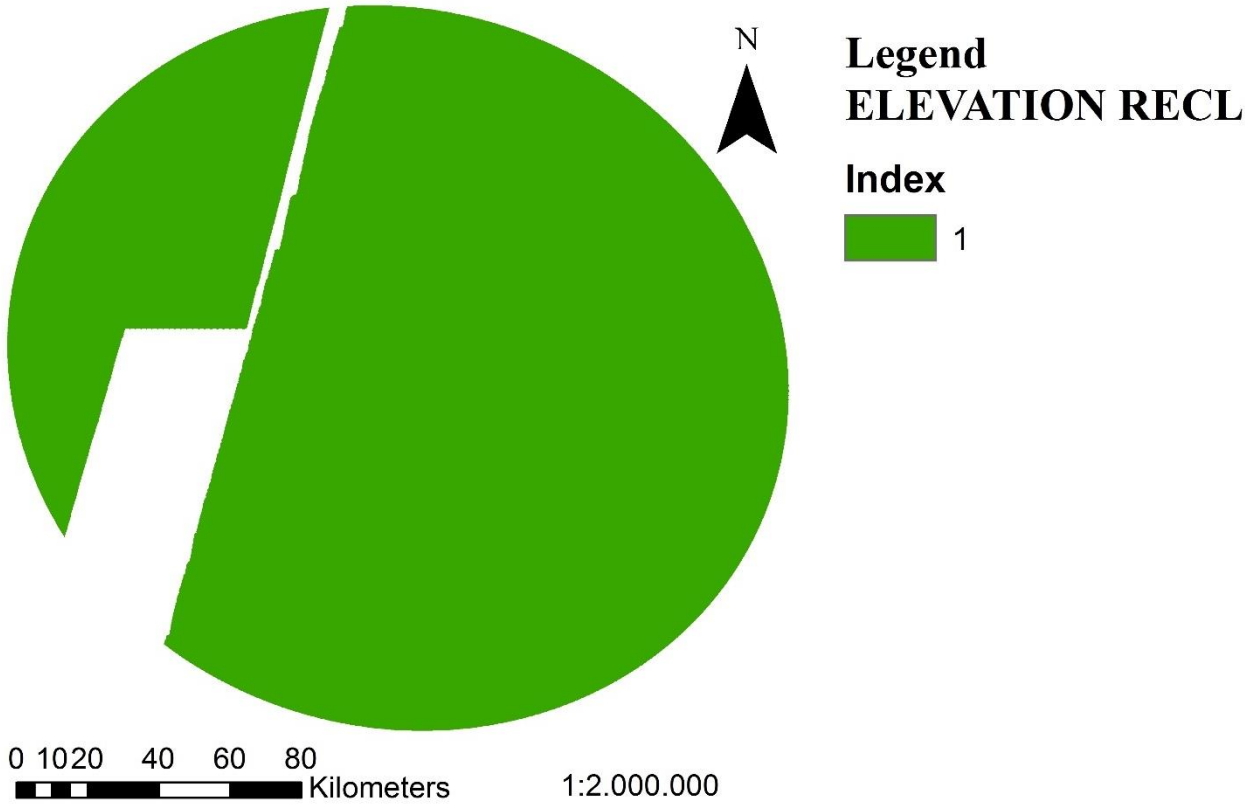

Figure 7-31. DMI EZ: Elevation Map and Elevation Reclassified Map

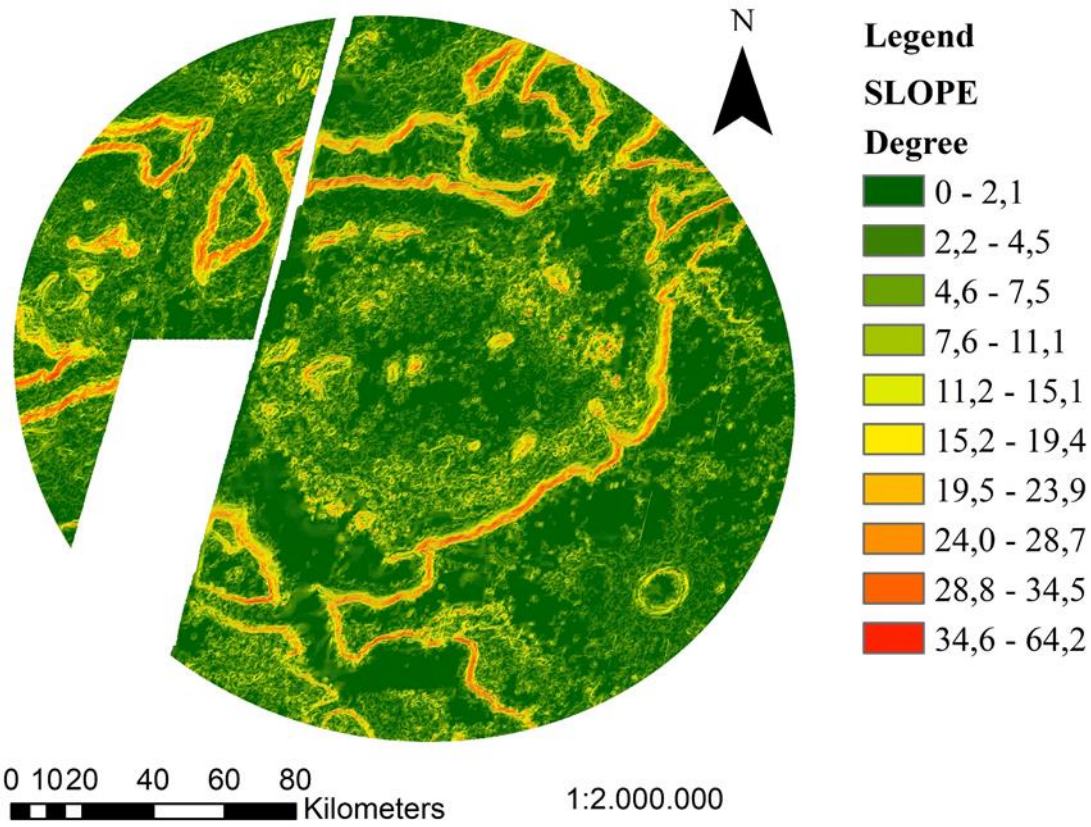

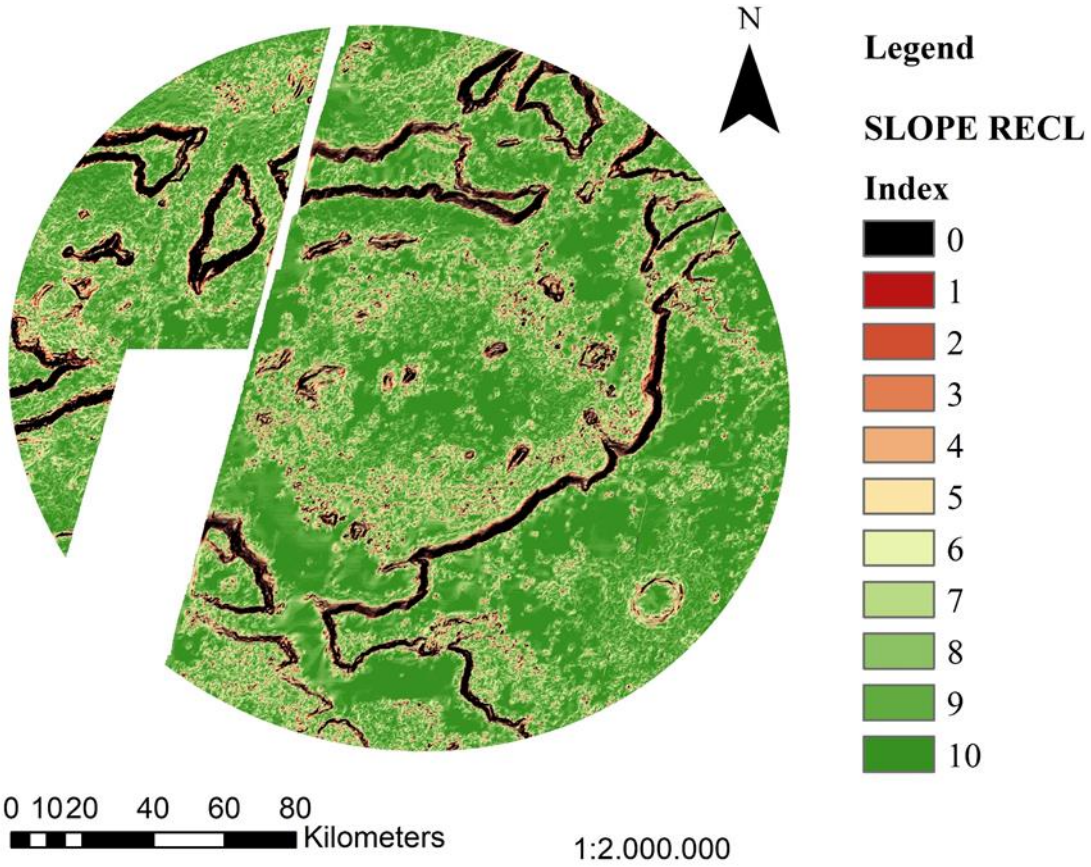

Figure 7-32. DMI EZ: Slope Map and Slope Reclassified Map

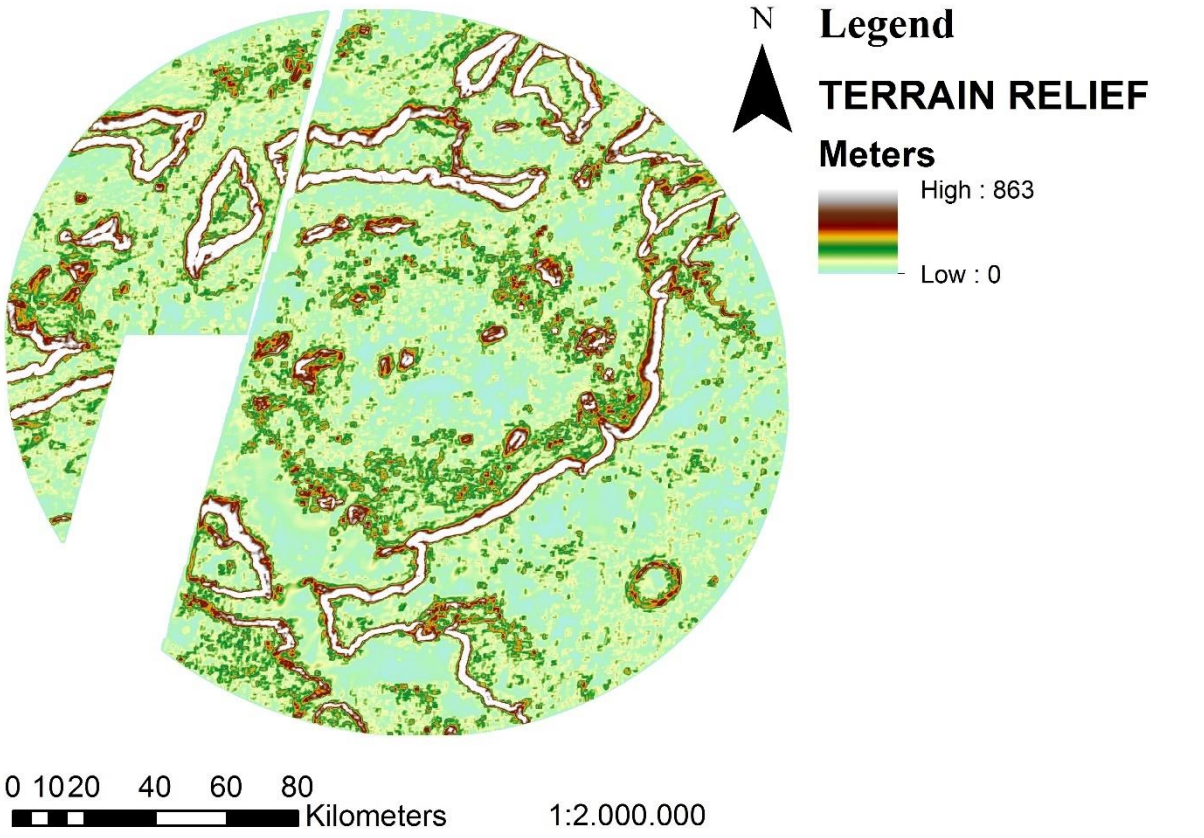

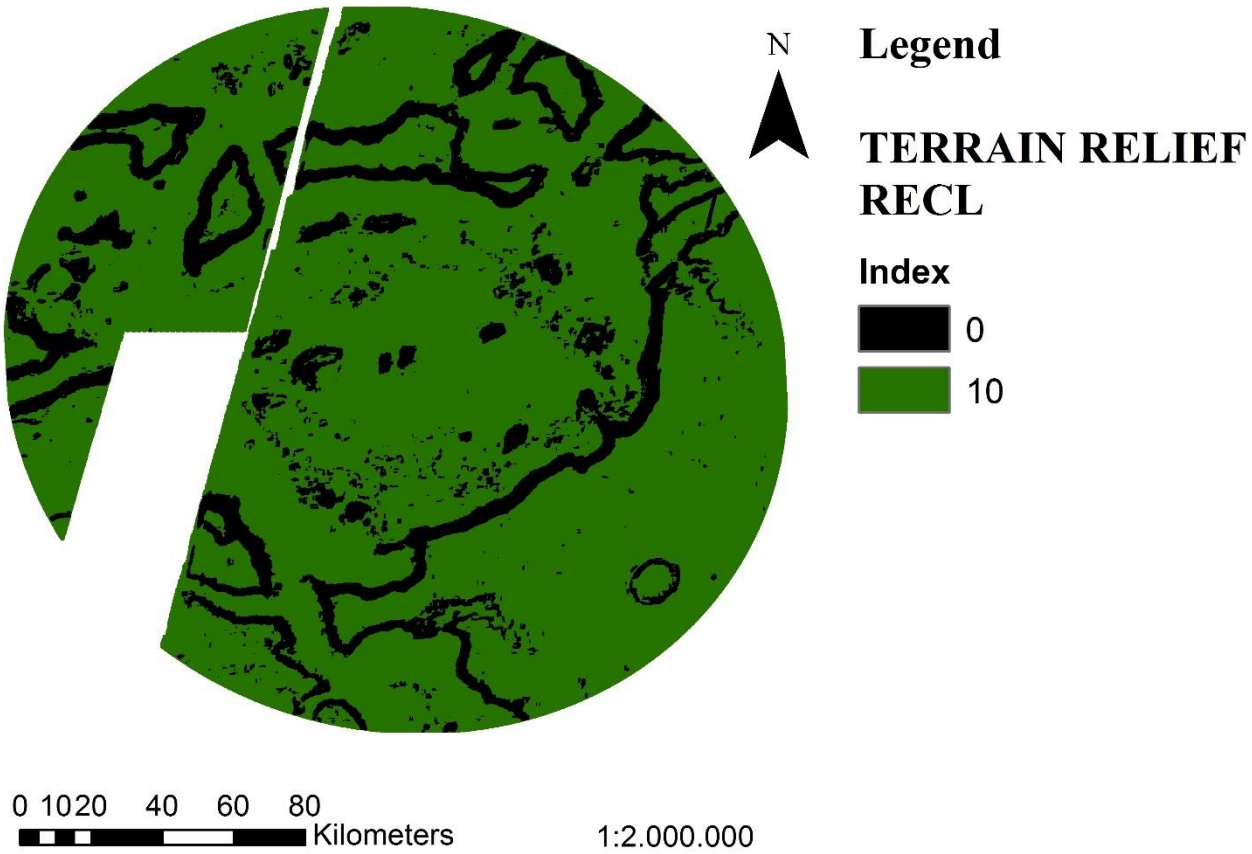

Figure 7-33. DMI EZ: Terrain Relief Map and Terrain Relief Reclassified Map

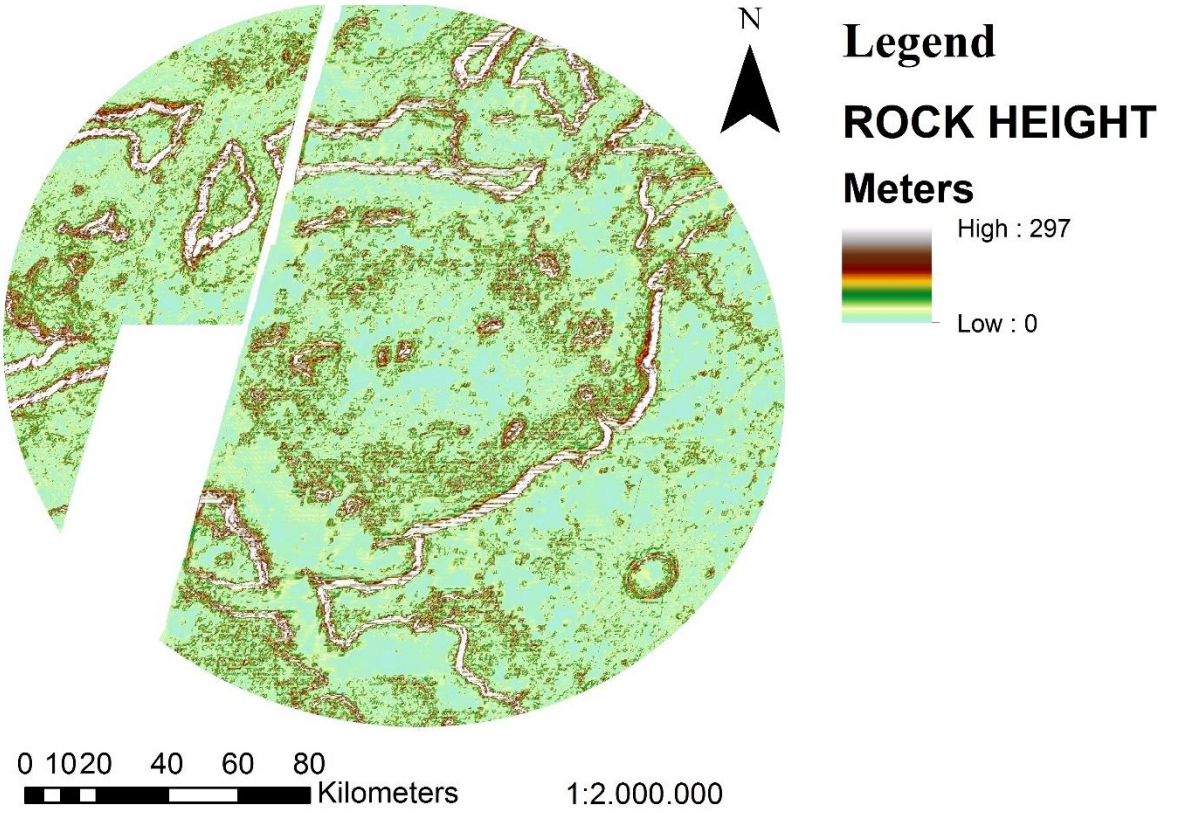

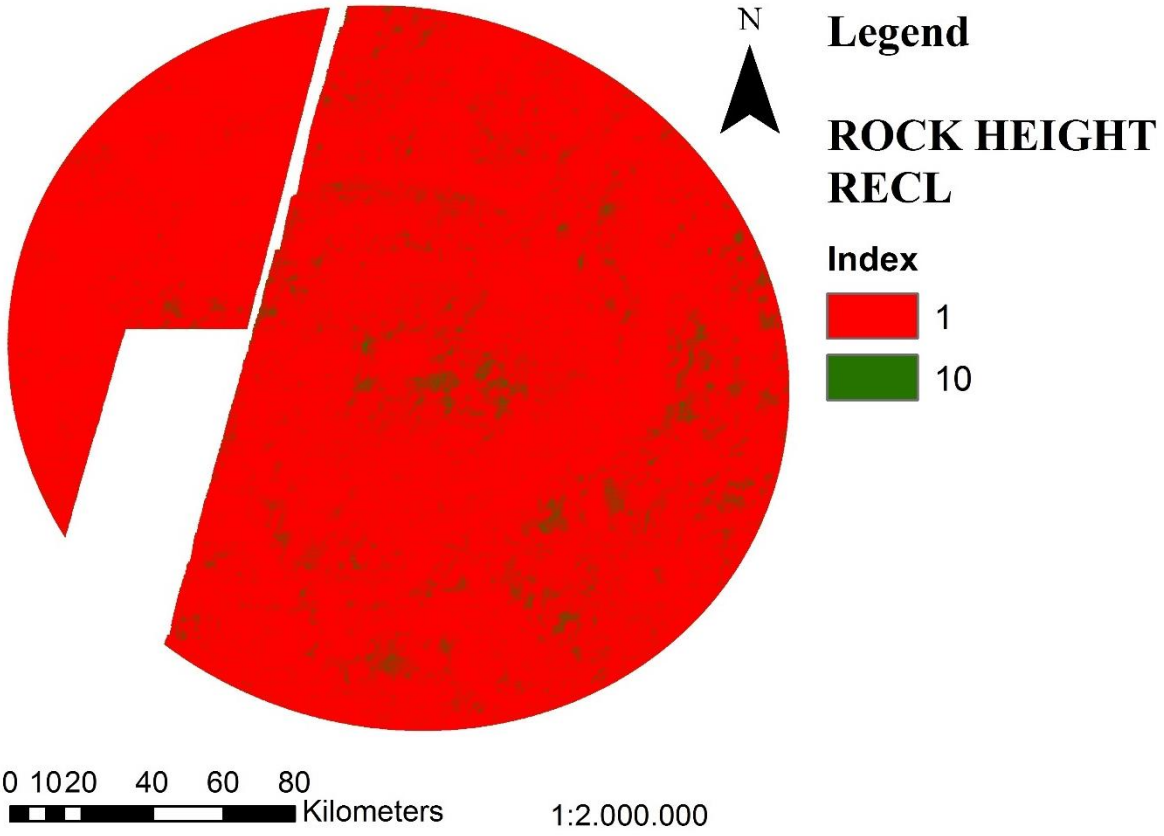

Figure 7-34. DMI EZ: Rock Height Map and Rock Height Reclassified Map

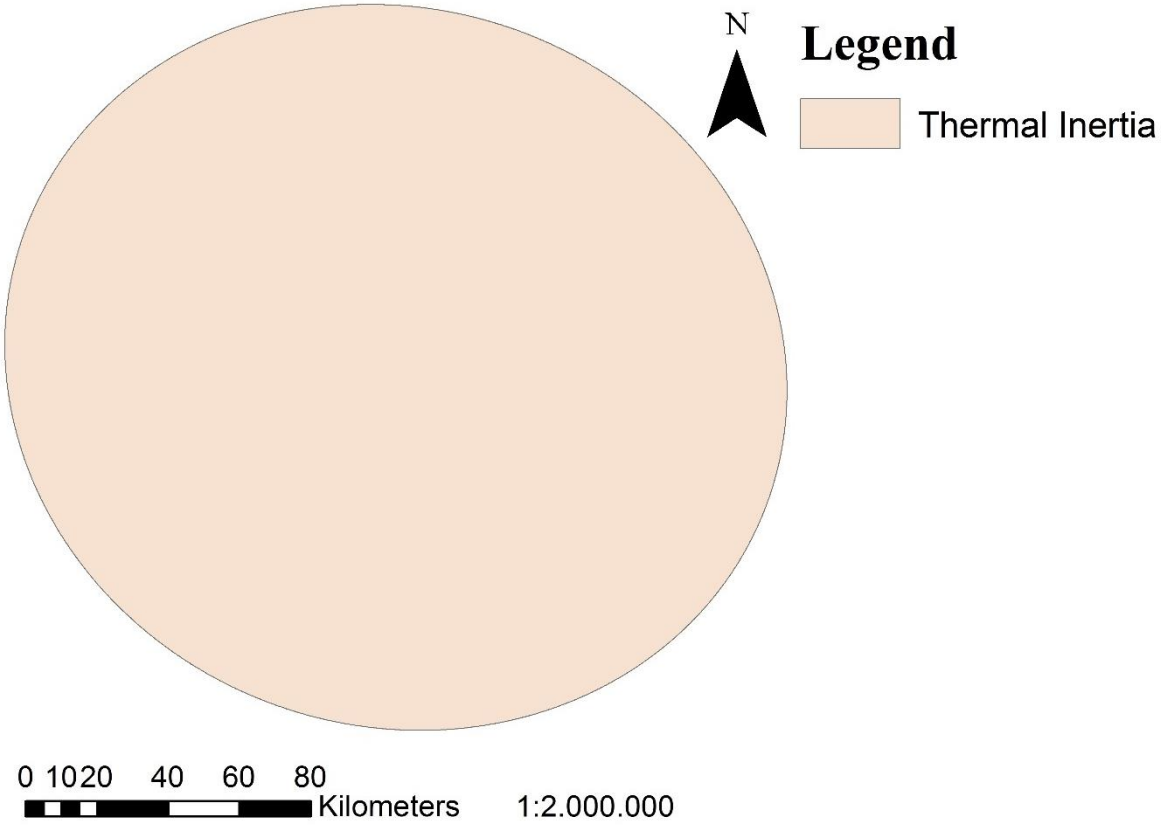

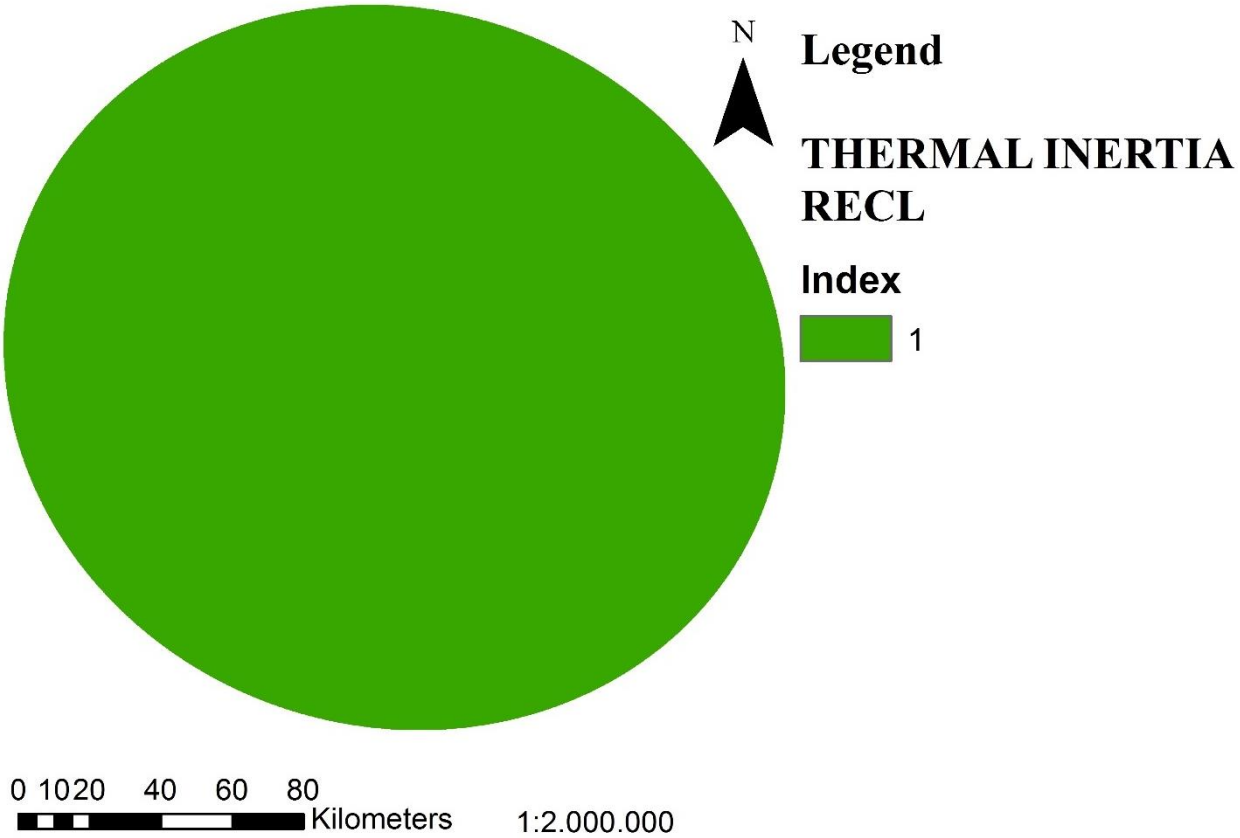

Figure 7-35. DMI EZ: Thermal Inertia Map and Thermal Inertia Reclassified Map

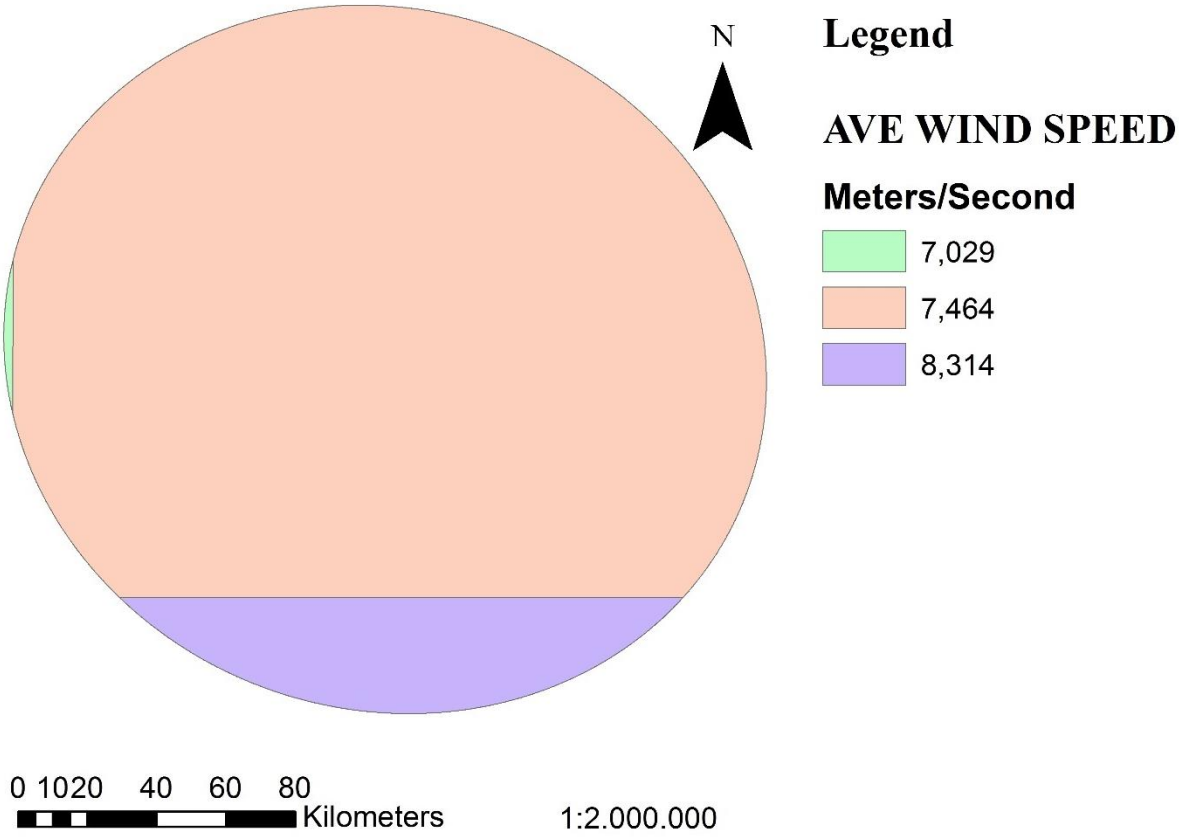

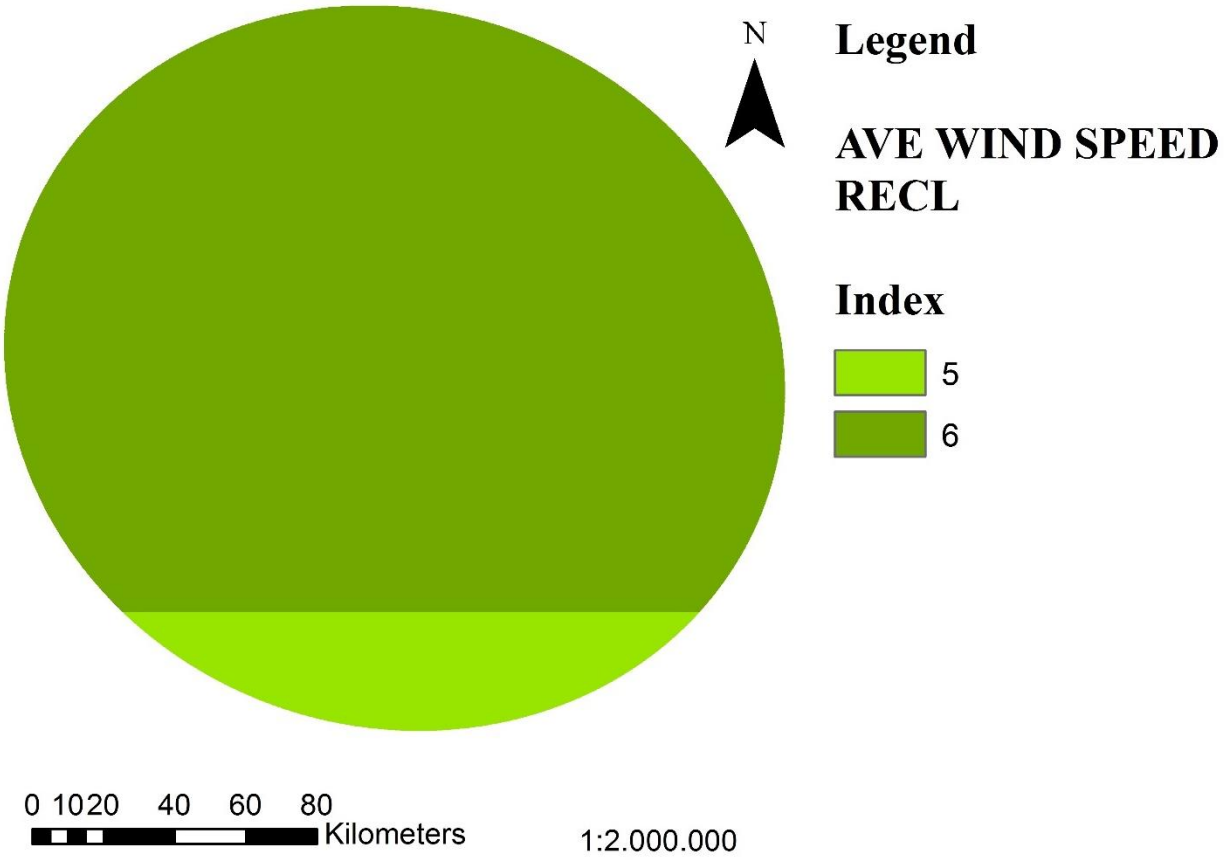

Figure 7-36. DMI EZ: Annual Average Wind Speed Map and Annual Average Wind Speed Reclassified Map

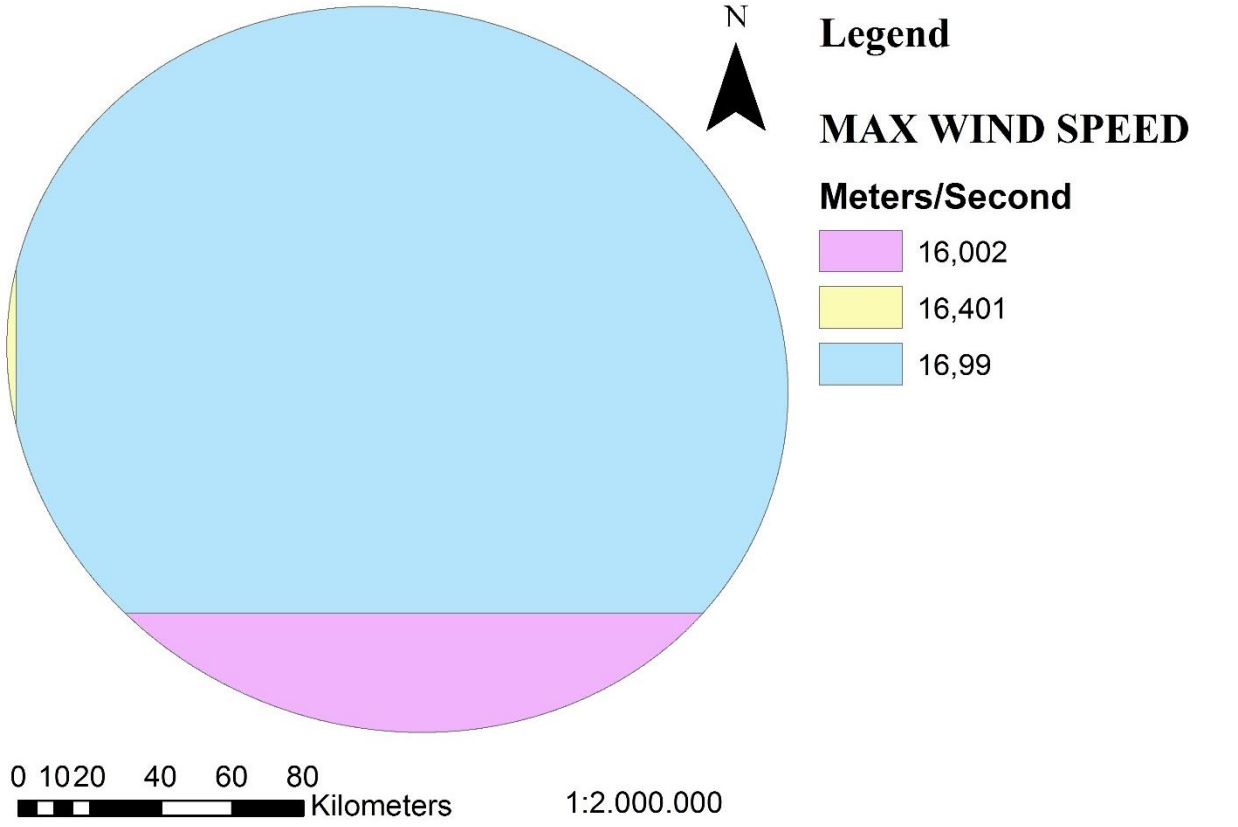

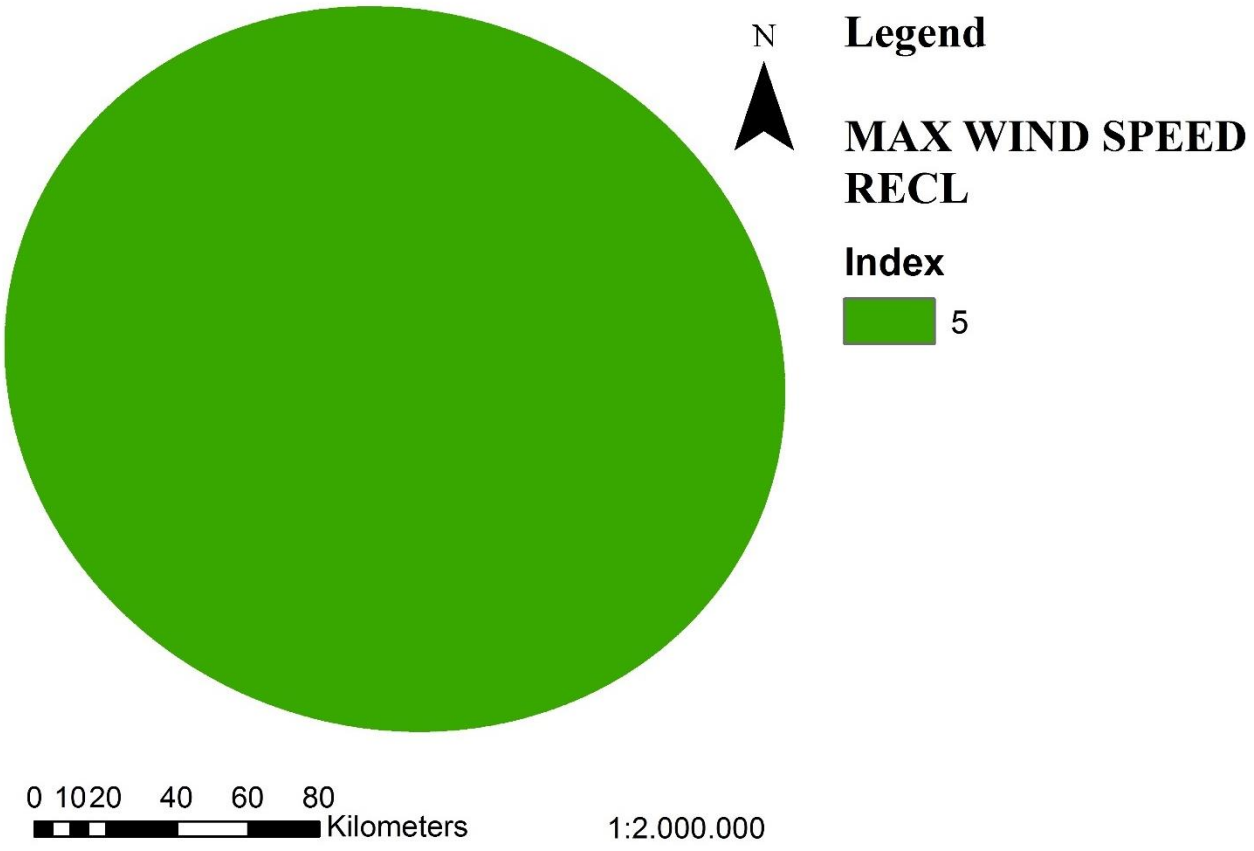

Figure 7-37. DMI EZ: Annual Maximum Wind Speed Map and Annual Maximum Wind Speed Reclassified Map

7.3.3 Final Map

Figure 7-38Figure 7-22 shows the raster map obtained as final result from the developed workflow in DMI.

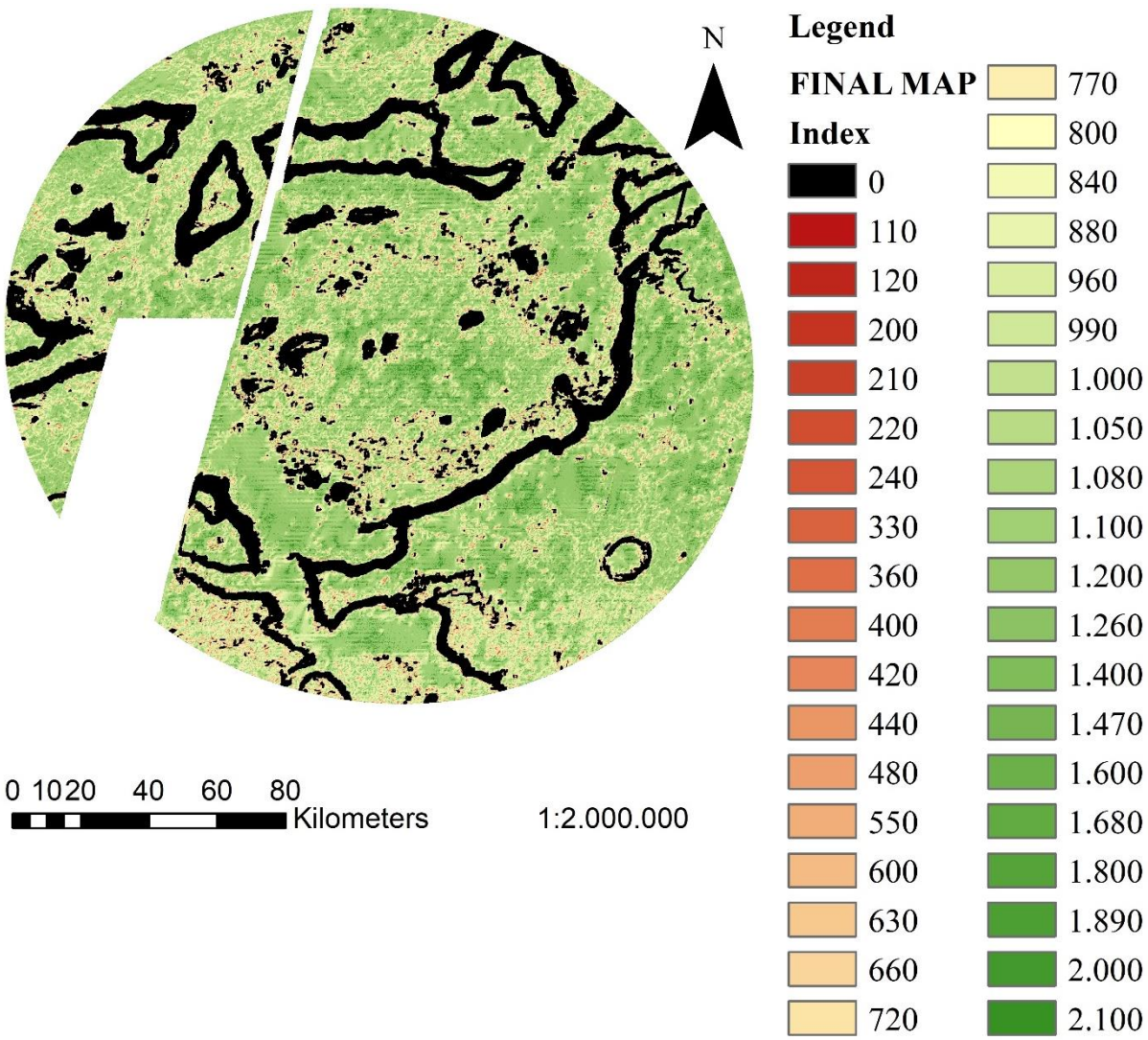

Figure 7-38. DMI EZ: Final Map

7.4 Deuteronilus Mensae II Exploration Zone

7.4.1 Geographical Framework

Figure 7-39 provides Deuteronilus Mensae II (DMII) Exploration Zone (EZ) geographical framework. DMII EZ's centre is located at 41°N.

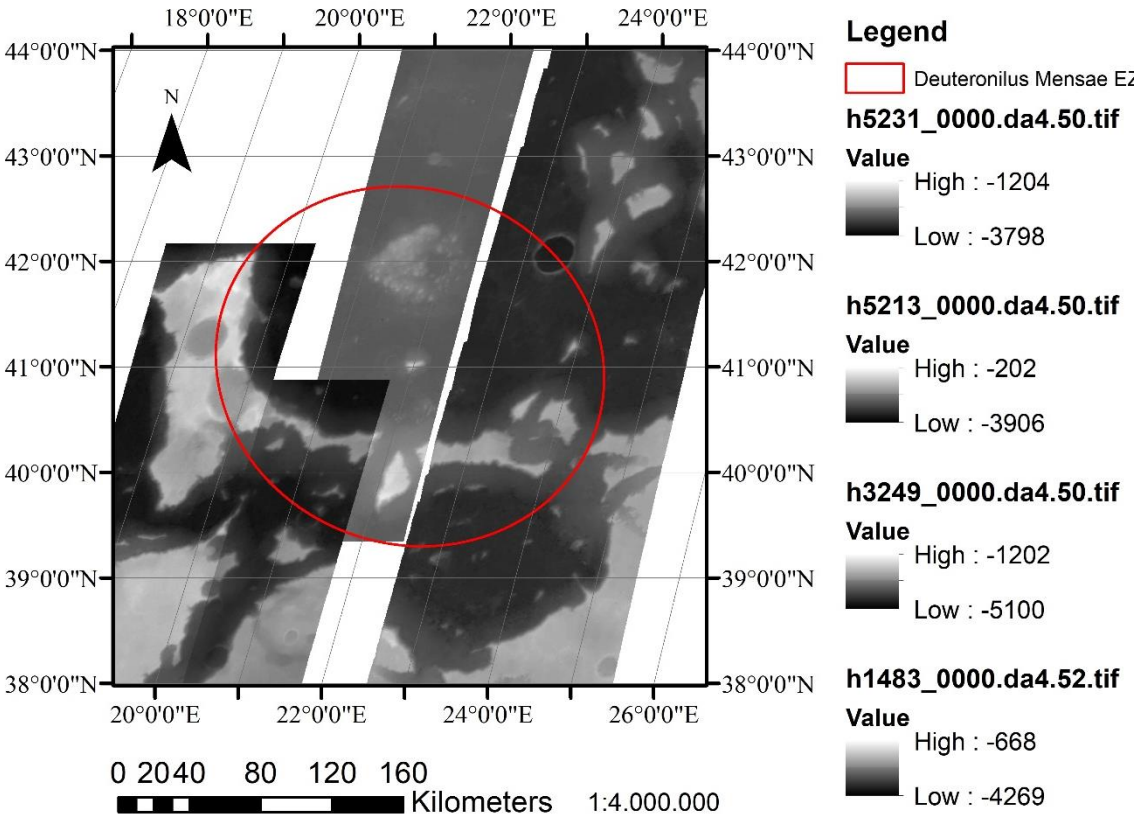

Figure 7-39. Deuteronilus Mensae II (DMII) Exploration Zone (EZ): geographical framework; HRSC DTM images 75 m/pixel resolution

7.4.2 Engineering Parameters Maps and Reclassified Maps

This Section reports the output maps obtained in Deuteronilus Mensae II (DMII) Exploration Zone (EZ).

The engineering map layers of (1) Elevation, (2) Slope, (3) Terrain Relief, and (4) Rock Height are automatically generated from the workflow developed in this thesis. Otherwise, (5) Thermal Inertia, (6) Annual Maximum Wind Speed, and (7) Annual Average Wind Speed engineering map layers are drawn as shapefiles and uploaded as input files in the model (see Section 6.1.3).

All these maps show how each engineering parameter varies within DMII. Each map is then reclassified by associating a specific index to a defined range of values. The associated indexes (1) are consistent with defined Engineering Constraints (see Table 6-3) and (2) are directly related to the goodness of each parameter.

All the introduced maps are shown in this Section.

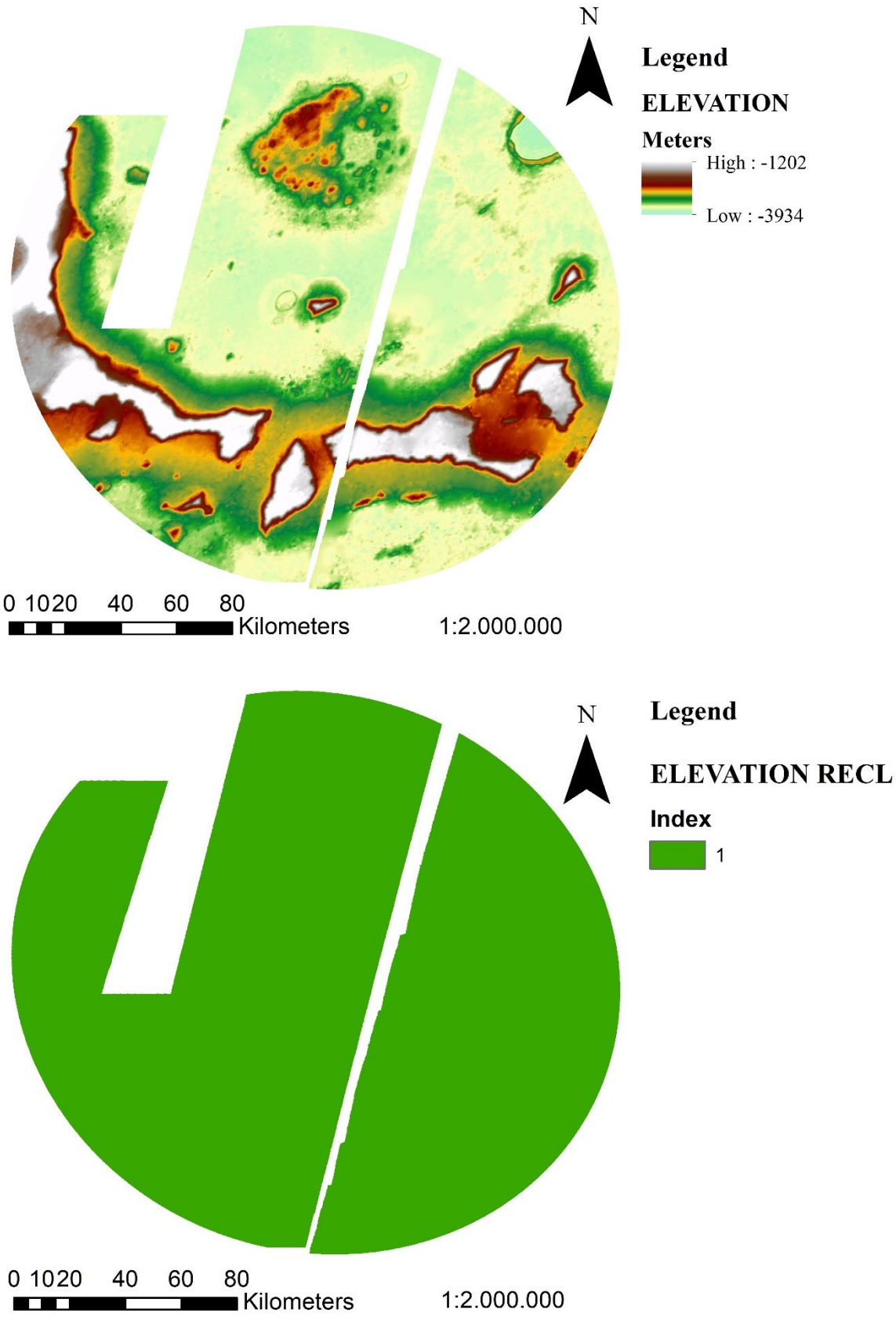

Figure 7-40. DMII EZ: Elevation Map and Elevation Reclassified Map

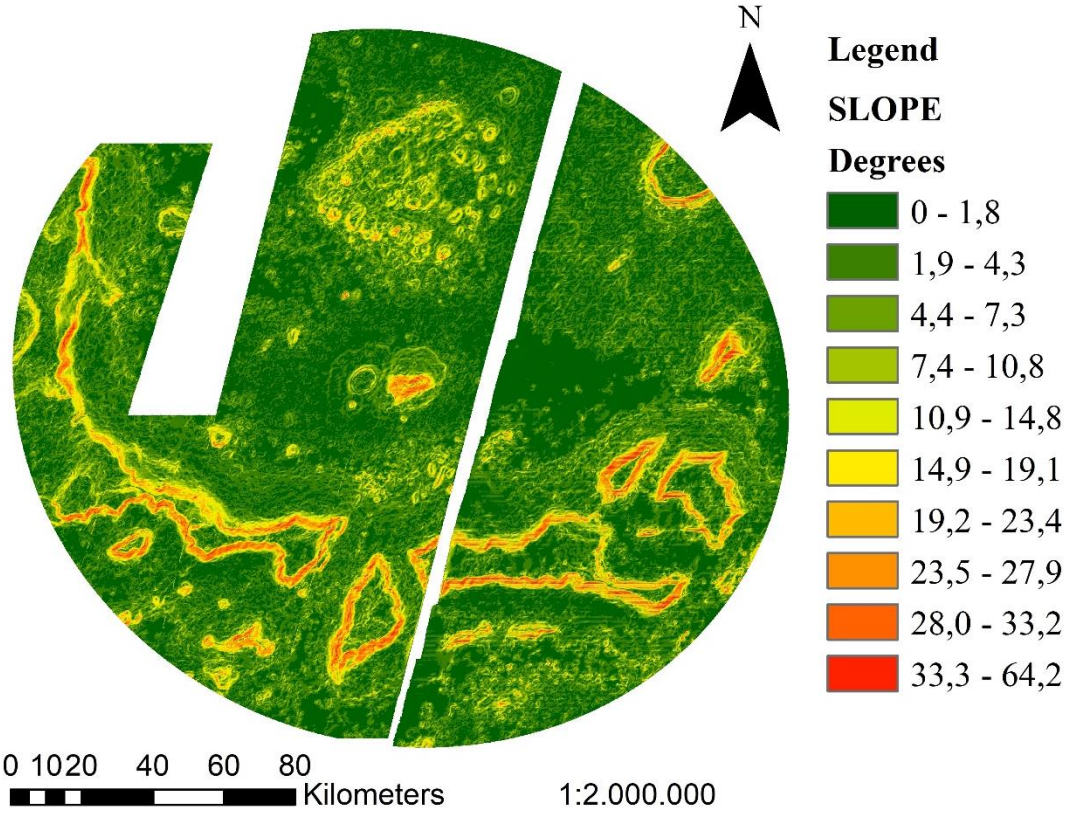

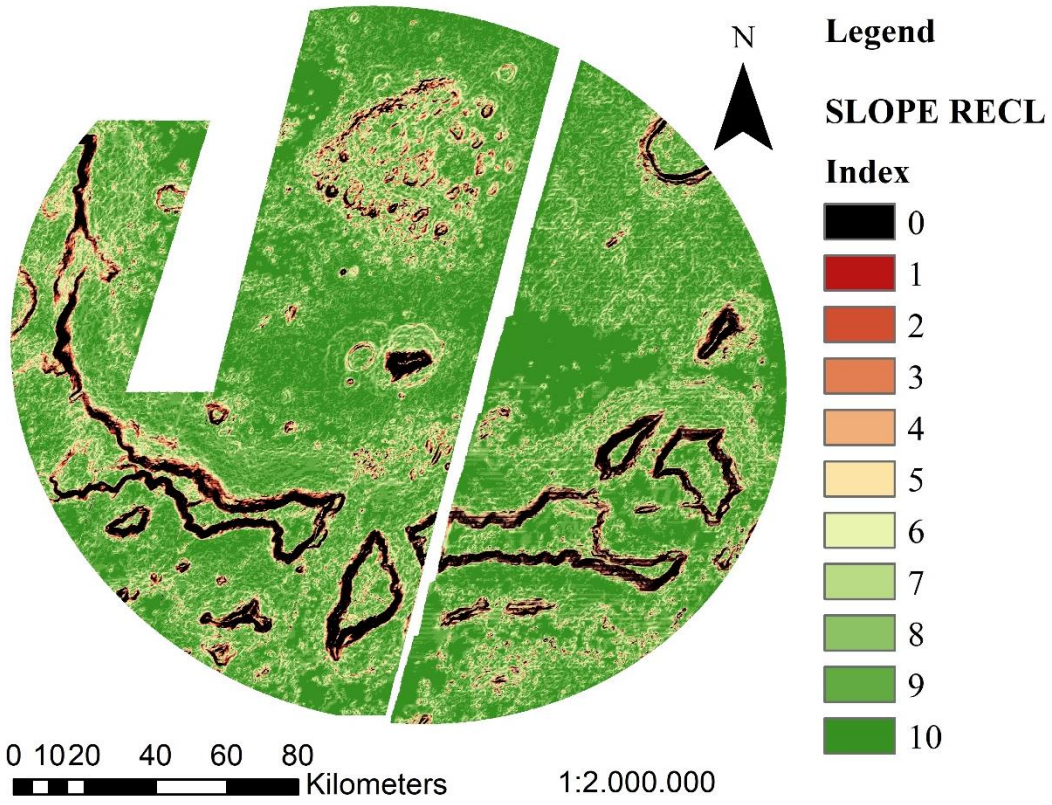

Figure 7-41. DMII EZ: Slope Map and Slope Reclassified Map

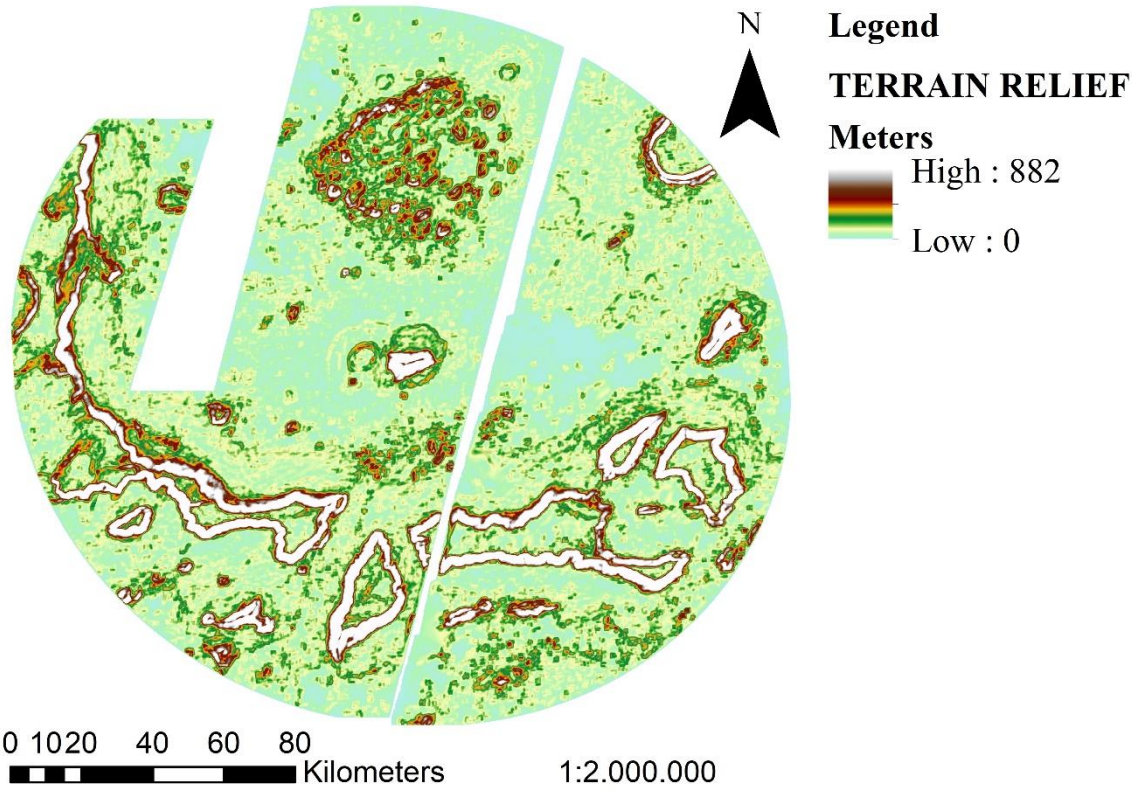

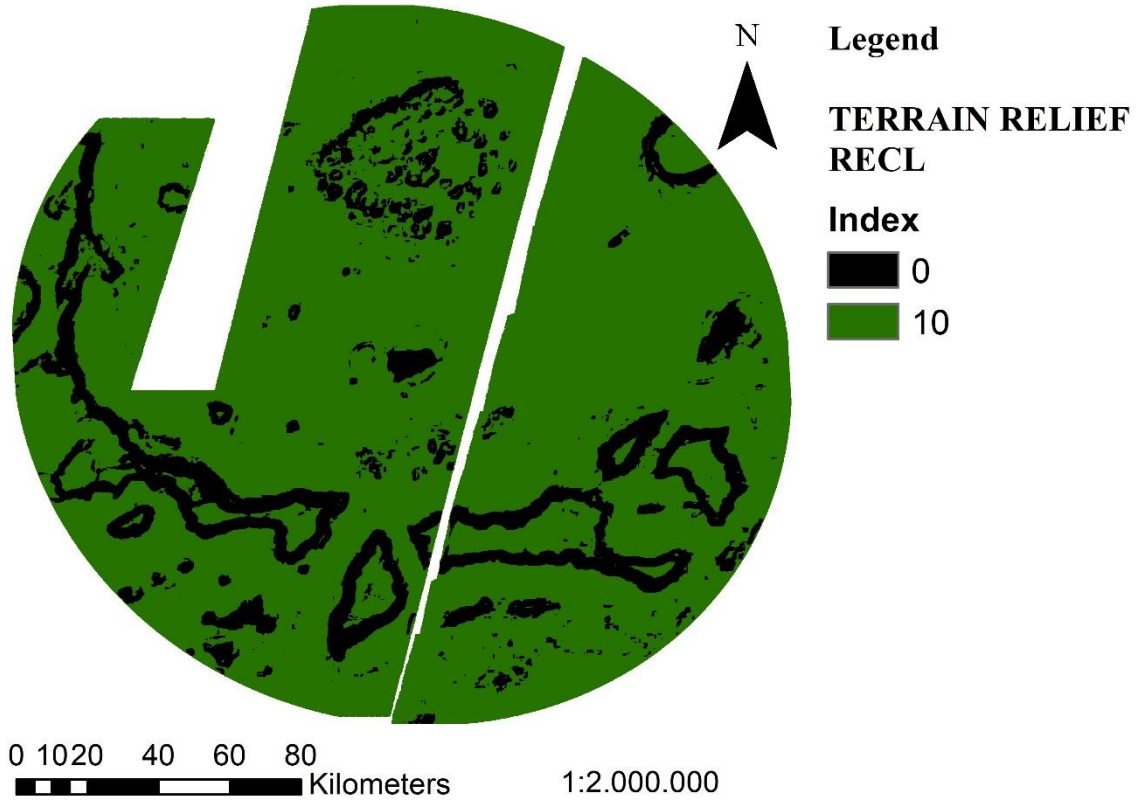

Figure 7-42. DMII EZ: Terrain Relief Map and Terrain Relief Reclassified Map

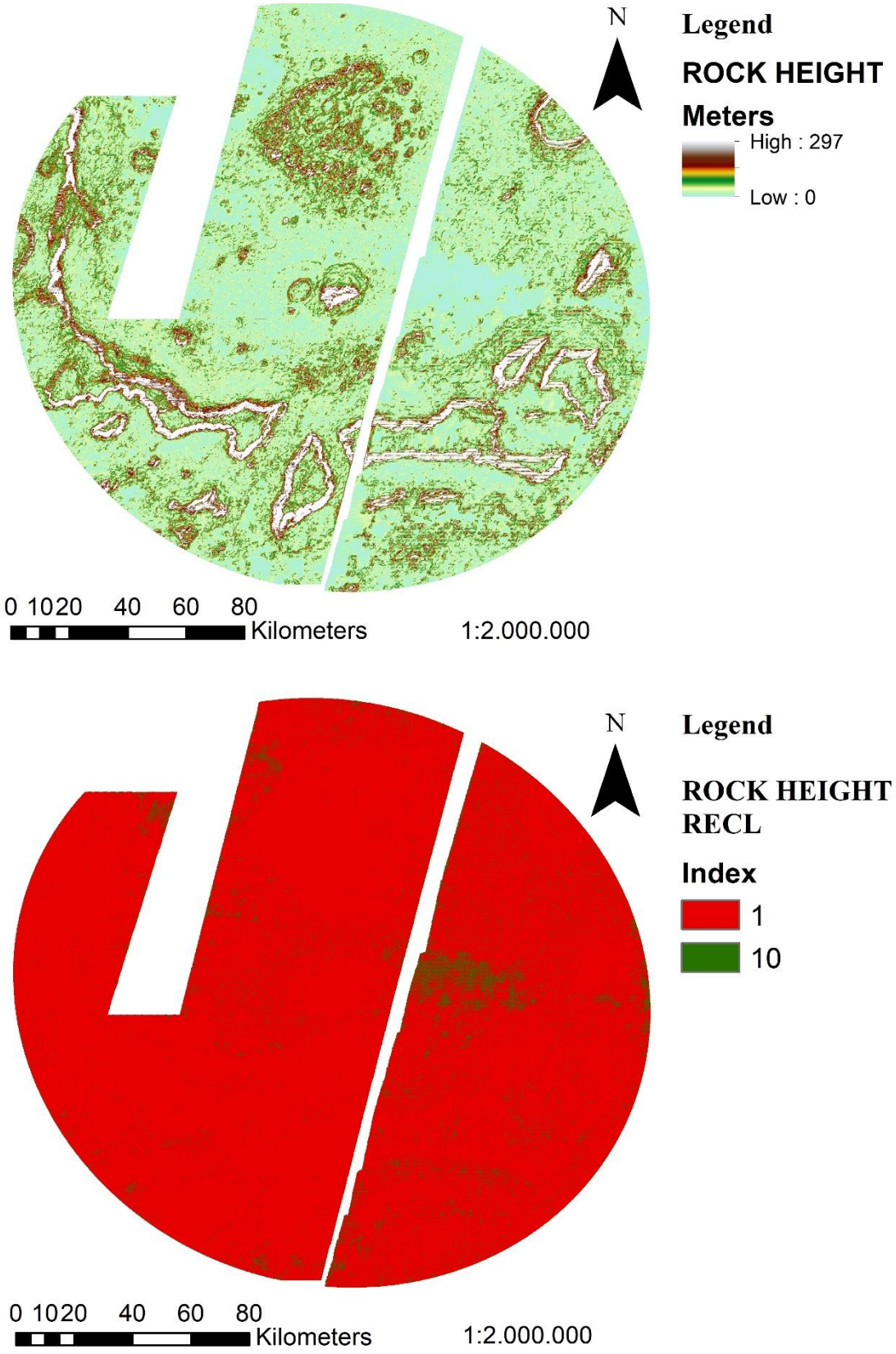

Figure 7-43. DMII EZ: Rock Height Map and Rock Height Reclassified Map

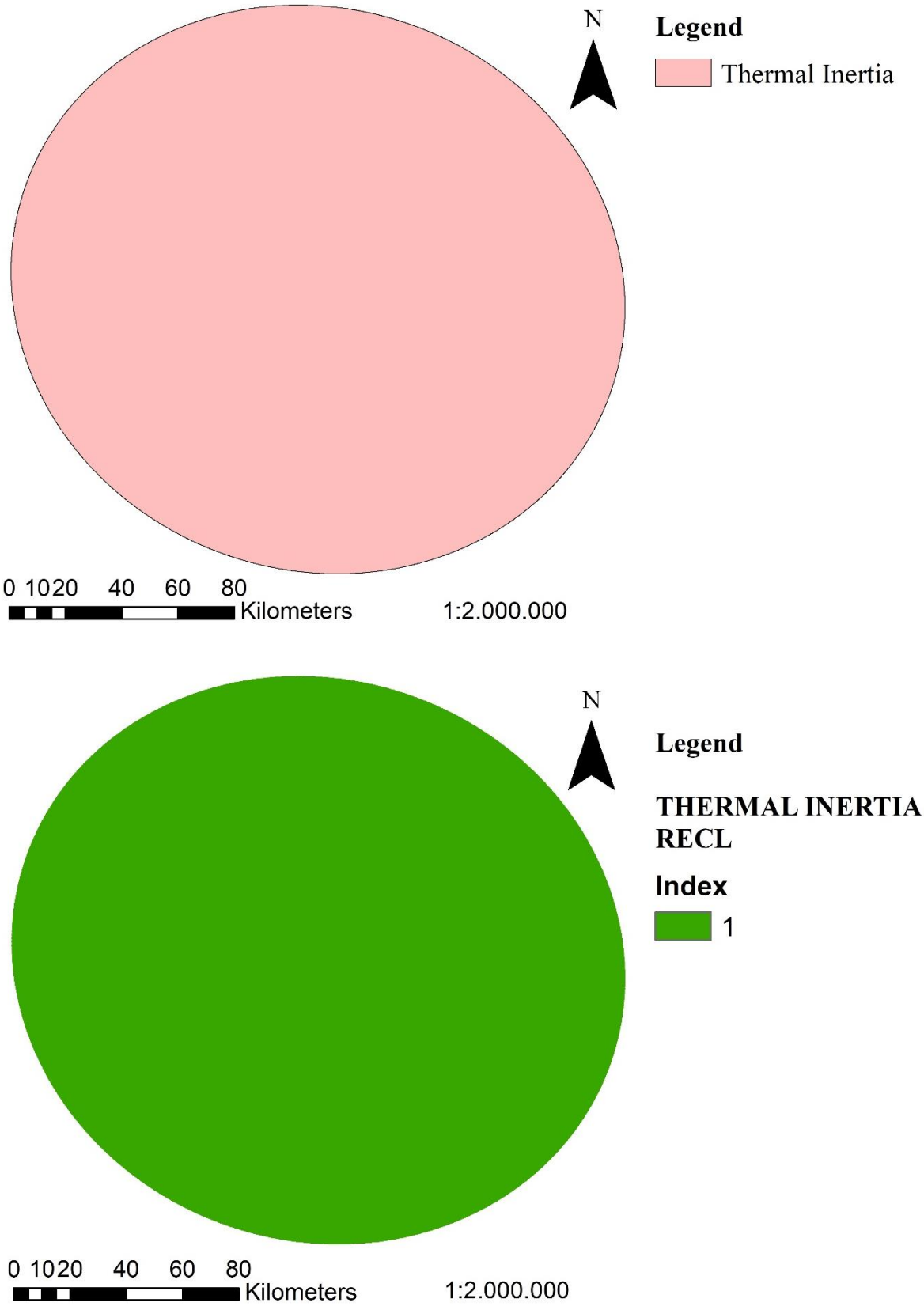

Figure 7-44. DMII EZ: Thermal Inertia Map and Thermal Inertia Reclassified Map

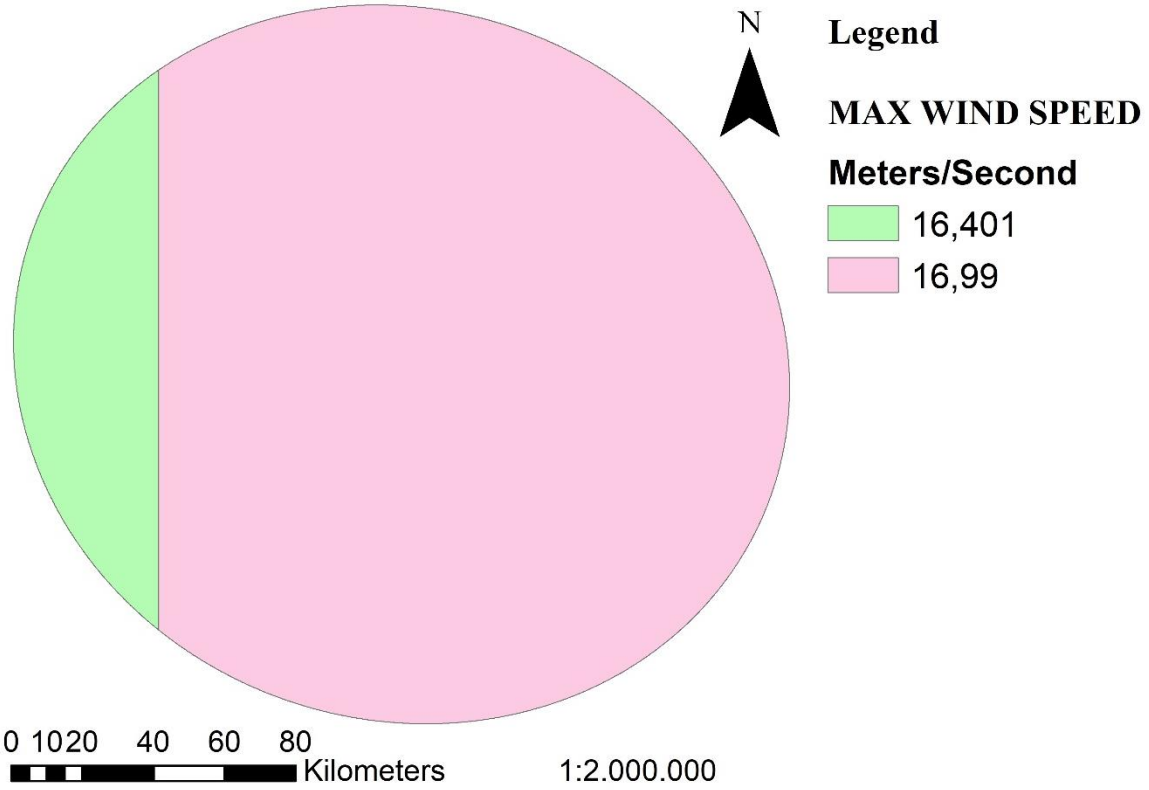

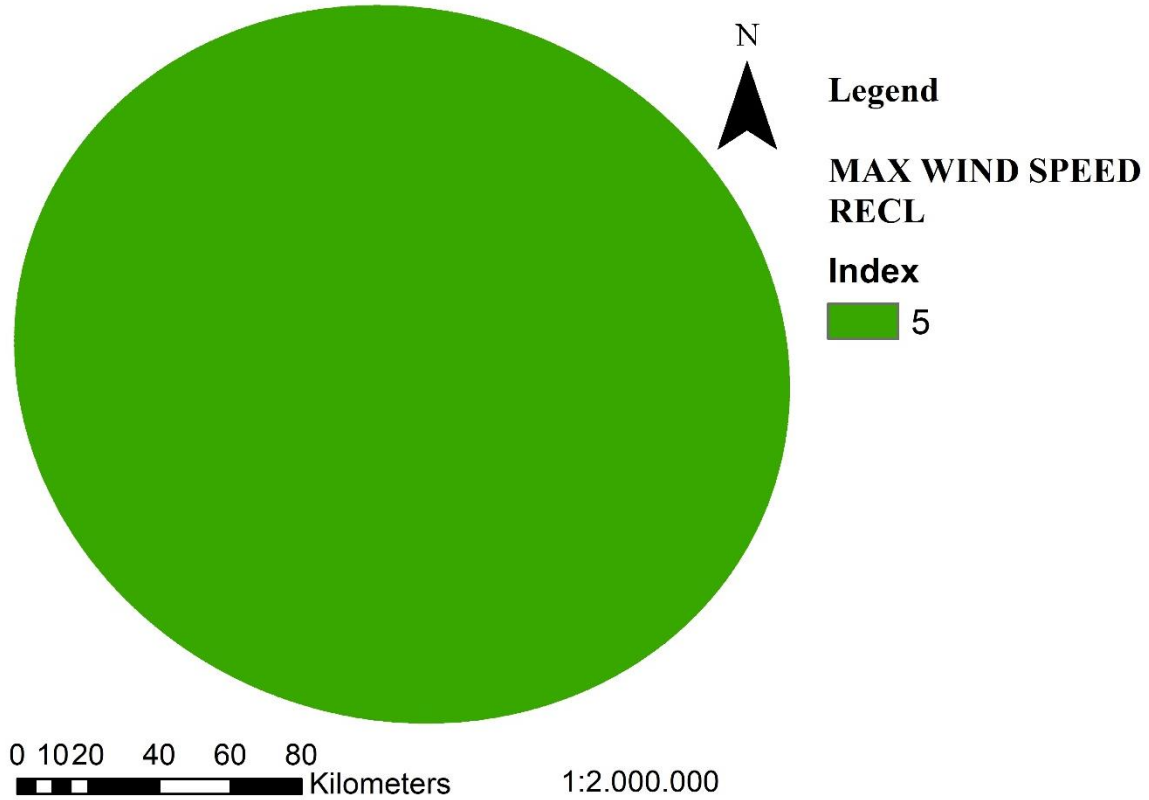

Figure 7-45. DMII EZ: Annual Maximum Wind Speed Map and Annual Maximum Wind Speed Reclassified Map

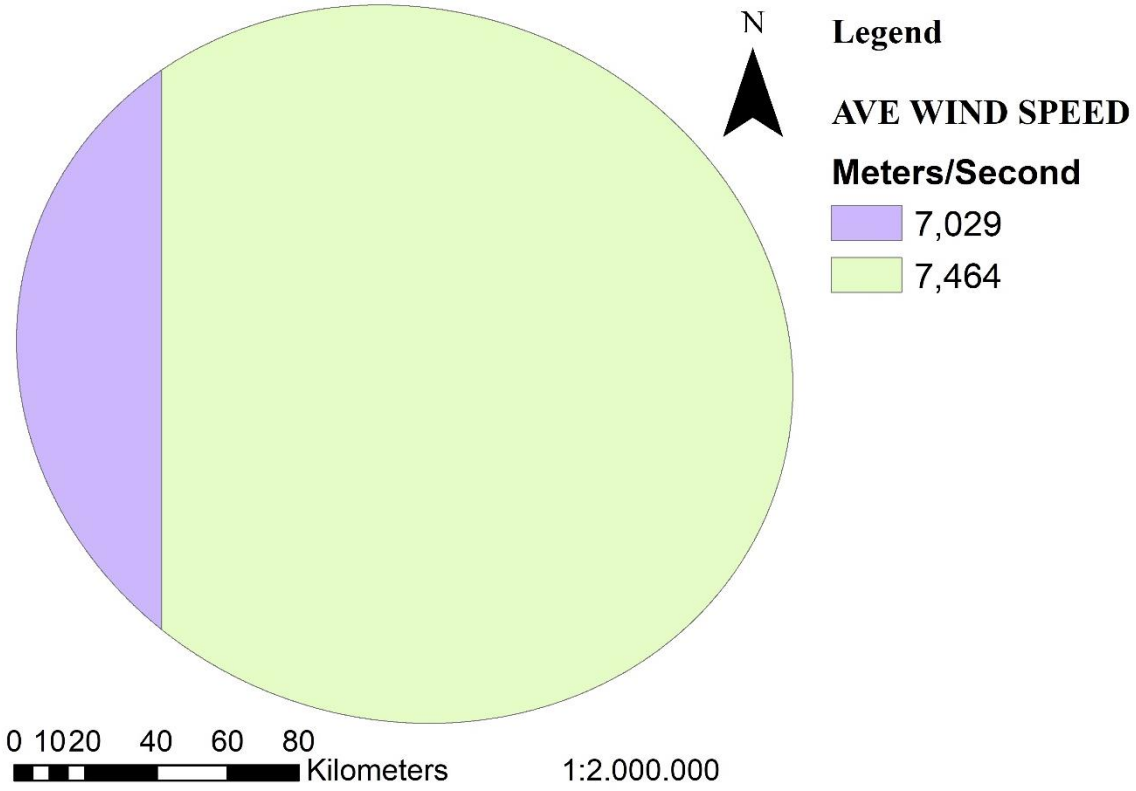

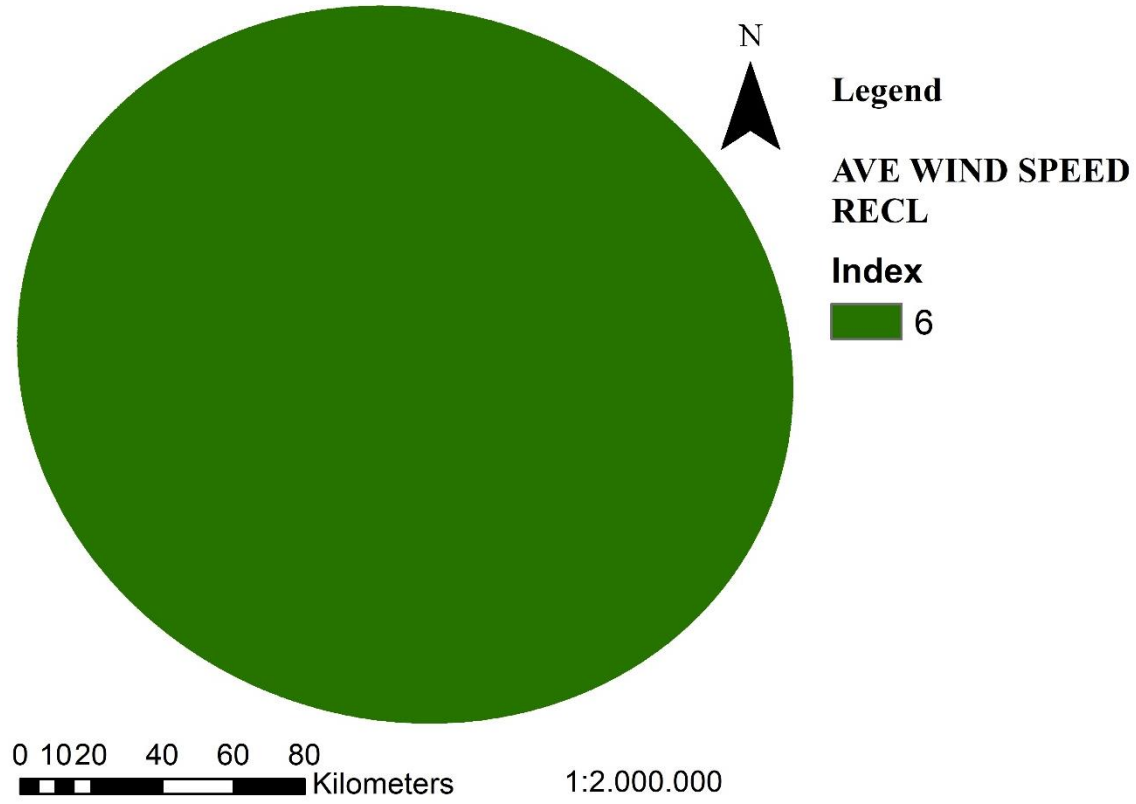

Figure 7-46. DMII EZ: Annual Average Wind Speed Map and Annual Average Wind Speed Reclassified Map

7.4.3 Final Map

Figure 7-47shows the raster map obtained as final result from the developed workflow in DMII.

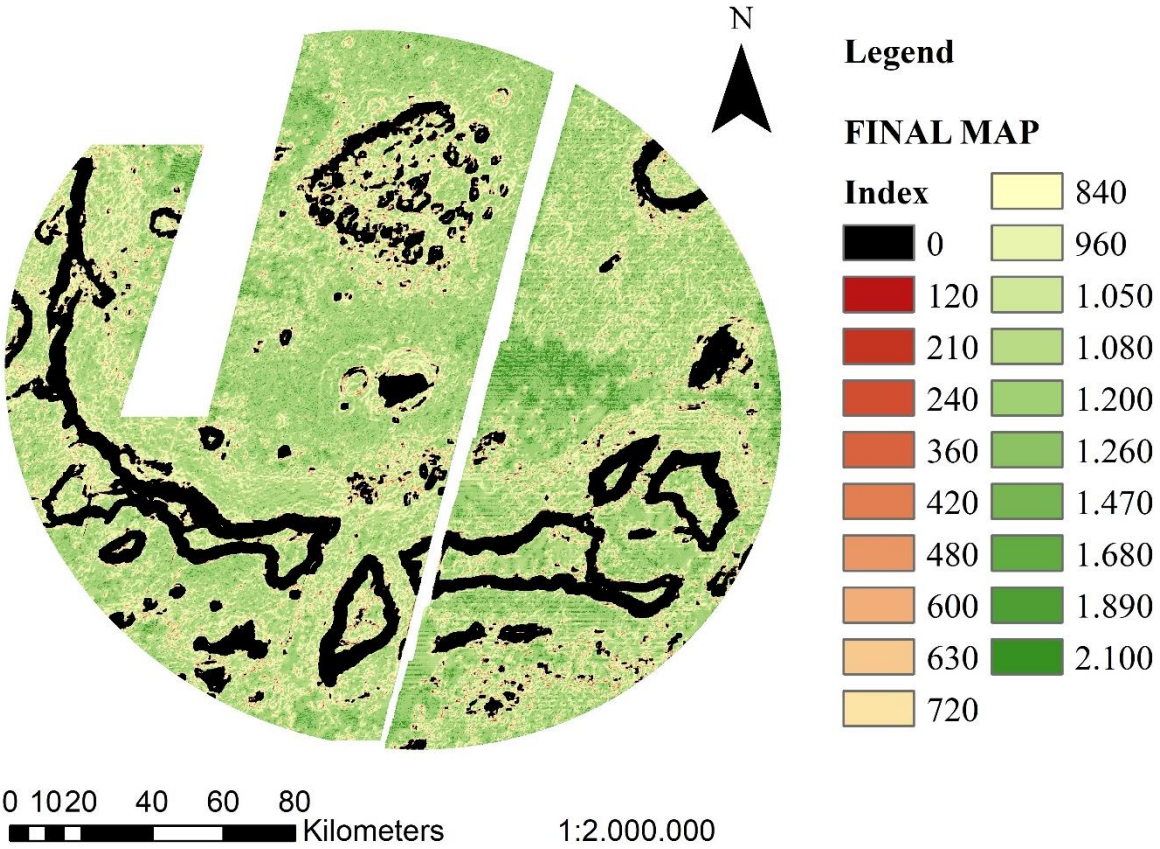

Figure 7-47. DMII EZ: Final Map

7.5 Comparison between final raster maps

This Section reports a comparison of indexes frequency histograms related to the final raster maps generated by the model developed in this work.
Each histogram shows how many times each attribute index, which is associated to a cell during the reclassification process, returns in the same final raster map.

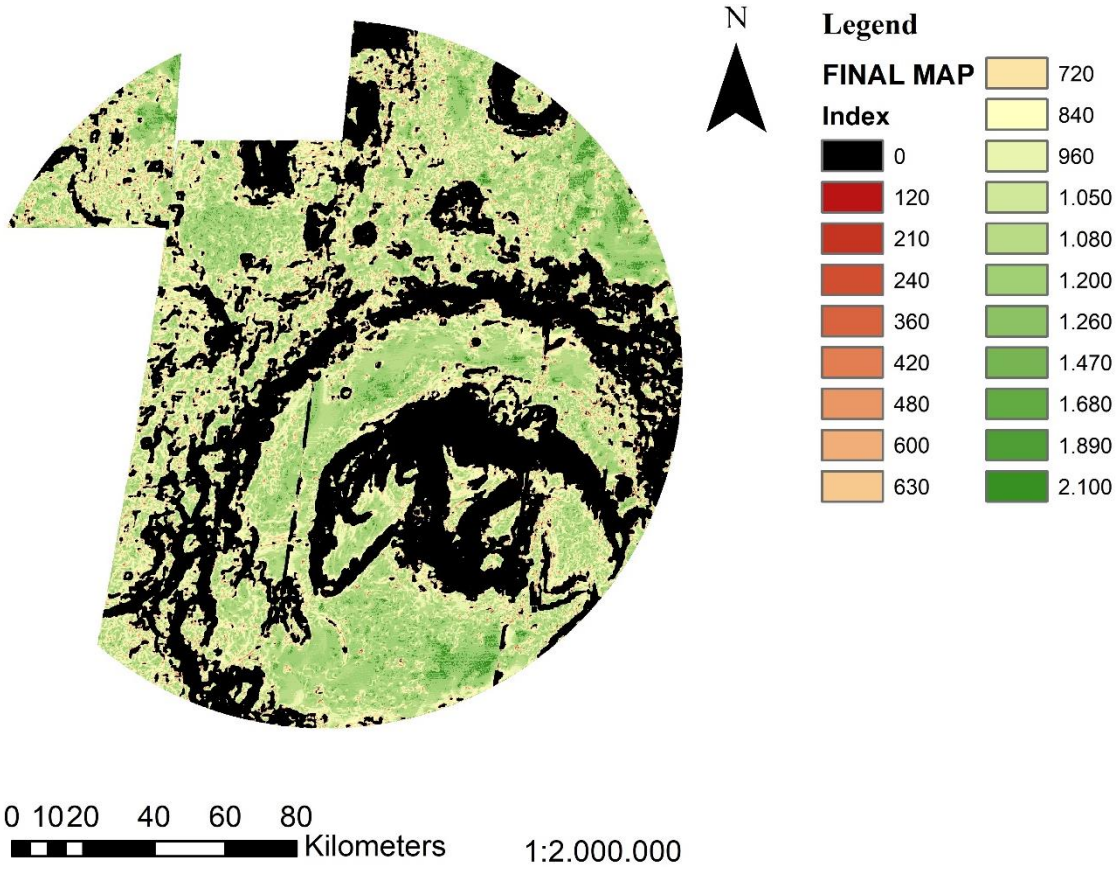

Figure 7-48. Final raster map in Gale Crater

Table 7-1. Indexes frequency histogram of the final raster map in Gale Crater

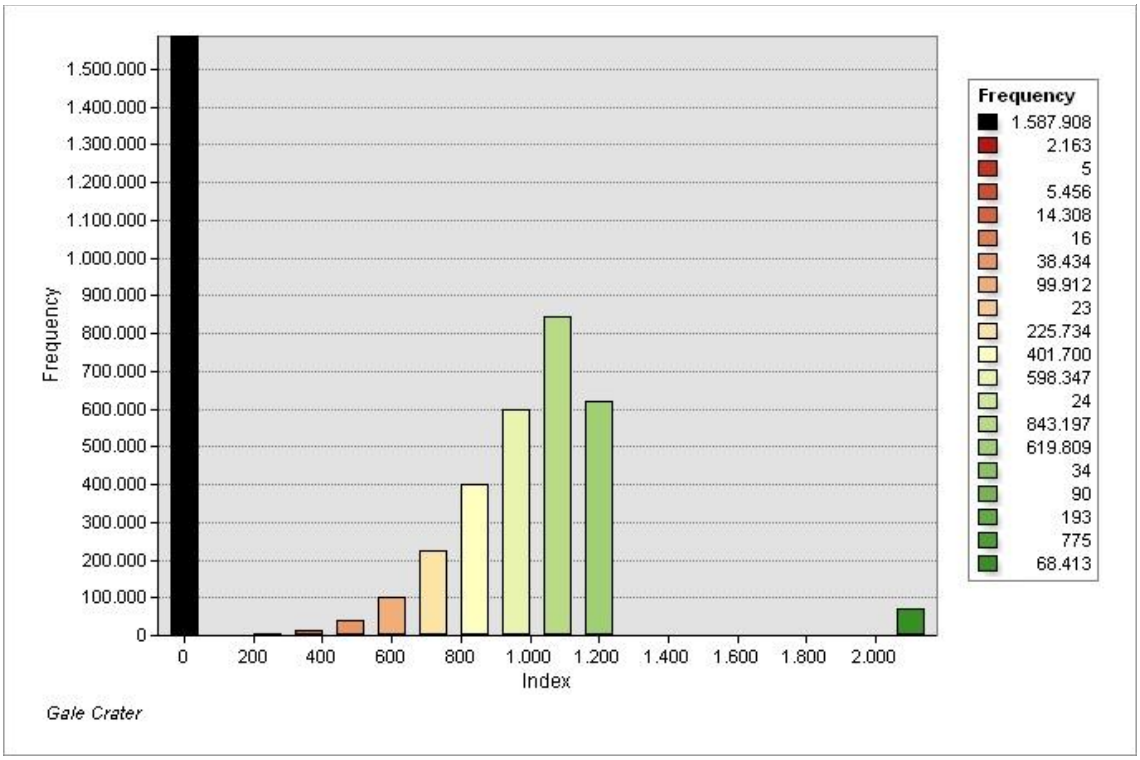

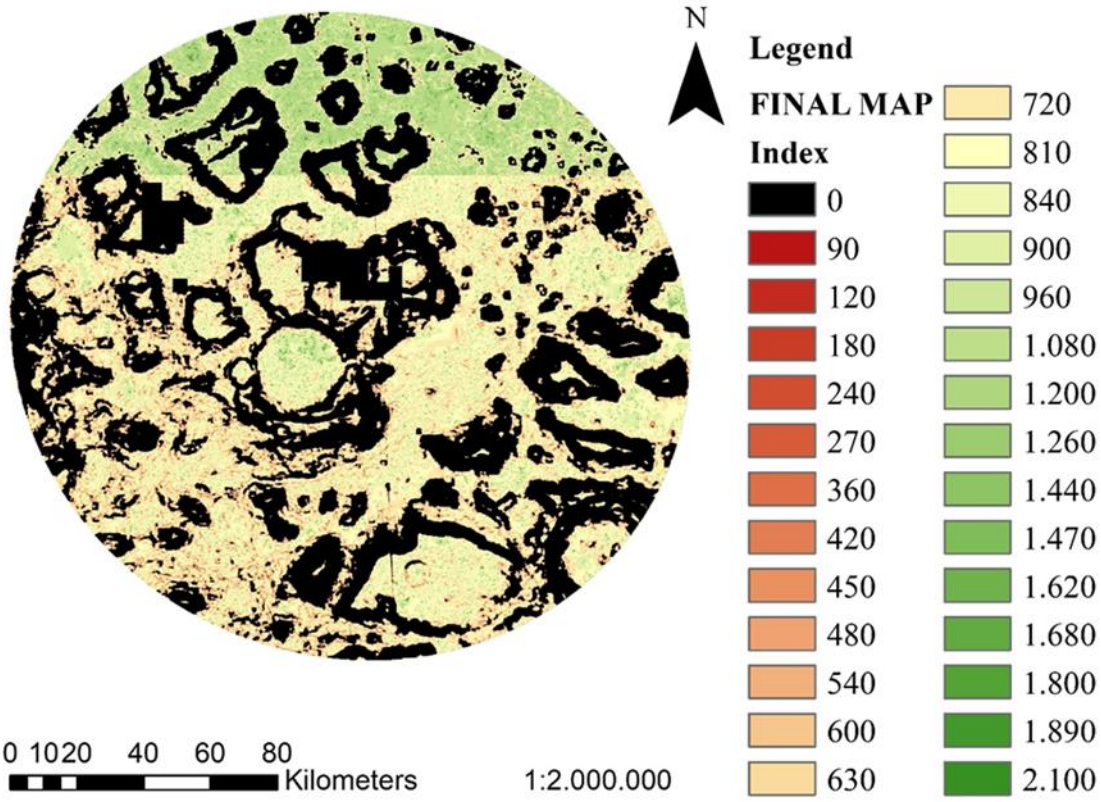

Figure 7-49. Final raster map in Protonilus Mensae

Table 7-2. Indexes frequency histogram of the final raster map in Protonilus Mensae

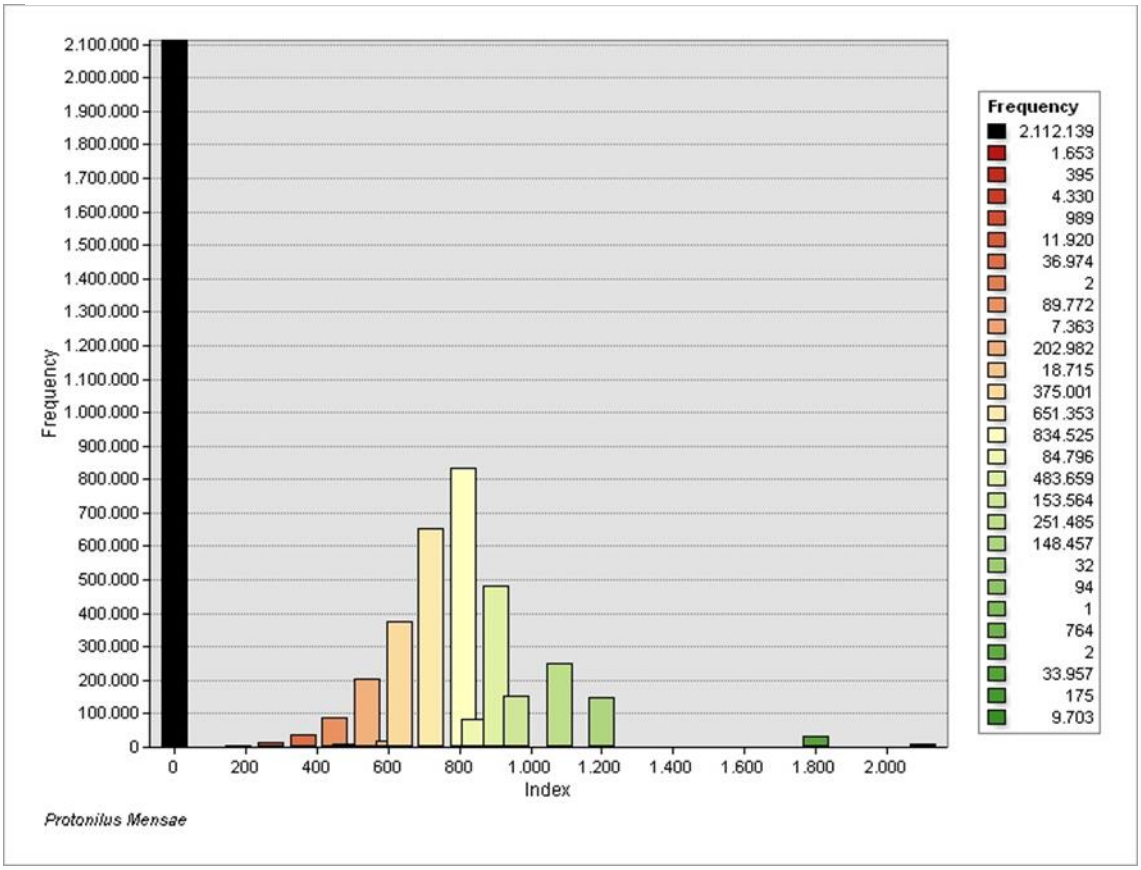

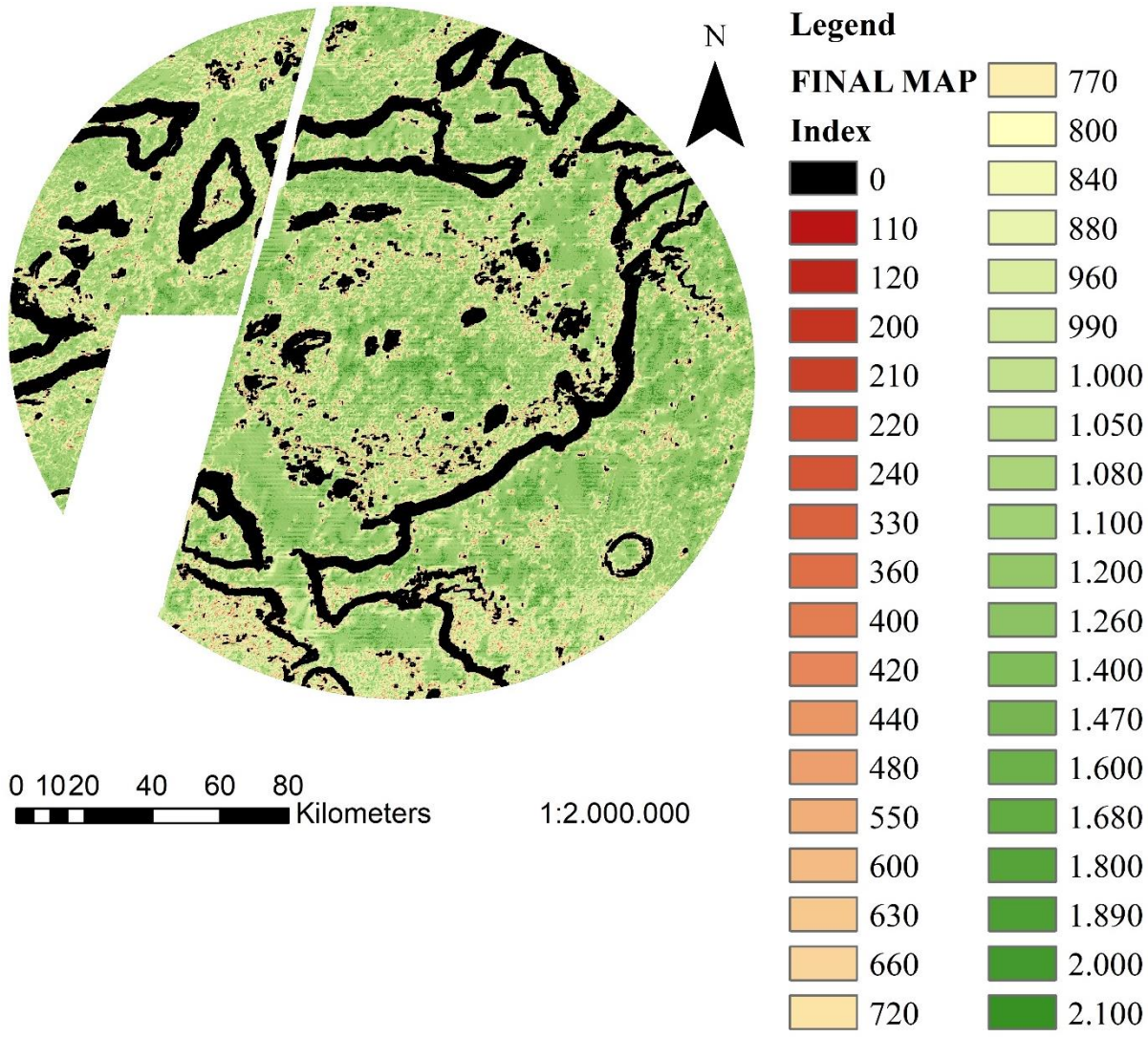

Figure 7-50. Final raster map in Deuteronilus Mensae I

Table 7-3. Indexes frequency histogram of the final raster map in Deuteronilus Mensae I

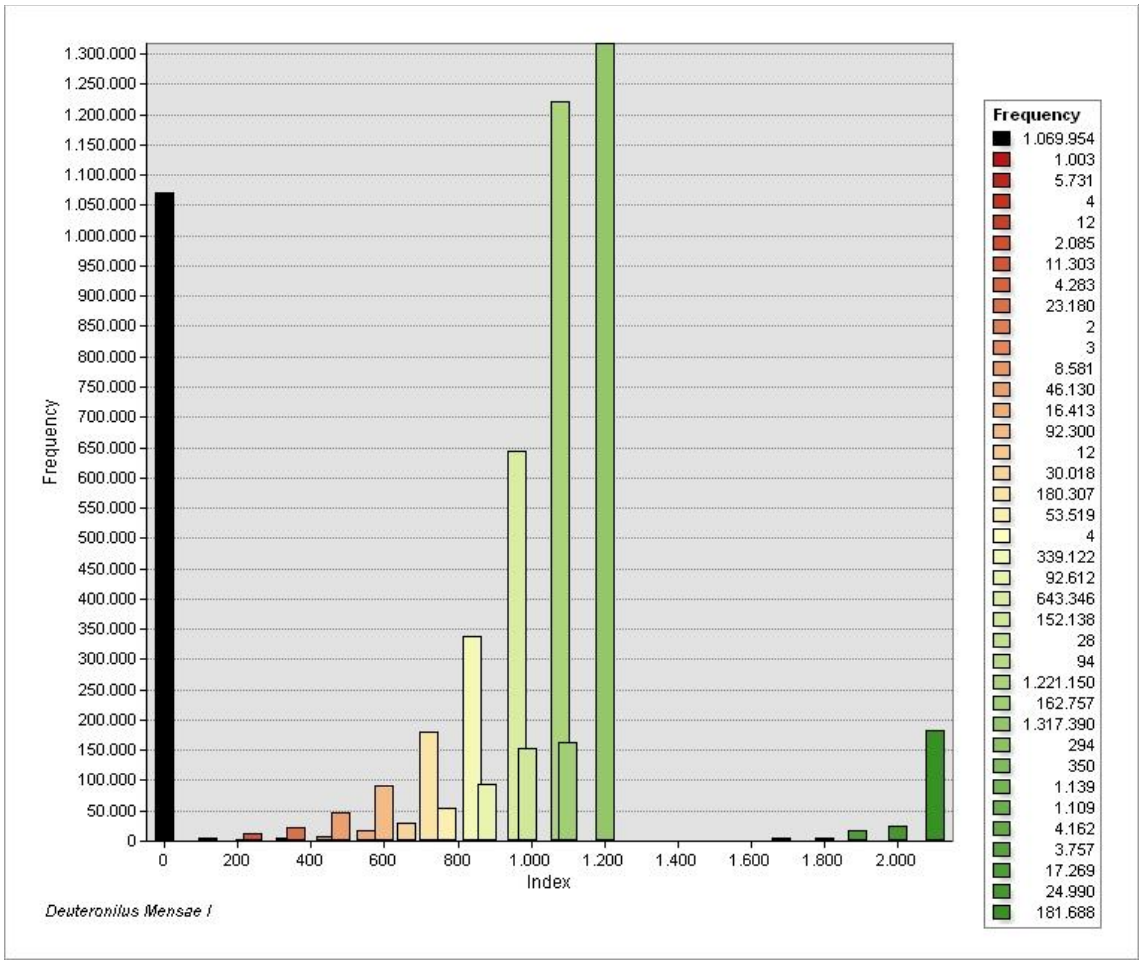

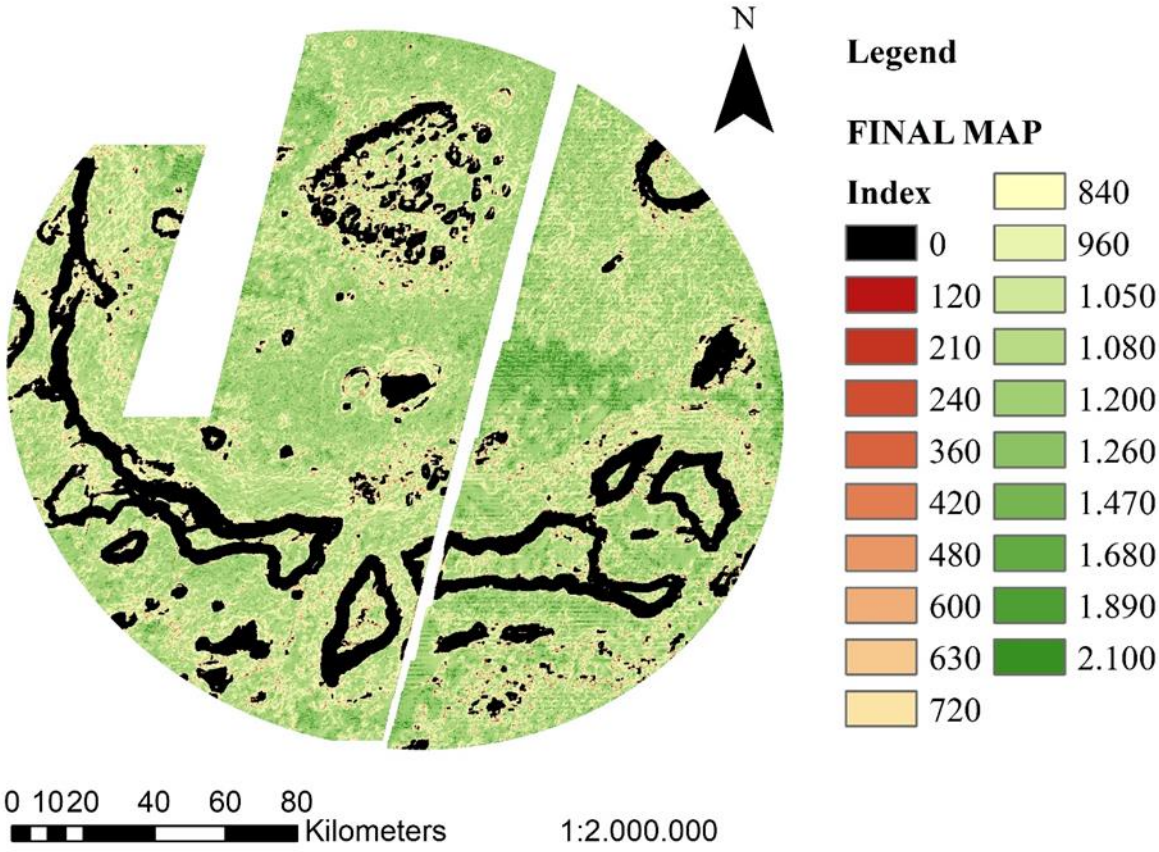

Figure 7-51. Final raster map in Deuteronilus Mensae II

Table 7-4. Indexes frequency histogram of the final raster map in Deuteronilus Mensae II

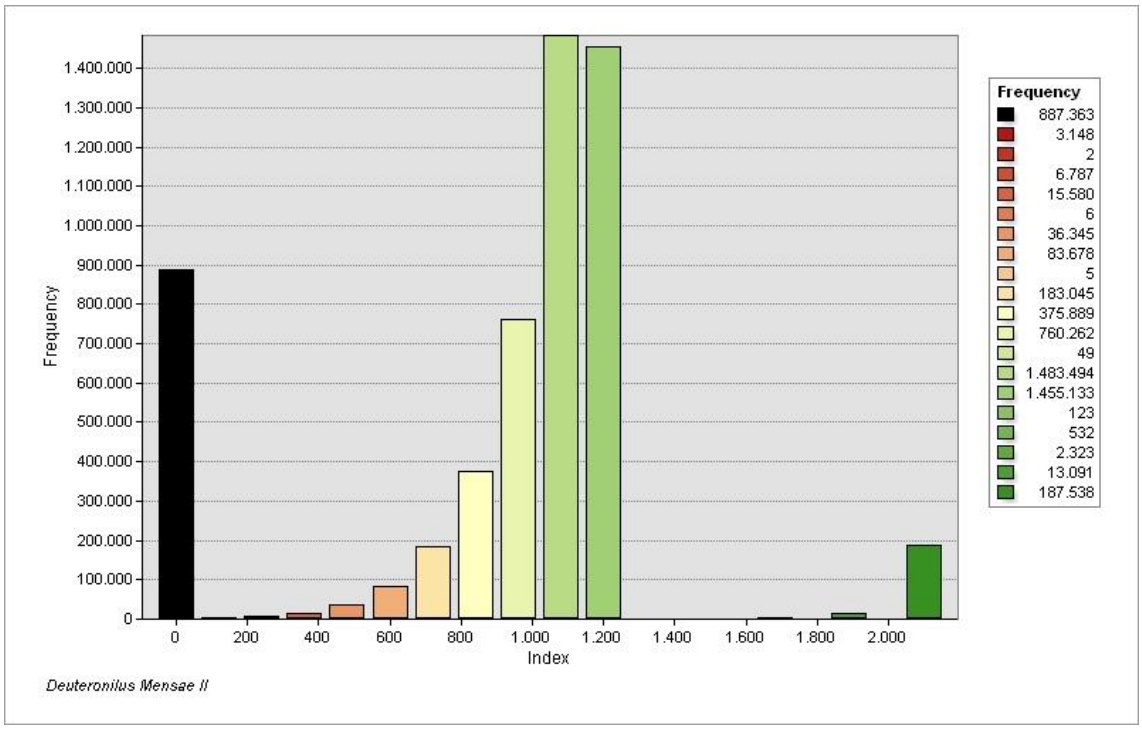

8 DISCUSSION

Processing input datasets with the automated model built in this thesis, which seeks to automate and optimise the Landing Site (LS) selection process for the first human mission to Mars, produced results (see Section 7) that will be discussed in this Section.
The developed workflow was run on four proposed Exploration Zones (EZs): (1) Gale Crater (GC), (2) Protonilus Mensae (PM), (3) Deuteronilus Mensae I (DMI), and (4) Deuteronilus Mensae II (DMII).

8.1 Model validation

Three different aspects to sustain and justify the model effectiveness will be discussed in this Section.

As specified in the previous Sections, the defined engineering requirements to safely land the first crew on Mars' surface are directly related to those used for the LS selection of Curiosity rover, the MSL's spacecraft that landed on GC in 2012. These Engineering Constraints (ECs) were incorporated into the developed tool (see Table 6-3).
Figure 7-11 clearly highlights a complete correspondence between the CTX image and the output final raster map. Indeed, Curiosity rover landed on Aeolis Palus (see Figure 7-1) and the indexes associate to its LS ranges between 1200 and 2100, that are the highest values attributed to the final map. Furthermore, the visual analysis of the LS confirms that Aeolis Palus' rocky ground is processed by the tool as the best landing area in the centre of the EZ (see Figure 7-11).

To provide further demonstration of the effectiveness of the model, different comparisons between the final map and CTX datasets in GC are provided in Figure 7-12 and Figure 7-13. Three zones show a direct correlation between surface morphology and reclassification output.
Zone 1 is representative of the well-defined subdivision between areas in which it is not possible to land, that are black zones with a 0-index associated as attribute to each cell,

and the others where the attribute index is as much higher as the increasing goodness of the analysed engineering parameters.
The output raster map obtained in *Zone 2* shows that the surface morphology is quite irregular, following the peaks that characterise this area.
This correspondence is also found in *Zone 3*, where a central rocky plain in markedly highlight by the associated indexes.

In view of the limitations and classifications set up on the base of the defined EC (see Section 6.1.3), it can be stated that each of the reclassified output maps is consistent to its input engineering map layer.
Some examples are provided referring to Section 7.1.2:

(1) *Elevation Reclassified Map* (see Figure 7-2) has a 1-index associated to all of its cells; indeed, this index is attributed for elevation values that are lower than 2 km in MOLA reference system (see Section 6.1.3.4) and GC's elevation ranges from -4676 to 838 m;

(2) The higher is the attribute index of *Slope Reclassified Map,* the lower is the slope value in *Slope Map* (see Figure 7-3). All the unacceptable cells with a slope higher than 15° are associated to a 0-index (see Section 6.1.3.5);

(3) Terrain relief ranges from 0 to 1031 m and cells with a value higher than 130 m over 975 m baseline are associated to a 0-index in *Terrain Relief Reclassified Map* (see Figure 7-5); otherwise, the attribute value is 10, consistently with justified assumptions made in Sections 6.1.3.7;

(4) *Rock Height Reclassified Map* demonstrates the limitations described in detail in Section 6.1.3.8 (see Figure 7-7); however, a 1-index is associated where the EC is not satisfied, otherwise a value of 10 is attributed to all the other cells.

(5) In GC EZ, thermal inertia EC is always satisfied: indeed, this parameter is always higher than 100 $Jm^{-2}K^{-1}s^{-1/2}$ (see Section 6.1.3.6) and, as consequence, there are no areas with a 0-index associated in *Thermal Inertia Reclassified Map* (see Figure 7-8);

(6) The annual average wind speed is 6.79 m/s in GC EZ; consistently with the implemented expression (see Section 6.1.3.10) and the set correlation between ranges of velocity and indexes (see Table 6-5) to reclassify the input map, the attribute value of the *Annual Average Wind Speed Reclassified Map* is 6 (see Figure 7-9);

(7) The annual maximum wind speed is 16 m/s in GC EZ; consistently with the implemented expression (see Section 6.1.3.9) and the set correlation between ranges of velocity and indexes (see Table 6-4) to reclassify the input map, the attribute value of the *Annual Maximum Wind Speed Reclassified Map* is 5 (see Figure 7-10).

These correlations between engineering maps and reclassified maps may be found in all the cases analysed through this work.

Consistency with Curiosity rover LS, correlations between surface morphology and reclassification output maps, and consequentiality between engineering map layers and reclassified output maps have been properly justified in this Section. As consequence, they represent three aspects that definitely support the model effectiveness.

8.2 Landing Site (LS) and Habitation Site (HS) selection

Once demonstrated the effectiveness and efficiency of the model, which are directly related to consistency and quality of results justified in Section 8.1, it can be stated that the developed tool satisfies the core focus of the work: it allows optimising the Landing Site (LS) selection process, replacing time consuming and subjective manual analysis of datasets with an automated flexible model based on defined Engineering Constraints (ECs).

The programmed model generates maps that represent a quantitative, fast and effective way to evaluate where it is and is not possible to land safely within an Exploration Zone (EZ). Indeed, black cells with an attribute 0-index associated (see Figure 7-11, Figure 7-22, Figure 7-38 and Figure 7-47) indicate areas that must be excluded from LS selection.

This first order analysis highlights the optimal landing areas from an engineering point of view.

This Section provides an overview on the successive phases that must be followed to properly interpret the final output map. Indeed, different areas may satisfy the engineering requirements and the following procedure help to select the optimum LS within an EZ.

The fundamental criteria evaluated to conduct a proper selection of the LS are to:

(1) Respect ECs requirements;

(2) Landing on a rocky ground;

(3) Identify Glacial Like Features (GLF) in the proximity of the LS;

(4) Satisfy LS/HS geometry requirements:

- $A_{LS} \cong 25km^2$,

where:

A_{LS} is the area of the Landing Site (LS),

- $Area_{HS} \cong 50km^2$,

where:

A_{HS} is the area of the Habitation Site (HS),

- $d_{LS-HS} \leq 5km$,

where:

$d_{LS\text{-}HS}$ is the distance between LS and HS;

(5) Select an area with a slope lower than 30° in the HS. This is an additional variable considered in this study to improve the LS/HS selection facilitating movements of the crew pressurised rovers within the HS. This condition is based on LPI (2015) considerations.

To provide an example, three different zones in PM, within both LS and HS have been located, are proposed in Section 7.2.5 (see Figure 7-25, Figure 7-27, Figure 7-28, and Figure 7-29).
It can be stated that all the required criteria are respected in the selected zones, indeed:

(1) The automated model generates final output maps where every site that must be excluded is associated to a 0-index on the base of defined ECs;

(2) The comparison between CTX and final output map allows distinguishing between rocky areas and zones that respect the defined ECs;

(3) All the proposed HS are close to the most typifying glacial bodies that are Lineated Valley Fill (LVF), Lobate Debris Aprons (LDA) or Concentric Crater Fill (CCF), all of them representing GLF (see Section 3.1.4) and constituting a fundamental resource for a feasible human mission to Mars;

(4) All the proposed LSs/HSs respect the defined geometrical conditions;

(5) All the HSs respect slope condition (see Figure 7-25 and Figure 7-26).

Zone 1 (see Figure 7-27) is located in the upper part of PM EZ. In this area, the goodness of indexes associated to its cells is high (see Figure 7-25). Nevertheless, it is recommendable to set the LS/HS location in the central part of the EZ to establish a good connection between the HS and both Resource and Scientific Regions of Interest (RROIs and SROIs). However, the boundaries of this EZ, proposed in 2015 at the First Landing Site/Exploration Zone Workshop for Human Missions to the Surface of Mars, do not necessary constitute a mandatory requirement. For this reason, if a zone is considered extremely good from an engineering point of view, it is possible to propose new potential EZ around this LS. However, when conducting a comparison between the final output map and the reclassified maps related to ECs, it is noticeable that both the Annual Maximum and Average Wind Speed parameters influence the division between the upper part of PM, associated to higher indexes, and the lower one, that is relatively penalized by this factor.

The left part of *Zone 1* is evidently characterised by the presence of glacial bodies that modify the geomorphic surface: LVF line the zone floors aligning the downslope direction. The requirements of landing on a rocky ground and close to GLF highlight the importance of integrate the model with geological analysis.
Hence, the need of safely land and the presence of exploitable and processable resources both represent fundamental requirements to achieve the goal of a successful mission to Mars. This careful evaluation necessitates a close cooperation of both engineering and geology complementary fields.
The analysis of resources is focused on finding glacial features because of the highest priority related to mining water on Mars both for life support and propellant production: indeed, (1) the natural scale of GLF present on Mars is far larger than the minimum required to produce 16 metric tons needed per crew (Abbud-Madrid et al., 2016), and (2) the chance of discover a glacial ice deposit that would yield less than 16 metric tons is considered non-existent (Abbud-Madrid et al., 2016); moreover, (3) metals, silicon and structural building material have secondary priority.
For these reasons, this study is focused to find evidence for glacial ice RROIs in the proximity of the selected LS.

Zone 2 (see Figure 7-28) is located in the middle of the EZ, where the majority of the attribute indexes ranges between 720 and 900. However, the analysis of indexes frequency histogram shown in Table 7-2 clarifies that this range of values is the most common in PM EZ final map. For this reason, the quality of this area is considered high enough if compared to the others. Furthermore, *Zone 2* is located in the central part of the EZ. As demonstrated for *Zone 1* case study, *Zone 2* is characterised by GLF presence: indeed, LDA originates from the escarpment flanks on the left side of the proposed LS.

Zone 3 (see Figure 7-29) is located in the proximity of a glacial landsystem: indeed, the northern area is characterised by the presence of a crater that, for its surface texture, constitutes a resource of ice; the lower part shows the presence of LDA that originate from mesas and of LVF that modify the surface texture.

To safely land the first crew on Mars' surface, all the proposed LSs and HSs are located on a rocky ground.

During this study, it has been clarified that the high thermal inertia requirement implemented to the model reconducts to ground properties. Thermal inertia is a measure of the ability of a material to store heat during the day and reradiate it during the night time and a rocky ground displays a much higher capability to heat and remain warm during the daily cycle. However, both the rocky ground and the boulders that constitutes the sublimation till of GLF (see Section 3.1.4) respect the defined engineering requirement. For this reason, a critical visual comparison between CTX and final map allows discerning between different geological bodies.
It is possible to note in Figure 7-24 both a LVF (*Zone 2*) and a crater (*Zone 3*), which could not be selected as possible LSs because of surface textures that indicate their glacial origin.

Figure 7-23 show the rocky upper part of a mesas. The steep flanks of this formation may represent an obstacle to safely moves between areas of the same EZ and, for this reason, excluding this zone from the LS selection may be considered a conservative choice.

Section 7.5 reports a comparison of indexes frequency histograms related to the final raster maps. Each histogram shows how many times each attribute index, which is associated to a cell during the reclassification process, returns in the same final raster map. These histograms allow:

(1) understanding indexes predominance and distribution within the same EZ to make considerations on the relative goodness of results (see PM example provided in this Section) and to analyse its homogeneity;

(2) analysing differences between EZs.

Indeed, both PM and GC histograms (see Table 7-1 and Table 7-2) show that the most frequent index in these EZ is 0; on the contrary, DMI and DMII present a higher concentration of values different from 0 (see Table 7-3 and Table 7-4).

Comparing indexes that are different from 0, 1080-index can be considered the most frequent one in both GC and DMII, 1200-index has the highest frequency in DMI and 810-index is the most frequent in PM.
To test the developed model, each EZ has been reclassified with indexes that range between 0 and 2100, on the base of the tool input set up. However, each final output map is reclassified with a different number of values that is directly proportional to engineering parameters homogeneity: for this reason, GC and DMII may be considered less heterogeneous than PM and DMI.

All the considerations made in this Section provide a tangible example of the procedure that must be followed to properly interpret the final output map obtained with the developed tool. It is evident that running this model definitely speeds up the LS selection process by furnishing a quantitative and easily interpretable final map that substitutes time consuming and subjective manual analysis of datasets.

8.3 Model flexibility

A distinctive aspect of the model developed in this work is its flexibility.
The output results obtained in GC, PM, DMI and DMII, exclusively represent one of the possible data processing realizations. Indeed, the model is set up on the base of reasonable assumptions and justifications made from an engineering point of view (see Section 6.1). Despite this consideration, the model is built with the attempt of creating a flexible tool that can be easily adapted to changeable circumstances, consistently with the dynamic mission's objectives and constraints evolution.
For this reason, (1) principles and assumptions adopted to reclassify input datasets, (2) ranges of values-indexes associations, (3) implemented parameter's weight assumed for the final output map, and (4) raster calculator expression's syntax may be easily varied. Moreover, (5) further parameters can be entered to the workflow whether requested.
It is proven that this model may be easily (6) run on different EZ and (7) may be implemented whether high-resolution datasets will be available.

8.4 Conclusion Statement

In view of the obtained results, this Section (1) provides evidence of workflow effectiveness, (2) highlights the analysis phases that must be followed to properly interpret the final output map to select the optimum LS within an EZ, and (3) justifies the model flexibility.

As consequence, it can be stated that the model developed is a tool which allows optimising the LS selection process for the first human mission to Mars.

9 CONCLUSIONS

Successfully sending humans to Mars represents one of the greatest achievements of the mankind. To ensure crews' safety and ongoing mission success, the selection of an optimised landing site for the construction of a human base is highly critical.
Site selection requires a multidisciplinary effort with significant planning to implement a successful strategy that is both flexible and adaptable.

In the view of results obtained with this study, the research objectives that have been met in this project are to:

i. Develop a flexible model based on defined engineering constraints using ArcGIS ModelBuilder, allowing automated selection of an optimised landing site location within a proposed exploration zone;

ii. Validate model effectiveness;

iii. Run the model on different exploration zones located on Mars;

iv. Propose possible configurations of the landing and habitation sites within a chosen exploration zone;

v. Incorporate the output results with a local glacial resources analysis.

The aim of proposing an automated landing site optimisation model for the first human mission to Mars has been achieved in this thesis. Indeed, a workflow based on defined engineering constraints, which works by integrating images processing tools, has been structured into three main phases, which consists of data processing, engineering parameter map layer development, and raster reclassification. The reclassified output maps have then been combined into a single map, which summarises all the properties analysed.

The effectiveness of the developed model has been supported by the correlations highlighted between surface morphology and reclassification output maps, by the

consistency identified between engineering map layers and reclassified output maps, and by coherence individualised in the final output raster in Gale Crater, which classifies Curiosity rover landing site as the optimum area in the middle of this exploration zone. Indeed, the constraints used for the landing of the Mars Science Laboratory spacecraft at Gale Crater were incorporated into the designed tool.

The output map replaces time consuming and subjective manual analysis of datasets; indeed, it speeds up the evaluation of safe landing sites within an exploration zone, and it allows both identifying the optimal landing areas from an engineering point of view and comparing different proposed exploration zones.

A distinctive aspect of the model developed in this work is its flexibility. Indeed, it has been designed with the attempt of creating a tool that can be easily adapted to changeable circumstances, consistently with the dynamic mission's objectives and constraints evolution. For this reason, principles and assumptions adopted to process input datasets, implemented parameters' weights on the final output map, number and typology of set up engineering constraints, and analysed zones can be easily modified.

Demonstrating the ability of producing commodities from local resources represents a fundamental requirement for a feasible and sustainable Off-Earth human mission. The attention must be focused on finding glacial resources, because of the highest priority related to mining water on Mars, both for life support and propellant production. Hence, the procedure that may be adopted to properly interpret the final raster map and to optimise the landing site selection process with the incorporation of a local glacial resources analysis has been described in this thesis.

Furthermore, considering both technological and resources requirements, some possible configuration for both the landing and habitation sites have been proposed in this study. The defined procedure highlights the great importance of conducting a landing site optimisation process that requires a synergic cooperation between engineering and geology complementary fields.

In conclusion, the model developed in this work represents a quantitative, fast, effective, resilient to changes way to optimise the landing site selection process for the pioneering human mission to Mars.

10 RECOMMENDATIONS

This Section provides an overview on possible areas of recommendation that may improve and enhance both validity and accuracy of the model developed in this thesis.

Indeed, to provide comprehensiveness to the model developed, some assumptions have been made and justified in this work to implement all the defined Engineering Constraints (ECs) in the designed model

However, recommendations to improve the developed tool include:

- The incorporation of HiRISE datasets to properly evaluate Rock Height (EC) since these high-resolution images will be available;
- The evaluation of Slope EC on a 20 m length scale.

Furthermore, the automated workflow may be implemented with additional analysis parameters, such as:

- Surface roughness;
- Sun exposure;
- Local resources classification.

The model developed works by integrating images processing tools: for this reason, it may be modified in the future to be run in different contexts such as the Lunar one.

11 REFERENCES

Abbud-Madrid, A., Beaty, D., Boucher, D., Bussey, B., Davis, R., Gertsch, L., Hays, L., Kleinhenz, J., Meyer, M., Moats, M., Mueller, R., Paz, A., Suzuki, N., van Susante, P., Whetsel, C., Zbinden, E., 2016. "Mars Water In-Situ Resource Utilization (ISRU) Planning (M-WIP) Study", California Institute of Technology [online]. Available from <https://mepag.jpl.nasa.gov/reports/Mars_Water_ISRU_Study.pdf> [Accessed: 04/08/2017].

Acuña, M.H., Connerney, J.E.P., Ness, N.F., Lin, R.P., Mitchell, D., Carlson, C.W., McFadden, J., Anderson, K.A., Rème, H., Mazelle, C., Vignes, D.,Wasilewski, P., Cloutier, P., 1999. "Global distribution of crustal magnetization discovered by the Mars Global Surveyor MAG/ER experiment", *Science*, v. 284, pp. 790-793.

Aharonson, O., Zuber, M.T., Rothman, D.H., 2001. "Statistics of Mars' topography from the Mars orbiter laser altimeter: slopes, correlations, and physical models", *Journal of Geophysical Research*, v. 109, 723-735.

Astropedia, n.d.. "Mars MGS MOLA Elevation Model 463m (MEGDR)" [online]. <https://astrogeology.usgs.gov/search/details/Mars/GlobalSurveyor/MOLA/Mars_MGS_MOLA_DEM_mosaic_global_463m/cub> [Accessed: 04/12/2017]

Boeing, n.d. "Path to Mars" [online]. Available from <http://beyondearth.com/path-to-mars/> [Accessed: 08/01/2018].

Boss, A.P., Durisen, R.H., 2005. "Chondrule-forming shock fronts in the Solar Nebula: A possible unified scenario for planet and chondrite formation", *The Astrophysical Journal*, v. 621, pp. L137-L140.

Bouvier, A.,Wadhwa, M., 2010. "The age of the Solar System redefined by the oldest Pb–Pb age of a meteoritic inclusion", *Nature Geoscience*, v. 3, pp. 637-641.

Carr, M.H., Head, J.W., 2010. "Geologic history of Mars", *Earth and Planetary Science Letters*, v. 294, pp. 185-203.

Connerney, J.E.P., Acuña, M.H., Wasilewski, P.J., Ness, N.F., Rème, H., Mazelle, C., Vignes, D., Lin, R.P., Mitchell, D.L., Cloutier, P.A., 1999. “Magnetic lineations in the ancient crust of Mars”, *Science*, v. 284, pp. 794-800.

Dickson, J.L., Head, J.W., Fassett, C.I., 2012. “Patterns of accumulation and flow of ice in the mid-latitudes of Mars during the Amazonian”, *Icarus*, v. 219, pp. 723-732.

DLR, 2017. “Mars Express; HRSC - High Resolution Stereo Camera” [online]. Available from <http://www.dlr.de/dlr/en/desktopdefault.aspx/tabid-10364/548_read-400/#/gallery/657> [Accessed: 28/02/2018].

Ehlmann, B.L., Edwards, C.S., 2014. “Mineralogy of the Martian Surface”, The Annual Review of Earth and Planetary Sciences, v. 42, pp. 291-315.

Esri, n.d.. “GIS Dictionary, Raster” [online]. Available from <https://support.esri.com/en/other-resources/gis-dictionary/term/raster> [Accessed: 25/02/2018].

Explore Mars Inc., 2017. “The Humans to Mars Report” [online]. Available from <https://www.exploremars.org/the-humans-to-mars-report> [Accessed: 08/11/2017].

Fassett, C.I., Head III J.W., 2008. “Valley network-fed, open-basin lakes on Mars: Distribution and implications for Noachian surface and subsurface hydrology”, *Icarus*, 198, pp. 37-56.

Freie Universität Berlin, n.d.. “HRSC view data explorer” [online]. Available from <http://hrscview.fu-berlin.de/cgi-bin/ion-p?page=entry2.ion> [Accessed: 22/12/2017].

Frey, H.V., 2003. “Buried impact basins and the earliest history of Mars”, Lunar and Planetary Science Conference 35, abstract 3104.

Goldreich, P., Ward, W.R., 1973. “The formation of planetesimals”, *The Astrophysical Journal*, v. 183, pp. 1051-1061.

Hartmann, W.K., Neukum, G., 2001. “Cratering chronology and the evolution of Mars”, *Space Science Review*, v. 96, pp. 165-194.

Head, J.W., Kreslavsky, M.A., Pratt, S., 2002. “Northern lowlands of Mars: evidence for widespread volcanic flooding and tectonic deformation in the Hesperian period”, *Journal of Geophysical Research*, v. 107, n. E1, 5003.

Head, J.W., Marchant, D.R., 2006a. “Evidence for global-scale northern mid-latitude glaciation in the Amazonian period of Mars: Debris-covered glacier and valley glacier deposits in the 30º-50º N latitude band”, *Lunar and Planetary Science Conference* 37, abstract 1127.

Head, J.W., Marchant, D.R., 2006b. “Modification of the walls of a Noachian crater in Northern Arabia Terra (24º E, 39º N) during northern mid-latitude Amazonian glacial epochs on Mars: Nature and evolution of Lobate Debris Aprons and their relationships to lineated valley fill and glacial systems”, *Lunar and Planetary Science Conference* 37, abstract 1126.

Head, J.W., Marchant, D.R., Agnew, M.C., Fassett, C.I., Kreslavsky, M.A., 2006. “Extensive valley glacier deposits in the northern mid-latitudes of Mars: Evidence for Late Amazonian obliquity-driven climate change”, *Earth and Planetary Science Letters*, v. 241, pp. 663-671.

Head, J.W., Nahm, A.L., Marchant, D.R., Neukum, G., 2006b. “Modification of the dichotomy boundary on Mars by Amazonian mid-latitude regional glaciation”, *Geophysical Research Letters, v.33, pp. 1-3.*

Howard, A.D., Moore, J.M., Irwin III, R.P., 2005a. “An intense terminal epoch of widespread fluvial activity on Mars: 1. valley network incision and associated deposits”, *Journal of Geophysical Research*, v. 110, E12S14.

Howard, A.D., Moore, J.M., Irwin III, R.P., Craddock, R.A., 2005b. “A sedimentary platform in Margaritifer Sinus, Meridiani Planum and Arabia”, *Lunar and Planetary Science Conference* 36, abstract 1545.

Human Mars, 2017. “Making Life Multiplanetary. Official schematics for BFR by Elon Musk, SpaceX” [online]. Available from <http://www.humanmars.net/2017/09/making-life-multiplanetary-official.html#more> [Accessed: 08/01/2018].

Jacosky, B.M., Carr, M.H., 1985. “Possible precipitation of ice at low latitudes of Mars during periods of high obliquity”, *Nature*, v. 315, pp. 559-561.

Jet Propulsion Laboratory, n.d. “Human Journey to Mars: Thoughts on an Executable Program”, California Institute of Technology [online]. Available from < https://www.nasa.gov/sites/default/files/files/Naderi_JPL_Study_of_Humans_to_Mars_NAC_Final_TAGGED.pdf> [Accessed: 08/01/2018].

Jet Propulsion Laboratory, 2015. “Ridge and Talus in Lycus Sulci”, California Institute of Technology, [online]. Available from <https://www.jpl.nasa.gov/spaceimages/details.php?id=PIA19870> [Accessed: 28/12/2017].

Kasting, J.F., 1991. “CO2 condensation and the climate of early Mars”, *Icarus*, v. 94, pp. 1-13.

Laskar, J., Robutel, P., 1993. “The chaotic obliquity of the planets”, *Nature*, v. 361, pp. 608-612.

Laskar, J., Correia, A.C.M., Gastineau, M., Joutel, F., Levrard, B. Robutel, P., 2004. “Long term evolution and chaotic diffusion of the insolation quantities of Mars”, *Icarus*, v. 170, pp. 343-364.

Leovy, C., 2001. “Weather and climate on Mars”, *Nature*, v. 412, pp. 245-249.

Levy, J.S., Head, J.W., Marchant, D.R., 2009. “Concentric crater fill in Utopia Planitia: Timing and transitions between glacial ‘‘brain terrain” and periglacial processes”, *Icarus*, v. 202, pp. 462-476.

Levy, J., Head, J.W., Marchant, D.R., 2010. “Concentric crater fill in the northern mid-latitudes of Mars: Formation processes and relationships to similar landforms of glacial origin”, *Icarus*, v. 209, pp. 390-404.

Litvak, M., Mitrofanov, I., Sanin, A., Lisov, D., Behar, A., Boynton, W., Deflores, L.,Fedosov, F., Golovin, D., Hardgrove, C., Harshman, K., Jun, I., Kozyrev, A., Kuzmin, R., Malakhov, A., Milliken, R., Mischna, M., Moersch, J., Mokrousov, M., Nikiforov, S., Shvetsov, V., Stack, K., Starr, R., Tate, C., Tret’yakov V, Vostrukhin, A., 2014’. “Local variations of bulk hydrogen and chlorine-equivalent neutron absorption content measured at the contact between the Sheepbed and

Gillespie Lake units in Yellowknife Bay, Gale Crater, using the DAN instrument onboard Curiosity" [online], *Journal of Geophysical Research: Planets*, v. 119, pp. 1259-1275. Available from: <www.onlinelibrary.wiley.com> [Accessed: 22/01/2018].

LPI, 2015. "First landing site/exploration zone workshop for human missions to the surface of Mars supplemental paper", Lunar and Planetary Institute, Huston, [online]. Available from <https://www.hou.usra.edu/meetings/explorationzone2015/program_presenter_info/Supplemental%20_Paper.pdf> [Accessed: 17/11/2017].

Mahaffy, P.R., Webster, C.R., Atreya, S.K., Franz, H., Wong, M., Conrad, P.G., Harpold, D., Jones, J.J., Leshin, L.A., Manning, H., Owen, T., Pepin, R.O., Squyres, S., Trainer, M., Kemppinen, O., Bridges, N., Johnson, J.R., Minitti, M., Cremers, D., Bell, J.F., Edgar, L., Farmer, J., Godber, A., Wadhwa, M., Wellington, D., McEwan, I., Newman, C., Richardson, M., Charpentier, A., et al., 2013. "Abundance and Isotopic Composition of Gases in the Martian Atmosphere from the Curiosity Rover", *Science*, v. 341, 263-266.

McGill, C.E., 2000. "Crustal history of north central Arabia Terra, Mars", *Journal of Geophysical Research: Planets*, v. 105, pp. 6945-6959.

Mitrofanov, I., Litvak, M., Sanin, A., Starr, R., Lisov, D., Kuzmin, R., Behar, A., Boynton, W., Hardgrove, C., Harshman, K., Jun, I., Milliken, R., Mischna, M., Moersch, J., Tate, C., 2014. "Water and chlorine content in the Martian soil along the first 1900 m of the Curiosity rover traverse as estimated by the DAN instrument" [online], *Journal of Geophysical Research: Planets*, v. 119, pp. 1579-1596. Available from: <http://onlinelibrary.wiley.com/doi/10.1002/2013JE004553/epdf> [Accessed: 22/01/2018].

Morgan, G.A., Head III, J.W., Marchant, D.R., 2009. "Lineated valley fill (LVF) and lobate debris aprons (LDA) in the Deuteronilus Mensae northern dichotomy boundary region, Mars: Constraints on the extent, age and episodicity of Amazonian glacial events", *Icarus*, v. 202, pp. 22-38.

McGill, G.E., Squyres, S.W., 1991. "Origin of the Marian Crustal Dichotomy: Evaluating Hypoteses", *Icarus*, v. 93, pp. 386-393.

Mitchell, Don P., 2004. “Soviet Mars Images” [online]. Available from <http://mentallandscape.com/C_CatalogMars.htm> [Accessed: 12/01/2018].

Murchie, S.L., the CRISM Science and Engineering Teams, 2008. “First results from the Compact Reconnaissance Imaging Spectrometer for Mars (CRISM)”, *Lunar and Planetary Science Conference* 39, abstract 1472.

NASA, 2015. “Seeks Ideas for Where on Mars the Next Giant Leap Will Take Place”, [online]. Available from <https://www.nasa.gov/journeytomars/mars-exploration-zones> [Accessed: 21/12/2017].

NASA, 2016a. “Mars Fact Sheet”, [online]. Available from < https://nssdc.gsfc.nasa.gov/planetary/factsheet/marsfact.html> [Accessed: 29/01/2018].

NASA, 2016b. “NASA’s Journey to Mars: Pioneering Next Steps in Space Exploration” [online]. Available from <https://www.nasa.gov/sites/default/files/atoms/files/journey-to-mars-next-steps-20151008_508.pdf> [Accessed: 13/11/2017].

NASA, 2017. “New Space Policy Directive Calls for Human Expansion Across Solar System”. Available from <https://www.nasa.gov/press-release/new-space-policy-directive-calls-for-human-expansion-across-solar-system> [Accessed: 08/01/2018].

NASA, n.d.a “2001 Mars Odissey” [online]. Available from <https://mars.nasa.gov/programmissions/missions/present/odyssey/> [Accessed: 15/12/2017].

NASA, n.d.b “Historical Log” [online]. Available from <https://mars.nasa.gov/programmissions/missions/log/> [Accessed: 04/12/2017].

NASA, n.d.c. “Mariner to Mercury, Venus and Mars” [online]. Available from <https://mars.nasa.gov/files/mep/Mars-Mission-Mariner-Fact-Sheet.pdf> [Accessed: 15/12/2017].

NASA, n.d.d. “Mars 3 Lander” [online]. Available from <https://nssdc.gsfc.nasa.gov/nmc/spacecraftDisplay.do?id=1971-049F> [Accessed: 22/12/2017]

NASA, n.d.e. “Mars Exploration Rover” [online]. Available from <https://mars.nasa.gov/mer/newsroom/factsheets/pdfs/Mars03Rover041020.pdf> [Accessed: 15/12/2017].

NASA, n.d.f. “Mars Global Surveyor” [online]. Available from <https://www.jpl.nasa.gov/news/fact_sheets/mgs.pdf> [Accessed: 15/12/2017].

NASA, n.d.g. “Mars Pathfinder” [online]. Available from <https://www.jpl.nasa.gov/news/fact_sheets/mpf.pdf> [Accessed: 15/12/2017].

NASA, n.d.h. “Mars Reconnaissance Orbiter” [online]. Available from <https://mars.nasa.gov/mro/files/mro/MRO-060303.pdf> [Accessed: 15/12/2017].

NASA, n.d.i. “Mars Science Laboratory/Curiosity” [online]. Available from <https://mars.nasa.gov/msl/news/pdfs/MSL_Fact_Sheet.pdf> [Accessed: 15/12/2017].

NASA, n.d.j. “Phoenix Mars Mission [online]. Available from http://phoenix.lpl.arizona.edu/pdf/fact_sheet.pdf [Accessed: 15/12/2017].

NASA, n.d.k. “Viking missions to Mars” [online]. Available from <https://www.jpl.nasa.gov/news/fact_sheets/viking.pdf> [Accessed: 15/12/2017].

Nimmo F., Tanaka K., “Early crustal evolution of Mars”, *Annual Review of Earth and Planetary Sciences*, v. 33, pp. 133-161, 2005.

Phillips, R.J., Zuber, M.T., Solomon, S.C., Golombek, M.P., Jakosky, B.M., Banerdt, W.B., Smith, D.E., Williams, R.M., Hynek, B.M., Aharonson, O., Hauck II, S.A., 2001. “Ancient geodynamics and global-scale hydrology on Mars”, *Science*, v. 291, pp. 2587-2591.

Planetary Science Institute, 2012. “Thermal Inertia Web Site” [online]. Available from <https://sharad.psi.edu/inertia/> [Accessed: 02/02/2018]

Saydam, S., Tapia Cortez, C., de Roche, T., Dempster, A.G., 2015. “An evaluation of Mars water extraction mission”, *Proceedings of the 26th Annual General Meeting and Conference of the Society of Mining Professors*, Saxony, Germany, pp. 75-82 (The Society of Mining Professors).

Schultz, R.A., Frey, H.V., 1990. “A new survey of multi-ring impact basins on Mars”, *Journal of Geophisical Research*, v. 95, pp. 14175-14189.

Scott, D.H., Tanaka, K.L., 1986. “Geologic map of the western equatorial region of Mars”, U.S. Geological Survey Misc. Inv. Map I-1802-A.

Sharp, R.P., 1973. “Mars: Fretted and chaotic terrains”, *Journal of Geophisical Research*, v. 78, pp. 4073-4083.

Solomon, S.C., Aharonson, O., Aurnou, J.M., Banerdt, W.B., Carr, M.H., Dombard, A.J., Frey, H.V., Golombek, M.P., Hauck II, S.A., Head, J.W., Jakosky, B.M., Johnson, C.L., McGovern, P.J., Neumann, G.A., Phillips, R.J., Smith, D.E., Zuber, M.T., 2005. “New perspectives on ancient Mars”, *Science*, v. 307, pp. 1214-1220.

SpaceX, 2017. “Making Life Multiplanetary” [online]. Available from < http://www.spacex.com/mars> [Accessed: 08/01/2018].

Squyres, S.W., 1978. “Martian fretted terrain: Flow of erosional debris”, *Icarus*, v. 34, pp. 600-613.

Squyres, S.W., 1979. “The distribution of lobate debris aprons and similar flows on Mars”, *Journal of Geophisical Research*, v. 84, pp. 8087-8096.

Strom, R.G., Croft, S.K., Barlow, N.G., 1992. In: Kieffer, H.H., Jakosky, B.M., Snyder, C.W., Matthews, M.S. (Eds.), “The Martian Impact Cratering Record”, *The University of Arizona Press*, Mars, pp. 383-423.

Zabludoff, A., 2003. “Lecture 13: The Nebular Theory of the origin of the Solar System”. Available from <http://atropos.as.arizona.edu/aiz/teaching/nats102/mario/solar_system.html> [Accessed: 28/12/201].

APPENDIX A

Missions summary (from NASA n.d.b)

S: successful mission

F: failed mission

#	Launch Date	Name	Country	Result	Reason
1	1960	Korabl 4	USSR (flyby)	F	Didn't reach Earth orbit
2	1960	Korabl 5	USSR (flyby)	F	Didn't reach Earth orbit
3	1962	Korabl 11	USSR (flyby)	F	Earth orbit only, spacecraft broke apart
4	1962	Mars 1	USSR (flyby)	F	Radio Failed
5	1962	Korabl 13	USSR (flyby)	F	Earth orbit only, spacecraft broke apart
6	1964	Mariner 3	US (flyby)	F	Shroud failed to jettison
7	1964	Mariner 4	US (flyby)	S	Returned 21 images
8	1964	Zond 2	USSR (flyby)	F	Radio failed
9	1969	Mars 1969A	USSR	F	Launch vehicle failure
10	1969	Mars 1969B	USSR	F	Launch vehicle failure
11	1969	Mariner 6	US (flyby)	S	Returned 75 images
12	1969	Mariner 7	US (flyby)	S	Returned 126 images
13	1971	Mariner 8	US	F	Launch failure
14	1971	Kosmos 419	USSR	F	Achieved Earth orbit only
15	1971	Mars 2 Orbiter/Lander	USSR	F	Orbiter arrived, but no useful data and Lander destroyed
16	1971	Mars 3 Orbiter/Lander	USSR	S	Orbiter obtained approximately 8 months of data and lander landed safely, but only 20 seconds of data
17	1971	Mariner 9	US	S	Returned 7,329 images
18	1973	Mars 4	USSR	F	Flew past Mars
19	1973	Mars 5	USSR	S	Returned 60 images, only lasted 9 days

20	1973	Mars 6 Orbiter/Lander	USSR	S/F	Occultation experiment produced data and Lander failure on descent
21	1973	Mars 7 Lander	USSR	F	Missed planet, now in solar orbit.
22	1975	Viking 1 Orbiter/Lander	US	S	Located landing site for Lander and first Successful landing on Mars
23	1975	Viking 2 Orbiter/Lander	US	S	Returned 16,000 images and extensive atmospheric data and soil experiments
24	1988	Phobos 1 Orbiter	USSR	F	Lost on route to Mars
25	1988	Phobos 2 Orbiter/Lander	USSR	F	Lost near Phobos
26	1992	Mars Observer	US	F	Lost prior to Mars arrival
27	1996	Mars Global Surveyor	US	S	More images than all Mars Missions
28	1996	Mars 96	Russia	F	Launch vehicle failure
29	1996	Mars Pathfinder	US	S	Technology experiment lasting 5 times longer than warranty
30	1998	Nozomi	Japan	F	No orbit insertion, fuel problems
31	1998	Mars Climate Orbiter	US	F	Lost on arrival
32	1999	Mars Polar Lander	US	F	Lost on arrival
33	1999	Deep Space 2 Probes (2)	US	F	Lost on arrival (carried on Mars Polar Lander)
34	2001	Mars Odyssey	US	S	High resolution images of Mars
35	2003	Mars Express Orbiter/Beagle 2 Lander	ESA	S/F	Orbiter imaging Mars in detail and lander lost on arrival
36	2003	Mars Exploration Rover - Spirit	US	S	Operating lifetime of more than 15 times original warranty
37	2003	Mars Exploration Rover - Opportunity	US	S	Operating lifetime of more than 15 times original warranty
38	2005	Mars Reconnaissance Orbiter	US	S	Returned more than 26 terabits of data (more than all other Mars missions combined)

39	2007	Phoenix Mars Lander	US	S	Returned more than 25 gigabits of data
40	2011	Mars Science Laboratory	US	S	Exploring Mars' habitability
41	2011	Phobos-Grunt/Yinghuo-1	Russia/China	F	Stranded in Earth orbit
42	2013	Mars Atmosphere and Volatile Evolution	US	S	Studying the Martian atmosphere
43	2013	Mars Orbiter Mission (MOM)	ISRO	S	Develop interplanetary technologies and explore Mars' surface features, mineralogy and atmosphere.
44	2016	ExoMars Orbiter/Schiaparelli EDL Demo Lander	ESA/Russia	S/F	Orbiter studying Martian atmosphere and EDL demo lander lost on arrival

APPENDIX B

Summary of proposed exploration zones (Bussey et al., 2017)

Author		Add'l Author(s)	Landing Site	Abstract No.	Longitude	Latitude
Ackiss	Sheridan	Niles, P.B.	Huygens Crater	1032	27	13.5S
Barker	Don		Phlegra Dorsa	1002	1	39N
Boatwright	Ben		Southern Nectaris Fossae	1005	2	29S
Calef	Fred		Gale Crater	1020	3	4.5S
Clarke	J		Endeavour Crater	1057	43	3S
Clifford	Stephen		Eastern Valles Marineris	1054	41	4S
Cohen	Barb		Meridiani Planum	1030	4	0.5N
Davila	Alfonso	Schulze-Makuch, D.	Hebrus Valles	1012	5	20N
Farrell	Winslow		Chryse – Viking	1019	22	22.5N
Gallegos	Zachary		Mesopotamia	1035	28	35.5S
Gallegos	Zachary		Protonilus Mensae	1053	40	42N
Gallegos	Zachary		Tempe Terra	1056	42	42N
Gupta	Sanjeev	Sefton-Nash, E.	Hypanis	1051	15	12N
Hamilton	John		Ausonia Cavus	1045	35	32S
Hamilton	John		Kasei Valles	1045	36	25N
Hamilton	John		Ausonia Cavus	1045	35	32S
Head	Jim		Deuteronilus Mensae	1033	9	39N
Hill	Jonathan		Noachis Terra	1021	23	37S
Horgan	Briony		Mawrth Vallis	1009	7	24.5N
Kerber	Laura		Apollinaris Sulci	1043	8	12.5S
Kochemasov	Gennady		Vallis Marineris Mouth	1006	10	20N
Laine	Pauli		Newton Crater	1015	20	40.5S
Lee	Pascal		Noctis Landing	1050	39	6.5S
Levy	Joe		Hellas Rim	1037	30	39S
Longo	Alex		Gusev Crater	1008	11	14.5S
Lynch	Kennda		Columbus Crater	1041	32	29S
Mangold	Nicolas		Ismenius Cavus	1027	19	33.5N
Markle	Loren		Nili Fossae	1010	12	22N
McEwen	Alfred		Melas Chasma	1007	13	12S
Michalski	Joe		McLaughlin Crater	1025	25	22N
Mitchell	Julie		Equatorial Vallis Marineris	1023	24	19S
Mojarro	A,	Carr, C.	Coprates Chasma	1036	29	11.5S
Montaño	Sui		Gale Crater	1040	3	4.5S
Mustard	Jack		Jezero Crater	1034	6	17.5N
Ori	Gian		Firsoff Crater	1026	14	0N
Plaut	Jeff		Deuteronilus Mensae	1044	34	41N
Rice	Jim		Eastern Hellas	1038	31	40S
Rice	Jim		Apollinaris Sulci	1046	37	13S
Sibille	Laurent		Aram Chaos	1048	38	2.5N
Skinner	Jim		Hadriacus Palus	1052	16	27S
Stillman	David		Hale Crater	1028	26	36S

Author		Add'l Author(s)	Landing Site	Abstract No.	Longitude	Latitude
Viola	Donna		Erberus Montes	1011	17	39N
Viola	Donna		Acheron Fossae	1011	18	40N
Westenberg	A		Copericus Crater	1029	44	49S
Wilkinson	Murray	McGovern, P.J.	Sinus Meridiani	1042	33	2S
Wright	Shawn		Cerberus	1017	21	10N
Yun	Paul		Gale Crater	1022	3	4.5S

APPENDIX C

List of analysed datasets

The format of all the following data is TIFF.

1. Global Map

MEGDR

Mars_MGS_MOLA_DEM_mosaic_global_463m

2. Gale Crater Exploration Zone

HRSC DTM

h1916_0000.da4.52

h1927_0000.da4.52

h1949_0000.da4.52

h5273_0000.da4.50

CTX

B07_012195_1750_XN_05S222W

B21_017786_1746_XN_05S222W

D03_028190_1746_XN_05S222W

F01_036339_1734_XN_06S222W

F03_037117_1751_XN_04S222W

F04_037407_1745_XN_05S221W

P01_001422_1747_XN_05S222W

P04_002530_1745_XI_05S223W

P05_003176_1746_XI_05S221W

3. Protonilus Mensae Exploration Zone

HRSC DTM

h1523_0000.da4.52

h1545_0000.da4.52

h2908_0000.da4.50

CTX

F04_037542_2217_XN_41N311Wf

P17_007715_2232_XN_43N312Wf

P16_007359_2220_XN_42N311Wf

P15_006937_2222_XN_42N308Wf

P15_006858_2226_XN_42N311Wf

4. Deuteronilus Mensae I Exploration Zone

HRSC DTM

h1461_0000.da4.52

h1483_0000.da4.52

h3249_0000.da4.50

h5213_0000.da4.50

5. Deuteronilus Mensae II Exploration Zone

HRSC DTM

h1483_0000.da4.52

h3249_0000.da4.50

h5213_0000.da4.50

h5231_0000.da4.50